Neural Plasticity

Glial Cells and Synaptic Plasticity

Guest Editors: Fushun Wang, Tifei Yuan, Alfredo Pereira Jr., Alexei Verkhratsky, and Jason H. Huang

Glial Cells and Synaptic Plasticity

Neural Plasticity

Glial Cells and Synaptic Plasticity

Guest Editors: Fushun Wang, Tifei Yuan, Alfredo Pereira Jr., Alexei Verkhratsky, and Jason H. Huang

Editorial Board

Contents

Glial Cells and Synaptic Plasticity
Fushun Wang, Tifei Yuan, Alfredo Pereira Jr., Alexei Verkhratsky, and Jason H. Huang
Volume 2016, Article ID 5042902, 3 pages

Astrocyte Hypertrophy Contributes to Aberrant Neurogenesis after Traumatic Brain Injury
Clark Robinson, Christopher Apgar, and Lee A. Shapiro
Volume 2016, Article ID 1347987, 10 pages

Modulation of Synaptic Plasticity by Glutamatergic Gliotransmission: A Modeling Study
Maurizio De Pittà and Nicolas Brunel
Volume 2016, Article ID 7607924, 30 pages

Role of MicroRNA in Governing Synaptic Plasticity
Yuqin Ye, Hongyu Xu, Xinhong Su, and Xiaosheng He
Volume 2016, Article ID 4959523, 13 pages

Housing Complexity Alters GFAP-Immunoreactive Astrocyte Morphology in the Rat Dentate Gyrus
Garrick Salois and Jeffrey S. Smith
Volume 2016, Article ID 3928726, 11 pages

Recent Advance in the Relationship between Excitatory Amino Acid Transporters and Parkinson's Disease
Yunlong Zhang, Feng Tan, Pingyi Xu, and Shaogang Qu
Volume 2016, Article ID 8941327, 8 pages

Anger Emotional Stress Influences VEGF/VEGFR2 and Its Induced PI3K/AKT/mTOR Signaling Pathway
Peng Sun, Sheng Wei, Xia Wei, Jieqiong Wang, Yuanyuan Zhang, Mingqi Qiao, and Jibiao Wu
Volume 2016, Article ID 4129015, 12 pages

The Plastic Glial-Synaptic Dynamics within the Neuropil: A Self-Organizing System Composed of Polyelectrolytes in Phase Transition
Vera Maura Fernandes de Lima and Alfredo Pereira Jr.
Volume 2016, Article ID 7192427, 20 pages

Glia and TRPM2 Channels in Plasticity of Central Nervous System and Alzheimer's Diseases
Jing Wang, Michael F. Jackson, and Yu-Feng Xie
Volume 2016, Article ID 1680905, 7 pages

Value of Functionalized Superparamagnetic Iron Oxide Nanoparticles in the Diagnosis and Treatment of Acute Temporal Lobe Epilepsy on MRI
Tingting Fu, Qingxia Kong, Huaqiang Sheng, and Lingyun Gao
Volume 2016, Article ID 2412958, 12 pages

Dynamic Alterations of miR-34c Expression in the Hypothalamus of Male Rats after Early Adolescent Traumatic Stress
Chuting Li, Yuan Liu, Dexiang Liu, Hong Jiang, and Fang Pan
Volume 2016, Article ID 5249893, 8 pages

Hindawi Publishing Corporation
Neural Plasticity
Volume 2016, Article ID 5042902, 3 pages
http://dx.doi.org/10.1155/2016/5042902

Editorial

Glial Cells and Synaptic Plasticity

Fushun Wang,[1,2,3] Tifei Yuan,[4] Alfredo Pereira Jr.,[5] Alexei Verkhratsky,[6] and Jason H. Huang[3,7]

[1]*Department of Psychology, Nanjing University of Chinese Medicine, Nanjing 210023, China*
[2]*Center of Translational Neuromedicine, Department of Neurosurgery, University of Rochester, Rochester, NY 14643, USA*
[3]*Department of Neurosurgery, Baylor Scott & White Health, Temple, TX 76508, USA*
[4]*Department of Psychology, Nanjing Normal University, Nanjing, Jiangsu 210023, China*
[5]*Institute of Bioscience of Botucatu, Sao Paulo State University, 18618-970 Botucatu, SP, Brazil*
[6]*Department of Life Science, University of Manchester, Oxford Road, Manchester M139PT, UK*
[7]*Department of Surgery, Texas A&M College of Medicine, Temple, TX 76504, USA*

Correspondence should be addressed to Fushun Wang; fushun_wang@urmc.rochester.edu

Received 28 March 2016; Accepted 29 March 2016

Neuroglia are composed of highly heterogeneous cellular populations of neural (astrocytes, oligodendrocytes, and NG2 glial cells) and nonneural (microglia) origin that are essential for maintaining efficient neurotransmission, homeostatic cascades, supply of energy metabolites, turnover of neurotransmitters, and establishment of the blood-brain barrier [1]. Astrocytes shape synaptic networks through essential roles in synaptogenesis, synaptic maturation, and synaptic extinction [2, 3]. Furthermore, astroglial cells secrete neurotransmitters (such as glutamate, ATP, and GABA), neuromodulators (such as adenosine and D-serine), neurohormones (such as atrial natriuretic peptide), and other humoral factors (such as eicosanoids) that modulate synaptic networks and affect information processing [4]. The concept of "multipartite synapse" formalizes the multicomponent nature of the synaptic concept that includes astroglial perisynaptic processes, microglial processes, and extracellular matrix [5, 6].

Potentiation and depression of synaptic connections are critical for learning, memory formation, and emotions [7, 8]. Long-term potentiation (LTP) and long-term depression (LTD) are triggered by patterned and repeated synaptic activities, depending on the complex dynamics of neurotransmitters (especially glutamate) in the synaptic cleft. Both the temporal course and spatial distribution of glutamate contribute to the coordinated activation of intracellular signaling cascades affecting synaptic strength [9]. The multipartite synapse concept has defined astrocyte as the key regulator of glutamate homeostasis (mediated through release and uptake) [10]. Astrocytes, for example, are capable of releasing D-serine to enhance the function of NMDA receptors [11]. In addition, astrocytes can change the buffering ability to take up extracellular K^+, thus modulating synaptic plasticity [12]. Calcium dynamics in astrocytes determine the release of glutamate and ATP molecules. At the synaptic level, the astroglial calcium signaling is activated in response to synaptic activities, such as repeated synaptic stimulation, through purinergic, glutamatergic, and cholinergic pathways. The hyperactivity of neural circuits (e.g., in epilepsy) results in altered calcium dynamics in astrocytes. These changes, in turn, contribute to the differential modulation of synaptic efficacy under physiological or pathological circumstances [13, 14].

The papers collected in this special issue focus on glial cells and synaptic plasticity. The reviews and experimental papers present the evidence that glial cells indeed affect long-term synaptic changes.

In "Housing Complexity Alters GFAP-Immunoreactive Astrocyte Morphology in the Rat Dentate Gyrus," G. Salois and J. S. Smith [15] demonstrate that the housing environment can affect neural plasticity. They found that an enriched environment results in considerable neuroplasticity in the rodent brain. They used confocal microscopy and found that

astrocytes play a key role in the process and induce changes in synaptic spines. These findings offer a hallmark feature for the understanding of numerous diseases, including the neurodegenerative ones.

In "Recent Advance in the Relationship between Excitatory Amino Acid Transporters and Parkinson's Disease," Y. Zhang et al. [16] reviewed their studies and also recent discoveries about the excitatory amino acid transporters (EAATs). Glutamate is the major excitatory neurotransmitter in the central nervous system, and it is mostly removed by astrocytes, where it is converted into glutamine. Impairment of astroglial glutamate uptake leads to the accumulation of glutamate in the synaptic cleft, which may contribute to various pathologies such as Parkinson's disease (PD).

Consistent with recent studies about astrocytic function in emotions, the paper "Anger Emotional Stress Influences VEGF/VEGFR2 and Its Induced PI3K/AKT/mTOR Signaling Pathway," by P. Sun et al. [17], reported changes of VEGR/VEGFR2 in both astrocytes and neurons, induced by the anger emotion; these changes, in turn, can stimulate neurogenesis.

In the review article "The Plastic Glial-Synaptic Dynamics within the Neuropil: A Self-Organizing System Composed of Polyelectrolytes in Phase Transition," V. M. F. de Lima and A. Pereira Jr. [18] reported another pathway for neuronal-glial interaction: the plastic nonlinear dynamics between glial and synaptic terminals; they also offered a model based on hydroionic waves within the neuropil.

In the paper "Glia and TRPM2 Channels in Plasticity of Central Nervous System and Alzheimer's Diseases," J. Wang et al. [19] review recent findings about synaptic plasticity in neurodegenerative diseases, mainly focusing on the transient receptor potential melastatin 2 (TRPM2) channels. The TRPM2 is a nonselective Ca^{2+} permeable channel expressed in both glial cells and neurons, which regulates synaptic plasticity and also the glial cells. In this review, authors summarized recent discoveries about the contribution of TRPM2 in physiological and pathological conditions.

In "Dynamic Alterations of miR-34c Expression in the Hypothalamus of Male Rats after Early Adolescent Traumatic Stress," C. Li et al. [20] reported experimental findings about neural plasticity under stress. They found that stress induces the overexpression of several types of microRNA notably including corticotrophin releasing factor 1 (CRFR1 mRNA) and miR-34c. Expression levels of the miR-34c in the hypothalamus represent an important factor involved in susceptibility to posttraumatic stress disorders.

In the subsequent paper "Role of MicroRNA in Governing Synaptic Plasticity," Y. Ye et al. reviewed the role of microRNA in neural plasticity. They explored recent findings demonstrating that miRNA exerts widespread regulation over the translation and degradation of target genes in the nervous systems and contributes to the pathophysiology of plasticity-related diseases.

In "Astrocyte Hypertrophy Contributes to Aberrant Neurogenesis after Traumatic Brain Injury," C. Robinson et al. reported their recent findings about astrocytic changes after traumatic brain injury (TBI). They analyzed the immunohistochemistry of glial fibrillary acidic protein and doublecortin and found a loss of radial glial-like processes extending through the granule cell layer after TBI. They further suggested that hypertrophied astrocytic processes form an ectopic glial scaffold that might facilitate the aberrant development of immature neurons in the dentate gyrus.

In "Modulation of Synaptic Plasticity by Glutamatergic Gliotransmission: A Modeling Study," M. De Pittà and N. Brunel reported a computational model about gliotransmitter releasing pathways related to modulation of synaptic release and postsynaptic slow inward currents. This model predicts that both pathways could profoundly affect synaptic plasticity.

Collectively, these studies demonstrate that glial cells play an important role in neural plasticity under physiological and pathological conditions. We hope that this special issue will stimulate interest in the field of glial cells modulating synaptic activities and will help to achieve a deeper understanding of the role of glial cells in neural plasticity.

Acknowledgments

This work was supported, in part, by NIH R01 NS067435 (Jason H. Huang), Scott & White Plummer Foundation Grant (Jason H. Huang), Jiangsu Specially Appointed Professorship Foundation (Fushun Wang), Jiangsu Nature Science Foundation BK20151565 (Fushun Wang), Jiangsu Traditional Chinese Medicine Foundation ZD201501 (Fushun Wang) and Jiangsu Six Talent Peak (2015YY006), and the Priority Academic Program Development (PAPD) of Jiangsu Higher Education Institute (Fushun Wang).

Fushun Wang
Tifei Yuan
Alfredo Pereira Jr.
Alexei Verkhratsky
Jason H. Huang

References

[1] A. Verkhratsky, M. Nedergaard, and L. Hertz, "Why are astrocytes important?" *Neurochemical Research*, vol. 40, no. 2, pp. 389–401, 2014.

[2] C. Eroglu and B. A. Barres, "Regulation of synaptic connectivity by glia," *Nature*, vol. 468, no. 7321, pp. 223–231, 2010.

[3] A. Verkhratsky and M. Nedergaard, "Astroglial cradle in the life of the synapse," *Philosophical Transactions of the Royal Society of London, Series B: Biological Sciences*, vol. 369, no. 1654, Article ID 20130595, 2014.

[4] A. Verkhratsky, M. Matteoli, V. Parpura, J. Mothet, and R. Zorec, "Astrocytes as secretory cells of the central nervous system: idiosyncrasies of vesicular secretion," *The EMBO Journal*, vol. 35, no. 3, pp. 239–257, 2016.

[5] V. Parpura, T. A. Basarsky, F. Liu, K. Jeftinija, S. Jeftinija, and P. G. Haydon, "Glutamate-mediated astrocyte-neuron signalling," *Nature*, vol. 369, no. 6483, pp. 744–747, 1994.

[6] E. Shigetomi, S. Patel, and B. S. Khakh, "Probing the complexities of astrocyte calcium signaling," *Trends in Cell Biology*, vol. 26, no. 4, pp. 300–312, 2016.

[7] S. Gu, F. Wang, T. Yuan, B. Guo, and J. Huang, "Differentiation of primary emotions through neuromodulators: review of

literature," *Internaiton Journal of Neurology Research*, vol. 1, no. 2, pp. 43–50, 2015.

[8] X. Cao, L.-P. Li, Q. Wang et al., "Astrocyte-derived ATP modulates depressive-like behaviors," *Nature Medicine*, vol. 19, pp. 773–777, 2013.

[9] N. Bazargani and D. Attwell, "Astrocyte calcium signaling: the third wave," *Nature Neuroscience*, vol. 19, pp. 182–189, 2016.

[10] M. M. Halassa and P. G. Haydon, "Integrated brain circuits: astrocytic networks modulate neuronal activity and behavior," *Annual Review of Physiology*, vol. 72, pp. 335–355, 2009.

[11] N. B. Hamilton and D. Attwell, "Do astrocytes really exocytose neurotransmitters?" *Nature Reviews. Neuroscience*, vol. 11, pp. 227–238, 2010.

[12] F. Wang, N. A. Smith, Q. Xu et al., "Astrocytes modulate neural network activity by Ca^2+-dependent uptake of extracellular K+," *Science Signaling*, vol. 5, no. 218, article ra26, 2012.

[13] F. Wang, N. A. Smith, Q. Xu et al., "Photolysis of caged Ca^{2+} but not receptor-mediated Ca^{2+} signaling triggers astrocytic glutamate release," *The Journal of Neuroscience*, vol. 33, no. 44, pp. 17404–17412, 2013.

[14] F. Wang, Q. Xu, W. Wang, T. Takano, and M. Nedergaard, "Bergmann glia modulate cerebellar Purkinje cell bistability via Ca^{2+}-dependent K^+ uptake," *Proceedings of the National Academy of Sciences of the United States of America*, vol. 109, no. 20, pp. 7911–7916, 2012.

[15] G. Salois and J. Smith, "Housing complexity alters GFAP-immunoreactive astrocyte morphology in the rat dentate gyrus," *Neural Plasticity*, vol. 2016, Article ID 3928726, 11 pages, 2016.

[16] Y. Zhang, F. Tan, P. Xu, and S. Qu, "Recent advance in the relationship between excitatory amino acid transporters and Parkinson's disease," *Neural Plasticity*, vol. 2016, Article ID 8941327, 8 pages, 2016.

[17] P. Sun, S. Wei, X. Wei et al., "Anger emotional stress influences VEGF/VEGFR2 and its induced PI3K/AKT/mTOR signaling pathway," *Neural Plasticity*, vol. 2016, Article ID 4129015, 12 pages, 2016.

[18] V. M. F. de Lima and A. Pereira Jr., "The plastic glial-synaptic dynamics within the neuropil: a self-organizing system composed of polyelectrolytes in phase transition," *Neural Plasticity*, vol. 2016, Article ID 7192427, 20 pages, 2016.

[19] J. Wang, M. F. Jackson, and Y.-F. Xie, "Glia and TRPM2 channels in plasticity of central nervous system and Alzheimer's diseases," *Neural Plasticity*, vol. 2016, Article ID 1680905, 7 pages, 2016.

[20] C. Li, Y. Liu, D. Liu, H. Jiang, and F. Pan, "Dynamic alterations of miR-34c expression in the hypothalamus of male rats after early adolescent traumatic stress," *Neural Plasticity*, vol. 2016, Article ID 5249893, 8 pages, 2016.

Hindawi Publishing Corporation
Neural Plasticity
Volume 2016, Article ID 1347987, 10 pages
http://dx.doi.org/10.1155/2016/1347987

Research Article

Astrocyte Hypertrophy Contributes to Aberrant Neurogenesis after Traumatic Brain Injury

Clark Robinson,[1,2] Christopher Apgar,[1,2] and Lee A. Shapiro[1,2,3]

[1]*Department of Surgery, Texas A&M University Health Science Center, College of Medicine, Temple, TX 76504, USA*
[2]*Central Texas Veterans Health Care System, Temple, TX 76504, USA*
[3]*Department of Neurosurgery, Neuroscience Research Institute, Scott & White Hospital, Temple, TX 76508, USA*

Correspondence should be addressed to Lee A. Shapiro; lshapiro@medicine.tamhsc.edu

Received 10 November 2015; Accepted 11 February 2016

Academic Editor: Fushun Wang

Traumatic brain injury (TBI) is a widespread epidemic with severe cognitive, affective, and behavioral consequences. TBIs typically result in a relatively rapid inflammatory and neuroinflammatory response. A major component of the neuroinflammatory response is astrocytes, a type of glial cell in the brain. Astrocytes are important in maintaining the integrity of neuronal functioning, and it is possible that astrocyte hypertrophy after TBIs might contribute to pathogenesis. The hippocampus is a unique brain region, because neurogenesis persists in adults. Accumulating evidence supports the functional importance of these newborn neurons and their associated astrocytes. Alterations to either of these cell types can influence neuronal functioning. To determine if hypertrophied astrocytes might negatively influence immature neurons in the dentate gyrus, astrocyte and newborn neurons were analyzed at 30 days following a TBI in mice. The results demonstrate a loss of radial glial-like processes extending through the granule cell layer after TBI, as well as ectopic growth and migration of immature dentate neurons. The results further show newborn neurons in close association with hypertrophied astrocytes, suggesting a role for the astrocytes in aberrant neurogenesis. Future studies are needed to determine the functional significance of these alterations to the astrocyte/immature neurons after TBI.

1. Introduction

Traumatic brain injuries (TBIs) have multiple causes, from motor vehicle accidents, falls, sports-related injuries, violence, and military activity, making TBI a serious health concern around the world. The World Health Organization has stated that the incidence and long-term consequences of TBIs will continue to increase over the next five years, representing a continual increase to this already existing major cause of death and disability [1]. Not only can TBI result in a patient's loss of function, but, in some cases, TBI may progress into early dementia, depression, personality changes, and posttraumatic epilepsy [2]. Therefore, understanding the complex cascades of biological consequences is vital to improving diagnostic and treatment options.

Similar to a typical response against any tissue damage, TBI induces inflammatory and neuroinflammatory processes [2–4]. Astrocytes and microglial cells are key central nervous system components of the neuroinflammatory response. Following a TBI, these glial cells become activated, resulting in the release of proinflammatory molecules such as interleukin 1 beta (IL-1β), interleukin 6 (IL-6), macrophage inflammatory protein (MIP), and CCL2 [5–10]. One method to discern activated astrocytes is by their morphology and GFAP expression [11, 12].

Amongst the neuroinflammatory consequences of astrocyte activation, previous studies have indicated that astrocyte hypertrophy can provide an anatomical substrate for the aberrant growth of newborn dentate granule cells [13–15]. More specifically, Shapiro et al. [13] demonstrated that because the glial cells at the border between the hilus and granule cell layer were closely apposed to the DCX+ processes, the latter processes grow into the hilus along an ectopic glial scaffold, where astrocytic processes preferentially orient into the hilus, rather than through the granule cell layer. This aberration is different than in the normal adult rodent brain,

where GFAP-expressing radial glial-like cells give birth to and wrap around new born dentate granule cells in a one-to-one relationship to nurture and guide the growth and integration of the newborn neurons. As part of this relationship, the radial glial cells extend a process that extends radially through the granule cell layer and the growing apical dendrite from the newborn neuron extends along this radial glial process. Thus, the radial glial-like cell helps to guide the newborn neurons as they migrate from the subgranular zone and grow into the granule cell layer [16, 17]. In addition to the growing apical dendrite, newborn neurons in the normal adult rodent brain often sprout a basal dendrite early in their development. In the normal rodent brain, after about 72 hours, this transient basal dendrite from the newborn neuron will begin to retract or curve back such that they course parallel to the granule cell layer [18]. However, following brain insults such as epileptogenic stimulus, neurogenesis is known to be altered, as is the relationship between newborn neurons and radial glial-like astrocytes [14–16].

Several studies have demonstrated a link between astrocyte activation and aberrant neurogenesis [14, 19–22]. These alterations to neurogenesis include increased and/or decreased numbers of newborn neurons and altered survival, migration, and integration of the newborn neurons into existing brain circuitry. For example, following TBIs or seizures, neurogenesis is typically increased in a transient fashion, such that, at short durations after injury or insult (<30 days after insult), subventricular zone and hippocampal neurogenesis is increased, whereas at >30 days after injury, a decrease in the number of newborn neurons is observed [23–25]. In addition, newborn neurons in the hippocampus have been observed to ectopically migrate into the hilus following seizures, and these ectopic cells contribute to aberrant hippocampal function [26, 27]. The growth and integration of newborn neurons are also observed after seizures, such that the newborn granule cells were observed to sprout basal dendrites that course deep into the hilus, where they are synaptically targeted by mossy fibers from granule cells [28–30]. This granule cell to granule cell connectivity constitutes a recurrent circuitry, and computational models as well as electrophysiological studies have demonstrated that such a circuit significantly disrupts normal hippocampal functioning [31, 32].

Considering the importance of hippocampal function to a wide variety of behavioral, emotional, reproductive, and cognitive functions, it is possible that alterations to hippocampal neurogenesis can negatively impact hippocampal function, leading to functional deficits that include disorders of learning and memory, affective behaviors, and cognitive dysfunction. Indeed, these types of short- and long-term deficits are often seen after TBI in humans [33–35] and in animal models [36, 37]. Thus, it is possible that changes to newborn neurons and their associated astrocytes might occur following a TBI, thereby contributing to functional deficits.

Previous studies have shown that cortical astrocytes are activated soon after a TBI [5, 6]. Other studies have demonstrated altered neurogenesis and activated astrocytes in the hippocampus at various time points and in various TBI animal models, as well as in clinical cases [38–40]. Given these data, we hypothesize that TBI causes astrocyte and neurogenic alterations in the hippocampus, such that the astrocytic changes provide an anatomical substrate for the aberrant growth of hilar basal dendrites from these newborn neurons. To test this hypothesis, we examined astrocytes, newborn neurons, and the relationship between these cell types in the hippocampus at 30 days following a TBI in mice.

2. Methods

2.1. Fluid Percussion Injury (FPI). Mice were randomly separated into two cohorts—a sham group ($N = 5$) and an FPI group ($N = 5$). Prior to sham or FPI procedures, all mice were anesthetized with an initial dose of 4% isoflurane and oxygen for anesthesia induction and maintained anesthesia on 2% isoflurane. Sham and FPI were performed as previously described [8, 41]. Briefly, once the mice were fully anesthetized, their heads were shaved. Strict sterile technique was followed throughout all surgical procedures. All animals were placed in a stereotaxic instrument with an attachment for mouse surgery (Stoelting, Inc., IL, USA). A 2 mm hole was drilled into the skull over the left parietal cortex, making sure to leave the dura intact. A female luer-lock (PlasticOne) was connected to the hole in the skull and mice in the FPI group received a pressure pulse of 1.5–1.7 atm from the FPI apparatus through the luer-lock for 12–16 ms. Sham animals received no pressure pulse while connected to the apparatus. Animals were housed singly after FPI with a 12-hour light-dark cycle (light on 6:00 and light off 18:00). All animals had continuous access to food and water.

2.2. Tissue Preparation. 30 days after surgery, mice in both groups were sacrificed and fixed under anesthesia by transcardial perfusion as previously described [6, 8]. Briefly, a peristaltic pump was used to deliver 0.9% saline through the left ventricle until the runoff through the cut right atrium ran clear. This was followed by pumping 4% paraformaldehyde through the left ventricle. The brains were allowed to postfix for 24 hrs in the skull, after which they were extracted and fixed for 24 hours in 4% paraformaldehyde and subsequently cut into 50-micrometer-thick serial coronal sections with a vibratome.

2.3. Doublecortin (DCX) Immunohistochemistry. Immature neurons were immunohistochemically stained for DCX as previously described [14, 16, 23]. Incubation of the primary antibody was done on tissue slices ($N = 4$ slices per mouse for each group) incubated in the dark, rotating at room temperature, for 24 hours, in PBS containing 0.005% tween, 5% normal horse serum, and DCX antibodies to the N and C termini (1 : 500 each, Santa Cruz Biotech). After staining, the tissue slices were rinsed 3 times for 5 minutes each in 0.01 M PBS. The tissue slices were next incubated for 90 minutes, rotating in the dark, at room temperature in PBS containing 0.005% tween, 5% normal horse serum, and fluorescently tagged donkey anti-goat antibody (1 : 200; Alexa Flour 488; Invitrogen). After 90 minutes, the tissue slices were rinsed 3 times for 5 minutes each in 0.01 M PBS, before being mounted onto glass slides. Slides were allowed to dry overnight and cover slips were applied with Vectashield Hardset (Vector

labs, Burlingame, CA). The slides were coded for subsequent analysis by reviewers blind to the condition of the tissue.

2.4. Glial Fibrillary Acidic Protein (GFAP) Immunohistochemistry. Astrocytes and radial glial-like astrocytes were labeled as previously described [13]. Briefly, tissue slices (N = 4-5 slices per mouse for each group) were incubated in the dark, at room temperature, for 24 hours in a mixture of 0.01 M PBS, 3% normal goat serum, and CY3 fluorescently tagged, primary GFAP antibody (1 : 1000; Sigma). After staining, the tissue slices were washed 3 times in 0.01 M PBS, mounted onto glass slides, and cover slips were applied with Vectashield Hardset (Vector labs, Burlingame, CA). As above, the slides were coded to eliminate potential reviewer bias.

2.5. Quantification of DCX-Labeled Cells in the Dentate Gyrus. A series of images from the ipsi- and contralateral dentate gyri were captured on the Olympus IX-81 laser scanning confocal microscope. These sections spanned the rostral-caudal extent of the hippocampus from −1.34 to −2.54 from bregma. Equal sampling of the hippocampi within these coordinates was ensured by an investigator separate from the blinded raters (e.g., the coordinate for each slice was identified by an independent reviewer who did not partake in the image analysis). Once the images were captured, they were loaded into PowerPoint (Microsoft 2010) and grids were superimposed over the images to allow random selection of the boxes for subsequent quantification at higher magnification. Cellular and neuropil landmarks were used in the low magnification images to ensure that the borders were accurately observed during high magnification counting. Upon loading into PowerPoint, the images were coded a second time, and a different rater traced the borders of the hilus, the borders of the suprapyramidal subgranular zone extending into the first 4 layers of granule cells, and the borders of the infrapyramidal subgranular zone extending into the first 4 layers of granule cells (Figure 1). Per stereological guidelines, a grid containing an array of numbered 5000 μm^2 boxes was overlaid upon the traced regions of interest (Figure 1). Areas to be counted were identified using a random number generator to select the boxes in which counting would be performed (https://www.random.org/integers/). The number of boxes to be counted was predetermined based on stereological estimates. In most cases, 3 boxes from each region of interest were randomly selected for analysis using the random number generator. However, in the most rostral slices (−1.34 to 1.55 from bregma), only 2 boxes were selected because of the decreased size of the granule cell layer and hilus. Alternatively, in the most caudal sections (−2.28 to 2.54 from bregma), 4 boxes were randomly selected because of the increased size of the granule cell layer and hilus. Within each box, 1 lateral and 1 horizontal border were chosen as inclusion lines, and the other two borders were exclusion lines. This schema was consistently maintained for all slices. All cells within the box, or touching the inclusion lines, were counted, whereas cells contacting the exclusion lines were omitted.

2.6. Radial Glial Process Counting. Images from the infra- and suprapyramidal cell layers of the left and right side of each slice were captured using the same blinding method as above for DCX counting. Areas for analysis were determined by drawing boundaries around the suprapyramidal and infrapyramidal granule cell layers. The area of each granule cell layer was calculated using Image J (NIH v.1.49) and multiplied by the section thickness, as determined using the confocal microscope. All primary processes were counted throughout the entire traced granule cell layer by an experimenter blinded to the animal's condition. Secondary and tertiary branches were counted separately if they arborized within the upper 3/5ths of the granule cell layer. Processes that branched deeper than this were not counted separately. The origin of these processes was not considered, as the cell body was often outside of the plane of focus and the perikaryal cytoplasm does not always robustly stain with GFAP. The data were then divided by the image's calculated volume to obtain the number of processes per cubic micron:

$$\frac{\text{number of radial glial processes}}{(\text{area of region of interest} \times \text{depth of image series})}. \quad (1)$$

2.7. Densitometry. In order to assess astrocyte hypertrophy in the hilus, we used a derivation of a previous densitometry

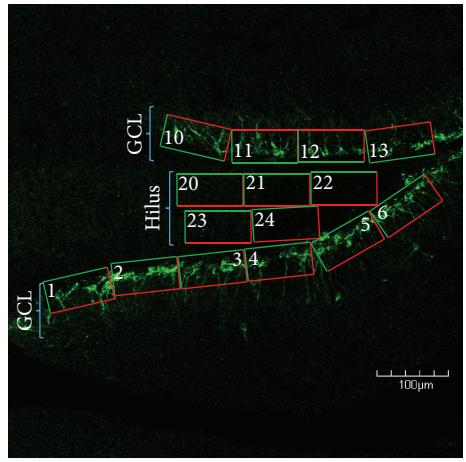

Figure 1: Confocal micrograph depicting the grid layout used to randomly select areas of the dentate gyrus in which newborn neurons were quantified. For each region of interest, we overlaid a series of numbered boxes. We then set the range of numbers in a random number generator and had it choose which grid numbers would be quantified at higher magnification. In this schema, the hilus and supra- and infrapyramidal blades of the granule cell layer (GCL) were quantified, in order to sample the entire dentate gyrus. Note that green portions of the grids are inclusion lines and red portions are exclusion lines. The grids along the GCL were positioned to include cells in the subgranular zone to the upper 3/5ths of the granule cell layer. The grids in the hilus were positioned to exclude cells in the subgranular zone, as DCX+ cells in this location are not necessarily hilar ectopic granule cells, and GFAP+ cells in this region typically display a morphology that is distinctly different than those in the hilus. It is pertinent to note that the apex and subjacent hilar areas are excluded from counting because cells in this region receive signals and cues from both the supra- and infrapyramidal blades of GCL. Scale bar = 100 μm.

protocol [42] to quantify the intensity of pixels using Image J (NIH v.1.49). Z-stack image series of 18 microns deep were captured on the confocal microscope, starting from the first visible astrocytic process at the top of the image for the right and left hilus, for all slices. All Z-stack images were captured from coded slides, by an experimenter blinded to the condition of the animal. For image analysis, the Z-stacks were merged into a single image (Olympus V.3.2) and thresholded into a binary image using Image J (NIH v.1.49). The autothreshold function was used for this portion of the analysis. As above, a second blinded reviewer randomly placed grids throughout these regions and used the Image J software (NIH v.1.49) to measure the mean grey values of the binary images. It should be noted that GFAP+ cells at the border of the subgranular zone were excluded from analysis. The reason for this is that these cells typically have a very different appearance compared to cells within the hilus, because many of the cells at the subgranular zone border are progenitor (neuronal and/or astrocytic) cells in varying stages in the cell cycle. As such, these cells often appear vastly different than the hilar astrocytes, most of which lack the capabilities to give rise to newborn neurons.

2.8. Statistics. For all analysis, a SPSS was used to run Student's t-test to compare FPI and sham groups. Data are reported as means with error bars representing standard error of the mean (±SEM).

3. Results

3.1. DCX. The appearance of DCX-labeled cells in the dentate gyrus of sham mice was relatively normal, whereas in FPI mice, the morphology and location of some of these cells appeared altered (Figures 2(a), 2(b), 2(d), and 2(e)). Analysis of the number of DCX-labeled cells in this region revealed no significant difference between the sham mice and the FPI mice ($t = 0.645$; $P = 0.441$, NS; Figure 2(c)). Conversely, there was a significant increase in the number of immature granule cells in the hilus of FPI mice compared to sham mice ($t = 10.961$; $P < 0.009$; Figure 2(f)).

3.2. Radial Glial-Like Processes. Qualitative analysis of the astrocytes at the border between the subgranular zone and the granule cell layer revealed that, compared to sham mice (Figure 3(a)), FPI mice exhibited a hypertrophied appearance and a change in their orientation, such that their processes preferentially extended toward the hilus, rather than towards the molecular layer (Figure 3(b)). As these processes are derived from the GFAP-expressing astrocytes at the border between the subgranular zone and the granule cell layer, we examined the appearance of this population of astrocytes. Quantitative analysis of the number of radial glial-like processes extending through the granule cell layer revealed that, at 30 days after FPI, the number of these processes is significantly decreased in FPI mice compared to sham mice ($t = 4.919$; $P < 0.05$; Figure 3(c)).

3.3. Density of GFAP-Labeling in the Hippocampus. The morphology of the GFAP+ astrocytes in the sham mice appeared relatively normal (Figure 3(d)), whereas some of these cells from FPI mice exhibited a moderate hypertrophy compared to the sham mice (Figure 3(e)). As the injury model we use is considered to be mild to moderate, we do not expect a robust hypertrophy to be observed [43], especially at the 30-day post-FPI time point. Despite these morphological alterations, the densitometric analysis of GFAP-labeling in the hilus revealed no significant difference in GFAP-labeling at 30 days after an FPI ($t = 0.894$; $P = 0.365$, NS; Figure 3(f)). It is pertinent to note that this analysis did not include the border region between the subgranular zone and the granule cell layer because the GFAP+ cells in this region have a distinctly different appearance than those in the hilus.

3.4. Basal Dendrites Grow along an Ectopic Glial Scaffold. Previous studies from pilocarpine-induced epileptic mice revealed that basal dendrites from newborn neurons aberrantly extend into the hilus by growing along the hypertrophied processes of radial glial-like cells. Because the model of FPI used in the current study is known to increase seizure susceptibility [41] and the sprouting of hilar basal dendrites and subsequent synaptic targeting is known to be proepileptic, we sought to determine if a similar anatomical substrate for basal dendrite sprouting was present following an FPI. The results show that basal dendrites from the DCX+ cells extend deep into the hilus at 30 days after FPI (Figures 4(a), 4(d), and 4(g)). Moreover, the results also show the presence of an ectopic glial scaffold that is comprised of the hypertrophied processes of GFAP-labeled astrocytes at the base of the granule cell layer (Figures 4(b), 4(e), and 4(h)). Interestingly, DCX-labeled basal processes from immature granule cells are observed in close apposition to these processes (Figures 4(c), 4(f), and 4(i)).

4. Discussion

The results from this study are the first to show ectopic migration of newborn granule cells into hilus, as well as an anatomical substrate for the aberrant growth of newborn neurons following an FPI. These results also indicate that astrocyte hypertrophy may contribute to detrimental neuronal plasticity, because the hypertrophied processes of radial glial-like astrocytes lose many of their radial glial processes and instead preferentially orient toward the hilus (Figure 4). The fact that the DCX+ basal dendrites that extend into the hilus are closely apposed to the GFAP+ processes suggests that the astrocytes provide an ectopic glial scaffold for the aberrant growth of newborn neurons. Therefore, targeting the astrocyte/neuronal interactions might be a novel strategy for normalizing neuronal function and treating the long-term consequences of TBIs.

Neuroinflammation is one of the well-known consequences of TBIs. While the precise mechanisms and positive or negative consequences of the inflammatory cascades that follow are not fully understood, it is known that glial activation and hypertrophy are typical anatomical manifestations of the neuroinflammatory response [11, 12]. Indeed, there are numerous reports of astrocyte and microglial hypertrophy from a number of different models of TBI and from clinical

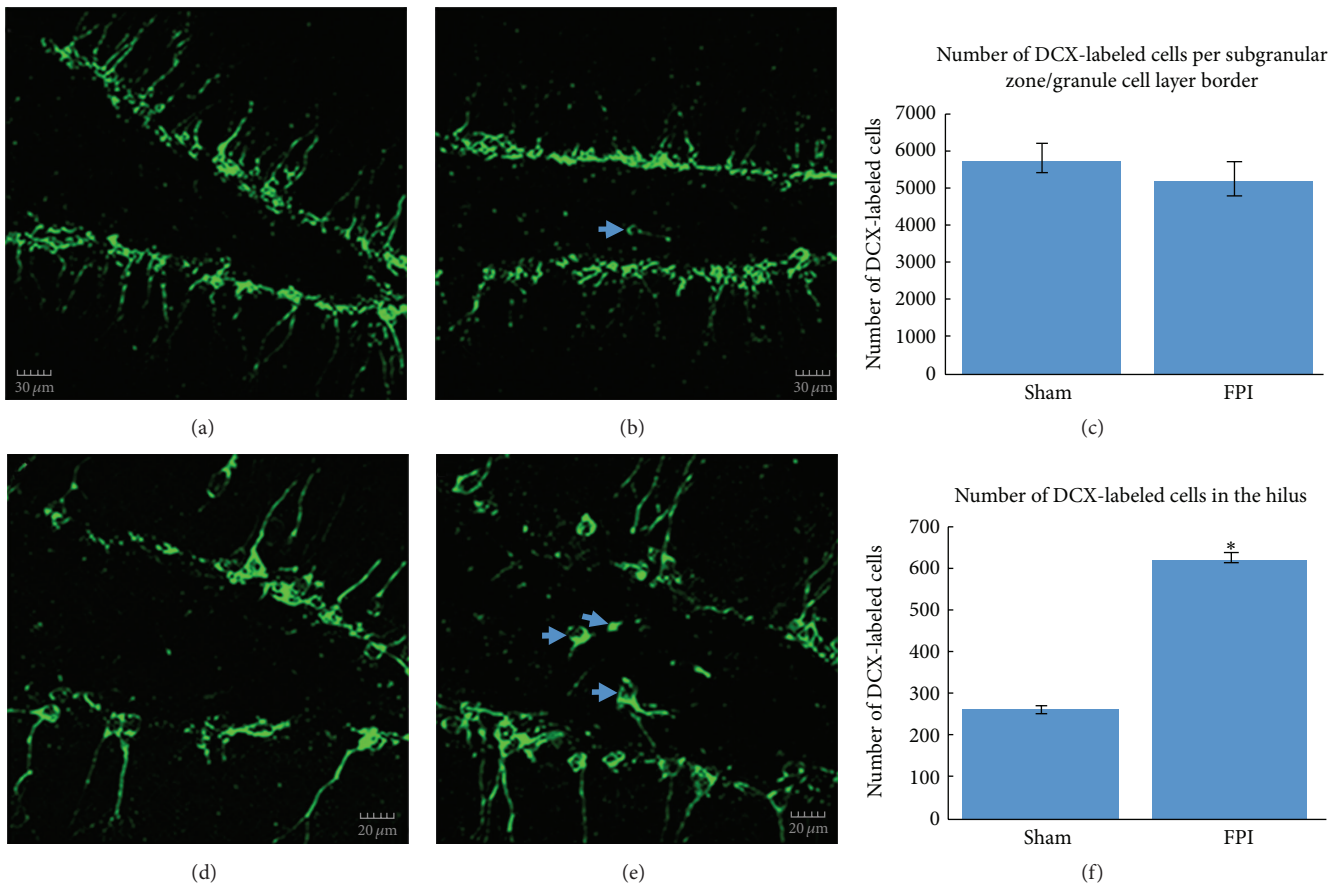

Figure 2: DCX-labeled immature neurons in the dentate gyrus. In (a), a relatively low magnification confocal micrograph is shown to depict both the infrapyramidal and suprapyramidal blades, as well as the hilus from a sham mouse. In (b), a fluorescent micrograph from an FPI mouse illustrates that, despite no significant differences in the number of DCX-labeled cells, the overall appearance of the DCX-labeled cells in the dentate gyrus is altered, as can be seen by the hilar ectopic granule cell (arrow). In (c), quantitative analysis of DCX-labeled cells at the subgranular zone/granule cell layer border revealed no significant differences between sham mice and FPI mice at 30 days after injury. In (d), a higher magnification confocal micrograph is shown to illustrate the typical appearance of granule cells in the dentate gyrus in a sham mouse. In (e), the confocal micrograph at higher magnification from an FPI mouse shows a relatively robust number of DCX-labeled hilar ectopic granule cells (arrows) at 30 days after a TBI. Such cells have been implicated in proepileptogenic circuits. In (f), quantitative analysis of the number of DCX-labeled hilar ectopic cells revealed a significant increase ($^{*}P < 0.009$) in FPI mice compared to sham mice. Scale bars in (a) & (b) = 30 μm and in (d) & (e) = 20 μm.

cases of TBI. What is of particular interest in this context is the fact that although injuries do not necessarily have to directly impact the hippocampus, glial activation is still often observed in this region [6, 41, 44, 45]. In this paper, the 30-day timepoint was selected to examine chronic, rather than acute changes to the hippocampus. While the acute changes may be more robust, the time course of development and integration of newborn neurons into the existing hippocampal circuitry is at minimal 2 weeks [46]. Moreover, most of the neurons that are affected during the early stages after brain insult die before they can be functionally integrated into the circuitry [47], as functional integration typically occurs beginning around 4 weeks after the birth of the newborn neurons [48]. Considering the notable role of the hippocampus in a number of cognitive and affective behaviors [44, 49], it is possible that glial activation within the hippocampus contributes to dysfunction of the hippocampal circuitry.

Examples of a role for glial activation in altered hippocampal functioning are observed in the adult neurogenesis literature. Hippocampal neurogenesis is ongoing throughout the lifespan of many mammals, including rodents, nonhuman primates, and humans [50–52]. A number of studies have documented the importance of adult neurogenesis in cognitive, affective, and reproductive behaviors [53–55]. In many of these studies, alterations to normal hippocampal neurogenesis result in varying degrees of functional alterations to behavioral and cognitive outcomes [56]. Our finding that the processes of hypertrophied astrocytes provide an ectopic glial scaffold (Figure 4) for the aberrant growth and/or migration of immature dentate granule cells represents one mechanism through which glial cells can contribute to altered hippocampal functioning.

Interestingly, previous studies have indicated that aberrantly sprouted basal dendrites from immature granule cells

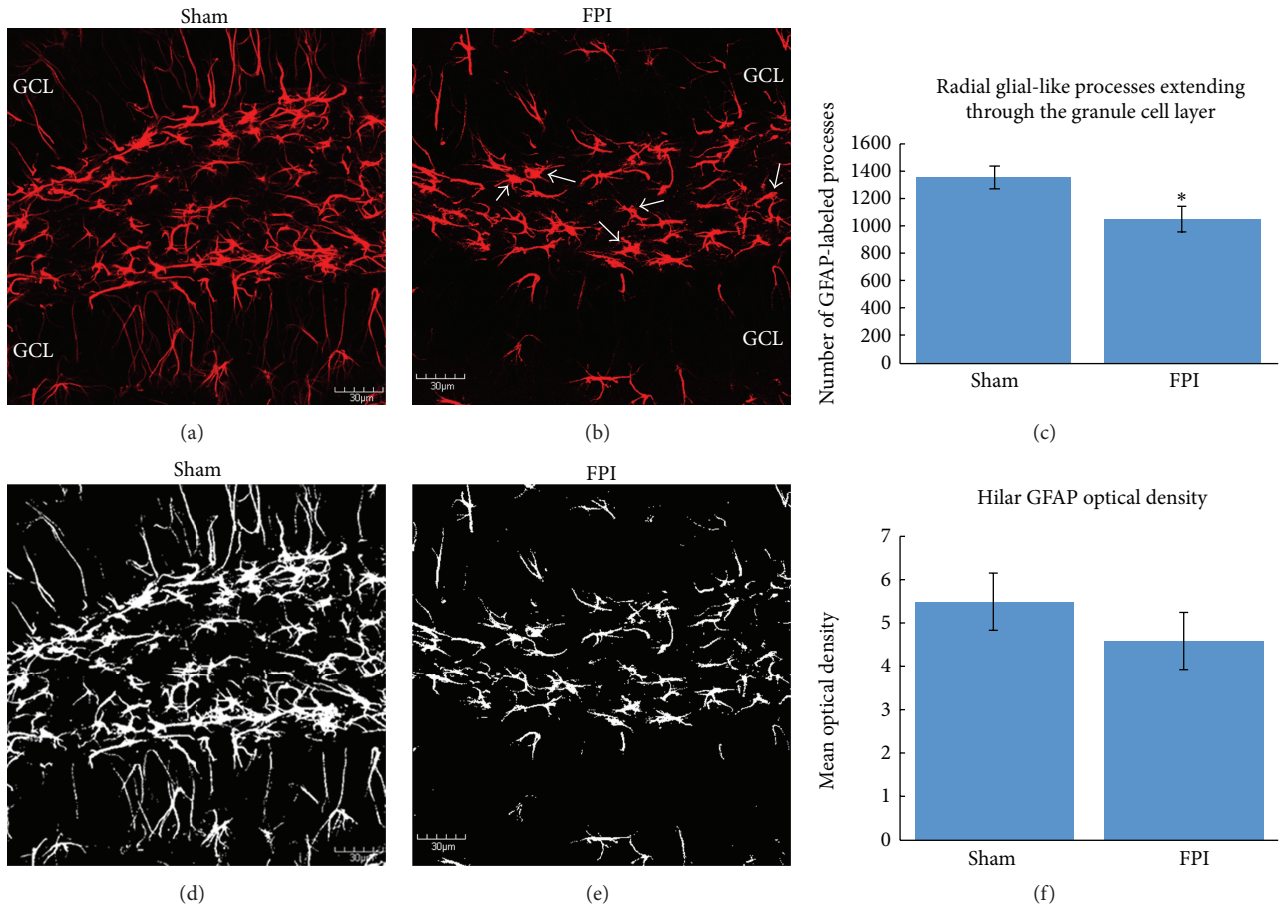

Figure 3: GFAP-labeled cells in the dentate gyrus. In (a), a confocal micrograph from a sham mouse is shown to depict the normal appearance of a robust number of radial glial processes extending through the granule cell layer (GCL). In (b), a representative confocal micrograph of an FPI mouse shows a decrease in the number of radial glial-like processes extending through the GCL. In addition to the lack of radial glial processes extending through the GCL, note that several GFAP-labeled astrocytes from FPI mice displayed varying levels of activated morphology in the hilus (arrows). In (c), quantitative analysis of the number of radial glial processes extending through the granule cell layer reveals a significant decrease ($^{*}P < 0.05$) in FPI mice compared to sham mice. In (d), the sham micrograph from (a) is shown after thresholding, to depict the technique used for densitometric analysis of GFAP-labeling in the hilus. Once thresholded, the Image J software (NIH v.1.49) automates the counting of white pixels. In (e), the micrograph from the FPI mouse is shown after thresholding. In (f), densitometric analysis of GFAP-labeled astrocytes in the hilus revealed no significant differences between sham and FPI mice at 30 days after FPI. It is pertinent to note that the subgranular zone was excluded from this analysis (as shown in Figure 1) because the cells in this region have a different appearance than they do in the hilus. Scale bars in all images = 30 μm.

can be targeted for synaptogenesis in the hilus [13, 16]. A previous report showed that, following a controlled cortical impact TBI, ectopic migration and dendritic branching of newborn dentate granule cells occur [57]. These newborn neurons were observed to be functionally integrated into the hippocampal circuitry and their potential for maladaptive plasticity was noted [57]. Despite the fact that we did not observe a difference in the number of DCX-labeled cells at the 30 days' post-FPI time point, the appearance of aberrant sprouting and ectopic migration suggests that neurogenesis is chronically altered after FPI. It is also possible that if we examine later time points, neurogenesis could significantly decrease. Thus, there are several mechanisms through which hypertrophied glial cells can directly influence hippocampal circuitry, and altered hippocampal circuitry can underlie functional deficits including increased seizure susceptibility and the development of posttraumatic epilepsy [58, 59].

Posttraumatic epilepsy (PTE) is the most common type of acquired epilepsy [60]. A number of mechanisms have been postulated to contribute to the development of PTE. These include oxidative and metabolic changes/dysfunction [61], ion channel alterations [62], inflammation [63, 64], synaptic plasticity [65], loss and/or reduced efficacy of inhibitory interneurons [66], and a number of other possibilities [67, 68]. Parallels can be drawn with the pilocarpine model of temporal lobe epilepsy in which an initial chemotactic, proconvulsive insult leads to status epilepticus. The status epilepticus is inhibited using benzodiazepines or other sedatives [69], after which a latent period of >2 weeks typically occurs with little to no seizure activity. Eventually, most, if

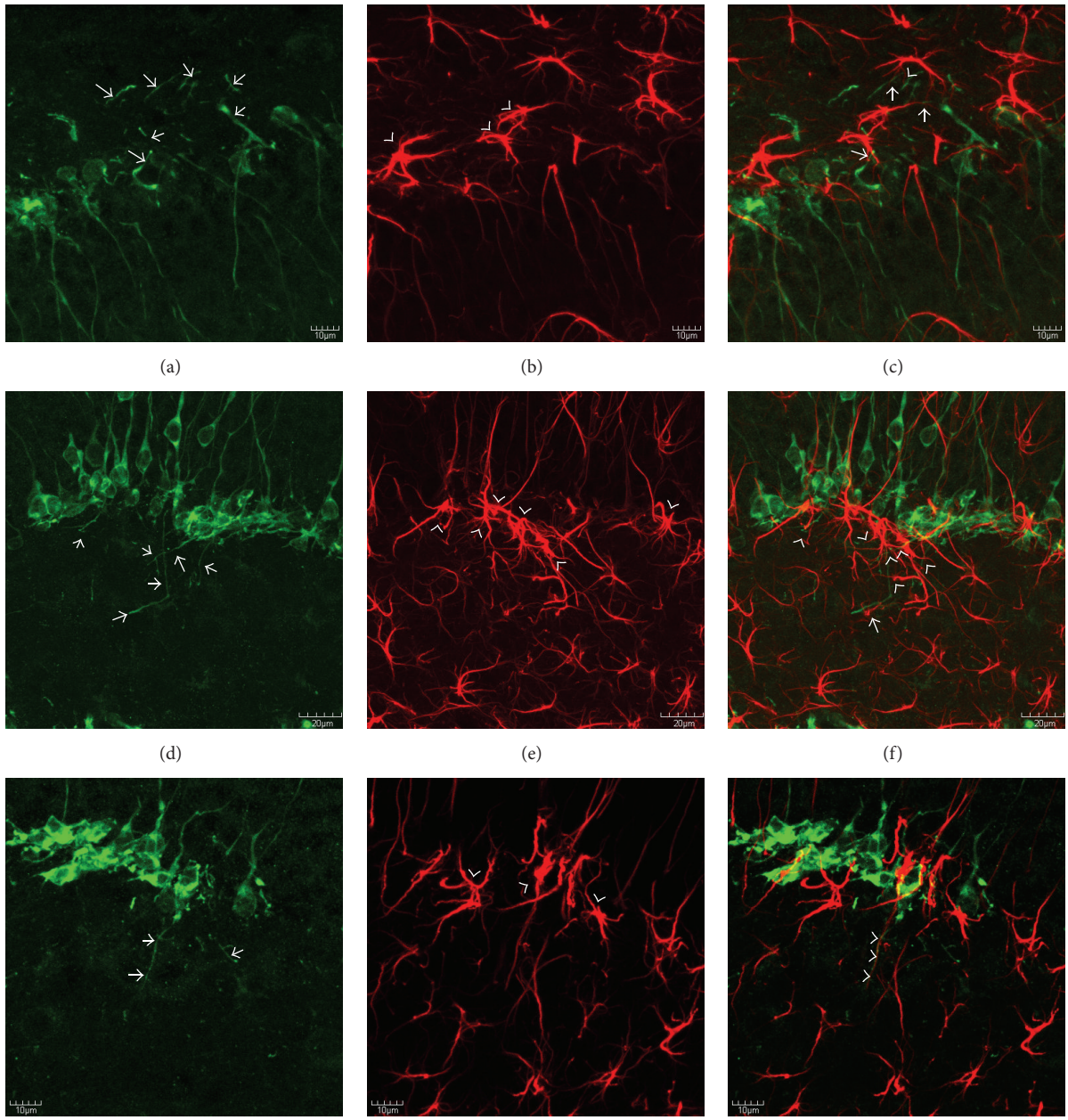

Figure 4: DCX-labeled basal dendrites grow along an ectopic glial scaffold. Confocal micrographs depicting DCX+ (a, d, g), GFAP+ (b, e, h), and merged, double-labeling for DCX (green) and GFAP (red) at 30 days after FPI. Note that (a)–(c) are taken from the infrapyramidal blade, whereas (d)–(i) are taken from the suprapyramidal blade. As can be seen in (a), (d), (g), DCX+ basal dendrites (arrows) are prominent features after FPI, and many of these basal dendrites extend deep into the hilus. Also note, in (b), (e), and (h), the hypertrophied appearance of GFAP+ cells at the base of the granule cell layer (arrowheads). Also note that the predominant orientation of the astrocytes from FPI mice at the border of the granule cell layer is oriented either parallel with the granule cell layer or toward the hilus. Such an orientation is consistent with an ectopic glial scaffold. The lack of radial glial processes extending through the granule cell layer is also notable in (b) and (h). In the merged images (c, f, i) the close relationship between the DCX+ basal dendrites and the GFAP+ processes can be appreciated (arrows). In (i), the apposition of the basal dendrite with the GFAP+ is so close that the two processes almost appear as if they are intertwined (arrowheads). Future studies using electron microscopy will determine if these cells/processes are aberrantly targeted for synaptogenesis in the hilus. Scale bars in (a)–(c) & (g)–(i) = 10 μm and in (d)–(f) = 20 μm. In (f) and (i), the appositions of the basal dendrites to the GFAP+ processes are so close that the two almost appear as if they are intertwined.

not all, of these rodents will go on to develop spontaneous epileptiform discharges that is analogous to temporal lobe epilepsy. In the pilocarpine model, as in our current study, hilar basal dendrite sprouting from immature granule cells is a prominent feature [13]. Of further interest is that, in the pilocarpine model, the hypertrophied astrocytes at the base of the granule cell layer were observed to express CCR2, which is the receptor for monocyte chemoattractant protein (MCP-1), also known as CCL2 [14]. Signaling through the CCR2/CCL2 receptor/ligand has been shown to be involved in chemotactic guidance of neuroblast migration [70–72]. Considering that we have previously demonstrated an increase of CCL2 protein in our FPI model [5, 6], it is possible that this mechanism is involved in the aberrant sprouting of basal dendrites from the newborn neurons, as well as the ectopic migration of some of these granule cells into the hilus (Figure 1). Future studies are warranted to examine this possibility

In conclusion, we demonstrate, for the first time, that radial glial fibers from GFAP+ astrocytes at the base of the granule cell layer are chronically reduced following FPI and that the hypertrophied astrocytes in this region can provide an anatomical substrate for the aberrant growth and migration of immature neurons in the hippocampus. Based on previous evidence of altered hippocampal function in response to such anatomical changes, future studies are needed to determine the potential of these alterations as targets for therapeutic intervention after TBI. Understanding these mechanisms could also lead to more efficacious regenerative therapy approaches.

Competing Interests

The authors declare that they have no competing interests.

Authors' Contributions

Clark Robinson and Christopher Apgar contributed equally to the paper.

Acknowledgments

The authors are grateful for the technical contributions of Sanjib Mukherjee, Jessica Kain, and Jaclyn Jenkins. This material is the result of work supported by the use of facilities at the Central Texas Veterans Health Care System, Temple, TX, USA.

References

[1] A. A. Hyder, C. A. Wunderlich, P. Puvanachandra, G. Gururaj, and O. C. Kobusingye, "The impact of traumatic brain injuries: a global perspective," *NeuroRehabilitation*, vol. 22, no. 5, pp. 341–353, 2007.

[2] I. P. Karve, J. M. Taylor, and P. J. Crack, "The contribution of astrocytes and microglia to traumatic brain injury," *British Journal of Pharmacology*, vol. 173, no. 4, pp. 692–702, 2016.

[3] S. M. Gentleman, P. D. Leclercq, L. Moyes et al., "Long-term intracerebral inflammatory response after traumatic brain injury," *Forensic Science International*, vol. 146, no. 2-3, pp. 97–104, 2004.

[4] D. Cederberg and P. Siesjö, "What has inflammation to do with traumatic brain injury?" *Child's Nervous System*, vol. 26, no. 2, pp. 221–226, 2010.

[5] S. Mukherjee, K. Katki, G. M. Arisi, M. L. Foresti, and L. A. Shapiro, "Early TBI-induced cytokine alterations are similarly detected by two distinct methods of multiplex assay," *Frontiers in Molecular Neuroscience*, vol. 4, no. 21, pp. 1–7, 2011.

[6] S. Mukherjee, P. C. Bricker, and L. A. Shapiro, "Alteration of hippocampal cytokines and astrocyte morphology observed in rats 24 hours after fluid percussion injury," *Journal of Neurological Disorders & Stroke*, vol. 2, no. 3, pp. 1–9, 2014.

[7] T. Frugier, M. C. Morganti-Kossmann, D. O'Reilly, and C. A. McLean, "In situ detection of inflammatory mediators in post mortem human brain tissue after traumatic injury," *Journal of Neurotrauma*, vol. 27, no. 3, pp. 497–507, 2010.

[8] R. P. Tobin, S. Mukherjee, J. M. Kain et al., "Traumatic brain injury causes selective, CD74-dependent peripheral lymphocyte activation that exacerbates neurodegeneration," *Acta Neuropathologica Communications*, vol. 2, no. 143, pp. 1–10, 2014.

[9] L. C. B. Ferreira, A. Regner, K. D. L. Miotto et al., "Increased levels of interleukin-6, -8 and -10 are associated with fatal outcome following severe traumatic brain injury," *Brain Injury*, vol. 28, no. 10, pp. 1311–1316, 2014.

[10] D. G. Hernandez-Ontiveros, N. Tajiri, S. Acosta, B. Giunta, J. Tan, and C. V. Borlongan, "Microglia activation as a biomarker for traumatic brain injury," *Frontiers in Neurology*, vol. 4, article 30, 2013.

[11] Y. Chen and R. A. Swanson, "Astrocytes and brain injury," *Journal of Cerebral Blood Flow and Metabolism*, vol. 23, no. 2, pp. 137–149, 2003.

[12] D. J. Myer, G. G. Gurkoff, S. M. Lee, D. A. Hovda, and M. V. Sofroniew, "Essential protective roles of reactive astrocytes in traumatic brain injury," *Brain*, vol. 129, no. 10, pp. 2761–2772, 2006.

[13] L. A. Shapiro, M. J. Korn, and C. E. Ribak, "Newly generated dentate granule cells from epileptic rats exhibit elongated hilar basal dendrites that align along GFAP-immunolabeled processes," *Neuroscience*, vol. 136, no. 3, pp. 823–831, 2005.

[14] M. L. Foresti, G. M. Arisi, K. Katki, A. Montañez, R. M. Sanchez, and L. A. Shapiro, "Chemokine CCL2 and its receptor CCR2 are increased in the hippocampus following pilocarpine-induced status epilepticus," *Journal of Neuroinflammation*, vol. 6, no. 40, pp. 1–11, 2009.

[15] M. L. Foresti, G. M. Arisi, and L. A. Shapiro, "Role of glia in epilepsy-associated neuropathology, neuroinflammation and neurogenesis," *Brain Research Reviews*, vol. 66, no. 1-2, pp. 115–122, 2011.

[16] L. A. Shapiro, M. J. Korn, Z. Shan, and C. E. Ribak, "GFAP-expressing radial glia-like cell bodies are involved in a one-to-one relationship with doublecortin-immunolabeled newborn neurons in the adult dentate gyrus," *Brain Research*, vol. 1040, no. 1-2, pp. 81–91, 2005.

[17] C. E. Ribak and L. A. Shapiro, "Dendritic development of newly generated neurons in the adult brain," *Brain Research Reviews*, vol. 55, no. 2, pp. 390–394, 2007.

[18] L. A. Shapiro and C. E. Ribak, "Integration of newly born dentate granule cells into adult brains: hypotheses based on normal and epileptic rodents," *Brain Research Reviews*, vol. 48, no. 1, pp. 43–56, 2005.

[19] M. Boccazzi, C. Rolando, M. P. Abbracchio, A. Buffo, and S. Ceruti, "Purines regulate adult brain subventricular zone cell

functions: contribution of reactive astrocytes," *Glia*, vol. 62, no. 3, pp. 428–439, 2014.

[20] R. S. Ashton, A. Conway, C. Pangarkar et al., "Astrocytes regulate adult hippocampal neurogenesis through ephrin-B signaling," *Nature Neuroscience*, vol. 15, no. 10, pp. 1399–1406, 2012.

[21] N. Kuzumaki, D. Ikegami, S. Imai et al., "Enhanced IL-1β production in response to the activation of hippocampal glial cells impairs neurogenesis in aged mice," *Synapse*, vol. 64, no. 9, pp. 721–728, 2010.

[22] F. Yang, Z.-R. Liu, J. Chen et al., "Roles of astrocytes and microglia in seizure-induced aberrant neurogenesis in the hippocampus of adult rats," *Journal of Neuroscience Research*, vol. 88, no. 3, pp. 519–529, 2010.

[23] L. A. Shapiro, S. Figueroa-Aragon, and C. E. Ribak, "Newly generated granule cells show rapid neuroplastic changes in the adult rat dentate gyrus during the first five days following pilocarpine-induced seizures," *European Journal of Neuroscience*, vol. 26, no. 3, pp. 583–592, 2007.

[24] J. M. Parent, T. W. Yu, R. T. Leibowitz, D. H. Geschwind, R. S. Sloviter, and D. H. Lowenstein, "Dentate granule cell neurogenesis is increased by seizures and contributes to aberrant network reorganization in the adult rat hippocampus," *Journal of Neuroscience*, vol. 17, no. 10, pp. 3727–3738, 1997.

[25] A. K. Shetty, V. Mishra, M. Kodali, and B. Hattiangady, "Blood brain barrier dysfunction and delayed neurological deficits in mild traumatic brain injury induced by blast shock waves," *Frontiers in Cellular Neuroscience*, vol. 8, article 232, 10 pages, 2014.

[26] H. E. Scharfman, J. H. Goodman, and A. L. Sollas, "Granule-like neurons at the hilar/CA3 border after status epilepticus and their synchrony with area CA3 pyramidal cells: functional implications of seizure-induced neurogenesis," *Journal of Neuroscience*, vol. 20, no. 16, pp. 6144–6158, 2000.

[27] H. Scharfman, J. Goodman, and D. McCloskey, "Ectopic granule cells of the rat dentate gyrus," *Developmental Neuroscience*, vol. 29, no. 1-2, pp. 14–27, 2006.

[28] J. P. Pierce, J. Melton, M. Punsoni, D. P. Mccloskey, and H. E. Scharfman, "Mossy fibers are the primary source of afferent input to ectopic granule cells that are born after pilocarpine-induced seizures," *Experimental Neurology*, vol. 196, no. 2, pp. 316–331, 2005.

[29] L. A. Shapiro and C. E. Ribak, "Newly born dentate granule neurons after pilocarpine-induced epilepsy have hilar basal dendrites with immature synapses," *Epilepsy Research*, vol. 69, no. 1, pp. 53–66, 2006.

[30] R. M. Sanchez, C. E. Ribak, and L. A. Shapiro, "Synaptic connections of hilar basal dendrites of dentate granule cells in a neonatal hypoxia model of epilepsy," *Epilepsia*, vol. 53, no. 1, pp. 98–108, 2012.

[31] H. E. Scharfman, A. L. Sollas, R. E. Berger, and J. H. Goodman, "Electrophysiological evidence of monosynaptic excitatory transmission between granule cells after seizure-induced mossy fiber sprouting," *Journal of Neurophysiology*, vol. 90, no. 4, pp. 2536–2547, 2003.

[32] M. Case and I. Soltesz, "Computational modeling of epilepsy," *Epilepsia*, vol. 52, no. 8, pp. 12–15, 2011.

[33] A. F. Ramlackhansingh, D. J. Brooks, R. J. Greenwood et al., "Inflammation after trauma: microglial activation and traumatic brain injury," *Annals of Neurology*, vol. 70, no. 3, pp. 374–383, 2011.

[34] V. E. Johnson, J. E. Stewart, F. D. Begbie, J. Q. Trojanowski, D. H. Smith, and W. Stewart, "Inflammation and white matter degeneration persist for years after a single traumatic brain injury," *Brain*, vol. 136, no. 1, pp. 28–42, 2013.

[35] A. I. Faden, J. Wu, B. A. Stoica, and D. J. Loane, "Progressive inflammation-mediated neurodegeneration after traumatic brain or spinal cord injury," *British Journal of Pharmacology*, vol. 173, no. 4, pp. 681–691, 2016.

[36] J. E. S. Pierce, D. H. Smith, J. Q. Trojanowski, and T. K. McIntosh, "Enduring cognitive, neurobehavioral and histopathological changes persist for up to one year following severe experimental brain injury in rats," *Neuroscience*, vol. 87, no. 2, pp. 359–369, 1998.

[37] D. J. Loane, A. Kumar, B. A. Stoica, R. Cabatbat, and A. I. Faden, "Progressive neurodegeneration after experimental brain trauma: association with chronic microglial activation," *Journal of Neuropathology and Experimental Neurology*, vol. 73, no. 1, pp. 14–29, 2014.

[38] P. K. Dash, S. A. Mach, and A. N. Moore, "Enhanced neurogenesis in the rodent following traumatic brain injury," *Journal of Neuroscience Research*, vol. 63, no. 4, pp. 313–319, 2001.

[39] S. Chirumamilla, D. Sun, M. R. Bullock, and R. J. Colello, "Traumatic brain injury induced cell proliferation in the adult mammalian central nervous system," *Journal of Neurotrauma*, vol. 19, no. 6, pp. 693–703, 2002.

[40] K. Nylén, M. Öst, L. Z. Csajbok et al., "Increased serum-GFAP in patients with severe traumatic brain injury is related to outcome," *Journal of the Neurological Sciences*, vol. 240, no. 1-2, pp. 85–91, 2006.

[41] S. Mukherjee, S. Zeitouni, C. F. Cavarsan, and L. A. Shapiro, "Increased seizure susceptibility in mice 30 days after fluid percussion injury," *Frontiers in Neurology*, vol. 4, article 28, 11 pages, 2013.

[42] L. A. Shapiro, L. Wang, and C. E. Ribak, "Rapid astrocyte and microglial activation following pilocarpine-induced seizures in rats," *Epilepsia*, vol. 49, no. 2, pp. 33–41, 2008.

[43] M. V. Sofroniew and H. V. Vinters, "Astrocytes: biology and pathology," *Acta Neuropathologica*, vol. 119, no. 1, pp. 7–35, 2010.

[44] L. R. Squire, "Memory and the hippocampus: a synthesis from findings with rats, monkeys, and humans," *Psychological Review*, vol. 99, no. 2, pp. 195–231, 1992.

[45] M. S. Grady, J. S. Charleston, D. Maris, B. M. Witgen, and J. Lifshitz, "Neuronal and glial cell number in the hippocampus after experimental traumatic brain injury: analysis by stereological estimation," *Journal of Neurotrauma*, vol. 20, no. 10, pp. 929–941, 2003.

[46] N. Toni, D. A. Laplagne, C. Zhao et al., "Neurons born in the adult dentate gyrus form functional synapses with target cells," *Nature Neuroscience*, vol. 11, no. 8, pp. 901–907, 2008.

[47] G. Kempermann, H. Song, and F. H. Gage, "Neurogenesis in the adult hippocampus," *Cold Spring Harbor Perspectives in Biology*, vol. 5, no. 7, pp. 1–16, 2015.

[48] C. Vivar and H. Van Praag, "Functional circuits of new neurons in the dentate gyrus," *Frontiers in neural circuits*, vol. 7, no. 15, pp. 1–13, 2013.

[49] W. Deng, J. B. Aimone, and F. H. Gage, "New neurons and new memories: how does adult hippocampal neurogenesis affect learning and memory?" *Nature Reviews Neuroscience*, vol. 11, no. 5, pp. 339–350, 2010.

[50] P. S. Eriksson, E. Perfilieva, T. Björk-Eriksson et al., "Neurogenesis in the adult human hippocampus," *Nature Medicine*, vol. 4, no. 11, pp. 1313–1317, 1998.

[51] H. Van Praag, A. F. Schinder, B. R. Christle, N. Toni, T. D. Palmer, and F. H. Gage, "Functional neurogenesis in the adult hippocampus," *Nature*, vol. 415, no. 6875, pp. 1030–1034, 2002.

[52] K. L. Spalding, O. Bergmann, K. Alkass et al., "Dynamics of hippocampal neurogenesis in adult humans," *Cell*, vol. 153, no. 6, pp. 1219–1227, 2013.

[53] A. Sahay and R. Hen, "Adult hippocampal neurogenesis in depression," *Nature Neuroscience*, vol. 10, no. 9, pp. 1110–1115, 2007.

[54] D. C. Lagace, M. H. Donovan, N. A. Decarolis et al., "Adult hippocampal neurogenesis is functionally important for stress-induced social avoidance," *Proceedings of the National Academy of Sciences of the United States of America*, vol. 107, no. 9, pp. 4436–4441, 2010.

[55] D. E. Peragine, J. A. Simpson, S. J. Mooney, M. B. Lovern, and M. M. Holmes, "Social regulation of adult neurogenesis in a eusocial mammal," *Neuroscience*, vol. 268, no. 11, pp. 10–20, 2014.

[56] B.-L. Zhang, X. Chen, T. Tan et al., "Traumatic brain injury impairs synaptic plasticity in hippocampus in rats," *Chinese Medical Journal*, vol. 124, no. 5, pp. 740–745, 2011.

[57] L. E. Villasana, K. N. Kim, G. L. Westbrook, and E. Schnell, "Functional integration of adult-born hippocampal neurons after traumatic brain injury," *eNeuro*, vol. 2, no. 5, pp. 1–17, 2015.

[58] G. Golarai, A. C. Greenwood, D. M. Feeney, and J. A. Connor, "Physiological and structural evidence for hippocampal involvement in persistent seizure susceptibility after traumatic brain injury," *Journal of Neuroscience*, vol. 21, no. 21, pp. 8523–8537, 2001.

[59] R. S. Briellmann, R. M. Kalnins, S. F. Berkovic, and G. D. Jackson, "Hippocampal pathology in refractory temporal lobe epilepsy: T2-weighted signal change reflects dentate gliosis," *Neurology*, vol. 58, no. 2, pp. 265–271, 2002.

[60] D. H. Lowenstein, "Epilepsy after head injury: an overview," *Epilepsia*, vol. 50, no. 2, pp. 4–9, 2009.

[61] L. J. Willmore, "Post-traumatic epilepsy: cellular mechanisms and implications for treatment," *Epilepsia*, vol. 31, no. 3, pp. 67–73, 1990.

[62] Z. Lei, P. Deng, J. Li, and Z. C. Xu, "Alterations of A-type potassium channels in hippocampal neurons after traumatic brain injury," *Journal of Neurotrauma*, vol. 29, no. 2, pp. 235–245, 2012.

[63] Y. Li, A. A. Korgaonkar, B. Swietek et al., "Toll-like receptor 4 enhancement of non-NMDA synaptic currents increases dentate excitability after brain injury," *Neurobiology of Disease*, vol. 74, no. 22, pp. 240–253, 2015.

[64] M. L. Diamond, A. C. Ritter, M. D. Failla et al., "IL-1β associations with posttraumatic epilepsy development: a genetics and biomarker cohort study," *Epilepsia*, vol. 56, no. 7, pp. 991–1001, 2015.

[65] A. R. Houweling, M. Bazhenov, I. Timofeev, M. Steriade, and T. J. Sejnowski, "Homeostatic synaptic plasticity can explain post-traumatic epileptogenesis in chronically isolated neocortex," *Cerebral Cortex*, vol. 15, no. 6, pp. 834–845, 2005.

[66] I. Pavlov, N. Huusko, M. Drexel et al., "Progressive loss of phasic, but not tonic, GABAA receptor-mediated inhibition in dentate granule cells in a model of post-traumatic epilepsy in rats," *Neuroscience*, vol. 194, no. 20, pp. 208–219, 2011.

[67] A. Agrawal, J. Timothy, L. Pandit, and M. Manju, "Post-traumatic epilepsy: an overview," *Clinical Neurology and Neurosurgery*, vol. 108, no. 5, pp. 433–439, 2006.

[68] R. F. Hunt, J. A. Boychuk, and B. N. Smith, "Neural circuit mechanisms of posttraumatic epilepsy," *Frontiers in Cellular Neuroscience*, vol. 7, no. 89, pp. 1–14, 2013.

[69] L. E. A. M. Mello, E. A. Cavalheiro, A. M. Tan et al., "Circuit mechanisms of seizures in the pilocarpine model of chronic epilepsy: cell loss and mossy fiber sprouting," *Epilepsia*, vol. 34, no. 6, pp. 985–995, 1993.

[70] A. Belmadani, P. B. Tran, D. Ren, and R. J. Miller, "Chemokines regulate the migration of neural progenitors to sites of neuroinflammation," *The Journal of Neuroscience*, vol. 26, no. 12, pp. 3182–3191, 2006.

[71] Y.-P. Yan, K. A. Sailor, B. T. Lang, S.-W. Park, R. Vemuganti, and R. J. Dempsey, "Monocyte chemoattractant protein-1 plays a critical role in neuroblast migration after focal cerebral ischemia," *Journal of Cerebral Blood Flow and Metabolism*, vol. 27, no. 6, pp. 1213–1224, 2007.

[72] X. S. Liu, Z. G. Zhang, R. L. Zhang et al., "Chemokine ligand 2 (CCL2) induces migration and differentiation of subventricular zone cells after stroke," *Journal of Neuroscience Research*, vol. 85, no. 10, pp. 2120–2125, 2007.

Hindawi Publishing Corporation
Neural Plasticity
Volume 2016, Article ID 7607924, 30 pages
http://dx.doi.org/10.1155/2016/7607924

Research Article

Modulation of Synaptic Plasticity by Glutamatergic Gliotransmission: A Modeling Study

Maurizio De Pittà[1,2] and Nicolas Brunel[1,3]

[1]*Department of Neurobiology, The University of Chicago, Chicago, IL 60637, USA*
[2]*Project-Team BEAGLE, INRIA Rhône-Alpes, 60097 Villeurbanne, France*
[3]*Departments of Statistics and Neurobiology, The University of Chicago, Chicago, IL 60637, USA*

Correspondence should be addressed to Maurizio De Pittà; maurizio.depitta@gmail.com

Received 5 January 2016; Accepted 15 February 2016

Academic Editor: Alfredo Pereira Jr.

Glutamatergic gliotransmission, that is, the release of glutamate from perisynaptic astrocyte processes in an activity-dependent manner, has emerged as a potentially crucial signaling pathway for regulation of synaptic plasticity, yet its modes of expression and function in vivo remain unclear. Here, we focus on two experimentally well-identified gliotransmitter pathways, (i) modulations of synaptic release and (ii) postsynaptic slow inward currents mediated by glutamate released from astrocytes, and investigate their possible functional relevance on synaptic plasticity in a biophysical model of an astrocyte-regulated synapse. Our model predicts that both pathways could profoundly affect both short- and long-term plasticity. In particular, activity-dependent glutamate release from astrocytes could dramatically change spike-timing-dependent plasticity, turning potentiation into depression (and vice versa) for the same induction protocol.

1. Introduction

In recent years, astrocytes have attracted great interest for their capacity to release neuroactive molecules, among which are neurotransmitters like glutamate, because these molecules could modulate neural activity and lead to a possible role for astrocytes in neural information processing [1–3]. Indeed, astrocyte-derived neurotransmitters, also called "gliotransmitters" for their astrocytic origin [4], have been shown to act on neurons and to regulate synaptic transmission and plasticity through a variety of mechanisms [5]. The binding of receptors located on either pre- or postsynaptic terminals by astrocyte-released glutamate has historically been the first pathway for gliotransmission to be discovered and, arguably, the most studied one experimentally for its several possible functional implications [6].

Activation of extrasynaptic receptors on presynaptic terminals by astrocytic glutamate modulates the probability of neurotransmitter release from those terminals [6]. In particular, depending on receptor type, such modulation may be either toward an increase or toward a decrease of the frequency of spontaneous [7–11] and evoked neurotransmitter release in both excitatory [2, 8, 10, 12] and inhibitory synapses [13–15]. Because synaptic release probability characterizes how a synapse filters or, in other words, "processes" presynaptic action potentials [16, 17], modulations of synaptic release probability by astrocytic glutamate are suggested to alter the computational properties of neural circuits [18].

Glutamate released by astrocytes may also bind to extrasynaptically located postsynaptic NMDA receptors, evoking slow inward currents (SICs) in nearby neurons [11, 19–26]. The depolarizing action of these currents modulates neural excitability with the potential to affect neuronal action potential firing [27]. Moreover, because single astrocytes are in close proximity to a large number (~100) of neurons [28], it has been suggested that an inward current can be generated in many adjacent neurons, thereby promoting synchrony of neuronal firing [19–21].

Although modulations of both synaptic release and SICs mediated by glutamatergic gliotransmission have been

recorded in the cortex and the hippocampus, as well as in several other brain regions [5], their physiological relevance remains elusive. In particular, beyond regulation of synaptic filtering and neuronal firing, theoretical arguments support a further possible role for both pathways in the regulation of NMDAR-mediated spike-timing-dependent plasticity (STDP) [29]. Both pathways have the potential to regulate activation of postsynaptic NMDA receptors and, in doing so, glutamatergic gliotransmission could ultimately regulate the STDP outcome, that is, either potentiation (LTP) or depression (LTD) [30, 31]. Consistent with this hypothesis, experiments have reported a lower threshold for LTP induction at hippocampal synapses when synaptic release is increased by astrocytic glutamate [9]. Moreover, long-term potentiation responses of neurons in the primary visual cortex by cholinergic activation of surrounding astrocytes has also been reported to be correlated with an increase of SIC frequency in those neurons [32].

While the potential impact on STDP of pre- or postsynaptic activity-dependent modulations of synaptic efficacy has widely been addressed both experimentally [33] and theoretically [34, 35], the possible effect on plasticity of the regulation of these modulations by glutamatergic gliotransmission (and by gliotransmission in general) has been investigated by very few theoretical studies. These studies suggest a potential role in LTP induction both for large increases of synaptic release and for large SICs mediated by astrocytic glutamate [36, 37]. This scenario seems however at odds with the majority of recent experimental observations that report modest signaling magnitudes for these two routes of gliotransmission. It is thus not clear under what biophysical conditions modulations of synaptic release or SICs mediated by glutamatergic gliotransmission could affect STDP. Astrocyte-mediated SICs, for example, are known to occur sporadically, being recorded in single neurons only as often as <5/min [26, 32], raising the question of whether and how, by occurring at such low rates, they could effectively play a role in STDP.

We thus set to investigating what conditions are required for glutamatergic gliotransmission to affect STDP by presynaptic modulations of neurotransmitter release or through postsynaptic SICs. We extend the model of an astrocyte-regulated synapse originally introduced by De Pittà et al. [73] to include a biophysically realistic description of synaptically evoked gliotransmitter release by the astrocyte as well as a mechanism for the generation of postsynaptic SICs and STDP. Extensive numerical investigations of our model lead to two major predictions. First, glutamatergic gliotransmission could change the nature of STDP by modifying the parameter ranges for LTP and LTD induction. Second, this effect crucially depends on the nature of gliotransmission, that is, whether it is release-increasing or release-decreasing, its strength, and its rate of occurrence and when it occurs with respect to pre/post pairs. Thus, while glutamatergic gliotransmission could potentially play a role in STDP and learning, in practice this effect must satisfy several biophysical and activity-dependent constraints, supporting the existence of specialized dynamic interactions between astrocytes and neurons.

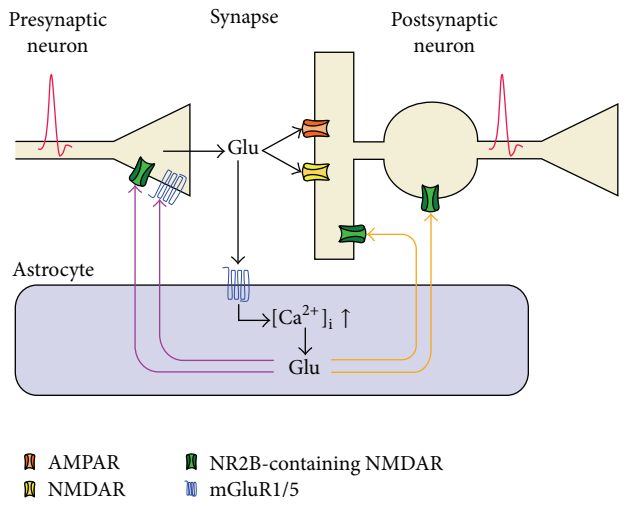

Figure 1: Pathways of glutamatergic gliotransmission. Perisynaptic astrocytic processes in several brain areas and different excitatory (but also inhibitory) synapses may release glutamate in a Ca^{2+}-dependent fashion. In turn, released astrocytic glutamate may increase (or decrease) synaptic neurotransmitter release by activating extrasynaptically located presynaptic receptors (*magenta arrows*) or contribute to postsynaptic neuronal depolarization by binding to extrasynaptic NMDA receptors (*orange arrows*) which mediate slow inward currents (SICs). These receptors often (but not always) contain NR2B subunits and are thus different with respect to postsynaptic NMDARs. Glutamate release by the astrocyte could be triggered either by activity from the same synapses that are regulated by the astrocyte (homosynaptic scenario) or by other synapses that are not directly reached by glutamatergic gliotransmission (heterosynaptic scenario).

2. Biophysical Modeling of a Gliotransmitter-Regulated Synapse

Although there may be several possible routes by which astrocytes release glutamate [38–40], Ca^{2+}-dependent glutamate release is likely the main one in physiological conditions [41, 42]. From a modeling perspective, as illustrated in Figure 1, Ca^{2+}-dependent glutamatergic gliotransmission consists of three distinct signaling pathways. One pathway (*black arrows*) initiates the release-triggering Ca^{2+} signal in the astrocyte and may be either exogenous or heterosynaptic or be triggered by the very synapses that are modulated by glutamatergic gliotransmission in a homosynaptic fashion. The other two pathways are instead represented by the two recognized routes for the action of glutamatergic gliotransmission on synaptic terminals: the presynaptic pathway whereby astrocytic glutamate modulates synaptic release (*magenta arrows*) and the postsynaptic pathway which mediates SICs in nearby neurons (*orange arrows*). Although both pathways could coexist at the same synapse in principle [11], their functional regulation is probably through different Ca^{2+}-dependent pathways [26], both in terms of spatiotemporal Ca^{2+}-dynamics [24] and in terms of pools of releasable glutamate resources and/or mechanism of release for these latter [43]. Thus, in the following, we set

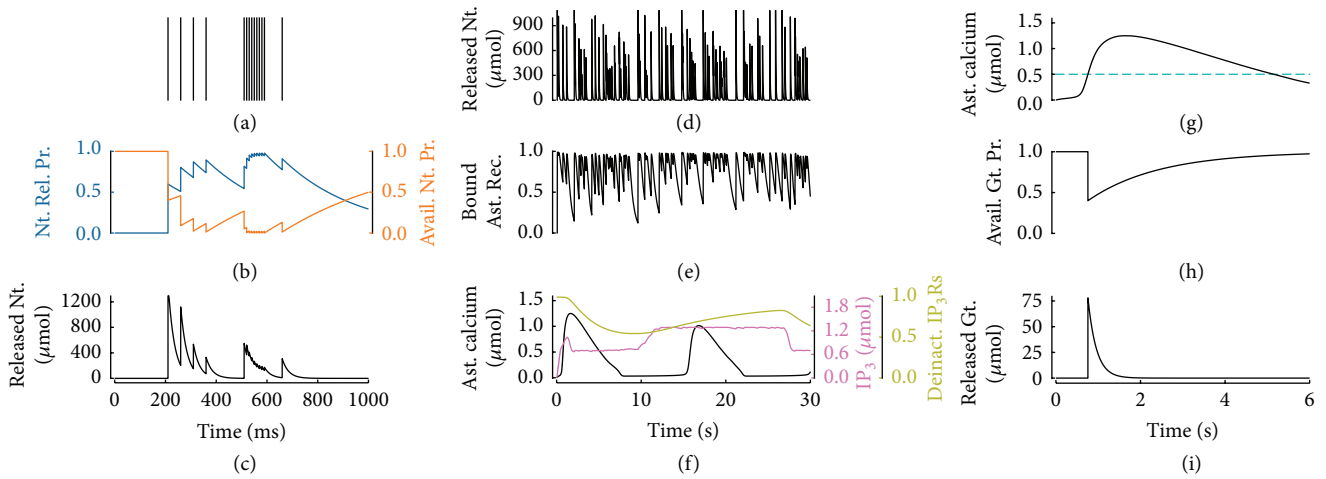

FIGURE 2: Biophysical modeling of a gliotransmitter-regulated synapse. ((a)–(c)) Model of synaptic release. Incoming presynaptic spikes (a) increase intrasynaptic Ca^{2+} levels which directly control the probability of release of available neurotransmitter resources ((b), Nt. Rel. Pr.) and decrease, upon release, the fraction (or probability) of neurotransmitter-containing vesicles available for release (Avail. Nt. Pr.). Each spike results in release of a quantum of neurotransmitter from the synapse ((c), Released Nt.) whose concentration in the perisynaptic space decays exponentially. Synapse parameters: $\tau_d = 0.5$ s, $\tau_f = 0.3$ s, and $U_0 = 0.6$. Stimulation by Poisson-distributed APs with an average rate of 5 Hz. ((d)–(f)) Model for astrocyte activation. Synaptically released neurotransmitter in the perisynaptic space (d) binds astrocytic receptors ((e), Bound Ast. Rec.), resulting in IP_3 production which triggers Ca^{2+} signaling in the astrocyte (f). This latter also depends on the fraction of deinactivated IP_3 receptors/Ca^{2+} channels (Deinact. IP_3Rs) on the astrocyte ER membrane (see Appendix A.1). ((g)–(i)) Model for gliotransmitter release. The increase of astrocytic Ca^{2+} beyond a threshold concentration ((g), *cyan dashed line*) results in the release of a quantum of gliotransmitter, which decreases the probability of further release of gliotransmitter ((h), Avail. Gt. Pr.) while transiently increasing extracellular gliotransmitter concentration ((i), Released Gt.). Model parameters as in Table 1.

to investigating the effect of synaptic transmission of each pathway independently of the other.

2.1. Calcium-Dependent Gliotransmitter Release. We begin our study by a description of a biophysically realistic model of synaptically evoked Ca^{2+}-dependent glutamate release from an astrocyte. At excitatory [44] and inhibitory synapses [45], astrocytes can respond to synaptically released neurotransmitters by intracellular Ca^{2+} elevations and release glutamate in turn [6]. Although morphological and functional details of the coupling between synaptic terminals and the surrounding astrocytic processes remain to be fully elucidated, the current hypothesis is that synaptically evoked glutamate-releasing astrocytic Ca^{2+} signaling is mainly by spillover of synaptic neurotransmitters and/or other factors, which bind to high-affinity astrocytic G protein-coupled receptors (GPCRs) [5] and thereby trigger inositol 1,4,5-trisphosphate (IP_3) production and Ca^{2+} release from the endoplasmic reticulum (ER) [46–48]. While early work mainly monitored somatic Ca^{2+} increases concluding that astrocytes respond only to intense neuronal firing patterns [49], recent experiments in astrocytic processes revealed that astrocytes may also respond to low levels of synaptic activity by Ca^{2+} elevations confined in subcellular regions of their processes [10, 48, 50], suggesting that the profile of astrocytic Ca^{2+} signaling and thus glutamate release could span the whole spectrum of neuronal (synaptic) activity [5].

To realistically describe synaptic release in the whole spectrum of neuronal firing, we consider the model of an activity-dependent synapse first introduced by Tsodyks and Markram [51]. This model captures the dependence of synaptic release on past activity, that is, presynaptic short-term plasticity, which substantially influences synaptic transmission at high enough rates of neuronal firing [52]. In particular, synaptic release results from the product of two quantities: (i) the probability of neurotransmiter-containing vesicles to be available for release and (ii) the probability of such vesicles to be effectively released by an action potential [53], which correlates with intrasynaptic Ca^{2+} [54]. At rest, it is assumed that all vesicles are available for release. The arrival of an action potential opens presynaptic voltage-dependent Ca^{2+} channels that trigger a transient increase of intrasynaptic Ca^{2+} which promotes release of a fraction u_S of available vesicles. Following release, the emptied vesicles are refilled in some characteristic time τ_d, while intrasynaptic Ca^{2+} and thus vesicle release probability decay to zero with a different time constant τ_f. For multiple action potentials incoming at time intervals of the order of these two time constants, neither vesicle replenishment nor intrasynaptic Ca^{2+} are restored to their resting values, so that the resulting synaptic release depends on the history of synaptic activity [55].

We illustrate the response of the synapse model to a train of action potentials in Figures 2(a)–2(c). The low rate of stimulation of the first four action potentials (Figure 2(a)) allows for the reintegration of most of the released neurotransmitter in between action potentials thereby keeping vesicle depletion limited (Figure 2(b), *orange trace*). In parallel, intrasynaptic Ca^{2+} grows, and so does vesicle release probability (Figure 2(b), *blue trace*), resulting in progressively

larger release of neurotransmitter per action potential or, in other words, in short-term facilitation of synaptic release (Figure 2(c), $t < 500$ ms). On the contrary, the presentation of a series of action potentials in rapid succession at $t = 500$ ms results in a sharp increase of vesicle release probability to a value close to saturation (i.e., Nt. Rel. Pr. $\simeq 1$) which causes exhaustion of neurotransmitter resources (i.e., Avail. Nt. Pr. $\simeq 0$). In this scenario, therefore, from one spike to the next one, progressively fewer neurotransmitter resources are available for release and the amount of released resources decreases with incoming action potentials, leading to depression of synaptic transmission. Such depression is short-lived, since synaptic release tends to recover after a sufficiently long period in which no action potentials occur, that is, the case, for example, of the last action potential at $t = 800$ ms.

Once released into the synaptic cleft, synaptic neurotransmitter is rapidly cleared by diffusion as well as by other mechanisms, including uptake by transporters and/or enzymatic degradation [56, 57]. In the simplest approximation, the contribution of these mechanisms can be modeled by a first-order reaction [58] which accounts for the exponentially decaying profile of neurotransmitter concentration in Figure 2(c) after synaptic release at each action potential. A fraction of released neurotransmitter molecules also spills out of the synaptic cleft to the perisynaptic space (Figure 2(d)) where it binds to GPCRs on the astrocyte (Figure 2(e)), therein triggering Ca^{2+} signaling (Figure 2(f)). To quantitatively describe this process, we modify the model of GPCR-mediated Ca^{2+} signaling originally introduced by De Pittà et al. [141] to account for dynamic regulation of astrocytic receptors by synaptic activity (see Appendix A, Section A.1). Accordingly, as illustrated in Figure 2(f), GPCR-mediated Ca^{2+} signaling is a result of the nonlinear interplay of three processes: (i) IP_3 production by GPCRs bound by synaptic neurotransmitter (*magenta trace*), (ii) Ca^{2+} release from the ER into the cytosol, which is triggered by IP_3-bound Ca^{2+} channels (IP_3Rs) and also modulates cytosolic IP_3 (*black trace*), and (iii) the effective fraction of available or, more exactly, "deinactivated" IP_3Rs [59] that can take part in Ca^{2+} release from the ER (*yellow trace*). Depending on the choice of parameter values, the astrocyte model may display both large, long-lasting somatic Ca^{2+} elevations and smaller and shorter Ca^{2+} increases, akin to those reported in astrocytic processes [47] (see Appendix B).

Glutamate release from the astrocyte is then assumed to occur every time that Ca^{2+} increases beyond a threshold concentration (Figure 2(g), *cyan dotted line*), in agreement with experimental observations [60, 61]. Although different mechanisms for glutamate release by the astrocyte could be possible, a large amount of evidence points to vesicular exocytosis as the main one to likely occur on a physiological basis [62]. Because astrocytic glutamate exocytosis bears several similarities with its synaptic homologue (reviewed in De Pittà et al. [29]), we model it in the same fashion. Thus, in line with experimental observations [63, 64], we postulate the existence of an astrocytic vesicular compartment that is competent for regulated glutamate exocytosis. Then, upon a suprathreshold Ca^{2+} elevation, a fixed fraction of astrocytic glutamate-containing vesicles releases glutamate into the extracellular space. Glutamate is then reintegrated into the astrocyte with some characteristic time constant (Figure 2(h)). In this fashion, glutamate concentration in the extracellular space abruptly increases by exocytosis from the astrocyte and then exponentially decays akin to neurotransmitter concentration in the synaptic cleft, yet, in general, at a different rate (Figure 2(h)) (Appendix B).

The description of gliotransmitter release hitherto introduced ignores the possible stochastic nature of astrocytic glutamate release [65] and reproduces the total amount of glutamate released, on *average*, by a single Ca^{2+} elevation beyond the release threshold. This description provides a simplified general framework to realistically capture synaptically evoked glutamate release by the astrocyte independently of the underlying mechanism of astrocytic exocytosis, which may either be in the form of a burst of synchronous vesicle fusion events that peaks within the first 50–500 ms from the Ca^{2+} rise underneath the plasma membrane [61, 65, 66] or occur at slower fusion rates in an asynchronous fashion [67, 68].

2.2. Gliotransmitter-Mediated Regulation of Synaptic Release and Short-Term Synaptic Plasticity. Once released, astrocyte-derived glutamate can diffuse in the extracellular space and bind extrasynaptic receptors located on presynaptic terminals. In particular, ultrastructural evidence suggests colocalization of glutamate-containing vesicles in perisynaptic astrocytic processes with those receptors [8], hinting a focal action of astrocytic glutamate on these latter. Such action is likely spatially confined and temporally precise, akin to that of a neurotransmitter on postsynaptic receptors, and is not affected by synaptic neurotransmitters [6]. Both ionotropic and metabotropic presynaptic receptors may be activated by astrocytic glutamate, yet their differential recruitment likely depends on developmental, regional, physiological, and cellular (synaptic) factors (reviewed in [29]). The details of the biochemical mechanisms of action of these receptors on synaptic physiology are not fully understood [69], but the simplest explanation is that they all modulate intrasynaptic Ca^{2+} levels, eventually increasing or decreasing synaptic release probability [18], although in a receptor-specific fashion [52, 69, 70].

From a modeling perspective, as originally proposed by De Pittà et al. [73], the common effect on synaptic release shared by different receptors allows expressing, in the simplest approximation, the synapse's resting release probability proportionally to the fraction of presynaptic receptors activated by astrocytic glutamate (Appendix A, Section A.1). In this fashion, as illustrated in Figure 3, the time evolution of the fraction of activated presynaptic receptors ensuing from a series of glutamate release events by the astrocyte (Figures 3(a) and 3(b)) is reflected by the dynamics of synaptic release probability at rest averaged across different trials (Figures 3(c) and 3(e)). The value of the coefficient of proportionality for the dependence of synaptic release probability on receptor activation sets the type of modulation of synaptic release by astrocytic glutamate which can be

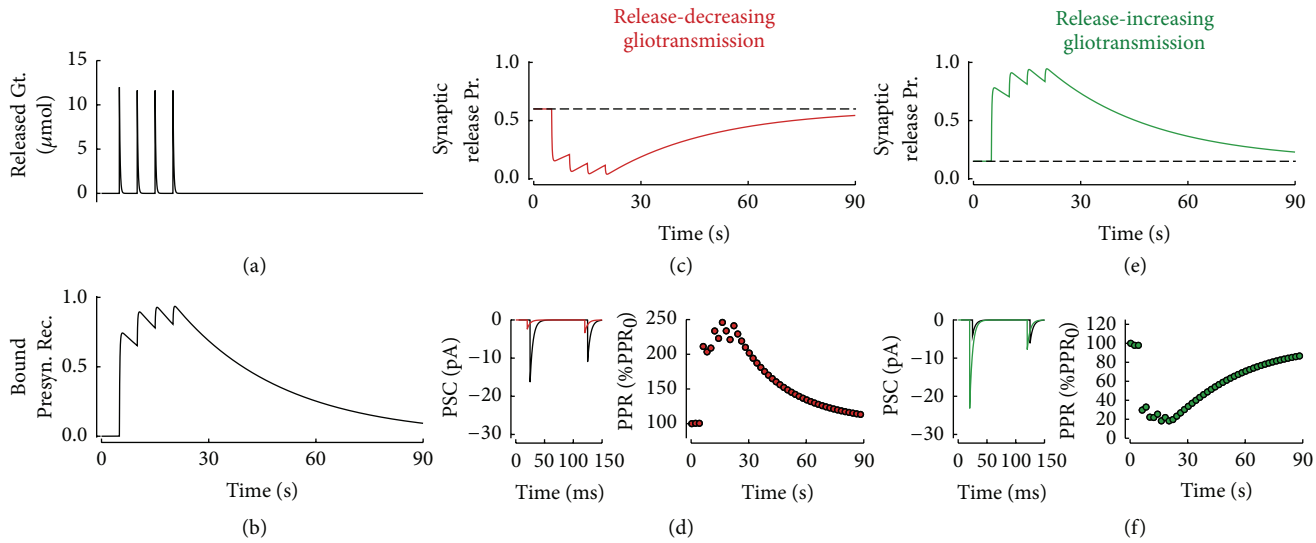

FIGURE 3: Presynaptic pathway of gliotransmission. Gliotransmitter released from the astrocyte (a) binds extrasynaptically located presynaptic receptors (b) thereby decreasing or increasing synaptic release depending on the type of gliotransmitter and receptor. In the release-decreasing case, synaptic release probability could approach zero by gliotransmission ((c), *red trace*, $\xi = 0$), although, in practice, less dramatic reductions are more likely to be measured with respect to the original value in the absence of gliotransmission (*black dashed line*). The reduction in synaptic release probability changes pair pulse plasticity increasing the pair pulse ratio (d). In the case of release-increasing gliotransmission, synaptic release probability could instead increase up to one ((e), *green trace*, $\xi = 1$). In turn, pair pulse plasticity changes towards a decrease of the ensuing pair pulse ratio (f). Parameters as in Table 1 except for $\varrho_e = 10^{-4}$, $O_P = 0.6\,\mu\text{M}^{-1}\,\text{s}^{-1}$, $\tau_P = 30\,\text{s}$, $\zeta = 0.54$, $J_S = 3\,\text{mV}$, and $R_{\text{in}} = 60\,\text{M}\Omega$.

either release-decreasing (Figure 3(c)), such as in the case of astrocytic glutamate-binding presynaptic kainate receptors or group II/III metabotropic receptors (mGluRs) [13, 14, 71], or release-increasing (Figure 3(e)), when astrocytic glutamate binds NMDARs or group I mGluRs [7–9, 11, 12, 26, 72]. The functional implications of these modulations of synaptic release by glutamatergic gliotransmission on synaptic transmission have been widely addressed in a series of previous studies [18, 29, 73], and the remainder of this section reviews and extends the main results from those studies about short-term synaptic plastic and synaptic filtering.

Figure 3(d) (*left panel*) shows how postsynaptic currents (PSCs) change in the presence of release-decreasing glutamatergic gliotransmission when elicited by two consecutive action potentials arriving to the resting synapse 20 ms after the onset of gliotransmission at $t = 5\,\text{s}$ (Figure 3(c)). Two differences with respect to the case without gliotransmission (*black trace*) may be observed. First the PSC amplitude overall decreases (*red trace*), consistent with a decrease of synaptic efficacy caused by the reduction of synaptic release by astrocytic glutamate. Then, the second PSC is larger than the first one, which is the opposite of what would be measured in the absence of gliotransmission. In other words, in agreement with experimental observations [13], the release-decreasing effect of astrocytic glutamate results in an increased pair pulse ratio (PPR) with respect to the case without gliotransmission (PPR_0). Notably, as shown in Figure 3(d) (*right panel*), this change in the PPR ratio is only transient and vanishes together with the effect of gliotransmission on synaptic release. Similar considerations also hold in the case of a release-increasing effect of astrocytic glutamate on synaptic transmission [8]: while PSC amplitude increases (Figure 3(f), *left panel*, *green trace*), this occurs to the detriment of PPR, which decreases instead (Figure 3(f), *right panel*). Thus, synapses whose release probability is increased by glutamatergic gliotransmission are likely to run out of neurotransmitter faster, exhibiting rapid onset of short-term depression, consistent with lower PPR values. On the contrary, synapses whose release probability is reduced by astrocyte-released glutamate deplete their neurotransmitter resources slower and may exhibit progressive facilitation (i.e., potentiation) of their efficacy to transmit action potentials and so larger PPR values [74]. That is, the plasticity mode of a synapse, namely, whether it is depressing or facilitating, may not be fixed but rather be modulated by glutamatergic gliotransmission by surrounding astrocytes in an activity-dependent fashion [29, 73].

An important consequence of short-term synaptic dynamics is that synapses can act as filters [16, 17, 75]. Hence, modulations of synaptic dynamics by glutamatergic gliotransmission are also expected to affect the synapse's filtering characteristics [18]. This scenario is illustrated in Figure 4 where the effect of release-decreasing versus release-increasing glutamatergic gliotransmission, respectively, on depressing and facilitating synapses, is shown in terms of changes of the filtering characteristics of these synapses, that is, their steady-state release as a function of the frequency of presynaptic stimulation [17]. In the absence of gliotransmission, depressing synapses, which are characterized by intermediate-to-high initial probability of release [74] (Figure 4(a), *black circles*), predominantly act as low-pass filters (Figure 4(b), *black circles*) that are most

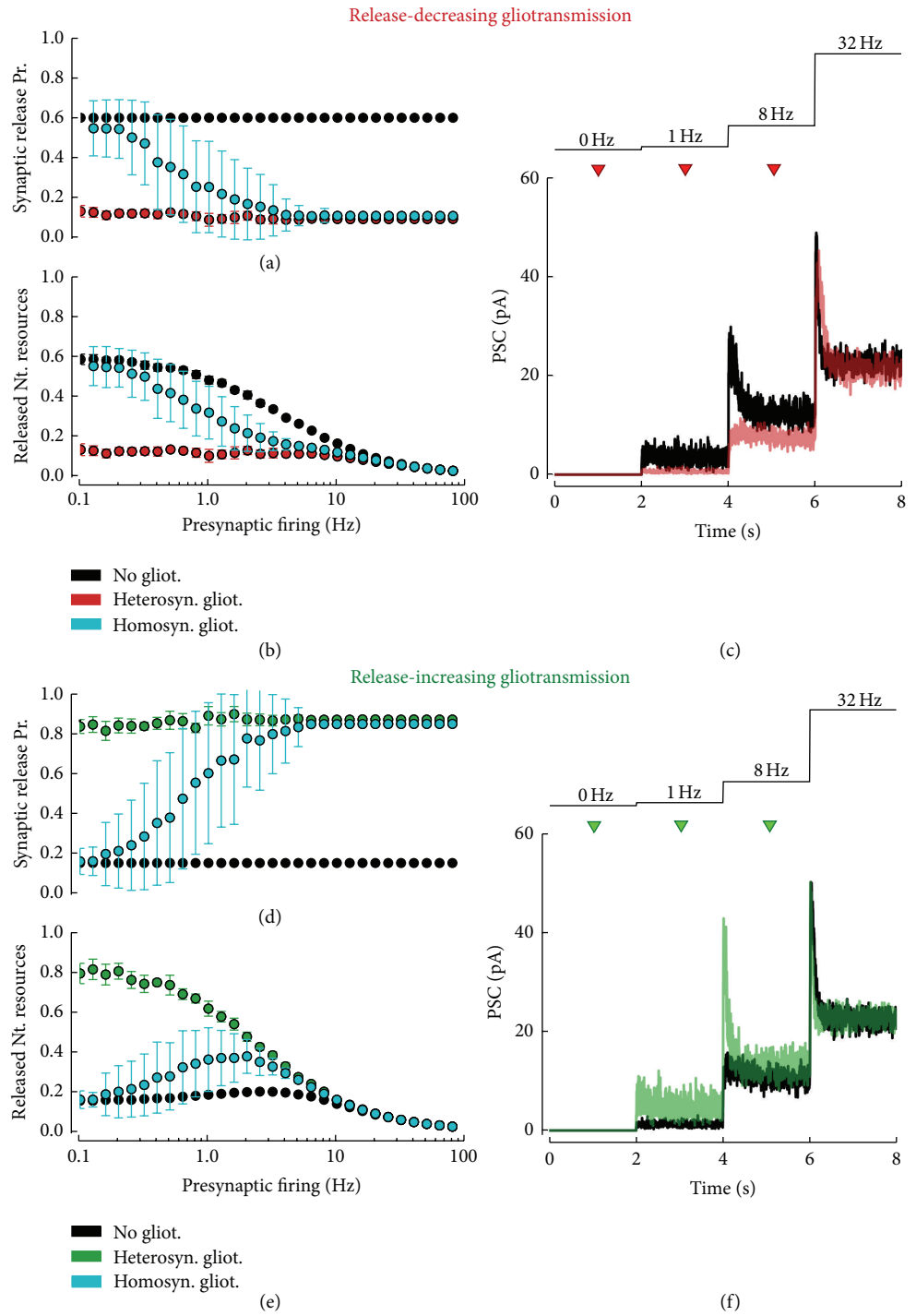

FIGURE 4: Gliotransmitter-mediated modulation of synaptic frequency response. Decrease (a) or increase (d) of synaptic release probability by gliotransmission modulates the average per-spike synaptic release, resulting in a change of the synapse frequency response. Monotonically decreasing frequency responses that are typical of depressing synapses could be flattened by release-decreasing gliotransmission ((b), *black* versus *red points*), and vice versa, almost nonmonotonic ones, characteristic of facilitating synapses, could turn into monotonically decreasing responses by release-increasing gliotransmission ((e), *black* versus *green points*). Changes in frequency response depend on whether gliotransmission impinges on the very synapse that is triggered by (homosynaptic/closed-loop scenario) or not (heterosynaptic/open-loop scenario). In the homosynaptic scenario, the synaptic response is expected to change only for presynaptic firing rates that are sufficiently high to trigger gliotransmitter release from the astrocyte ((b), (e), *cyan points*). Data points and error bars: mean ± STD for $n = 20$ (no gliot. and heterosyn. gliot.) or $n = 200$ simulations (homosyn. gliot.) with 60 s long Poisson-distributed presynaptic spike trains. ((c), (f)) The change of synaptic frequency response mediated by gliotransmission (three consecutive gliotransmitter releases at the time instants marked by *triangles*) leads to changes in how presynaptic firing rates (*top panels*) are transmitted by the synapse (*bottom panels*). Simulated postsynaptic currents (PSCs) are shown as average traces of $n = 1000$ simulations for gliotransmitter release at 1 Hz. Release-decreasing gliotransmission was achieved for $\xi = 0$, whereas $\xi = 1$ was used for release-increasing gliotransmission. Depressing synapse in ((a), (b)): $\tau_d = 0.5$ s, $\tau_f = 0.3$ s, and $U_0 = 0.6$; facilitating synapse in ((d), (e)): $\tau_d = 0.5$ s, $\tau_f = 0.5$ s, and $U_0 = 0.15$. Other model parameters as in Figure 3 except for $R_{\text{in}} = 300$ MΩ.

effective at transmitting low frequency presynaptic spike trains (Figure 4(c), *black traces*). On the contrary, facilitating synapses, with a low-to-intermediate initial probability of neurotransmitter release [74] (Figure 4(a), *black circles*), function as high-pass or band-pass filters (Figure 4(b), *black circles*); that is, they are mostly effective at transmitting action potentials in an intermediate range of presynaptic activity (Figure 4(c), *black trace*).

In the presence of glutamate release by the astrocyte, these two scenarios could be reversed. Consider indeed the simple heterosynaptic case where glutamatergic gliotransmission is stimulated by other means compared to by the very synapses it impinges on. It may be noted that release-decreasing gliotransmission flattens the synaptic steady-state release towards zero for all frequencies of stimulation (Figure 4(b), *red circles*), ensuing in synaptic transmission that resembles the one of a facilitating, band-pass synapse (compare the *red* PSC *trace* in Figure 4(c) with the *black* PSC *trace* in Figure 4(f)). Vice versa, release-increasing gliotransmission could turn band-pass features of transmission by a facilitating synapse (Figure 4(e), *green circles*) into low-pass, reminiscent of a more depressing synapse (compare the *green* PSC *trace* in Figure 4(f) with the *black* PSC *trace* in Figure 4(c)). On the other hand, when gliotransmission is stimulated by the same synapses that it modulates, that is, in the homosynaptic scenario of gliotransmission, inspection of the ensuing synaptic filtering characteristics (Figures 4(b) and 4(e), *cyan circles*) reveals that these latter coincide with those obtained in the absence of gliotransmission for low frequencies of presynaptic activity, while they tend to equal those observed with heterosynaptic gliotransmission as the frequency of stimulation increases. This coexistence of mixed features from apparently opposite scenarios, that is, no gliotransmission versus heterosynaptic gliotransmission, can be explained by the fact that the release of glutamate from the astrocyte requires intracellular Ca^{2+} to cross a threshold concentration. Hence, in the homosynaptic scenario, synapses that impinge on the astrocyte must be stimulated at rate sufficiently high to allow astrocytic Ca^{2+} to increase beyond such a threshold.

The modulation of synaptic filtering by glutamatergic gliotransmission offers the possibility that the same stimulus could be differently filtered (i.e., processed) and transmitted by a synapse in the presence (or not) of glutamate release by surrounding astrocytic processes, ultimately endowing that synapse with processing versatility with respect to incoming action potentials. Moreover, to the extent that synaptic dynamics critically shape the computations performed by the neural circuitry, such versatility could also be reflected at the network level, leading to the possibility that the same neuron-glia network could be involved in different computational tasks defined, time by time, by activity-dependent gliotransmitter release by astrocytes in the network.

2.3. Astrocyte-Mediated Slow Inward Currents. Induction of slow inward (i.e., depolarizing) currents (SICs) by activation of extrasynaptically located postsynaptic NMDA receptors is the other mechanism considered in this study whereby glutamatergic gliotransmission could affect synaptic information transfer. While astrocyte-mediated SICs have been reported in several brain regions, the pathway underlying glutamate release by astrocytes has not been fully elucidated [76, 77]. It is likely that, similar to the presynaptic route for glutamatergic gliotransmission discussed above, multiple pathways for glutamate release could be used by the same astrocyte [39], but their deployment depends on developmental, regional, and physiological factors [27]. Astrocytic Ca^{2+} activity seems to be a crucial factor in the regulation of astrocyte-mediated SICs [19–23, 25, 78]. In particular, SIC frequency and amplitude have been shown to increase upon Ca^{2+} elevations mediated by GPCRs on astrocytes such as mGluRs [19–23, 72, 79], the metabotropic purinergic P2Y1 receptor [25], the endocannabinoid CB1 receptor [80], or the protease-activated receptor 1 (PAR1) [24]. Remarkably, stimulation of PAR1s on hippocampal astrocytes was shown to trigger, under physiological conditions, Ca^{2+}-dependent glutamate release from these cells through Bestrophin-1 anion channel [81, 82], and this pathway of glutamate release has been suggested as a candidate mechanism for SICs [83]. Channel-mediated glutamate release is expected to account for prolonged (>10 s) release of transmitter but in small amounts per unit time [82] thus ensuing in modest, very slow rising and decaying inward currents. While similar SICs have indeed been recorded [71, 84], most experiments reported SICs within a wide range of amplitudes to last only few seconds at most and rise in correlation with astrocytic Ca^{2+} increases, with rise time much shorter than their decay [20–22, 24, 26, 32, 85, 86] akin to currents that would ensue from a quantal mechanism of gliotransmitter release [62].

Based on these arguments, we assume glutamate exocytosis as the candidate mechanism for glutamate release by astrocytes that mediates SICs. Accordingly, we adopt the description of astrocytic glutamate exocytosis previously introduced (Figures 2(g)–2(i)) to also model astrocyte-mediated SICs. In this fashion, glutamate exocytosis by the astrocyte into the extracellular space (Figure 5(a)) results in activation of extrasynaptically located NMDARs on nearby neuronal dendrites which trigger SICs (Figure 5(b)) that cause slow depolarizing postsynaptic potentials (PSP, Figure 5(c)).

An important functional consequence of SIC-mediated depolarizations is that they can modulate neuronal excitability [21–23, 85]. As illustrated in Figures 5(d) and 5(e), astrocyte-mediated SICs (*cyan trace*) may add to regular synaptic currents (*black trace*) resulting in depolarizations of postsynaptic neurons closer to their firing threshold [23]. In turn, these larger depolarizations could dramatically change generation and timing of action potentials by those neurons in response to incoming synaptic stimuli (Figure 5(f)). This could ultimately affect several neurons within the reach of glutamate released by an astrocyte, leading to synchronous transient increases of their firing activity [21]. Remarkably, this concerted increase of neuronal excitability has often been observed in correspondence with large amplitude (i.e., >100 pA) SICs [21, 25, 85, 87], but experiments report the majority of SICs to be generally smaller, with amplitudes < 80 pA [11, 21, 22, 26, 32, 87]. It is therefore unclear whether SIC-mediated increase of neuronal excitability could occur [88] or not [87, 89, 90] in physiological conditions.

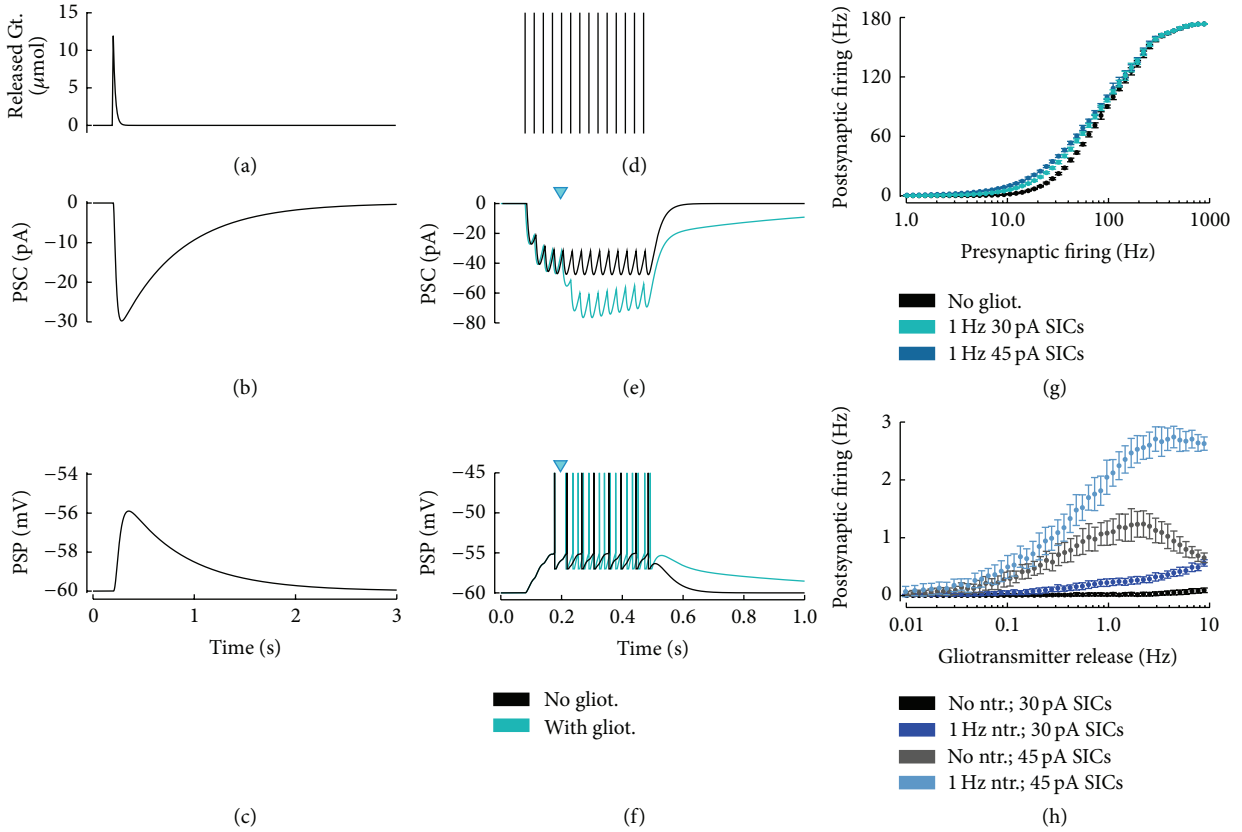

FIGURE 5: Postsynaptic pathway of gliotransmission by slow inward currents. The transient increase of gliotransmitter concentration in the perisynaptic space (a) triggers a slow inward (depolarizing) current (SIC) in the postsynaptic neuron ((b), (c)). Such SIC adds to postsynaptic currents triggered by presynaptic spikes ((d), (e), *cyan triangle* marks gliotransmitter release/SIC onset) and may dramatically alter postsynaptic firing (f). In general postsynaptic firing frequency increases with both SIC amplitude (g) and frequency (h). In this latter case, however, SICs as ample as 30 pA (similar to what reported in several experiments) need to impinge on the postsynaptic neuron at unrealistically high rates ($\gg$0.1 Hz) in order to trigger a sensible change in the neuron's firing rate (*black data points*). Lower, more realistic SIC rates may affect neuronal firing only for larger SIC amplitudes (e.g., 45 pA, *grey data points*). The entity of SIC-mediated increase of postsynaptic neuronal firing further depends on the neuron's state of depolarization at SIC timings which is set by synaptic inputs (*blue* and *cyan data points*). Data points and error bars: mean ± STD out of $n = 50$ simulations with presynaptic Poisson-distributed spike trains. Parameters as in Table 1 except for $\varrho_e = 10^{-4}$, $\tau_e = 200$ ms, $\tau_S^r = 10$ ms, and $R_{\text{in}} = 150$ MΩ.

In Figure 5(g), we consider postsynaptic firing in a standard leaky integrate-and-fire neuron model [91, 92] as a function of presynaptic activity for SICs of different amplitudes (30–45 pA, see Appendix B) randomly occurring at an average rate of 1 Hz based on a binomial process for glutamate release from astrocytes as suggested by experiments [65] (see Appendix A). In line with experimental evidence [93], the input-output transfer function in the absence of gliotransmission has a typical sigmoidal shape (*black dots*) which reflects the following: (i) gradual emergence of firing for low (>10 Hz) fluctuating synaptic inputs; (ii) the progressive, quasi-linear increase of the firing rate for presynaptic activity beyond ~30 Hz; and finally, (iii) saturation of the firing rate for sufficiently strong synaptic inputs such that timing of action potential generation approaches the neuron's refractory period (which was fixed at 2 ms in the simulations, Appendix B) [92]. The addition of astrocyte-mediated SICs alters the firing characteristics of the neuron due to the ensuing larger depolarization. In particular the neuron could generate action potentials for lower rates of presynaptic activity (*cyan*/*blue dots*). Clearly, the larger the SIC is, the more the postsynaptic firing increases with respect to the case without SICs, for a given level of presynaptic activity.

As previously mentioned, these results assume an average 1 Hz rate for astrocyte-mediated SICs. While such a rate cannot be excluded, it seems unlikely for the following reasons. The weak correlation of SIC amplitude with somatic Ca^{2+} elevations observed in experiments favors indeed the idea that glutamate-mediated SICs are highly localized events, occurring within subcellular domains at astrocytic processes [22]. In turn, Ca^{2+} elevations in astrocytic processes could be as short-lived as ~0.5 s [10, 50], thus in principle allowing for glutamate release rates of the order of 1 Hz. However, in practice, reported SIC frequency is much lower, that is,

<5/min (i.e., ~0.08 Hz) [11, 22]. Hence, it may be expected that the effect of SICs on neuronal firing could be considerably reduced with respect to the case in Figure 5(g).

We consider this possibility more closely in Figure 5(h), where we analyze postsynaptic firing in function of the average frequency of astrocyte-mediated SICs, both in the absence of synaptic activity (*black* and *dark blue dots*) and in the case of presynaptic activity at an average rate ~ 1 Hz, which corresponds to typical levels of spontaneous activity in vivo [94] (*grey* and *light blue dots*). It may be noted that the effect of SICs of typical amplitudes on postsynaptic firing rate is generally small, that is, <0.5 Hz, except for unrealistic (>0.1 Hz) SIC rates, while it gets stronger in association with synaptic activity. In this latter case however the possible increase in postsynaptic firing by astrocyte-mediated SICs is limited by the rate of reintegration of released glutamate resources in the astrocyte (fixed at ~1 Hz, Appendix B). Analogously to short-term synaptic depression in fact, our description of gliotransmitter release predicts that, for release rates that exceed the rate of reintegration of released glutamate by the astrocyte, exhaustion of astrocytic glutamate resources available for further release will result in SICs of smaller amplitude. In this fashion, due to depletion of astrocytic glutamate, the effect of large rates of glutamate release and thus of SICs on neuronal firing tends to be equivalent to that of considerably lower ones.

Taken together, the above results do not exclude a possible role of SICs in modulation of neuronal excitability and firing but suggest that such modulation could effectively occur only in coincidence with proper levels of synaptic activity. In this fashion, astrocyte-mediated SICs could be regarded to operate a sort of coincidence detection between synaptic activity and astrocytic glutamate release [22], whose readout would then be a temporally precise, cell-specific increase of neuronal firing (Figure 5(f)).

3. Astrocyte-Mediated Regulation of Long-Term Plasticity

The strength of a synaptic connection between two neurons can be modified by activity, in a way that depends on the timing of neuronal firing on both sides of the synapse, through a series of processes collectively known as spike-timing-dependent plasticity (STDP) [95]. As both pre- and postsynaptic pathways of glutamatergic gliotransmission potentially change EPSC magnitude, thereby affecting postsynaptic firing, it may be expected that they could also influence STDP.

Although the molecular mechanisms of STDP remain debated, and different mechanisms could be possible depending on type of synapse, age, and induction protocol [34], at several central excitatory synapses postsynaptic calcium concentration has been pointed out as a necessary factor in induction of synaptic changes by STDP [31, 96–99]. Remarkably, amplitude and, likely, time course of postsynaptic Ca^{2+} could control the direction of plasticity: smaller, slower increases of postsynaptic Ca^{2+} give rise to spike-timing-dependent long-term depression (LTD), whereas larger, more rapid increases cause spike-timing-dependent long-term potentiation (LTP) [31, 96, 97]. In calcium-based STDP models, this is also known as the "Ca^{2+}-control hypothesis" [35, 100, 101]. According to this hypothesis, no modification of synaptic strength occurs when Ca^{2+} is below a threshold θ_d that is larger than the resting Ca^{2+} concentration. If calcium resides in an intermediate concentration range, between θ_d and a second threshold $\theta_p > \theta_d$, the synaptic strength is decreased. Finally, if calcium increases above the second threshold, θ_p, the synaptic strength is potentiated.

Figures 6(a1) and 6(b1) exemplify the operational mechanism of the Ca^{2+}-control hypothesis within the framework of a nonlinear Ca^{2+}-based model for STDP at glutamatergic synapses originally introduced by Graupner and Brunel [102]. At most glutamatergic synapses, postsynaptic Ca^{2+} is mainly regulated by two processes: (i) postsynaptic Ca^{2+} entry mediated by NMDARs [103] and (ii) Ca^{2+} influx by voltage-dependent Ca^{2+} channels (VDCCs) [31, 33, 99, 104]. In this fashion, each presynaptic action potential generates a long-lasting Ca^{2+} transient by opening NMDAR channels, while postsynaptic firing results in a short-lasting Ca^{2+} transient due to opening of VDCCs by dendritic depolarization through back-propagating action potentials (bAPs) [95]. Presynaptic action potentials alone do not trigger changes in synaptic strength, but they do so in correlation with postsynaptic bAPs [105]. Notably [106], in a typical STDP induction pairing protocol, LTD is induced if the postsynaptic neuron fires before the presynaptic one, that is, post → pre pairing at negative spike-timing intervals Δt (Figure 6(a1)). Contrarily, LTP is induced when the presynaptic cell fires before the postsynaptic cell, that is, for pre → post pairing at positive Δt intervals (Figure 6(a1)). This is possible because, when a presynaptic action potential is followed shortly after by a postsynaptic bAP, the strong depolarization by this latter drastically increases the voltage-dependent NMDAR-mediated Ca^{2+} current due to removal of the NMDAR magnesium block [107, 108], thereby resulting in supralinear superposition of the NMDAR- and VDCC-mediated Ca^{2+} influxes.

In the framework of the Ca^{2+}-control hypothesis, these observations may be summarized as follows. For large Δt, pre- and postsynaptic Ca^{2+} transients do not interact, and the contributions from potentiation and depression by pre/post pairs (or vice versa) cancel each other, leading to no synaptic changes on average (Figure 6(c), *black curves*). For short, negative Δt, the presynaptically evoked Ca^{2+} transient rises instead above the depression threshold (θ_d) but not beyond the potentiation threshold (θ_p). Consequently, depression increases whereas potentiation remains constant, which leads to LTD induction. For short, positive Δt however the postsynaptically evoked calcium transient rises on top of the presynaptic transient by the NMDAR nonlinearity and increases activation of both depression and potentiation. Because the rate of potentiation is larger than the rate of depression (Appendix C), this results in LTP induction.

For the same number of pre/post pairs (or vice versa), mapping of the average synaptic modification as a function

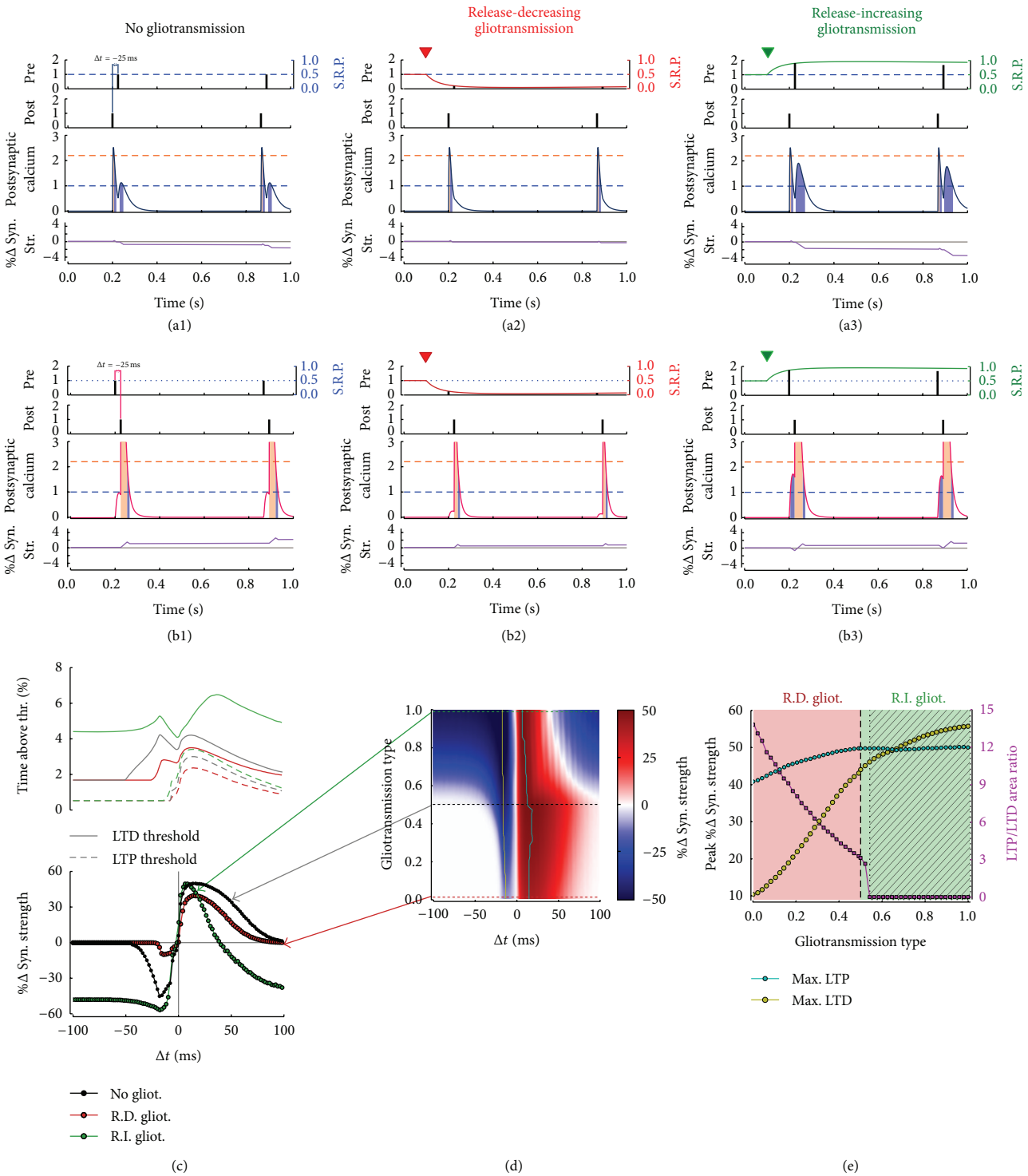

FIGURE 6: STDP modulation by gliotransmitter regulation of synaptic release. ((a), (b)) Rationale of LTD and LTP without ((a1), (b1)) and with either release-decreasing ((a2), (b2), $\xi = 0$) or release-increasing gliotransmission ((a3), (b3), $\xi = 1$) setting on at the *red*/*green marks*. (c) Percentage of time spent by postsynaptic Ca^{2+} transients (*left panel*) above depression (*dashed lines*) and potentiation thresholds (*solid lines*) for spike-timing intervals (Δt) within ±100 ms and resulting STDP curves (*right panel*) in the absence of gliotransmission (no gliot., *black curve*) and with maximal release-decreasing (RD, *red curve*) or release-increasing gliotransmission (RI, *green circles*). (d) In general, strength and direction (i.e., "type") of gliotransmission may dramatically modulate STDP. For example, synaptic changes are attenuated when synaptic release is decreased by gliotransmission (area below the *black dashed line*). Conversely, for sufficiently strong release-increasing gliotransmission (area above the *black dotted line*), the LTP window shrinks and LTD may be measured for all $\Delta t < 0$, as well as for sufficiently large $\Delta t > 0$. (e) A closer inspection of STDP curves indeed reveals that LTD (*yellow curve*) increases for larger synaptic release accounted by gliotransmission, while the ratio between areas underneath the LTP and LTD (*magenta curve*), initially in favor of the former (i.e., for release-decreasing gliotransmission), reduces to zero for large enough release-increasing gliotransmission, when two open LTD windows appear outside a small LTP window center for small $\Delta t > 0$ (*hatched area*). Synaptic parameters: $\tau_d = 0.33$ s, $\tau_f = 0.33$ s, and $U = 0.5$ s. Other parameters as in Table 1 except for $\varrho_e = 10^{-4}$, $\tau_c = 1$ ms, $W_N = 78.7$, $\tau_P = 5$ s in ((a), (b)), and $\tau_P = 30$ s otherwise.

of the spike-timing interval Δt ultimately provides an STDP curve that qualitatively resembles the classic curve originally described by Bi and Poo [123] (Figure 6(c), *right panel*, *black curve*). In the following, we will focus on parameters that lead to such a STDP curve and investigate how this curve is affected in the presence of glutamatergic gliotransmission, through the pre- and postsynaptic pathways of regulation discussed above.

3.1. Presynaptic Pathway. The very nature of synaptic transmission crucially depends on the synapse's initial probability of neurotransmitter release, insofar as this latter sets both the tone of synaptic transmission, that is, how much neurotransmitter is released per action potential by the synapse on average, and whether the synapse displays short-term depression or facilitation [17]. Synapses with low-to-intermediate values of initial neurotransmitter release probability, for example, Schaffer collateral synapses [74], or some cortical synapses [16], are indeed prone to display facilitation, whereas synapses that are characterized by large release probability are generally depressing [16]. Because synaptic release probability also dictates the degree of activation of NMDARs and consequently the magnitude of postsynaptic Ca^{2+} influx, it is expected that both the tone of synaptic transmission and its short-term dynamics could affect STDP [34]. The relative weight of these two factors in shaping synaptic changes however likely depends on the protocol for STDP induction. Short-term plasticity could indeed sensibly regulate STDP induction only for rates of presynaptic action potentials high enough to allow facilitation or depression of synaptic release from one AP to the following one [109, 110]. In this study, we consider low pre/post frequencies of 1 Hz. At such frequencies we expect short-term plasticity to have a negligible effect, and thus we only focus on how changes in the tone of synaptic transmission by glutamatergic gliotransmission affect STDP.

Figures 6(a2) and 6(b2), respectively, show the outcome of LTD and LTP induction for two consecutive pre → post and pre → post pairings preceded by the onset of release-decreasing gliotransmission at 0.1 s (*top panels*, *black marks*). A comparison of the ensuing postsynaptic Ca^{2+} dynamics with respect to the case without gliotransmission (Figures 6(a1) and 6(b1)) reveals that the strong decrease of synaptic release probability (SRP, *top panels*, *red curves*) caused by gliotransmission remarkably reduces the NMDAR-mediated contribution to postsynaptic Ca^{2+} influx (*middle panels*), resulting in smaller variations of synaptic strength (*bottom panels*). In this fashion, at the end of the pairing protocol, release-decreasing gliotransmission accounts for less time spent by Ca^{2+} above both LTD and LTP thresholds (Figure 6(c), *left panel*, *red traces*). The resulting STDP curve thus displays strongly attenuated LTD and LTP (Figure 6(c), *right panel*, *red curve*), with LTP windows spanning a considerably smaller range of Δts values than in the curve obtained without gliotransmission (*black curve*).

Similar considerations apply to the case of release-increasing gliotransmission (Figures 6(a3) and 6(b3)). In this case, the NMDAR component of postsynaptic Ca^{2+} could increase by gliotransmission even beyond the θ_d threshold (*dashed blue line*), thus favoring depression while reducing potentiation (*bottom panels*). In particular, for short positive Δt, the maximal LTP does not change but the Δt range for LTP induction shrinks. For $\Delta t > 40$ ms in fact, the time that Ca^{2+} spends above the LTD threshold increases with respect to the time spent by Ca^{2+} above the LTP threshold, thereby resulting in LTD induction (Figure 6(c), *left panel*, *green traces*). In this fashion, the STDP curve in the presence of release-increasing gliotransmission displays a narrow 0–40 ms LTP window outside which LTD occurs instead (Figure 6(c), *right panel*, *green curve*).

Figure 6(d) summarizes how the STDP curve changes for the whole spectrum of glutamatergic gliotransmission. In this figure, a y-axis value of "gliotransmission type" equal to 0 corresponds to maximum release-decreasing gliotransmission (*red curve* in Figure 3(c)); a value equal to 1 stands instead for maximum release-increasing gliotransmission (as in the case of the *green curve* in Figure 3(c)); finally, a value of 0.5 corresponds to no effect of gliotransmission on synaptic release (*black curve* in Figure 3(c)). It may be noted that gliotransmission may affect the STDP curve in several ways, changing both strength of plastic changes (*color code*) and shape and areas of LTP and LTD windows. In particular, as revealed by Figure 6(e), maxima of LTP (*cyan circles*) and LTD (*yellow circles*) decrease with decreasing values of gliotransmission type, consistently with smaller postsynaptic Ca^{2+} influx for larger decreases of synaptic release by gliotransmission. This suggests that release-decreasing gliotransmission (*red-shaded area*) could attenuate STDP yet in a peculiar fashion, counteracting LTD more than LTP induction, as reflected by increasing values of LTP/LTD area ratio (*magenta curve*).

On the contrary, the effect of release-increasing gliotransmission (Figure 6(e), *green-shaded area*) could be dramatically different. For sufficiently strong increases of synaptic release by gliotransmission in fact, the LTP/LTD area ratio drops to zero (*hatched area*) in correspondence with the appearance of two "open" LTD windows, one for $\Delta t < 0$ and the other for sufficiently large positive spike-timing intervals. In parallel, consistently with the fact that release-increasing gliotransmission tends to increase the fraction of time spent by postsynaptic Ca^{2+} above the threshold for LTD thereby promoting this latter (Figure 6(c)), the range for LTP induction also tends to shrink to lower Δt values as release-increasing gliotransmission grows stronger (Figure 6(d), *red color-coded areas* for gliotransmission type > 0.5).

In summary, our analysis reveals that modulation of synaptic release by glutamatergic gliotransmission could change STDP both quantitatively and qualitatively, from hindering its induction for release-decreasing modulations to altering both shape and existence of LTD windows for release-increasing modulations. However, whether and how this could effectively be observed in experiments remain to be investigated. Supported both by experimental evidence and theoretical arguments is the notion that regulations of the tone of synaptic transmission by glutamatergic gliotransmission likely require specific morphological and functional

constraints to be fulfilled by the nature of astrocyte-synapse coupling [5, 18]. Similar arguments may ultimately hold true also for modulation of STDP; insofar as for this modulation to be measured in our simulations, we required both a sufficiently strong increase/decrease of synaptic release by gliotransmission and a decay time of such increase/decrease long enough for this latter to be present during the induction protocol. Should these two aspects not have been fulfilled in our simulations, then modulation of STDP by gliotransmitter-mediated changes of synaptic release would likely have been negligible or even undetectable.

3.2. Postsynaptic Pathway. We now turn our analysis to the possible impact of astrocyte-mediated SICs on STDP. Because SICs are through extrasynaptic NMDA receptors and these receptors are mainly permeable to Ca^{2+} ions [111], then SICs could contribute to postsynaptic Ca^{2+} thereby affecting STDP. Nevertheless, we should note that it is unclear whether and how extrasynaptic NMDARs contribute to plasticity, independently of the occurrence of SICs [77]. For example, theta-burst LTP induction in CA1 neurons of rat hippocampal slices is turned into LTD when extracellular NMDARs are selectively stimulated [112], but it is unknown whether these receptors have a role in STDP [113]. In general, for a given STDP induction protocol, two factors that could crucially regulate how Ca^{2+} transients mediated by extrasynaptic NMDARs are involved in STDP are the location of these receptors on the spine and the morphology of this latter in terms of spine head and neck [114, 115]. Unfortunately both these factors remain unknown in the current knowledge of SIC-mediating extrasynaptic NMDARs and, for the remainder of this study, we assume that, in spite of their possible location away from the postsynaptic density along the spine neck or the dendritic shaft [116], SIC-mediating extrasynaptic NMDARs could still regulate spine Ca^{2+} dynamics [27].

Based on the above rationale, we thus model SICs as slow postsynaptic Ca^{2+} transients that will add to presynaptically and postsynaptically triggered ones and study their effect on the induction of SDTP by classic pairing protocols. For the sake of generality, we express the peak of SIC-mediated Ca^{2+} transients in units of NMDAR-mediated EPSCs. However, since in our STDP description individual EPSCs do not trigger any synaptic modification [102], then we may expect that only SICs sufficiently larger than EPSCs could effectively affect STDP. On the other hand, smaller SICs could also combine with Ca^{2+} transients by pre/post pairings, resulting in Ca^{2+} elevations beyond either LTD or LTP thresholds that would ultimately cause synaptic changes (Figures 7(a) and 7(b)). Hence, based on these considerations, we deem amplitude and timing of SICs, in terms of both frequency of occurrence and onset with respect to STDP-inducing stimuli, to be crucial factors in shaping how SICs affect STDP, and thus we set to analyzing these three factors separately.

Figure 7(c) summarizes the results of our simulations for SICs as large as 0.5, 1, or 1.5 times typical EPSCs, occurring at a fixed rate of 0.1 Hz and starting 100 ms before the delivery of 60 STDP-inducing pre/post pairings at 1 Hz. As illustrated in Figures 7(a) and 7(b), for the same SIC kinetics, these simulations guarantee superposition between Ca^{2+} influxes mediated by SICs and pre/post pairings such that the extension of the ensuing Ca^{2+} transient beyond LTD and LTP thresholds (*dashed lines*) merely depends on SIC amplitude. In this fashion, it may be noted that SICs of amplitude smaller than or equal to typical EPSCs (Figure 7(c), *turquoise circles* and *black circles,* resp.), which alone would not produce any synaptic modification, do not sensibly change the STDP curve with respect to the previously considered case of an alike synapse in the absence of gliotransmission (Figure 6(c), *black circles*). Conversely, large SICs could dramatically affect STDP, shifting the STDP curve towards negative synaptic changes (*blue circles*), and this negative shift increases the larger SICs grow beyond the θ_d threshold (results not shown). In this case, STDP generally results in LTD with the exception of a LTP window that is comprised between ~0 ms and positive Δt values that are smaller than those in the absence of gliotransmission (Figure 6(c), *green circles*). This resembles what was previously observed for STDP curves in the presence of release-increasing gliotransmission, with the only difference that, for large $|\Delta t|$ values, LTD strength in the presence of astrocyte-mediated SICs is found to be the same, regardless of Δt (compare the *blue curve* in Figure 7(c) with the *green curve* in Figure 6(c)).

In Figure 7(d) we consider the alternative scenario where only SICs as large as typical EPSCs impinge on the postsynaptic neuron at different rates, yet always 100 ms before STDP-inducing pairings. Akin to what happens for SIC amplitudes, the larger the SIC frequency is, the more the STDP curve changes. Indeed, as SIC frequency increases above SIC decay rate (i.e., $1/\tau_A$, Appendix A, Section A.1.4), SIC-mediated Ca^{2+} transients start adding up, so that the fraction of time spent by Ca^{2+} beyond the LTD threshold increases favoring LTD induction. In this fashion, the ensuing STDP curve, once again, consists of a narrow LTP window for $\Delta t \geq 0$, outside which only LTD is observed (*red curve*). In practice however, because SICs occur at rates that are much slower than their typical decay (Appendix B), they likely affect STDP in a more subtle fashion. This may be readily understood considering the *pink* STDP *curve* obtained for SICs at 0.1 Hz, that is, the maximum rate experimentally recorded for these currents [22]. Inspection of this curve indeed suggests that SICs could effectively modulate LTD and LTP maxima as well as the outer sides of the LTD/LTP windows, which dictate how fast depression/potentiation decay for large $|\Delta t|$, but overall the qualitative features of the STDP curve are preserved with respect to the case without gliotransmission (*black curve*).

Clearly, the extent of the impact of SIC amplitude and frequency on STDP discussed in Figures 7(c) and 7(d) ultimately depends on when SICs occur with respect to ongoing STDP-inducing pairings. Had we set SICs to occur ~200 ms after pre/post Ca^{2+} transients in our simulations, then, as illustrated in Figures 8(a) and 8(b), we would have not detected any sensible alteration of STDP, unless SICs were larger than typical EPSCs and/or occurred at sufficiently high rate to generate Ca^{2+} transients beyond the plasticity thresholds

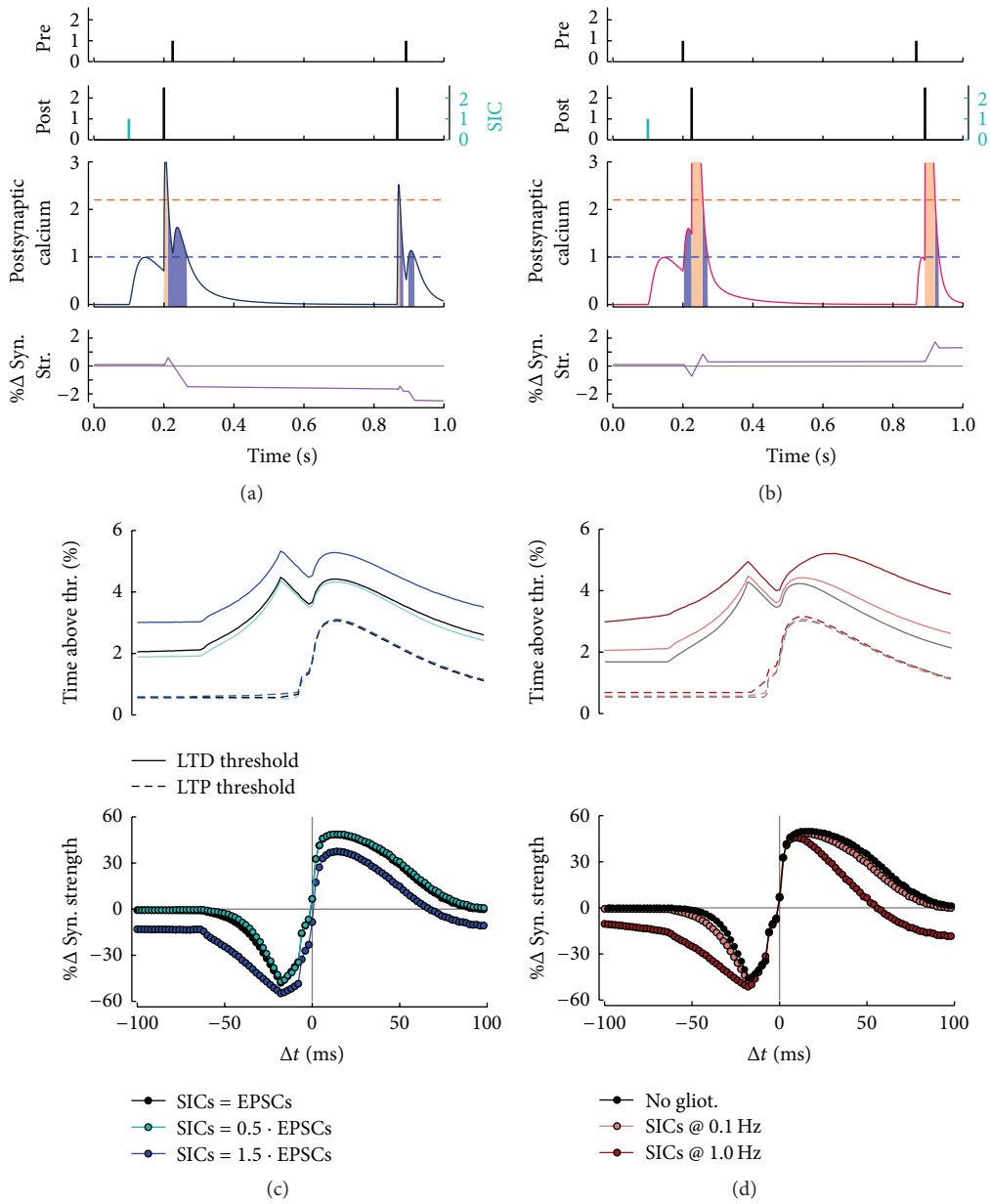

FIGURE 7: STDP modulation by gliotransmitter-mediated SICs. ((a), (b)) Inspection of postsynaptic Ca^{2+} in the initial part of a pairing protocol that includes a gliotransmitter-mediated slow inward current (SIC) arriving to the postsynaptic neuron at $t = 0.1$ s illustrates how SICs have the potential to modulate postsynaptic Ca^{2+} thereby regulating LTD and LTP. (c) The magnitude of modulation depends on how large SICs are with respect to synaptic inputs (EPSCs) as well as at (d) what rate they occur. ((c), (d)) STDP curves were calculated for 60 pre/post pairings at 1 Hz and included SICs starting 0.1 s before the first pairing and occurring at 0.1 Hz. Synaptic parameters: $\tau_d = 0.33$ s, $\tau_f = 0.33$ s, and $U_0 = 0.5$ s. Other parameters as in Table 1 except for $\varrho_e = 10^{-4}$, $\tau_c = 1$ ms, $\tau_e = 200$ ms, $\tau_S^r = 5$ ms, and $\tau_S = 100$ ms.

(results not shown). To seek understanding of how timing of SICs versus pre/post pairings could alter LTD and/or LTP, we simulated STDP induction by pairing as the time interval ($\Delta\varsigma$) between SIC and pre/post pairs was systematically varied (with SIC rate fixed at 0.2 Hz) (Figures 8(c)–8(e)). In doing so, we adopted the convention that negative $\Delta\varsigma$ values stand for SICs preceding pre/post (or post/pre) pairings while positive $\Delta\varsigma$ values refer to the opposite scenario of SICs that follow pairings (Figure 8(c), *top schematics*). Then, it may be observed that, for $\Delta\varsigma$ approximately in between −300 ms and 0 ms, LTD could be induced for any negative Δt as well as for large positive Δt (Figure 8(c), *blue tones*), in this latter case to the detriment of the LTP window, whose upper bound moves to lower Δt values (Figure 8(c), *red tones*). This results in STDP curves (e.g., Figure 8(f), *yellow curve* for $\Delta\varsigma = -75$ ms) that bear strong analogy with the blue and red curves in Figures 7(c) and 7(d), respectively, obtained for SICs of large amplitude and frequency and suggest that depression grows

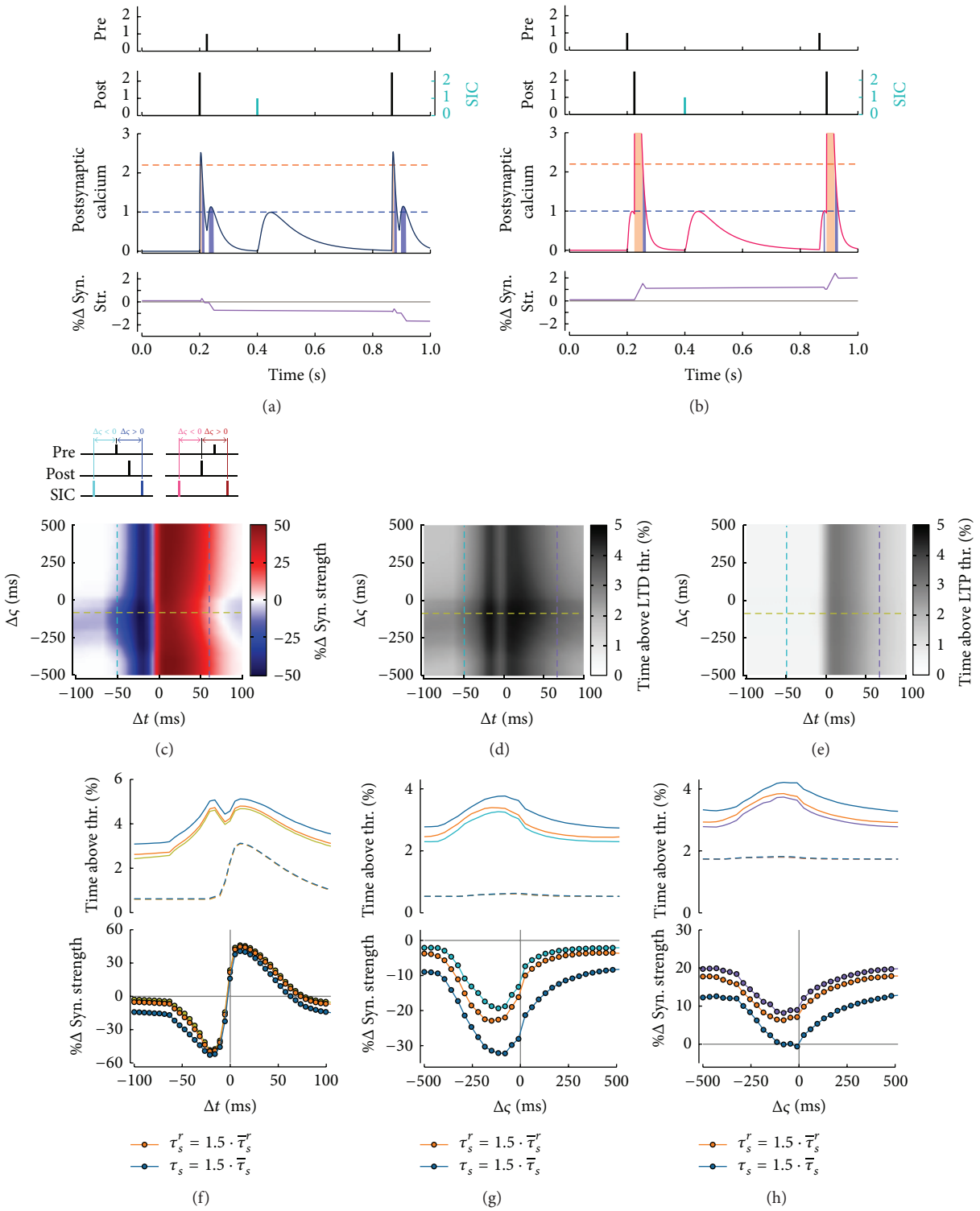

FIGURE 8: Effect on STDP of SIC timing with respect to pairings. ((a), (b)) Impact on plasticity of a SIC occurring 0.2 ms after the first pairing instead of 0.1 s before it as previously considered in Figures 7(a), 7(b). (c) STDP curves as a function of the SIC pre/post pair delay ($\Delta\varsigma$) show how LTD could get stronger while the LTP window shrink for small-to-intermediate $\Delta\varsigma \leq 0$ in correspondence with ((d), (e)) a maximum of the duration of Ca^{2+} transients above the LTD threshold. These results were obtained assuming SIC rise and decay time constants, respectively, equal to $\tau_s^r = \overline{\tau}_s^r = 20$ ms and $\tau_s = \overline{\tau}_s = 200$ ms. ((f), (h)) Peak and range of this LTD increase ultimately depend on SIC kinetics as reflected by the change of sample curves for specific $\Delta\varsigma$ (*yellow curve*) and spike-timing intervals (*cyan* and *purple curves*) when SIC rise and/or decay time constants were slowed down 1.5-fold (*orange* and *blue curves,* resp.). ((c), (h)) The same pairing protocol of Figures 7(c) and 7(d) was used but with a SIC frequency of 0.2 Hz and variable SIC onset and kinetics according to $\Delta\varsigma$, τ_S^r, and τ_S. Parameters as in Figure 7.

as SICs tend to concur with pre/post pairings. An inspection of postsynaptic Ca^{2+} transients (Figures 8(d) and 8(e)) indeed reveals that coincidence of SICs and pre/post pairings, which occurs at negative $\Delta\varsigma$ of the order of SIC rise time (see Appendix B), corresponds to the longest time spent by Ca^{2+} above the LTD threshold, thereby resulting in maximum LTD (Figure 8(g)) and thus minimum LTP (Figure 8(h)). Clearly, the $\Delta\varsigma$ range for which coincidence of SICs with pre/post pairings enhances LTD induction ultimately depends on kinetics of SICs, as reflected by their rise (τ_s^r) and/or decay time constants (τ_s), and spans $\Delta\varsigma$ values approximately comprised within ± SIC duration (i.e., $\simeq \tau_s^r + \tau_s$). As SIC duration increases in fact, because of either larger τ_s^r or larger τ_s or both, so does the $\Delta\varsigma$ range for LTD enhancement, as reflected by the *orange* and *blue curves* in Figures 8(f)–8(h).

In conclusion the simulations in Figures 8(c)–8(h) point to both timing and duration of SICs with respect to pre/post pairing-mediated Ca^{2+} transients as a further, potentially crucial factor in setting strength and polarity of STDP at glutamatergic synapses. It is noteworthy to emphasize that, however, to appreciate some effect on STDP, we had to assume in those simulations SICs occurring at 0.2 Hz, that is, twofold the maximum SIC rate (i.e., ~0.1 Hz) experimentally observed [22]. Indeed, analogous simulations run with realistic SIC rates $\leq$ 0.1 Hz did produce only marginal changes to STDP curves, akin to those previously observed for the *pink* STDP curve in Figure 7(d). The potential functional implications (or lack thereof) of this perhaps puzzling result are addressed in Discussion.

4. Discussion

A large body of evidence has accumulated over the last years suggesting an active role of astrocytes in many brain functions. Collectively, these data fuelled the concept that synapses could be tripartite rather than bipartite, since in addition to the pre- and postsynaptic terminals, the astrocyte could be an active element in synaptic transmission [1, 49, 117]. Using a computational modeling approach, we showed here that glutamatergic gliotransmission could indeed play several roles in synaptic information transfer, either modulating synaptic filtering or controlling postsynaptic neuronal firing, as well as regulating both short- and long-term forms of synaptic plasticity. Supported by experimental observations [8, 9, 13, 23, 118], these results complement and extend previous theoretical work on astrocyte-mediated regulations of synaptic transmission and plasticity [18, 29] and pinpoint biophysical conditions for a possible role of glutamatergic gliotransmission in spike-timing-dependent plasticity.

An important prediction of our model indeed is that both pathways of regulation of synaptic transmission by astrocytic glutamate considered in this study, presynaptic modulation of transmitter release and postsynaptic SICs, could affect STDP, potentially altering induction of LTP and LTD. This alteration could encompass changes in the timing between pre- and postsynaptic firing that is required for plasticity induction, as well as different variations of synaptic strength in response to the same stimulus. With this regard, the increase of LTP observed in our simulations, when moving from release-decreasing to release-increasing gliotransmission (Figure 6(e)), agrees with the experimental observation that LTP induction at hippocampal synapses requires weaker stimuli in the presence of endogenous glutamatergic gliotransmission rather than when gliotransmission is inhibited thereby decreasing synaptic release probability [9].

Notably, spike-timing-dependent plasticity in the hippocampus is not fully understood insofar as STDP induction by pairing protocols has produced a variety of seemingly contradicting observations for this brain region [119]. Recordings in hippocampal slices, for example, showed that pairing of single pre- and postsynaptic action potentials at positive spike-timing intervals could trigger LTP [120–122], as effectively expected by the classic STDP curve [123], but also induce either LTD [124] or no plasticity at all [121]. Although different experimental and physiological factors could account for these diverse observations [119, 125], we may speculate that glutamatergic gliotransmission by astrocytes, which in those experiments was not explicitly taken into account, could also provide an alternative explanation. For example, the prediction of our model that release-increasing glutamatergic gliotransmission could account for multiple LTD windows, at either positive or negative spike-timing intervals (Figure 6), indeed supports the possibility that LTD in the hippocampus could also be induced by proper presentations of pre $\rightarrow$ post pairings sequences [124]. On the same line of reasoning, the possibility that astrocyte-mediated SICs could transiently increase postsynaptic firing (Figure 5(f)) could explain why, in some experiments, precise spike timing in the induction of synaptic plasticity in the hippocampus could exist only when single EPSPs are paired with postsynaptic bursts [124, 126]. Moreover, it was also shown that postsynaptic firing is relatively less important than EPSP amplitude for the induction of STDP in the immature hippocampus compared to the mature network, possibly due to a reduced backpropagation of somatic APs in juvenile animals [121]. Remarkably, these diverse modes of plasticity induction could also ensue from different dynamics of glutamatergic gliotransmission, as likely mirrored by the developmental profile of somatic Ca^{2+} signals in hippocampal astrocytes [47], which have been reported to be much more frequent in young mice [127]. Insofar as somatic Ca^{2+} signals may result in robust astrocytic glutamate release that could trigger, in turn, similar increases of synaptic release and/or SICs [5, 62], the frequent occurrence of these latter could then ultimately guarantee a level of dendritic depolarization sufficient to produce LTP in mice pups [128].

High amplitude/rate SICs, or large increases of synaptic release mediated by glutamatergic gliotransmission, result, in our simulations, in LTD induction for any spike-timing interval except for a narrow LTP window at small-to-intermediate $\Delta t > 0$. This is in stark contrast with STDP experiments, where the observed plasticity always depends, to some extent, on the coincidence of pre- and postsynaptic activity, as EPSPs or postsynaptic action potentials fail to induce plasticity by their own [95, 105]. Apart from the consideration that large SIC amplitudes/rates and large increases of synaptic release by astrocytic glutamate may not reflect physiological conditions

[76, 90], this contrast may be further resolved on the basis of the following arguments.

A first consideration is that we simulated plasticity induction assuming either persistent occurrence of SICs or continuous modulations of synaptic release during the whole induction protocol. While this rationale proved useful to identify the possible mechanisms of regulation of STDP by glutamatergic gliotransmission, it may likely not reflect what occurs in reality. Indeed, modulations of synaptic release by glutamatergic gliotransmission could last only few tens of seconds [7, 8] and thus be short-lived with respect to typical induction protocols which are of the order of minutes [33, 105, 129]. Moreover, the morphology of astrocytic perisynaptic processes is not fixed but likely undergoes dynamical reshaping in an activity-dependent fashion during plasticity induction [118, 130], thereby potentially setting time and spatial range of action of gliotransmission on nearby synaptic terminals [18]. In this fashion, LTD for large spike-timing intervals could be induced only transiently and at selected synapses, focally targeted by glutamatergic gliotransmission, while leaving unchanged the qualitative features of the classic STDP curve obtained by somatic recordings in the postsynaptic neuron [129].

A further aspect that we did not take into account in our simulations is also the possible voltage dependence of astrocyte-triggered SICs. The exact nature of this dependence remains to be elucidated and likely changes with subunit composition of NMDA receptors that mediate SICs in different brain regions and at different developmental stages [77]. Regardless, it may be generally assumed that slow inward currents through NMDA receptors become substantial only for intermediate postsynaptic depolarizations when the voltage-dependent Mg^{2+} block of these receptors is released [108]. In this fashion, the possible effect of SICs on STDP would be confined in a time window around $\Delta t \geq 0$ for which coincidence with pre- and postsynaptic spikes allows for robust depolarization of postsynaptic spines. Outside this window instead, SICs would be negligible, and plasticity induction would essentially depend on mere pre- and postsynaptic spiking rescuing the experimental observation of no synaptic modification for large spike-timing intervals [95, 105].

On the other hand, even without considering voltage dependence of SIC-mediating NMDARs, the precise timing of SICs with respect to pre/post pairs is predicted by our analysis, to be potentially critical to determine strength and sign of plasticity. Similar considerations could also hold for the onset time and duration of modulations of synaptic release triggered by gliotransmission with respect to the temporal features of plasticity-inducing stimuli [29]. This ultimately points to timing of glutamate release by the astrocyte (and its downstream effects on synaptic transmission) as a potential additional factor for associative (Hebbian) learning, besides sole correlation between pre- and postsynaptic activities [131, 132]. Remarkably, this could also provide a framework to conciliate the possibility that modest, sporadic SICs that we predict would not substantially affect STDP (Figure 7) could do so instead [32]. Indeed our predictions are based on the average number of SICs within a given time window, as documented in literature, rather than on the precise timing of those SICs in that time window. In this fashion, for example, there is no distinction in terms of effect on STDP in our simulations, between a hypothetical scenario of three SICs randomly occurring on average every ~10 s in a 30 s time frame and the alternative scenario of three SICs taking place within the same time frame but in rapid succession (Figure 5b in [22]), as could happen following an exocytic burst of glutamate release by the astrocyte [61, 62, 65]. Yet the latter case could result in a dramatically different plasticity outcome with respect to the former. While individual SICs likely fail to induce synaptic modification alone in fact, their occurrence in rapid succession would instead allow postsynaptic Ca^{2+} levels to quickly increase beyond one of the thresholds for plasticity induction. Furthermore, this increase could further be boosted by coincidence of SICs with pre- and postsynaptic activity, ultimately accounting for robust LTP, as indeed predicted by other theoretical investigations [36]. However, to complicate this intriguing scenario is the observation that glutamatergic gliotransmission [65] and even more so astrocyte-mediated SICs [19, 25] are likely not deterministic but rather stochastic processes. Therefore, it would ultimately be interesting to understand how this stochasticity could affect neuronal activity and shape learning [133].

To conclude, our analysis provides theoretical arguments in support of the hypothesis that, beyond neuronal firing, astrocytic gliotransmission could represent an additional factor in the regulation of activity-dependent plasticity and learning [18, 134, 135]. This could occur in a variegated fashion by both presynaptic and postsynaptic elements targeted by glutamatergic gliotransmission, with possibly diverse functional consequences. Nonetheless, the practical observation in future experiments of a possible mechanism of action of glutamatergic gliotransmission on activity-dependent plasticity will depend on the implementation of novel specific plasticity-inducing protocols that match possible stringent temporal and spatial dynamical constraints defining the complex nature of neuron-astrocyte interactions.

Appendix

A. Modeling Methods

A.1. Synapse Model with Glutamatergic Gliotransmission

A.1.1. Synaptic Release. To study modulation of short-term synaptic plasticity by gliotransmitter-bound extrasynaptically located presynaptic receptors we extend the model originally introduced by De Pittà et al. [73] for astrocyte-mediated heterosynaptic modulation of synaptic release to also account for the homosynaptic scenario. For the sake of clarity, in the following we will limit our description to excitatory (glutamatergic) synapses. Accordingly, synaptic glutamate release is described following Tsodyks [55], whereby upon arrival of an action potential (AP) at time t_k, the probability of glutamate resources to be available for release (u_S) increases by a factor u_0, while the readily releasable glutamate resources (x_S) decrease by a fraction $r_S(t_k) = u_S(t_k^+)x_S(t_k^-)$, corresponding to the fraction of

effectively released glutamate. In between APs, glutamate resources are reintegrated at a rate of $1/\tau_d$ while u_S decays to zero at a rate of $1/\tau_f$. The equations for u_S, x_S thus read [55]

$$\begin{aligned}\tau_f \frac{\mathrm{d}}{\mathrm{d}t} u_S &= -u_S + \sum_k u_0 \left(1 - u_S\right) \delta\left(t - t_k\right) \tau_f, \\ \tau_d \frac{\mathrm{d}}{\mathrm{d}t} x_S &= 1 - x_S - \sum_k r_S\left(t\right) \delta\left(t - t_k\right) \tau_d.\end{aligned} \tag{A.1}$$

The parameter u_0 in the above equations may be interpreted as the synaptic release probability at rest. Indeed, the synapse is "at rest" when $u_S \to 0$ and $x_S \to 1$, which occurs when the period of incoming Aps is much larger than the synaptic time scales τ_d, τ_f. Then, in this case, the probability of glutamate release from the synapse by an AP equals u_0.

A.1.2. Neurotransmitter Time Course. Assuming a total vesicular glutamate concentration of Y_T, the released glutamate, expressed as concentration in the synaptic cleft, is then equal to $Y_{\mathrm{rel}}(t_k) = \varrho_c Y_T r_S(t_k)$, where ϱ_c represents the ratio between vesicular and synaptic cleft volumes. The time course of synaptically released glutamate in the cleft (Y_S) depends on several mechanisms, including clearance by diffusion, uptake, and/or degradation [56, 57]. In the simplest approximation, the contribution of these mechanisms to glutamate time course in the cleft may be modeled by a first-order degradation reaction of characteristic time τ_c [58] so that

$$\tau_c \frac{\mathrm{d}}{\mathrm{d}t} Y_S = -Y_S + \sum_k Y_{\mathrm{rel}} \delta\left(t - t_k\right) \tau_c. \tag{A.2}$$

A.1.3. Astrocytic Calcium Dynamics. We assume that only a fraction ζ of released glutamate binds to postsynaptic receptors, while the remainder $1 - \zeta$ fraction spills out of the cleft and activates astrocytic metabotropic receptors which trigger astrocytic Ca^{2+} signaling. The latter is modeled following Wallach et al. [136] and results from the interplay of four quantities: (i) the fraction of activated astrocytic receptors (γ_A); (ii) the cytosolic IP_3 (I) and (iii) Ca^{2+} concentrations (C) in the astrocyte; and (iv) the fraction of deinactivated IP_3 receptors (IP_3Rs) on the membrane of the astrocyte's endoplasmic reticulum (ER) that mediate Ca^{2+}-induced Ca^{2+}-release (h). In particular, considering each quantity separately, the fraction of astrocytic receptors bound by synaptic glutamate may be approximated, at first instance, by a first-order binding reaction and thus evolves according to [136]

$$\tau_A \frac{\mathrm{d}}{\mathrm{d}t} \gamma_A = -\gamma_A + O_M \left(1 - \zeta\right) Y_S \left(1 - \gamma_A\right) \tau_A, \tag{A.3}$$

with τ_A representing the characteristic receptor deactivation (unbinding) time constant. Cytosolic IP_3 results instead from the complex Ca^{2+}-modulated interplay of phospholipase Cβ- and Cδ-mediated production and degradation by IP_3 3-kinase (3K) and inositol polyphosphatase 5-phosphatase (5P) [137–140] and evolves according to the mass balance equation [141]:

$$\frac{\mathrm{d}}{\mathrm{d}t} I = J_\beta\left(\gamma_A\right) + J_\delta\left(C, I\right) - J_{3\mathrm{K}}\left(C, I\right) - J_{5\mathrm{P}}\left(I\right), \tag{A.4}$$

where

$$\begin{aligned}J_\beta\left(\gamma_A\right) &= O_\beta \gamma_A, \\ J_\delta\left(C, I\right) &= O_\delta \frac{\kappa_\delta}{\kappa_\delta + I} \mathscr{H}\left(C^2, K_\delta\right), \\ J_{3\mathrm{K}}\left(C\right) &= O_{3\mathrm{K}} \mathscr{H}\left(C^4, K_D\right) \mathscr{H}\left(I, K_3\right), \\ J_{5\mathrm{P}}\left(I\right) &= \Omega_{5\mathrm{P}} I\end{aligned} \tag{A.5}$$

and $\mathscr{H}(x^n, K)$ denotes the sigmoid (Hill) function $x^n/(x^n + K^n)$. Finally, cytosolic Ca^{2+} and the IP_3R gating are described by a set of Hodgkin-Huxley-like equations according to the model originally introduced by Li and Rinzel [142]:

$$\begin{aligned}\frac{\mathrm{d}}{\mathrm{d}t} C &= J_C\left(C, h, I\right) + J_L\left(C\right) - J_P\left(C\right), \\ \frac{\mathrm{d}}{\mathrm{d}t} h &= \frac{h_\infty\left(C, I\right) - h}{\tau_h\left(C, I\right)},\end{aligned} \tag{A.6}$$

where J_C, J_L, and J_P, respectively, denote the IP_3R-mediated Ca^{2+}-induced Ca^{2+}-release from the ER (J_C), the Ca^{2+} leak from the ER (J_L), and the Ca^{2+} uptake from the cytosol back to the ER by serca-ER Ca^{2+}/ATPase pumps (J_P) [141]. These terms, together with the IP_3R deinactivation time constant (τ_h) and steady-state probability (h_∞), are given by [142, 143]

$$\begin{aligned}J_C\left(C, h, I\right) &= \Omega_C m_\infty^3 h^3 \left(C_T - \left(1 + \varrho_A\right) C\right), \\ m_\infty\left(C, I\right) &= \mathscr{H}\left(I, d_1\right) \mathscr{H}\left(C, d_5\right), \\ J_L\left(C\right) &= \Omega_L \left(C_T - \left(1 + \varrho_A\right) C\right), \\ J_P\left(C\right) &= O_P \mathscr{H}\left(C^2, K_P\right), \\ h_\infty\left(C, I\right) &= d_2 \frac{I + d_1}{d_2\left(I + d_1\right) + \left(I + d_3\right) C}, \\ \tau_h\left(C, I\right) &= \frac{I + d_3}{\Omega_2\left(I + d_1\right) + O_2\left(I + d_3\right) C}.\end{aligned} \tag{A.7}$$

A detailed explanation of the parameters of the astrocyte model may be found in Table 1.

A.1.4. Calcium-Dependent Glutamatergic Gliotransmission. Astrocytic glutamate exocytosis is modeled akin to synaptic glutamate release, assuming that a fraction $x_A(t)$ of gliotransmitter resources is available for release at any time t. Then, every time t_j that astrocytic Ca^{2+} increases beyond a threshold concentration C_θ, a fraction of readily releasable astrocytic glutamate resources, that is, $r_A(t_j) = U_A x_A(t_j^-)$, is released into the periastrocytic space and later reintegrated at rate $1/\tau_A$. Hence, $x_A(t)$ evolves according to [73]

$$\tau_G \frac{\mathrm{d}}{\mathrm{d}t} x_A = 1 - x_A - \sum_j r_A\left(t\right) \delta\left(t - t_j\right) \tau_G. \tag{A.8}$$

Similarly to (A.2), we may estimate the contribution to glutamate concentration in the periastrocytic space (G_A), resulting from a quantal glutamate release event by the astrocyte at $t = t_j$, as $G_{\text{rel}}(t_j) = \varrho_e G_T r_A(t_j)$, where G_T represents the total vesicular glutamate concentration in the astrocyte and ϱ_e is the volume ratio between glutamate-containing astrocytic vesicles and periastrocytic space. Then, assuming a clearance rate of glutamate of $1/\tau_e$, the time course of astrocyte-derived glutamate in the extracellular space comprised between the astrocyte and the surrounding synaptic terminals is given by

$$\tau_e \frac{\mathrm{d}}{\mathrm{d}t} G_A = -G_A + \sum_j G_{\text{rel}}(t)\, \delta\left(t - t_j\right) \tau_e. \tag{A.9}$$

A.1.5. Presynaptic Pathway for Glutamatergic Gliotransmission. The extracellular glutamate concentration sets the fraction of bound extrasynaptically located presynaptic receptors (γ_S) according to [73]

$$\tau_P \frac{\mathrm{d}}{\mathrm{d}t} \gamma_S = -\gamma_S + O_P\left(1 - \gamma_S\right) G_A \tau_P, \tag{A.10}$$

where O_P and τ_P, respectively, denote the rise rate and the decay time of the effect of gliotransmission on synaptic glutamate release. It is then assumed that modulations of synaptic release by gliotransmitter-bound presynaptic receptors are brought forth by modulations of the resting synaptic release probability; that is, $u_0 = u_0(\gamma_S)$. In an attempt to consider a mechanism as general as possible, rather than focusing on a specific functional dependence for $u_0(\gamma_S)$, we consider only the first-order expansion of this latter [73]; that is,

$$u_0\left(\gamma_S\right) \approx U_0 + \left(\xi - U_0\right) \gamma_S, \tag{A.11}$$

where U_0 denotes the synaptic release probability at rest in the absence of gliotransmission, whereas the parameter ξ lumps, in a phenomenological way, the information on the effect of gliotransmission on synaptic release. For $0 \le \xi < U_0$, u_0 decreases with γ_S, consistent with a "release-decreasing" effect of astrocytic glutamate on synaptic release. This could be the case, for example, of astrocytic glutamate binding to presynaptic kinate receptors or group II/III mGluRs [13, 14, 71]. For $U_0 < \xi \le 1$, u_0 increases with γ_S, consistent with a "release-increasing" effect of astrocytic gliotransmitter on synaptic release, as in the case of presynaptic NMDARs or group I mGluRs [2, 7–9, 11, 12, 72]. Finally, the special case where $\xi = U_0$ corresponds to occlusion, that is, coexistence and balance between release-decreasing and release-increasing glutamatergic gliotransmission at the same synapse resulting in no net effect of this latter on synaptic release.

Although based on glutamatergic synapses, the set of (A.1)–(A.11) provides a general description for modulations of synaptic release mediated by glutamatergic gliotransmission that could also be easily extended to other types of excitatory synapses [144] as well as inhibitory synapses [14, 45, 145, 146].

A.1.6. Postsynaptic Pathways for Glutamatergic Gliotransmission: Slow Inward Currents. Postsynaptic astrocyte-mediated slow inward currents take place through extrasynaptic NMDA receptors. The subunit composition of these receptors however remains unclear [77]. Several studies reported SICs to be inhibited by antagonists of NR2B-containing NMDARs [21, 24, 78]; however there is also evidence that other NMDAR types could be involved, possibly containing subunits NR2C or NR2D [25]. Being mediated by NMDA receptors, SICs are likely affected by voltage dependence of the Mg^{2+} block of these receptors. Although there is evidence that SICs rate and frequency could indeed depend on extracellular Mg^{2+} [21], the effective nature of the possible voltage dependence of SICs has not been elucidated. Moreover, the potential diversity of subunit composition of receptors mediated SICs could also result in different voltage dependencies, strong for NR2B-containing receptors, akin to postsynaptic NMDARs, and weak otherwise [111]. Accordingly, in this study we neglect the possible voltage dependence of SICs arguing that this is not substantially changing the essence of our results (see Discussion). In this fashion, denoting postsynaptic SICs by $i_A(t)$, we model them by a difference of exponentials according to

$$\tau_S^r \frac{\mathrm{d}}{\mathrm{d}t} i_A(t) = -i_A(t) + \widehat{I}_A B_A(t)\, \tau_S^r, \tag{A.12}$$

$$\tau_S \frac{\mathrm{d}}{\mathrm{d}t} B_A(t) = -B_A(t) + \widehat{J}_A G_A(t)\, \tau_S, \tag{A.13}$$

where τ_S^r and τ_S, respectively, are rise and decay time constants for SICs. The two scaling factors $\widehat{I}_A$ and $\widehat{J}_A$ are taken such that the SIC maximum in correspondence with an event of glutamate release by the astrocyte is equal to a constant value I_A (see Appendix B).

A.1.7. Postsynaptic Neuron. Postsynaptic action potential firing is modeled by a leaky integrate-and-fire (LIF) neuron [91, 92]. Accordingly, the membrane potential (v) of the postsynaptic neuron evolves as

$$\tau_m \frac{\mathrm{d}}{\mathrm{d}t} v = E_L - v + i_S(t) + i_A(t), \tag{A.14}$$

where τ_m denotes the membrane time constant and $i_S(t)$ represents the excitatory synaptic input to the neuron. Every time v crosses the firing threshold v_θ, an AP is emitted and the membrane potential is reset to v_r and kept at this value for the duration of a refractory period τ_r.

For synaptic currents, we only consider the AMPA receptor-mediated fast component of EPSCs. Accordingly, we consider two possible descriptions for $i_S(t)$. In Figures 3 and 4, we assume that the rise time of synaptic currents is very short compared to the relaxation time of these latter [147–149], so that $i_S(t)$ can be modeled by a sum of instantaneous jumps of

amplitude $\widehat{J}_S$, each followed by an exponential decay [91]; that is,

$$\tau_N \frac{\mathrm{d}}{\mathrm{d}t} i_S(t) = -i_S(t) + \widehat{J}_S \zeta Y_S(t)\, \tau_N. \tag{A.15}$$

In the presence of gliotransmitter-mediated slow inward currents instead (Figure 5), we model synaptic currents similarly to these latter; that is,

$$\tau_N^r \frac{\mathrm{d}}{\mathrm{d}t} i_S(t) = -i_S(t) + \widehat{I}_S B_S(t)\, \tau_N^r, \tag{A.16}$$

$$\tau_N \frac{\mathrm{d}}{\mathrm{d}t} B_S(t) = -B_S(t) + \widehat{J}_S \zeta Y_S(t)\, \tau_N, \tag{A.17}$$

where τ_N^r, τ_N, respectively, denote EPSC rise and decay time constants; the scaling factor $\widehat{J}_S$ is taken such that synaptic releases result in unitary increases of the gating variable B_S, and similarly, $\widehat{I}_S$ is set such that an increase in synaptic current ensuing from quantal synaptic release equals to I_S.

A.2. Spike-Timing-Dependent Plasticity

A.2.1. Postsynaptic Calcium Dynamics. Spike-timing-dependent plasticity is modeled by the nonlinear calcium model introduced by Graupner and Brunel [102], which was modified to include short-term synaptic plasticity as well as astrocyte-mediated SIC contribution to postsynaptic Ca^{2+}. Accordingly, postsynaptic Ca^{2+} dynamics, $c(t)$, result from the sum of three contributions: (i) Ca^{2+} transients mediated by NMDA receptors, activated by synaptic glutamate whose release probability from the presynaptic bouton may be modulated by gliotransmission (c_{pre}), (ii) Ca^{2+} transients mediated by gliotransmitter-triggered NMDA-mediated SICs (c_{sic}), and (iii) Ca^{2+} transients due to activation of voltage-dependent Ca^{2+} channels (VDCCs) by postsynaptic backpropagating APs (c_{post}). All three Ca^{2+} transients are accounted for by a difference of exponentials. In particular, presynaptic Ca^{2+} transients are described by

$$\begin{aligned} \tau_{\mathrm{pre}}^r \frac{\mathrm{d}}{\mathrm{d}t} c_{\mathrm{pre}} &= -c_{\mathrm{pre}} + \widehat{C}_{\mathrm{pre}} R_{\mathrm{pre}} \tau_{\mathrm{pre}}^r, \\ \tau_{\mathrm{pre}} \frac{\mathrm{d}}{\mathrm{d}t} R_{\mathrm{pre}} &= -R_{\mathrm{pre}} + W_N \zeta Y_S \tau_{\mathrm{pre}}, \end{aligned} \tag{A.18}$$

where $\tau_{\mathrm{pre}}^r, \tau_{\mathrm{pre}}$ are rise and decay time constants of the Ca^{2+} transient; $\widehat{C}_{\mathrm{pre}}$ is a normalization constant such that the maximal amplitude of the transient is C_{pre}; W_N is the "weight" of presynaptic Ca^{2+} transients triggered by synaptic glutamate (Y_S, equation (A.2)).

Similarly to presynaptic ones, calcium transients due to SICs mediated by gliotransmission are given by

$$\begin{aligned} \tau_{\mathrm{sic}}^r \frac{\mathrm{d}}{\mathrm{d}t} c_{\mathrm{sic}} &= -c_{\mathrm{sic}} + \widehat{C}_{\mathrm{sic}} R_{\mathrm{sic}} \tau_{\mathrm{sic}}^r, \\ \tau_{\mathrm{sic}} \frac{\mathrm{d}}{\mathrm{d}t} R_{\mathrm{sic}} &= -R_{\mathrm{sic}} + W_A G_A \tau_{\mathrm{sic}}, \end{aligned} \tag{A.19}$$

where τ_{sic}^r and τ_{sic}^d are the rise and decay time constants of the Ca^{2+} transient; and $\widehat{C}_{\mathrm{sic}}$ is a normalization constant such that the maximal amplitude of the transient is C_{sic}; W_A is the "weight" of SIC-mediated Ca^{2+} transients triggered by perisynaptic gliotransmitter (G_A, equation (A.9)).

Finally, postsynaptic Ca^{2+} transients caused by bAPs are modeled by [102]

$$\begin{aligned} \tau_{\mathrm{post}}^r \frac{\mathrm{d}}{\mathrm{d}t} c_{\mathrm{post}} &= -c_{\mathrm{post}} + \widehat{C}_{\mathrm{post}} R_{\mathrm{post}} \tau_{\mathrm{post}}^r, \\ \tau_{\mathrm{post}} \frac{\mathrm{d}}{\mathrm{d}t} R_{\mathrm{post}} &= -R_{\mathrm{post}} \\ &\quad + \left(1 + \eta c_{\mathrm{pre}}\right) \sum_i \delta\left(t - t_i\right) \tau_{\mathrm{post}}, \end{aligned} \tag{A.20}$$

where the sum goes over all postsynaptic APs occurring at times t_i; τ_{post}^r and τ_{post} are the rise and decay time constants of the Ca^{2+} transient; $\widehat{C}_{\mathrm{post}}$ is a scaling factor such that the maximal amplitude of the transient is C_{post}, and the parameter η denotes how much a bAP-evoked Ca^{2+} transient is increased by preceding presynaptic stimulation.

A.2.2. Synaptic Efficacy. The temporal evolution of synaptic efficacy $\rho(t)$ depends on postsynaptic Ca^{2+} dynamics $c(t) = c_{\mathrm{pre}}(t) + c_{\mathrm{sic}}(t) + c_{\mathrm{post}}(t)$ and is described by the first-order differential equation [102]:

$$\begin{aligned} \tau_\rho \frac{\mathrm{d}}{\mathrm{d}t} \rho &= -\rho\left(1 - \rho\right)\left(\rho_\star - \rho\right) \\ &\quad + \gamma_p \left(1 - \rho\right) \Theta\left(c(t) - \theta_p\right) \\ &\quad - \gamma_d \rho \Theta\left(c(t) - \theta_d\right) + \mathrm{Noise}(t), \end{aligned} \tag{A.21}$$

where $\rho_\star$ is the boundary of the basins of attraction of UP and DOWN states of synaptic efficacy, that is, the states for which $\rho = 1$ and $\rho = 0$, respectively; θ_d, θ_p denote the depression (LTD) and potentiation (LTP) thresholds, and γ_d, γ_p measure the corresponding rates of synaptic decrease and increase when these thresholds are exceeded; $\Theta(\cdot)$ denotes the Heaviside function, that is, $\Theta(c - \theta) = 0$ for $c < \theta$ and $\Theta(c - \theta) = 1$ for $c \geq \theta$. The last term lumps an activity-dependent noise term in the form of $\mathrm{Noise}(t) = \sigma\sqrt{\tau_\rho}\sqrt{\Theta(c(t) - \theta_d) + \Theta(c(t) - \theta_p)} \cdot \varpi(t)$, where $\varpi(t)$ is a Gaussian white noise process with unit variance density. This term accounts for activity-dependent fluctuations stemming from stochastic neurotransmitter release, stochastic channel opening, and diffusion [102].

A.3. STDP Curves. To construct the STDP curves of Figures 6–8, we follow the rationale originally described by Graupner and Brunel [102] and consider the average synaptic strength of a synaptic population after a stimulation protocol of n pre-post (or post-pre) pairs presented at time interval T. With this aim, synaptic strength is surmised to be linearly related to ρ as $w = w_0 + \rho(w_1 - w_0)$, where w_0 and w_1 are the synaptic strength of the DOWN/UP

states for which ρ_0, that is, the initial value of ρ at $t = 0$, is 0 or 1, respectively. In this fashion, w may be thought of as a rescaled version of equivalent experimental measures of synaptic strength such as the excitatory postsynaptic potential (EPSP) or excitatory postsynaptic current (EPSC) amplitude, the initial EPSP slope, or the current in 2 ms windows at the EPSC peak. Accordingly, before a stimulus protocol, a fraction β of the synapses is taken in the DOWN state, so that the average initial synaptic strength is $\overline{w}_0 = \beta w_0 + (1-\beta)w_1$. Then, after the stimulation protocol, the ensuing average synaptic strength is $\overline{w}_1 = w_0((1-\mathcal{U})\beta + \mathcal{D}(1-\beta)) + w_1(\mathcal{U}\beta + (1-\mathcal{D})(1-\beta))$, where $\mathcal{U}$ and $\mathcal{D}$ represent the UP and DOWN transition probabilities, respectively. As in experiments, we consider the change in synaptic strength as the ratio between the average synaptic strengths after and before the stimulation; that is,

$$\Delta\rho = \frac{(1-\mathcal{U})\,\beta + \mathcal{D}\,(1-\beta) + b\,(\mathcal{U}\beta + (1-\mathcal{D})\,(1-\beta))}{\beta + (1-\beta)\,b}, \tag{A.22}$$

with $b = w_1/w_0$. Under the hypotheses of this study, that is, $T \ll \tau_\rho$ and γ_d, γ_p are large, the transition probabilities $\mathcal{U}$ and $\mathcal{D}$ may be analytically solved and read [102]:

$$\begin{aligned}\mathcal{U}(\rho_0) &= \frac{1}{2}\left(1 + \operatorname{erf}\left(-\frac{\rho_\star - \overline{\rho} + (\rho-\rho_0)\,\mathrm{e}^{-nT/\tau}}{\sqrt{\sigma_\rho}\,(1-\mathrm{e}^{-2nT/\tau})}\right)\right),\\ \mathcal{D}(\rho_0) &= \frac{1}{2}\left(1 - \operatorname{erf}\left(-\frac{\rho_\star - \overline{\rho} + (\rho-\rho_0)\,\mathrm{e}^{-nT/\tau}}{\sqrt{\sigma_\rho}\,(1-\mathrm{e}^{-2nT/\tau})}\right)\right),\end{aligned} \tag{A.23}$$

where erf denotes the standard error function, defined as $\operatorname{erf}(x) = (2/\sqrt{\pi})\int_0^x \mathrm{e}^{-t^2}\mathrm{d}t$ and

$$\begin{aligned}\overline{\rho} &= \frac{\Gamma_p}{\Gamma_d + \Gamma_p},\\ \sigma_\rho^2 &= \frac{\alpha_d + \alpha_p}{\Gamma_d + \Gamma_p}\sigma^2,\\ \tau &= \frac{\tau_\rho}{\Gamma_d + \Gamma_p},\end{aligned} \tag{A.24}$$

with $\Gamma_i = \gamma_i\alpha_i$ and $\alpha_i = (1/nT)\int_0^{nT}\Theta(c(t)-\theta_i)\mathrm{d}t$ with $i = d, p$.

A.4. Simulations. The model was implemented in Brian 2.0 [150]. Simulations and data analysis were serendipitously designed and performed by the open source programming language Python 2.7 [151]. The code is available online and can be downloaded from terminal by "git clone https://mauriziodepitta@bitbucket.org/mauriziodepitta/public.code.git -b NeuralPlasticity-2016."

B. Parameter Estimation

B.1. Synaptic Parameters. Glutamate release probability U_0 of central excitatory synapses is generally comprised between ~0.09 [152] and ~0.6–0.9 [153, 154], with lower values mostly consistent with facilitating synapses [155]. Facilitation time constants τ_f may be estimated by the decay time of intracellular Ca^{2+} increases at presynaptic terminals upon arrival of action potentials [156, 157]. With this regard, typical decay times for Ca^{2+} transients are reported to be <500 ms [157], with an upper bound within 0.65–2 s [156]. Concerning depression time constants instead, experiments have reported glutamate-containing vesicles in the readily releasable pool to preferentially undergo rapid endocytosis within 1-2 s after release [158], although vesicle recycling could also be as fast as 10–20 ms [153, 159].

Estimates in hippocampal synapses suggest that the readily releasable pool could contain between 2 and 27 vesicles [152] which are essentially spherical with average outer diameter d_S equal to 39.2 ± 11.4 nm and in the range of 23–49 nm [160, 161]. Subtracting to this value a 6 nm thick vesicular membrane [152], the inner diameter of a vesicle can then be estimated within 16–38 nm, corresponding to a mean vesicular volume Λ_S in the range of $2.1\cdot10^{-21}$–$28.7\cdot10^{-21}$ dm^3. Given that vesicular glutamate concentration is reported in the range of 60–210 mM [160–162], then, considering a pool of 10 vesicles with average diameter of 30 nm (i.e., average volume $\Lambda_S \approx 14.1\cdot10^{-21}$ dm^3) and average vesicular neurotransmitter concentration of 60–100 mM [161], the total neurotransmitter vesicular content ranges up to $Y_T = (10)(60\text{–}100\ \mathrm{mM}) = 300\text{–}1000\ \mathrm{mM}$. Assuming a typical neurotransmitter release time of $t_{\mathrm{rel}} = 25\,\mu\mathrm{s}$ [163] and a diffusion constant for glutamate in the synaptic cleft of $D_{\mathrm{Glu}} = 0.33\,\mu\mathrm{m}^2/\mathrm{ms}$ [164], the average diffusion length (ℓ_c) of a glutamate molecule from the release site can be estimated by the Einstein-Smoluchowski relationship [152] whereby $\ell_c = \sqrt{(2\cdot D_{\mathrm{Glu}}\cdot t_{\mathrm{rel}})} = \sqrt{(2\cdot 0.33\,\mu\mathrm{m}^2/\mathrm{ms}\cdot 0.025\ \mathrm{ms})} \approx 0.129\,\mu\mathrm{m}$. Thus, the associated mixing volume Λ_c, namely, the effective diffusion volume which the released glutamate has rapid access to, can be estimated by the volume of the disk of radius ℓ_c and thickness h_c equal to the average width of the synaptic cleft [165]. Considering $h_c = 20$ nm [152], it is $\Lambda_c = \pi\ell_c^2 h_c = \pi\cdot(0.129\,\mu\mathrm{m})^2(0.020\,\mu\mathrm{m}) \approx 8.89\cdot10^{-18}$ dm^3 which falls in the experimental range of volumes of nonsynaptic interfaces at hippocampal synapses elsewhere reported [166]. Considering vesicular release from at least 3 independent sites [167], it follows that the ratio between vesicle volume and mixing volume is $\varrho_c = \Lambda_S/\Lambda_c = (3)(14.1\cdot10^{-21}\ \mathrm{dm}^3)/(8.89\cdot10^{-18}\ \mathrm{dm}^3) \approx 0.005$, so that the contribution to the concentration of glutamate in the extracellular space following a release event is $Y_{\mathrm{rel}} = \varrho_c\cdot U_0\cdot Y_T$. Hence, for a sample value of $U_0 = 0.5$ [153] with a choice of $Y_T = 500$ mM, for example, the latter equals $Y_{\mathrm{rel}} = (0.005)(0.5)(500\ \mathrm{mM}) \approx 1.25$ mM.

Such released glutamate is then rapidly cleared from the extracellular space by combined action of diffusion and uptake by transporters [168]. As a result the time course of glutamate in the synaptic cleft is short, with an estimated decay constant within ~2–10 ms [57, 169]. However, slower

clearance times could also be possible since resting glutamate concentrations in the extracellular space surrounding activated synapses are recovered only ~100 ms after the stimulus [170, 171]. Based on these considerations, we consider an intermediate value of glutamate clearance time of $\tau_c = 25$ ms.

B.2. Astrocyte Parameters. Astrocyte parameters reported in Appendix C were estimated on extensive numerical explorations of the astrocyte model aimed at reproducing experimental whole-cell Ca^{2+} elevations with rise and decay time constants, respectively, in the ranges of 3–20 s and 3–25 s and with full-width half-maximum (FWHM) values within 5–160 s [172–174]. In doing so, we considered a ratio between ER and cytoplasmic volumes (ϱ_A) of 0.18 in line with the experimental observation that the probability of ER localization in the cytoplasmic space at astrocytic somata is within ~20–70% [175]. Moreover, the cell's total Ca^{2+} concentration (measured with respect to the cytoplasmic volume) was fixed at $C_T = 2\,\mu$M, while Ca^{2+} affinity of sarco-ER pumps (SERCAs) was taken equal to 0.05 μM [176, 177], assuring peak Ca^{2+} concentrations < 5 μM in agreement with experiments [178, 179].

Activation rate and unbinding time constants O_A, τ_A of astrocytic receptors may be estimated by rise times of agonist-triggered Ca^{2+} signals. With this regard, application of 50 μM of DHPG, a potent agonist of group I subtype 5 mGluRs, the main type of mGluRs expressed by astrocytes [180], triggered submembrane Ca^{2+} signals characterized by a rise time $\tau_r = 0.272 \pm 0.095$ s. Because mGluR5 affinity ($K_{0.5}$) for DHPG is ~2 μM [181], which is much smaller than the applied agonist concentration, receptor saturation may be assumed in those experiments so that the receptor activation rate by DHPG (O_{DHPG}) can be expressed as a function of τ_r [165] whereby $O_{\mathrm{DHPG}} \approx \tau_r(50\,\mu\mathrm{M})^{-1} = 0.055$–$0.113\,\mu\mathrm{M}^{-1}\,\mathrm{s}^{-1}$ and, accordingly, $\Omega_{\mathrm{DHPG}} = 1/O_{\mathrm{DHPG}}K_{0.5} \approx$ 4–10 s. Corresponding rate constants for glutamate may then be estimated by the latter, assuming similar kinetics yet with $K_{0.5} = K_A = 1/O_A\tau_A \approx 3$–$10\,\mu$M [182], that is, 1.5–5-fold larger than $K_{0.5}$ for DHPG. Moreover, since rise times of Ca^{2+} signals triggered by nonsaturating physiological stimuli are somehow faster than in the case of DHPG [10], it may be assumed that $O_N > O_{\mathrm{DHPG}}$. With this regard, for a choice of $O_A \approx 3O_{\mathrm{DHPG}} = 0.3\,\mu\mathrm{M}^{-1}\,\mathrm{s}^{-1}$, with $K_A = 6\,\mu$M such that $\tau_A = 1/(0.3\,\mu\mathrm{M}^{-1}\mathrm{s}^{-1})/(6\,\mu\mathrm{M}) = 0.55$ s, a peak synaptic glutamate concentration of $Y_{\mathrm{rel}} = 1200\,\mu$M, with $\tau_c = 25$ ms, results in a maximum average fraction of bound receptors of ~0.75–0.9 that occurs within ~70 ms from synaptic release, in good agreement with experimentally reported rise times.

B.3. Gliotransmission. Exocytosis of glutamate from astrocytes is reported to occur by Ca^{2+} concentrations increasing beyond a threshold value $C_\theta \approx 0.15$–$0.8\,\mu$M. In this study we specifically consider $C_\theta = 0.5\,\mu$M. Glutamate-containing vesicles found in astrocytic processes have regular (spherical) shape with typical diameters (d_A) within ~20–110 nm [63, 183]. The corresponding vesicular volume Λ_A then is within ~2–$700\cdot10^{-21}\,\mathrm{dm}^3$. Vesicular glutamate content is approximately the same, or at least as low as one-third of synaptic vesicles in adjacent nerve terminals [8, 161, 184]. Thus, considering a range of synaptic vesicular glutamate content within ~60–150 mM [162], astrocytic vesicular glutamate concentration (G_v) is likely within ~20–150 mM [161].

The majority of glutamate vesicles in astrocytic processes clusters in close proximity (i.e., <100 nm) to the plasma membrane, but about half of them are found within a distance of 40–60 nm from the ventral side of the membrane, suggesting existence of "docked" vesicles in astrocytic processes akin to synaptic terminals [8, 161]. Borrowing the synaptic rationale whereby docked vesicles approximately correspond to readily releasable ones [152], then the average number of astrocytic glutamate vesicles available for release (n_A) could be within ~1–6 [8]. Hence, the total vesicular glutamate releasable by an astrocyte may be estimated within $G_T = n_A G_A = 20$–900 mM.

Astrocytic vesicle recycling (τ_G) likely depends on the mode of exocytosis. Both full-fusion of vesicles and kiss-and-run events have been observed in astrocytic processes [63] with the latter seemingly occurring more often [63, 185]. The fastest recycling pathway corresponds to kiss-and-run fusion, where the rate is mainly limited by vesicle fusion with plasma membrane and subsequent pore opening [186]. Indeed, reported pore-opening times in this case can be as short as 2.0 ± 0.3 ms [185]. The actual recycling time however could be considerably longer if we take into account that, even for fast release events confined within 100 nm from the astrocyte plasma membrane, vesicle reacidification could last ~1.5 s [187].

Considering a value for the diffusion constant of glutamate in the extracellular space of $D_{\mathrm{Glu}} = 0.2\,\mu\mathrm{m}^2/\mathrm{ms}$ [164] and a vesicle release time $t_{\mathrm{rel}} \approx 1$ ms [185], the average diffusion distance travelled by astrocytic glutamate molecules into the extracellular space is [152] $\ell_e = \sqrt{(2 \cdot 0.2\,\mu\mathrm{m}^2/\mathrm{ms} \cdot 1\,\mathrm{ms})} \approx 0.63\,\mu$m. Then, assuming that the mixing volume of released glutamate Λ_e in the extracellular space coincides with one-tenth (i.e., 0.1) of the ideal diffusion volume in free space [188], it is $\Lambda_e = (0.1)4\pi\ell_e^3/3 \approx 10^{-16}\,\mathrm{dm}^3$. Accordingly, considering an average vesicular diameter $d_A = 50$ nm, so that $\Lambda_A \approx 65 \cdot 10^{-21}\,\mathrm{dm}^3$, the ratio ϱ_e between vesicular and mixing volumes for astrocytic glutamate diffusion can be estimated to be of the order of $\varrho_e = \Lambda_A/\Lambda_e = (65 \cdot 10^{-21}\,\mathrm{dm}^3)/10^{-16}\,\mathrm{dm}^3 \approx 6.5 \cdot 10^{-4}$. For an astrocytic pool of releasable glutamate of $G_T = 200$ mM and a release probability $U_A = 0.6$, it follows that the extracellular peak glutamate concentration after exocytosis is $\widehat{G}_A = (6.5 \cdot 10^{-4})(0.6)(200\,\mathrm{mM}) \approx 78\,\mu$M, in agreement with experimental measurements [189]. Finally, imaging of extrasynaptic glutamate dynamics in hippocampal slices hints that glutamate clearance is fast and mainly carried out within <300 ms of exocytosis [171]. Therefore, we consider a characteristic clearance time constant for glutamate in the periastrocytic space of $\tau_e = 200$ ms.

B.4. Presynaptic Receptors. We set the activation rate and inactivation time constants of presynaptic receptors, that is,

O_P and τ_P, to reproduce the experimentally reported rapid onset of the modulatory effect on synaptic release exerted by those receptors, namely, within 1–5 s from glutamate exocytosis by the astrocyte and the slow decay of this modulation, which is of the order of tens of seconds at least [7, 8]. In particular, inhibition of synaptic release following activation of presynaptic mGluRs by astrocytic glutamate could last from tens of seconds [71] to ~2–3 min [13]. Similarly, group I mGluR-mediated enhancement of synaptic release following a single Ca^{2+} elevation in an astrocyte process may last as long as ~30–60 s [2, 7]. Values within ~1-2 min however have also been reported in the case of an involvement of NMDARs [8, 190]. No specific assumption is made on the possible ensuing peak of receptor activation by a single glutamate release by the astrocyte.

B.5. Postsynaptic Neuron. The membrane time constant of pyramidal neurons is typically within 20–70 ms [191, 192] in correspondence with a membrane potential at rest in the range of -66.5 ± 11.7 mV [147, 148, 192–196]. Firing threshold (v_θ) values are on average around -53 ± 2 mV [195, 197, 198], resulting in after-spike reset potentials (v_r) that are 2-3 mV below the firing threshold [192, 195, 199]. The peak of action potentials is artificially set in simulations to $v_p = 30$ mV [193, 197], whereas the refractory period for neuronal action potential generation is fixed at $\tau_r = 2$ ms [93, 195, 197].

B.6. Postsynaptic Currents. AMPA receptor-mediated EPSCs recorded at central synapses are characterized by small rise time constants (τ_N^r), namely, within 0.2–0.6 ms [147–149, 196], and decay time constants (τ_N) in the range of 2.7–11.6 ms [149, 191, 196, 200]. Furthermore, whole-cell recordings of EPSCs for quantal-like glutamatergic stimulation report amplitudes for these currents generally within ~15.5–30 pA [191, 196], and similarly, corresponding somatic depolarizations (EPSPs) are in a wide range of values comprised within ~0.5–7.2 mV, consistent with large quantal size variability of glutamate release from presynaptic terminals [201]. Accordingly, in the simulations of Figure 5 we set $\tau_N^r = 0.5$ ms and $\tau_N = 10$ ms and take the two scaling factors $\widehat{J}_S, \widehat{I}_S$ in (A.16) such that [202]

$$\widehat{J}_S = \frac{J_S}{\varrho_c Y_T \tau_N},$$
$$\widehat{I}_S = \frac{I_S\left(\left(1/\tau_N\right) - \left(1/\tau_N^r\right)\right)}{\left(\tau_N^r/\tau_N\right)^{\left(\tau_N/\left(\tau_N-\tau_N^r\right)\right)} - \left(\tau_N^r/\tau_N\right)^{\left(\tau_N^r/\left(\tau_N-\tau_N^r\right)\right)}}. \tag{B.1}$$

In this fashion, with 3/4 of released neurotransmitter reaching postsynaptic receptors (i.e., $\zeta = 0.75$), setting $J_S = 4.27$ results in EPSP amplitudes approximately equal to I_S. In order to convert PSCs and SICs from voltage to current units, we divide them by typical neuronal input resistance (R_{in}) values which are generally reported in the range of ~60–150 MΩ [192, 193, 196].

B.7. Slow Inward Currents. Astrocyte-mediated SICs are documented in a wide range of amplitudes that spans from >10 pA [11, 21, 22, 26, 32] to >200 pA [21, 25, 85, 87], although their majority is mostly found within 30–80 pA in physiological conditions [21, 26]. SICs kinetics also likely vary depending on subunit composition of SIC-mediating NMDA receptors [203]. In general, assuming NR2B-containing NMDARs as the main receptor type mediating SICs [77], mean SICs rise and decay times are, respectively, reported in ~30–90 ms and ~100–800 [20, 21]. Accordingly, in the simulations of Figure 5 we set $\tau_S^r = 30$ ms and $\tau_N = 600$ ms and take the two scaling factors $\widehat{J}_S, \widehat{I}_S$ in (A.12) such that

$$\widehat{J}_A = \frac{J_A}{\varrho_e G_T \tau_S},$$
$$\widehat{I}_A = \frac{I_A\left(\left(1/\tau_S\right) - \left(1/\tau_S^r\right)\right)}{\left(\tau_S^r/\tau_S\right)^{\left(\tau_N/\left(\tau_N-\tau_S^r\right)\right)} - \left(\tau_S^r/\tau_S\right)^{\left(\tau_S^r/\left(\tau_S-\tau_S^r\right)\right)}}. \tag{B.2}$$

In this fashion, we ultimately choose the value of J_S to account for SIC-mediated depolarizations approximately equal to I_A. As SIC amplitudes are generally reported in terms of current rather than voltage units, we estimate somatic depolarizations ensuing from SICs by expressing these latter in terms of typical EPSCs. Thus, for example, or individual EPSCs of 30 pA that generate 2 mV EPSPs, realistic SICs could be regarded on average to be ~1–5-fold these EPSCs and thus contribute to a similar extent to 1–5 times typical EPSPs, that is, ~2–10 mV.

B.8. Spike-Timing-Dependent Plasticity. We consider the set of parameters for the nonlinear Ca^{2+} model by Graupner and Brunel [102, Figure S6] originally proposed by these authors to qualitatively reproduce the classic STDP curve [123]. In addition, SIC-mediated postsynaptic Ca^{2+} transients are assumed similar to presynaptically triggered Ca^{2+} transients but with likely longer rise and decay times. Finally, both presynaptically mediated and SIC-mediated Ca^{2+} transients are rescaled by equations analogous to (B.1) and (B.2) in order to obtain transient peak amplitudes equal to C_{pre} and C_{sic}, respectively.

C. Parameter Ranges and Values

Values of model parameters used in our simulations are summarized in Table 1. Blank table entries are for those parameters whose value was either taken from previously published studies [102, 136, 141] or estimated on the basis of other model parameters (see Appendix B). Simulation specific (s.s.) parameter values are instead specified within figure captions.

Table 1

Symbol	Description	Range	Value	Units
	Synaptic dynamics			
τ_d	Depression time constant	>0.01–2	s.s.	s
τ_f	Facilitation time constant	>0.5–2	s.s.	s
U_0	Resting synaptic release probability	<0.09–0.9	s.s.	—
	Neurotransmitter release and time course			
Y_T	Total vesicular glutamate concentration	300–1000	500	mM
ϱ_c	Vesicular versus mixing volume ratio		0.005	—
τ_c	Glutamate clearance time constant	2–100	25	ms
ζ	Efficacy of synaptic transmission	0-1	0.75	—
	Astrocyte GPCR kinetics			
O_A	Agonist binding rate		0.3	$\mu M^{-1}s^{-1}$
τ_A	Agonist unbinding time		0.55	s
	IP_3R kinetics			
O_2	Inact. Ca^{2+} binding rate (with Ca^{2+} act.)	0.04–0.18	0.2	$\mu M^{-1}s^{-1}$
d_1	IP_3 binding affinity	0.1–0.15	0.13	μM
d_2	Inact. Ca^{2+} binding affinity (Ca^{2+} act.)		1.05	μM
d_3	IP_3 binding affinity (Ca^{2+} inact.)		0.9434	μM
d_5	Act. Ca^{2+} binding affinity		0.08	μM
	Calcium fluxes			
ϱ_A	ER-to-cytoplasm volume ratio	0.4–0.7	0.18	—
C_T	Total ER Ca^{2+} content	3–5	2	μM
Ω_L	Max. Ca^{2+} leak rate	0.05–0.1	0.1	s^{-1}
Ω_C	Max. Ca^{2+} release rate by IP_3Rs	>6	6	s^{-1}
K_P	Ca^{2+} affinity of SERCA pumps	0.05–0.1	0.05	μM
O_P	Max. Ca^{2+} uptake rate	0.4–1.3	0.9	$\mu M\,s^{-1}$
	IP_3 production			
O_β	Max. rate of IP_3 production by PLCβ	0.05–2	1	$\mu M\,s^{-1}$
K_δ	Ca^{2+} affinity of PLCδ	0.1–1	0.5	μM
κ_δ	Inhibiting IP_3 affinity of PLCδ	1–1.5	1	μM
O_δ	Max. rate of IP_3 production by PLCδ	<0.8	0.05	$\mu M\,s^{-1}$
	IP_3 degradation			
Ω_{5P}	Max. rate of IP_3 degradation by IP-5P	>0.05–0.25	0.1	s^{-1}
K_D	Ca^{2+} affinity of IP_3-3K	0.4–0.5	0.5	μM
K_{3K}	IP_3 affinity of IP_3-3K	0.7–1	1	μM
O_{3K}	Max. rate of IP_3 degradation by IP_3-3K	>0.6	4.5	$\mu M\,s^{-1}$
	Gliotransmitter release and time course			
C_θ	Ca^{2+} threshold for exocytosis	0.15–0.8	0.5	μM
τ_G	Glutamate recycling time constant	0.003–1.5	1.66	s
U_A	Resting glutamate release probability	<0.9	0.6	—
ϱ_e	Vesicular versus mixing volume ratio		$6.5 \cdot 10^{-4}$	—
τ_e	Glutamate clearance time constant	≤300	200	ms
	Presynaptic receptors			
O_P	Activation rate	>0.3	1.5	$\mu M^{-1}s^{-1}$
τ_P	Inactivation time constant	>30–180	120	s
ξ	Gliotransmission type	0-1	s.s.	—
	Postsynaptic neuron			
τ_m	Membrane time constant	20–70	40	ms
τ_r	Refractory period	1–5	2	ms
E_L	Resting potential	−78.2–−54.8	−60	mV
v_θ	Firing threshold	−55–−51	−55	mV

Table 1: Continued.

Symbol	Description	Range	Value	Units
v_r	Reset potential	−58–−53	−57	mV
v_p	Peak AP amplitude	29.8–41.2	30	mV
R_{in}	Input resistance	60–150	s.s.	MΩ
	Postsynaptic currents			
τ_N^r	EPSC rise time	0.4–0.6	0.5	ms
τ_N	EPSC decay time	2.7–11.6	10	ms
J_S	Synaptic efficacy		4.3	—
I_S	EPSP amplitude	0.5–7.5	2	mV
	Slow inward currents			
τ_S^r	SIC rise time	20–70	20	ms
τ_S	SIC decay time	100–800	600	ms
J_A	SIC efficacy		68	—
I_A	SIC amplitude	1–10	4.5	mV
	Spike-timing-dependent plasticity			
C_{pre}	NMDAR-mediated Ca^{2+} increase per AP		1.0	—
τ_{pre}^r	NMDAR Ca^{2+} rise time		10	ms
τ_{pre}	NMDAR Ca^{2+} decay time		30	ms
W_N	Synaptic weight		39.7	—
C_{post}	VDCC-mediated Ca^{2+} increase per AP		2.5	—
τ_{post}^r	VDCC Ca^{2+} rise time		2	ms
τ_{post}	VDCC Ca^{2+} decay time		12	ms
C_{sic}	SIC-mediated Ca^{2+} increase per AP		1.0	—
τ_{sic}^r	SIC Ca^{2+} rise time		5	ms
τ_{sic}	SIC Ca^{2+} decay time		100	ms
W_A	SIC weight		10.6	—
η	Amplification of NMDAR-mediated Ca^{2+}		4	—
θ_d	LTD threshold		1.0	—
θ_p	LTP threshold		2.2	—
γ_d	LTD learning rate		0.57	s^{-1}
γ_p	LTP learning rate		2.32	s^{-1}
$\rho_\star$	Boundary between UP/DOWN states		0.5	—
τ_ρ	Decay time of synaptic change		1.5	s
σ	Noise amplitude		0.1	—
β	Fraction of synapses in the DOWN state		0.5	—
b	UP/DOWN Synaptic strength ratio		4	—

Abbreviations

AMPAR: α-Amino-3-hydroxy-5-methyl-4-isoxazolepropionic acid receptor
AP: Action potential
bAP: Back-propagating action potential
ER: Endoplasmic reticulum
GPCR: G protein-coupled receptor
LTD: Long-term depression
LTP: Long-term potentiation
mGluR: Metabotropic glutamate receptor
NMDA(R): N-Methyl-D-aspartate (receptors)
PAR1: Protease-activated receptor 1
PPR: Pair pulse ratio
(E)PSC: (Excitatory) postsynaptic current
(E)PSP: (Excitatory) postsynaptic potential
SIC: Slow inward current
SERCA: Sarco/endoplasmic reticulum Ca^{2+}/ATPase
STDP: Spike-timing-dependent plasticity
VDCC: Voltage-dependent calcium channel.

Competing Interests

The authors declare that they have no competing interests.

Acknowledgments

Maurizio De Pittà wishes to thank Hugues Berry for insightful discussions, Marcel Stimberg, Romain Brette, and members of Brette's group at the Institut de la Vision (Paris)

for hospitality and assistance in implementing part of the code in Brian 2.0 used in the simulations of this study. This work was supported by a FP7 Maria Skłodowska-Curie International Outgoing Fellowship to Maurizio De Pittà (Project 331486 "Neuron-Astro-Nets").

References

[1] A. Volterra and J. Meldolesi, "Astrocytes, from brain glue to communication elements: the revolution continues," *Nature Reviews Neuroscience*, vol. 6, no. 8, pp. 626–640, 2005.

[2] G. Perea and A. Araque, "Astrocytes potentiate transmitter release at single hippocampal synapses," *Science*, vol. 317, no. 5841, pp. 1083–1086, 2007.

[3] M. M. Halassa and P. G. Haydon, "Integrated brain circuits: astrocytic networks modulate neuronal activity and behavior," *Annual Review of Physiology*, vol. 72, pp. 335–355, 2009.

[4] P. Bezzi and A. Volterra, "A neuron-glia signalling network in the active brain," *Current Opinion in Neurobiology*, vol. 11, no. 3, pp. 387–394, 2001.

[5] A. Araque, G. Carmignoto, P. G. Haydon, S. H. R. Oliet, R. Robitaille, and A. Volterra, "Gliotransmitters travel in time and space," *Neuron*, vol. 81, no. 4, pp. 728–739, 2014.

[6] M. Santello and A. Volterra, "Synaptic modulation by astrocytes via Ca^{2+}-dependent glutamate release," *Neuroscience*, vol. 158, no. 1, pp. 253–259, 2009.

[7] T. A. Fiacco and K. D. McCarthy, "Intracellular astrocyte calcium waves in situ increase the frequency of spontaneous AMPA receptor currents in CA1 pyramidal neurons," *The Journal of Neuroscience*, vol. 24, no. 3, pp. 722–732, 2004.

[8] P. Jourdain, L. H. Bergersen, K. Bhaukaurally et al., "Glutamate exocytosis from astrocytes controls synaptic strength," *Nature Neuroscience*, vol. 10, no. 3, pp. 331–339, 2007.

[9] C. Bonansco, A. Couve, G. Perea, C. Á. Ferradas, M. Roncagliolo, and M. Fuenzalida, "Glutamate released spontaneously from astrocytes sets the threshold for synaptic plasticity," *European Journal of Neuroscience*, vol. 33, no. 8, pp. 1483–1492, 2011.

[10] A. Panatier, J. Vallée, M. Haber, K. K. Murai, J.-C. Lacaille, and R. Robitaille, "Astrocytes are endogenous regulators of basal transmission at central synapses," *Cell*, vol. 146, no. 5, pp. 785–798, 2011.

[11] G. Perea, A. Yang, E. S. Boyden, and M. Sur, "Optogenetic astrocyte activation modulates response selectivity of visual cortex neurons in vivo," *Nature Communications*, vol. 5, article 3262, 2014.

[12] M. Navarrete and A. Araque, "Endocannabinoids potentiate synaptic transmission through stimulation of astrocytes," *Neuron*, vol. 68, no. 1, pp. 113–126, 2010.

[13] Q. Liu, Q.-S. Xu, J. Kang, and M. Nedergaard, "Astrocyte activation of presynaptic metabotropic glutamate receptors modulates hippocampal inhibitory synaptic transmission," *Neuron Glia Biology*, vol. 1, no. 4, pp. 307–316, 2004.

[14] Q.-S. Liu, Q. Xu, G. Arcuino, J. Kang, and M. Nedergaard, "Astrocyte-mediated activation of neuronal kainate receptors," *Proceedings of the National Academy of Sciences of the United States of America*, vol. 101, no. 9, pp. 3172–3177, 2004.

[15] B. Benedetti, V. Matyash, and H. Kettenmann, "Astrocytes control GABAergic inhibition of neurons in the mouse barrel cortex," *Journal of Physiology*, vol. 589, no. 5, pp. 1159–1172, 2011.

[16] H. Markram, Y. Wang, and M. Tsodyks, "Differential signaling via the same axon of neocortical pyramidal neurons," *Proceedings of the National Academy of Sciences of the United States of America*, vol. 95, no. 9, pp. 5323–5328, 1998.

[17] L. F. Abbott and W. G. Regehr, "Synaptic computation," *Nature*, vol. 431, no. 7010, pp. 796–803, 2004.

[18] M. De Pittà, N. Brunel, and A. Volterra, "Astrocytes: orchestrating synaptic plasticity?" *Neuroscience*, 2015.

[19] H. R. Parri, T. M. Gould, and V. Crunelli, "Spontaneous astrocytic Ca^{2+} oscillations in situ drive NMDAR-mediated neuronal excitation," *Nature Neuroscience*, vol. 4, no. 8, pp. 803–812, 2001.

[20] M. C. Angulo, A. S. Kozlov, S. Charpak, and E. Audinat, "Glutamate released from glial cells synchronizes neuronal activity in the hippocampus," *Journal of Neuroscience*, vol. 24, no. 31, pp. 6920–6927, 2004.

[21] T. Fellin, O. Pascual, S. Gobbo, T. Pozzan, P. G. Haydon, and G. Carmignoto, "Neuronal synchrony mediated by astrocytic glutamate through activation of extrasynaptic NMDA receptors," *Neuron*, vol. 43, no. 5, pp. 729–743, 2004.

[22] G. Perea and A. Araque, "Properties of synaptically evoked astrocyte calcium signal reveal synaptic information processing by astrocytes," *Journal of Neuroscience*, vol. 25, no. 9, pp. 2192–2203, 2005.

[23] M. D'Ascenzo, T. Fellin, M. Terunuma et al., "mGluR5 stimulates gliotransmission in the nucleus accumbens," *Proceedings of the National Academy of Sciences of the United States of America*, vol. 104, no. 6, pp. 1995–2000, 2007.

[24] E. Shigetomi, D. N. Bowser, M. V. Sofroniew, and B. S. Khakh, "Two forms of astrocyte calcium excitability have distinct effects on NMDA receptor-mediated slow inward currents in pyramidal neurons," *The Journal of Neuroscience*, vol. 28, no. 26, pp. 6659–6663, 2008.

[25] R. Bardoni, A. Ghirri, M. Zonta et al., "Glutamate-mediated astrocyte-to-neuron signalling in the rat dorsal horn," *Journal of Physiology*, vol. 588, no. 5, pp. 831–846, 2010.

[26] R. Martín, R. Bajo-Grañeras, R. Moratalla, G. Perea, and A. Araque, "Circuit-specific signaling in astrocyte-neuron networks in basal ganglia pathways," *Science*, vol. 349, no. 6249, pp. 730–734, 2015.

[27] M. M. Halassa, T. Fellin, and P. G. Haydon, "The tripartite synapse: roles for gliotransmission in health and disease," *Trends in Molecular Medicine*, vol. 13, no. 2, pp. 54–63, 2007.

[28] M. M. Halassa, T. Fellin, H. Takano, J.-H. Dong, and P. G. Haydon, "Synaptic islands defined by the territory of a single astrocyte," *The Journal of Neuroscience*, vol. 27, no. 24, pp. 6473–6477, 2007.

[29] M. De Pittà, V. Volman, H. Berry, V. Parpura, A. Volterra, and E. Ben-Jacob, "Computational quest for understanding the role of astrocyte signaling in synaptic transmission and plasticity," *Frontiers in Computational Neuroscience*, vol. 6, article 98, 2012.

[30] T. Mizuno, I. Kanazawa, and M. Sakurai, "Differential induction of LTP and LTD is not determined solely by instantaneous calcium concentration: an essential involvement of a temporal factor," *European Journal of Neuroscience*, vol. 14, no. 4, pp. 701–708, 2001.

[31] T. Nevian and B. Sakmann, "Spine Ca^{2+} signaling in spike-timing-dependent plasticity," *The Journal of Neuroscience*, vol. 26, no. 43, pp. 11001–11013, 2006.

[32] N. Chen, H. Sugihara, J. Sharma et al., "Nucleus basalis-enabled stimulus-specific plasticity in the visual cortex is mediated by

astrocytes," *Proceedings of the National Academy of Sciences of the United States of America*, vol. 109, no. 41, pp. E2832–E2841, 2012.

[33] P. J. Sjöström, E. A. Rancz, A. Roth, and M. Häusser, "Dendritic excitability and synaptic plasticity," *Physiological Reviews*, vol. 88, no. 2, pp. 769–840, 2008.

[34] R. C. Froemke, D. Debanne, and G.-Q. Bi, "Temporal modulation of spike-timing-dependent plasticity," *Frontiers in Synaptic Neuroscience*, vol. 2, article 19, 16 pages, 2010.

[35] M. Graupner and N. Brunel, "Mechanisms of induction and maintenance of spike-timing dependent plasticity in biophysical synapse models," *Frontiers in Computational Neuroscience*, vol. 4, no. 136, pp. 1–19, 2010.

[36] J. J. Wade, L. J. McDaid, J. Harkin, V. Crunelli, and J. A. S. Kelso, "Bidirectional coupling between astrocytes and neurons mediates learning and dynamic coordination in the brain: a multiple modeling approach," *PLoS ONE*, vol. 6, no. 12, Article ID e29445, 2011.

[37] M. Naeem, L. J. McDaid, J. Harkin, J. J. Wade, and J. Marsland, "On the role of astroglial syncytia in self-repairing spiking neural networks," *IEEE Transactions on Neural Networks and Learning Systems*, vol. 26, no. 10, pp. 2370–2380, 2015.

[38] Y. Ni, E. B. Malarkey, and V. Parpura, "Vesicular release of glutamate mediates bidirectional signaling between astrocytes and neurons," *Journal of Neurochemistry*, vol. 103, no. 4, pp. 1273–1284, 2007.

[39] V. Parpura and R. Zorec, "Gliotransmission: exocytotic release from astrocytes," *Brain Research Reviews*, vol. 63, no. 1-2, pp. 83–92, 2010.

[40] R. Zorec, A. Araque, G. Carmignoto, P. G. Haydon, A. Verkhratsky, and V. Parpura, "Astroglial excitability and gliotransmission: an appraisal of Ca^{2+} as a signalling route," *ASN Neuro*, vol. 4, no. 2, Article ID e00080, pp. 103–119, 2012.

[41] B. A. Barres, "The mystery and magic of glia: a perspective on their roles in health and disease," *Neuron*, vol. 60, no. 3, pp. 430–440, 2008.

[42] V. Parpura, V. Grubišic, and A. Verkhratsky, "Ca^{2+} sources for the exocytotic release of glutamate from astrocytes," *Biochimica et Biophysica Acta—Molecular Cell Research*, vol. 1813, no. 5, pp. 984–991, 2011.

[43] N. B. Hamilton and D. Attwell, "Do astrocytes really exocytose neurotransmitters?" *Nature Reviews Neuroscience*, vol. 11, no. 4, pp. 227–238, 2010.

[44] G. Perea, M. Navarrete, and A. Araque, "Tripartite synapses: astrocytes process and control synaptic information," *Trends in Neurosciences*, vol. 32, no. 8, pp. 421–431, 2009.

[45] G. Losi, L. Mariotti, and G. Carmignoto, "GABAergic interneuron to astrocyte signalling: a neglected form of cell communication in the brain," *Philosophical Transactions of the Royal Society B: Biological Sciences*, vol. 369, no. 1654, Article ID 20130609, 2014.

[46] A. Nimmerjahn, "Astrocytes going live: advances and challenges," *The Journal of Physiology*, vol. 587, no. 8, pp. 1639–1647, 2009.

[47] A. Volterra, N. Liaudet, and I. Savtchouk, "Astrocyte Ca^{2+} signalling: an unexpected complexity," *Nature Reviews Neuroscience*, vol. 15, no. 5, pp. 327–335, 2014.

[48] N. Bazargani and D. Attwell, "Astrocyte calcium signaling: the third wave," *Nature Neuroscience*, vol. 19, no. 2, pp. 182–189, 2016.

[49] P. G. Haydon, "Glia: listening and talking to the synapse," *Nature Reviews Neuroscience*, vol. 2, no. 3, pp. 185–193, 2001.

[50] M. A. Di Castro, J. Chuquet, N. Liaudet et al., "Local Ca^{2+} detection and modulation of synaptic release by astrocytes," *Nature Neuroscience*, vol. 14, no. 10, pp. 1276–1284, 2011.

[51] M. V. Tsodyks and H. Markram, "The neural code between neocortical pyramidal neurons depends on neurotransmitter release probability," *Proceedings of the National Academy of Sciences of the United States of America*, vol. 94, no. 2, pp. 719–723, 1997.

[52] R. S. Zucker and W. G. Regehr, "Short-term synaptic plasticity," *Annual Review of Physiology*, vol. 64, pp. 355–405, 2002.

[53] J. Del Castillo and B. Katz, "Quantal components of the end-plate potential," *The Journal of Physiology*, vol. 124, no. 3, pp. 560–573, 1954.

[54] T. C. Südhof, "The synaptic vesicle cycle," *Annual Review of Neuroscience*, vol. 27, pp. 509–547, 2004.

[55] M. Tsodyks, "Activity-dependent transmission in neocortical synapses," in *Methods and Models in Neurophysics*, C. C. Chow, B. Gutkin, D. Hansel, C. Meunier, and J. Dalibard, Eds., pp. 245–265, Elsevier, 2005.

[56] J. D. Clements, "Transmitter timecourse in the synaptic cleft: its role in central synaptic function," *Trends in Neurosciences*, vol. 19, no. 5, pp. 163–171, 1996.

[57] J. S. Diamond, "Deriving the glutamate clearance time course from transporter currents in CA1 hippocampal astrocytes: transmitter uptake gets faster during development," *Journal of Neuroscience*, vol. 25, no. 11, pp. 2906–2916, 2005.

[58] A. Destexhe, Z. F. Mainen, and T. J. Sejnowski, "Synthesis of models for excitable membranes, synaptic transmission and neuromodulation using a common kinetic formalism," *Journal of Computational Neuroscience*, vol. 1, no. 3, pp. 195–230, 1994.

[59] G. W. De Young and J. Keizer, "A single-pool inositol 1,4,5-trisphosphate-receptor-based model for agonist-stimulated oscillations in Ca^{2+} concentration," *Proceedings of the National Academy of Sciences of the United States of America*, vol. 89, no. 20, pp. 9895–9899, 1992.

[60] L. Pasti, A. Volterra, T. Pozzan, and G. Carmignoto, "Intracellular calcium oscillations in astrocytes: a highly plastic, bidirectional form of communication between neurons and astrocytes in situ," *The Journal of Neuroscience*, vol. 17, no. 20, pp. 7817–7830, 1997.

[61] J. Marchaland, C. Calì, S. M. Voglmaier et al., "Fast subplasma membrane Ca^{2+} transients control exo-endocytosis of synaptic-like microvesicles in astrocytes," *The Journal of Neuroscience*, vol. 28, no. 37, pp. 9122–9132, 2008.

[62] D. A. Sahlender, I. Savtchouk, and A. Volterra, "What do we know about gliotransmitter release from astrocytes?" *Philosophical Transactions of the Royal Society B*, vol. 369, Article ID 20130592, 2014.

[63] P. Bezzi, V. Gundersen, J. L. Galbete et al., "Astrocytes contain a vesicular compartment that is competent for regulated exocytosis of glutamate," *Nature Neuroscience*, vol. 7, no. 6, pp. 613–620, 2004.

[64] L. H. Bergersen and V. Gundersen, "Morphological evidence for vesicular glutamate release from astrocytes," *Neuroscience*, vol. 158, no. 1, pp. 260–265, 2009.

[65] M. Santello, P. Bezzi, and A. Volterra, "TNFα controls glutamatergic gliotransmission in the hippocampal dentate gyrus," *Neuron*, vol. 69, no. 5, pp. 988–1001, 2011.

[66] M. Domercq, L. Brambilla, E. Pilati, J. Marchaland, A. Volterra, and P. Bezzi, "P2Y1 receptor-evoked glutamate exocytosis from astrocytes: control by tumor necrosis factor-α and

prostaglandins," *The Journal of Biological Chemistry*, vol. 281, no. 41, pp. 30684–30696, 2006.

[67] M. Kreft, M. Stenovec, M. Rupnik et al., "Properties of Ca^{2+}-dependent exocytosis in cultured astrocytes," *Glia*, vol. 46, no. 4, pp. 437–445, 2004.

[68] E. B. Malarkey and V. Parpura, "Temporal characteristics of vesicular fusion in astrocytes: examination of synaptobrevin 2-laden vesicles at single vesicle resolution," *The Journal of Physiology*, vol. 589, no. 17, pp. 4271–4300, 2011.

[69] P. S. Pinheiro and C. Mulle, "Presynaptic glutamate receptors: physiological functions and mechanisms of action," *Nature Reviews Neuroscience*, vol. 9, no. 6, pp. 423–436, 2008.

[70] A. Banerjee, R. S. Larsen, B. D. Philpot, and O. Paulsen, "Roles of presynaptic NMDA receptors in neurotransmission and plasticity," *Trends in Neurosciences*, vol. 39, no. 1, pp. 26–39, 2016.

[71] A. Araque, V. Parpura, R. P. Sanzgiri, and P. G. Haydon, "Glutamate-dependent astrocyte modulation of synaptic transmission between cultured hippocampal neurons," *European Journal of Neuroscience*, vol. 10, no. 6, pp. 2129–2142, 1998.

[72] M. Navarrete, G. Perea, D. F. de Sevilla et al., "Astrocytes mediate in vivo cholinergic-induced synaptic plasticity," *PLoS Biology*, vol. 10, no. 2, Article ID e1001259, 2012.

[73] M. De Pittà, V. Volman, H. Berry, and E. Ben-Jacob, "A tale of two stories: astrocyte regulation of synaptic depression and facilitation," *PLoS Computational Biology*, vol. 7, no. 12, Article ID e1002293, 2011.

[74] J. S. Dittman, A. C. Kreitzer, and W. G. Regehr, "Interplay between facilitation, depression, and residual calcium at three presynaptic terminals," *Journal of Neuroscience*, vol. 20, no. 4, pp. 1374–1385, 2000.

[75] E. S. Fortune and G. J. Rose, "Short-term synaptic plasticity as a temporal filter," *Trends in Neurosciences*, vol. 24, no. 7, pp. 381–385, 2001.

[76] C. Agulhon, J. Petravicz, A. B. McMullen et al., "What is the role of astrocyte calcium in neurophysiology?" *Neuron*, vol. 59, no. 6, pp. 932–946, 2008.

[77] T. Papouin and S. H. R. Oliet, "Organization, control and function of extrasynaptic NMDA receptors," *Philosophical Transactions of the Royal Society B: Biological Sciences*, vol. 369, no. 1654, Article ID 20130601, 2014.

[78] T. M. Pirttimaki, S. D. Hall, and H. R. Parri, "Sustained neuronal activity generated by glial plasticity," *The Journal of Neuroscience*, vol. 31, no. 21, pp. 7637–7647, 2011.

[79] M. Navarrete, G. Perea, L. Maglio, J. Pastor, R. García de Sola, and A. Araque, "Astrocyte calcium signal and gliotransmission in human brain tissue," *Cerebral Cortex*, vol. 23, no. 5, pp. 1240–1246, 2013.

[80] M. Navarrete and A. Araque, "Endocannabinoids mediate neuron-astrocyte communication," *Neuron*, vol. 57, no. 6, pp. 883–893, 2008.

[81] S.-J. Oh, K.-S. Han, H. Park et al., "Protease activated receptor 1-induced glutamate release in cultured astrocytes is mediated by Bestrophin-1 channel but not by vesicular exocytosis," *Molecular Brain*, vol. 5, no. 1, article 38, 2012.

[82] D. H. Woo, K.-S. Han, J. W. Shim et al., "TREK-1 and Best1 channels mediate fast and slow glutamate release in astrocytes upon GPCR activation," *Cell*, vol. 151, no. 1, pp. 25–40, 2012.

[83] T. Papouin, L. Ladépêche, J. Ruel et al., "Synaptic and extrasynaptic NMDA receptors are gated by different endogenous coagonists," *Cell*, vol. 150, no. 3, pp. 633–646, 2012.

[84] C. J. Lee, G. Mannaioni, H. Yuan, D. H. Woo, M. B. Gingrich, and S. F. Traynelis, "Astrocytic control of synaptic NMDA receptors," *The Journal of Physiology*, vol. 581, no. 3, pp. 1057–1081, 2007.

[85] H. Nie, H. Zhang, and H.-R. Weng, "Bidirectional neuron–glia interactions triggered by deficiency of glutamate uptake at spinal sensory synapses," *Journal of Neurophysiology*, vol. 104, no. 2, pp. 713–725, 2010.

[86] D. Reyes-Haro, J. Müller, M. Boresch et al., "Neuron-astrocyte interactions in the medial nucleus of the trapezoid body," *The Journal of General Physiology*, vol. 135, no. 6, pp. 583–594, 2010.

[87] N. Kang, J. Xu, Q. Xu, M. Nedergaard, and J. Kang, "Astrocytic glutamate release-induced transient depolarization and epileptiform discharges in hippocampal CA1 pyramidal neurons," *Journal of Neurophysiology*, vol. 94, no. 6, pp. 4121–4130, 2005.

[88] T. Fellin, M. Gomez-Gonzalo, S. Gobbo, G. Carmignoto, and P. G. Haydon, "Astrocytic glutamate is not necessary for the generation of epileptiform neuronal activity in hippocampal slices," *The Journal of Neuroscience*, vol. 26, no. 36, pp. 9312–9322, 2006.

[89] G.-F. Tian, H. Azmi, T. Takano et al., "An astrocytic basis of epilepsy," *Nature Medicine*, vol. 11, no. 9, pp. 973–981, 2005.

[90] S. Ding, T. Fellin, Y. Zhu et al., "Enhanced astrocytic Ca^{2+} signals contribute to neuronal excitotoxicity after status epilepticus," *The Journal of Neuroscience*, vol. 27, no. 40, pp. 10674–10684, 2007.

[91] N. Fourcaud and N. Brunel, "Dynamics of the firing probability of noisy integrate-and fire neurons," *Neural Computation*, vol. 14, no. 9, pp. 2057–2110, 2002.

[92] A. N. Burkitt, "A review of the integrate-and-fire neuron model: I. Homogeneous synaptic input," *Biological Cybernetics*, vol. 95, no. 1, pp. 1–19, 2006.

[93] A. Rauch, G. La Camera, H.-R. Lüscher, W. Senn, and S. Fusi, "Neocortical pyramidal cells respond as integrate-and-fire neurons to in vivo-like input currents," *Journal of Neurophysiology*, vol. 90, no. 3, pp. 1598–1612, 2003.

[94] T. Hromádka, M. R. DeWeese, and A. M. Zador, "Sparse representation of sounds in the unanesthetized auditory cortex," *PLoS Biology*, vol. 6, no. 1, article e16, 2008.

[95] N. Caporale and Y. Dan, "Spike timing-dependent plasticity: a hebbian learning rule," *Annual Review of Neuroscience*, vol. 31, pp. 25–46, 2008.

[96] J. C. Magee and D. Johnston, "A synaptically controlled, associative signal for Hebbian plasticity in hippocampal neurons," *Science*, vol. 275, no. 5297, pp. 209–213, 1997.

[97] I. Ismailov, D. Kalikulov, T. Inoue, and M. J. Friedlander, "The kinetic profile of intracellular calcium predicts long-term potentiation and long-term depression," *The Journal of Neuroscience*, vol. 24, no. 44, pp. 9847–9861, 2004.

[98] T. Nevian and B. Sakmann, "Single spine Ca^{2+} signals evoked by coincident EPSPs and backpropagating action potentials in spiny stellate cells of layer 4 in the juvenile rat somatosensory barrel cortex," *The Journal of Neuroscience*, vol. 24, no. 7, pp. 1689–1699, 2004.

[99] V. A. Bender, K. J. Bender, D. J. Brasier, and D. E. Feldman, "Two coincidence detectors for spike timing-dependent plasticity in somatosensory cortex," *The Journal of Neuroscience*, vol. 26, no. 16, pp. 4166–4177, 2006.

[100] H. Z. Shouval, M. F. Bear, and L. N. Cooper, "A unified model of NMDA receptor-dependent bidirectional synaptic plasticity," *Proceedings of the National Academy of Sciences of the United States of America*, vol. 99, no. 16, pp. 10831–10836, 2002.

[101] Y. Cai, J. P. Gavornik, L. N. Cooper, L. C. Yeung, and H. Z. Shouval, "Effect of stochastic synaptic and dendritic dynamics on synaptic plasticity in visual cortex and hippocampus," *Journal of Neurophysiology*, vol. 97, no. 1, pp. 375–386, 2007.

[102] M. Graupner and N. Brunel, "Calcium-based plasticity model explains sensitivity of synaptic changes to spike pattern, rate, and dendritic location," *Proceedings of the National Academy of Sciences of the United States of America*, vol. 109, no. 10, pp. 3991–3996, 2012.

[103] R. C. Malenka and M. F. Bear, "LTP and LTD: an embarrassment of riches," *Neuron*, vol. 44, no. 1, pp. 5–21, 2004.

[104] J. C. Magee and D. Johnston, "Plasticity of dendritic function," *Current Opinion in Neurobiology*, vol. 15, no. 3, pp. 334–342, 2005.

[105] P. J. Sjöström and S. B. Nelson, "Spike timing, calcium signals and synaptic plasticity," *Current Opinion in Neurobiology*, vol. 12, no. 3, pp. 305–314, 2002.

[106] L. F. Abbott and S. B. Nelson, "Synaptic plasticity: taming the beast," *Nature*, vol. 3, pp. 1178–1183, 2000.

[107] L. Nowak, P. Bregestovski, P. Ascher, A. Herbet, and A. Prochiantz, "Magnesium gates glutamate-activated channels in mouse central neurones," *Nature*, vol. 307, no. 5950, pp. 462–465, 1984.

[108] C. E. Jahr and C. F. Stevens, "Voltage dependence of NMDA-activated macroscopic conductances predicted by single-channel kinetics," *The Journal of Neuroscience*, vol. 10, no. 9, pp. 3178–3182, 1990.

[109] R. C. Froemke and Y. Dan, "Spike-timing-dependent synaptic modification induced by natural spike trains," *Nature*, vol. 416, no. 6879, pp. 433–438, 2002.

[110] R. C. Froemke, I. A. Tsay, M. Raad, J. D. Long, and Y. Dan, "Contribution of individual spikes in burst-induced long-term synaptic modification," *Journal of Neurophysiology*, vol. 95, no. 3, pp. 1620–1629, 2006.

[111] S. Cull-Candy, S. Brickley, and M. Farrant, "NMDA receptor subunits: diversity, development and disease," *Current Opinion in Neurobiology*, vol. 11, no. 3, pp. 327–335, 2001.

[112] D.-D. Liu, Q. Yang, and S.-T. Li, "Activation of extrasynaptic NMDA receptors induces LTD in rat hippocampal CA1 neurons," *Brain Research Bulletin*, vol. 93, pp. 10–16, 2013.

[113] R. C. Evans and K. T. Blackwell, "Calcium: amplitude, duration, or location?" *The Biological Bulletin*, vol. 228, no. 1, pp. 75–83, 2015.

[114] B. L. Bloodgood and B. L. Sabatini, "Ca^{2+} signaling in dendritic spines," *Current Opinion in Neurobiology*, vol. 17, no. 3, pp. 345–351, 2007.

[115] D. A. Rusakov, A. Scimemi, M. C. Walker, and D. M. Kullmann, "Comment on 'Role of NMDA receptor subtypes in governing the direction of hippocampal synaptic plasticity'," *Science*, vol. 305, article 1912, 2004.

[116] R. S. Petralia, Y. X. Wang, F. Hua et al., "Organization of NMDA receptors at extrasynaptic locations," *Neuroscience*, vol. 167, no. 1, pp. 68–87, 2010.

[117] A. Araque, V. Parpura, R. P. Sanzgiri, and P. G. Haydon, "Tripartite synapses: glia, the unacknowledged partner," *Trends in Neurosciences*, vol. 22, no. 5, pp. 208–215, 1999.

[118] A. Perez-Alvarez, M. Navarrete, A. Covelo, E. D. Martin, and A. Araque, "Structural and functional plasticity of astrocyte processes and dendritic spine interactions," *The Journal of Neuroscience*, vol. 34, no. 38, pp. 12738–12744, 2014.

[119] K. A. Buchanan and J. R. Mellor, "The activity requirements for spike timing-dependent plasticity in the hippocampus," *Frontiers in Synaptic Neuroscience*, vol. 2, no. 11, pp. 1–5, 2010.

[120] R. M. Meredith, A. M. Floyer-Lea, and O. Paulsen, "Maturation of long-term potentiation induction rules in rodent hippocampus: role of GABAergic inhibition," *The Journal of Neuroscience*, vol. 23, no. 35, pp. 11142–11146, 2003.

[121] K. A. Buchanan and J. R. Mellor, "The development of synaptic plasticity induction rules and the requirement for postsynaptic spikes in rat hippocampal CA1 pyramidal neurones," *The Journal of Physiology*, vol. 585, no. 2, pp. 429–445, 2007.

[122] E. Campanac and D. Debanne, "Spike timing-dependent plasticity: a learning rule for dendritic integration in rat CA1 pyramidal neurons," *The Journal of Physiology*, vol. 586, no. 3, pp. 779–793, 2008.

[123] G.-Q. Bi and M.-M. Poo, "Synaptic modifications in cultured hippocampal neurons: dependence on spike timing, synaptic strength, and postsynaptic cell type," *The Journal of Neuroscience*, vol. 18, no. 24, pp. 10464–10472, 1998.

[124] G. M. Wittenberg and S. S.-H. Wang, "Malleability of spike-timing-dependent plasticity at the CA3-CA1 synapse," *The Journal of Neuroscience*, vol. 26, no. 24, pp. 6610–6617, 2006.

[125] D. E. Shulz and V. Jacob, "Spike-timing-dependent plasticity in the intact brain: counteracting spurious spike coincidences," *Frontiers in Synaptic Neuroscience*, vol. 1, article 137, 2010.

[126] F. G. Pike, R. M. Meredith, A. W. A. Olding, and O. Paulsen, "Postsynaptic bursting is essential for 'Hebbian' induction of associative long-term potentiation at excitatory synapses in rat hippocampus," *The Journal of Physiology*, vol. 518, no. 2, pp. 571–576, 1999.

[127] W. Sun, E. McConnell, J.-F. Pare et al., "Glutamate-dependent neuroglial calcium signaling differs between young and adult brain," *Science*, vol. 339, no. 6116, pp. 197–200, 2013.

[128] N. L. Golding, N. P. Staff, and N. Spruston, "Dendritic spikes as a mechanism for cooperative long-term potentiation," *Nature*, vol. 418, no. 6895, pp. 326–331, 2002.

[129] G.-Q. Bi and M.-M. Poo, "Synaptic modification by correlated activity: hebb's postulate revisited," *Annual Review of Neuroscience*, vol. 24, pp. 139–166, 2001.

[130] M. Lavialle, G. Aumann, E. Anlauf, F. Pröls, M. Arpin, and A. Derouiche, "Structural plasticity of perisynaptic astrocyte processes involves ezrin and metabotropic glutamate receptors," *Proceedings of the National Academy of Sciences of the United States of America*, vol. 108, no. 31, pp. 12915–12919, 2011.

[131] D. O. Hebb, *The Organization of Behavior; A Neuropsychological Theory*, John Wiley & Sons, New York, NY, USA, 1949.

[132] W. Gerstner and W. M. Kistler, "Mathematical formulations of Hebbian learning," *Biological Cybernetics*, vol. 87, no. 5-6, pp. 404–415, 2002.

[133] A. B. Porto-Pazos, N. Veiguela, P. Mesejo et al., "Artificial astrocytes improve neural network performance," *PLoS ONE*, vol. 6, no. 4, Article ID e19109, 2011.

[134] J. S. Bains and S. H. R. Oliet, "Glia: they make your memories stick!," *Trends in Neurosciences*, vol. 30, no. 8, pp. 417–424, 2007.

[135] R. Min, M. Santello, and T. Nevian, "The computational power of astrocyte mediated synaptic plasticity," *Frontiers in Computational Neuroscience*, vol. 6, article 93, 2012.

[136] G. Wallach, J. Lallouette, N. Herzog et al., "Glutamate mediated astrocytic filtering of neuronal activity," *PLoS Computational Biology*, vol. 10, no. 12, Article ID e1003964, 2014.

[137] B.-X. Zhang, H. Zhao, and S. Muallem, "Ca^{2+}-dependent kinase and phosphatase control inositol 1,4,5-trisphosphate-mediated Ca^{2+} release. Modification by agonist stimulation," *The Journal of Biological Chemistry*, vol. 268, no. 15, pp. 10997–11001, 1993.

[138] C. E. Sims and N. L. Allbrittont, "Metabolism of inositol 1,4,5-trisphosphate and inositol 1,3,4,5-tetrakisphosphate by the oocytes of *Xenopus laevis*," *Journal of Biological Chemistry*, vol. 273, no. 7, pp. 4052–4058, 1998.

[139] M. J. Rebecchi and S. N. Pentyala, "Structure, function, and control of phosphoinositide-specific phospholipase C," *Physiological Reviews*, vol. 80, no. 4, pp. 1291–1335, 2000.

[140] M. J. Berridge, M. D. Bootman, and H. L. Roderick, "Calcium signalling: dynamics, homeostasis and remodelling," *Nature Reviews Molecular Cell Biology*, vol. 4, no. 7, pp. 517–529, 2003.

[141] M. De Pittà, M. Goldberg, V. Volman, H. Berry, and E. Ben-Jacob, "Glutamate regulation of calcium and IP_3 oscillating and pulsating dynamics in astrocytes," *Journal of Biological Physics*, vol. 35, no. 4, pp. 383–411, 2009.

[142] Y.-X. Li and J. Rinzel, "Equations for $InsP_3$ receptor-mediated $[Ca^{2+}]_i$ oscillations derived from a detailed kinetic model: a Hodgkin-Huxley like formalism," *Journal of Theoretical Biology*, vol. 166, no. 4, pp. 461–473, 1994.

[143] M. De Pittà, V. Volman, H. Levine, and E. Ben-Jacob, "Multimodal encoding in a simplified model of intracellular calcium signaling," *Cognitive Processing*, vol. 10, no. 1, pp. 55–70, 2009.

[144] Y. Pankratov, U. Lalo, A. Verkhratsky, and R. A. North, "Quantal release of ATP in mouse cortex," *Journal of General Physiology*, vol. 129, no. 3, pp. 257–265, 2007.

[145] J. Kang, L. Jiang, S. A. Goldman, and M. Nedergaard, "Astrocyte-mediated potentiation of inhibitory synaptic transmission," *Nature Neuroscience*, vol. 1, no. 8, pp. 683–692, 1998.

[146] A. Serrano, N. Haddjeri, J.-C. Lacaille, and R. Robitaille, "GABAergic network activation of glial cells underlies hippocampal heterosynaptic depression," *The Journal of Neuroscience*, vol. 26, no. 20, pp. 5370–5382, 2006.

[147] N. Spruston, P. Jonas, and B. Sakmann, "Dendritic glutamate receptor channels in rat hippocampal CA3 and CA1 pyramidal neurons," *The Journal of Physiology*, vol. 482, no. 2, pp. 325–352, 1995.

[148] J. C. Magee and E. P. Cook, "Somatic EPSP amplitude is independent of synapse location in hippocampal pyramidal neurons," *Nature Neuroscience*, vol. 3, no. 9, pp. 895–903, 2000.

[149] B. K. Andrásfalvy and J. C. Magee, "Distance-dependent increase in AMPA receptor number in the dendrites of adult hippocampal CA1 pyramidal neurons," *The Journal of Neuroscience*, vol. 21, no. 23, pp. 9151–9159, 2001.

[150] M. Stimberg, D. F. M. Goodman, V. Benichoux, and R. Brette, "Equation-oriented specification of neural models for simulations," *Frontiers in Neuroinformatics*, vol. 8, article 6, 2014.

[151] Python Software Foundation, *Python Language Reference, Version 2.7*, Python Software Foundation, 2015.

[152] T. Schikorski and C. F. Stevens, "Quantitative ultrastructural analysis of hippocampal excitatory synapses," *The Journal of Neuroscience*, vol. 17, no. 15, pp. 5858–5867, 1997.

[153] C. F. Stevens and Y. Wang, "Facilitation and depression at single central synapses," *Neuron*, vol. 14, no. 4, pp. 795–802, 1995.

[154] H. Markram, D. Pikus, A. Gupta, and M. Tsodyks, "Potential for multiple mechanisms, phenomena and algorithms for synaptic plasticity at single synapses," *Neuropharmacology*, vol. 37, no. 4-5, pp. 489–500, 1998.

[155] V. N. Murthy, T. J. Sejnowski, and C. F. Stevens, "Heterogeneous release properties of visualized individual hippocampal synapses," *Neuron*, vol. 18, no. 4, pp. 599–612, 1997.

[156] W. G. Regehr, K. R. Delaney, and D. W. Tank, "The role of presynaptic calcium in short-term enhancement at the hippocampal mossy fiber synapse," *Journal of Neuroscience*, vol. 14, no. 2, pp. 523–537, 1994.

[157] N. J. Emptage, C. A. Reid, and A. Fine, "Calcium stores in hippocampal synaptic boutons mediate short-term plasticity, store-operated Ca^{2+} entry, and spontaneous transmitter release," *Neuron*, vol. 29, no. 1, pp. 197–208, 2001.

[158] J. L. Pyle, E. T. Kavalali, E. S. Piedras-Rentería, and R. W. Tsien, "Rapid reuse of readily releasable pool vesicles at hippocampal synapses," *Neuron*, vol. 28, no. 1, pp. 221–231, 2000.

[159] D. L. Brody and D. T. Yue, "Release-independent short-term synaptic depression in cultured hippocampal neurons," *The Journal of Neuroscience*, vol. 20, no. 7, pp. 2480–2494, 2000.

[160] K. M. Harris and P. Sultan, "Variation in the number, location and size of synaptic vesicles provides an anatomical basis for the nonuniform probability of release at hippocampal CA1 synapses," *Neuropharmacology*, vol. 34, no. 11, pp. 1387–1395, 1995.

[161] L. H. Bergersen, C. Morland, L. Ormel et al., "Immunogold detection of L-glutamate and D-serine in small synaptic-like microvesicles in adult hippocampal astrocytes," *Cerebral Cortex*, vol. 22, no. 7, pp. 1690–1697, 2012.

[162] N. C. Danbolt, "Glutamate uptake," *Progress in Neurobiology*, vol. 65, no. 1, pp. 1–105, 2001.

[163] S. Raghavachari and J. E. Lisman, "Properties of quantal transmission at CA1 synapses," *Journal of Neurophysiology*, vol. 92, no. 4, pp. 2456–2467, 2004.

[164] T. A. Nielsen, D. A. DiGregorio, and R. A. Silver, "Modulation of glutamate mobility reveals the mechanism underlying slow-rising AMPAR EPSCs and the diffusion coefficient in the synaptic cleft," *Neuron*, vol. 42, no. 5, pp. 757–771, 2004.

[165] B. Barbour, "An evaluation of synapse independence," *The Journal of Neuroscience*, vol. 21, no. 20, pp. 7969–7984, 2001.

[166] R. Ventura and K. M. Harris, "Three-dimensional relationships between hippocampal synapses and astrocytes," *The Journal of Neuroscience*, vol. 19, no. 16, pp. 6897–6906, 1999.

[167] T. G. Oertner, B. L. Sabatini, E. A. Nimchinsky, and K. Svoboda, "Facilitation at single synapses probed with optical quantal analysis," *Nature Neuroscience*, vol. 5, no. 7, pp. 657–664, 2002.

[168] B. Barbour and M. Häusser, "Intersynaptic diffusion of neurotransmitter," *Trends in Neurosciences*, vol. 20, no. 9, pp. 377–384, 1997.

[169] J. D. Clements, R. A. J. Lester, G. Tong, C. E. Jahr, and G. L. Westbrook, "The time course of glutamate in the synaptic cleft," *Science*, vol. 258, no. 5087, pp. 1498–1501, 1992.

[170] M. A. Herman and C. E. Jahr, "Extracellular glutamate concentration in hippocampal slice," *The Journal of Neuroscience*, vol. 27, no. 36, pp. 9736–9741, 2007.

[171] Y. Okubo, H. Sekiya, S. Namiki et al., "Imaging extrasynaptic glutamate dynamics in the brain," *Proceedings of the National Academy of Sciences of the United States of America*, vol. 107, no. 14, pp. 6526–6531, 2010.

[172] H. Hirase, L. Qian, P. Barthó, and G. Buzsáki, "Calcium dynamics of cortical astrocytic networks *in vivo*," *PLoS Biology*, vol. 2, no. 4, article e96, 2004.

[173] A. Nimmerjahn, F. Kirchhoff, J. N. D. Kerr, and F. Helmchen, "Sulforhodamine 101 as a specific marker of astroglia in the neocortex *in vivo*," *Nature Methods*, vol. 1, no. 1, pp. 31–37, 2004.

[174] X. Wang, N. Lou, Q. Xu et al., "Astrocytic Ca^{2+} signaling evoked by sensory stimulation *in vivo*," *Nature Neuroscience*, vol. 9, no. 6, pp. 816–823, 2006.

[175] T. Pivneva, B. Haas, D. Reyes-Haro et al., "Store-operated Ca^{2+} entry in astrocytes: different spatial arrangement of endoplasmic reticulum explains functional diversity *in vitro* and *in situ*," *Cell Calcium*, vol. 43, no. 6, pp. 591–601, 2008.

[176] J. Lytton, M. Westlin, S. E. Burk, G. E. Shull, and D. H. MacLennan, "Functional comparisons between isoforms of the sarcoplasmic or endoplasmic reticulum family of calcium pumps," *Journal of Biological Chemistry*, vol. 267, no. 20, pp. 14483–14489, 1992.

[177] I. Vandecaetsbeek, M. Trekels, M. De Maeyer et al., "Structural basis for the high Ca^{2+} affinity of the ubiquitous SERCA2b Ca^{2+} pump," *Proceedings of the National Academy of Sciences of the United States of America*, vol. 106, no. 44, pp. 18533–18538, 2009.

[178] V. Parpura and P. G. Haydon, "Physiological astrocytic calcium levels stimulate glutamate release to modulate adjacent neurons," *Proceedings of the National Academy of Sciences of the United States of America*, vol. 97, no. 15, pp. 8629–8634, 2000.

[179] M. Kang and H. G. Othmer, "Spatiotemporal characteristics of calcium dynamics in astrocytes," *Chaos*, vol. 19, no. 3, Article ID 037116, 2009.

[180] E. Aronica, J. A. Gorter, H. Ijlst-Keizers et al., "Expression and functional role of mGluR3 and mGluR5 in human astrocytes and glioma cells: opposite regulation of glutamate transporter proteins," *European Journal of Neuroscience*, vol. 17, no. 10, pp. 2106–2118, 2003.

[181] I. Brabet, S. Mary, J. Bockaert, and J.-P. Pin, "Phenylglycine derivatives discriminate between mGluR1- and mGluR5-mediated responses," *Neuropharmacology*, vol. 34, no. 8, pp. 895–903, 1995.

[182] L. P. Daggett, A. I. Sacaan, M. Akong et al., "Molecular and functional characterization of recombinant human metabotropic glutamate receptor subtype 5," *Neuropharmacology*, vol. 34, no. 8, pp. 871–886, 1995.

[183] D. Crippa, U. Schenk, M. Francolini et al., "Synaptobrevin2-expressing vesicles in rat astrocytes: insights into molecular characterization, dynamics and exocytosis," *The Journal of Physiology*, vol. 570, no. 3, pp. 567–582, 2006.

[184] V. Montana, E. B. Malarkey, C. Verderio, M. Matteoli, and V. Parpura, "Vesicular transmitter release from astrocytes," *Glia*, vol. 54, no. 7, pp. 700–715, 2006.

[185] X. Chen, L. Wang, Y. Zhou, L.-H. Zheng, and Z. Zhou, ""Kiss-and-run" glutamate secretion in cultured and freshly isolated rat hippocampal astrocytes," *Journal of Neuroscience*, vol. 25, no. 40, pp. 9236–9243, 2005.

[186] F. Valtorta, J. Meldolesi, and R. Fesce, "Synaptic vesicles: is kissing a matter of competence?" *Trends in Cell Biology*, vol. 11, no. 8, pp. 324–328, 2001.

[187] D. N. Bowser and B. S. Khakh, "Two forms of single-vesicle astrocyte exocytosis imaged with total internal reflection fluorescence microscopy," *Proceedings of the National Academy of Sciences of the United States of America*, vol. 104, no. 10, pp. 4212–4217, 2007.

[188] D. A. Rusakov and D. M. Kullmann, "Extrasynaptic glutamate diffusion in the hippocampus: ultrastructural constraints, uptake, and receptor activation," *Journal of Neuroscience*, vol. 18, no. 9, pp. 3158–3170, 1998.

[189] B. Innocenti, V. Parpura, and P. G. Haydon, "Imaging extracellular waves of glutamate during calcium signaling in cultured astrocytes," *The Journal of Neuroscience*, vol. 20, no. 5, pp. 1800–1808, 2000.

[190] A. Araque, R. P. Sanzgiri, V. Parpura, and P. G. Haydon, "Calcium elevation in astrocytes causes an NMDA receptor-dependent increase in the frequency of miniature synaptic currents in cultured hippocampal neurons," *Journal of Neuroscience*, vol. 18, no. 17, pp. 6822–6829, 1998.

[191] Y. V. Pankratov and O. A. Krishtal, "Distinct quantal features of AMPA and NMDA synaptic currents in hippocampal neurons: implication of glutamate spillover and receptor saturation," *Biophysical Journal*, vol. 85, no. 5, pp. 3375–3387, 2003.

[192] B. N. Routh, D. Johnston, K. Harris, and R. A. Chitwood, "Anatomical and electrophysiological comparison of CA1 pyramidal neurons of the rat and mouse," *Journal of Neurophysiology*, vol. 102, no. 4, pp. 2288–2302, 2009.

[193] J. C. Magee, "Dendritic hyperpolarization-activated currents modify the integrative properties of hippocampal CA1 pyramidal neurons," *The Journal of Neuroscience*, vol. 18, no. 19, pp. 7613–7624, 1998.

[194] N. A. Otmakhova, N. Otmakhov, and J. E. Lisman, "Pathway-specific properties of AMPA and NMDA-mediated transmission in CA1 hippocampal pyramidal cells," *Journal of Neuroscience*, vol. 22, no. 4, pp. 1199–1207, 2002.

[195] S. Gasparini, M. Migliore, and J. C. Magee, "On the initiation and propagation of dendritic spikes in CA1 pyramidal neurons," *Journal of Neuroscience*, vol. 24, no. 49, pp. 11046–11056, 2004.

[196] C. M. McDermott, M. N. Hardy, N. G. Bazan, and J. C. Magee, "Sleep deprivation-induced alterations in excitatory synaptic transmission in the CA1 region of the rat hippocampus," *The Journal of Physiology*, vol. 570, no. 3, pp. 553–565, 2006.

[197] C. M. McDermott, G. J. LaHoste, C. Chen, A. Musto, N. G. Bazan, and J. C. Magee, "Sleep deprivation causes behavioral, synaptic, and membrane excitability alterations in hippocampal neurons," *The Journal of Neuroscience*, vol. 23, no. 29, pp. 9687–9695, 2003.

[198] S. Gasparini and J. C. Magee, "State-dependent dendritic computation in hippocampal CA1 pyramidal neurons," *The Journal of Neuroscience*, vol. 26, no. 7, pp. 2088–2100, 2006.

[199] A. E. Metz, T. Jarsky, M. Martina, and N. Spruston, "R-type calcium channels contribute to afterdepolarization and bursting in hippocampal CA1 pyramidal neurons," *The Journal of Neuroscience*, vol. 25, no. 24, pp. 5763–5773, 2005.

[200] M. A. Smith, G. C. R. Ellis-Davies, and J. C. Magee, "Mechanism of the distance-dependent scaling of Schaffer collateral synapses in rat CA1 pyramidal neurons," *The Journal of Physiology*, vol. 548, no. 1, pp. 245–258, 2003.

[201] A. Loebel, G. Silberberg, D. Helbig, H. Markram, M. Tsodyks, and M. J. E. Richardson, "Multiquantal release underlies the distribution of synaptic efficacies in the neocortex," *Frontiers in Computational Neuroscience*, vol. 3, article 27, 2009.

[202] N. J. Abbott, "Astrocyte-endothelial interactions and blood-brain barrier permeability," *Journal of Anatomy*, vol. 200, no. 6, pp. 629–638, 2002.

[203] S. F. Traynelis, L. P. Wollmuth, C. J. McBain et al., "Glutamate receptor ion channels: Structure, regulation, and function," *Pharmacological Reviews*, vol. 62, no. 3, pp. 405–496, 2010.

Hindawi Publishing Corporation
Neural Plasticity
Volume 2016, Article ID 4959523, 13 pages
http://dx.doi.org/10.1155/2016/4959523

Review Article

Role of MicroRNA in Governing Synaptic Plasticity

Yuqin Ye,[1,2] Hongyu Xu,[1] Xinhong Su,[1] and Xiaosheng He[1]

[1]*Department of Neurosurgery, Xijing Hospital, Fourth Military Medical University, Xi'an 710032, China*
[2]*Department of Neurosurgery, Second Affiliated Hospital of Hunan Normal University (PLA 163 Hospital), Changsha 410000, China*

Correspondence should be addressed to Xiaosheng He; hexiaos@fmmu.edu.cn

Received 29 October 2015; Revised 6 January 2016; Accepted 14 February 2016

Academic Editor: Alexei Verkhratsky

Although synaptic plasticity in neural circuits is orchestrated by an ocean of genes, molecules, and proteins, the underlying mechanisms remain poorly understood. Recently, it is well acknowledged that miRNA exerts widespread regulation over the translation and degradation of target gene in nervous system. Increasing evidence suggests that quite a few specific miRNAs play important roles in various respects of synaptic plasticity including synaptogenesis, synaptic morphology alteration, and synaptic function modification. More importantly, the miRNA-mediated regulation of synaptic plasticity is not only responsible for synapse development and function but also involved in the pathophysiology of plasticity-related diseases. A review is made here on the function of miRNAs in governing synaptic plasticity, emphasizing the emerging regulatory role of individual miRNAs in synaptic morphological and functional plasticity, as well as their implications in neurological disorders. Understanding of the way in which miRNAs contribute to synaptic plasticity provides rational clues in establishing the novel therapeutic strategy for plasticity-related diseases.

1. Introduction

Synaptic plasticity, as a specific form of neural plasticity, not only plays an important role in maintaining neural physiological function but also contributes to many nervous system diseases including neurotrauma, neurodegenerative disease, and mental disorder [1, 2]. Actually, synapse structural plasticity and functional plasticity are collectively referred to as the term of synaptic plasticity. The structural plasticity covers the changes of synaptic morphology and number in adapting to activity-induced neural network variation, including dendritic spine modification, axonal sprouting, and new synaptic formation [3]. The functional plasticity encompasses the alterations of synaptic transmission and efficacy in response to neural activity, such as long-term potentiation (LTP), long-term depression (LTD), and homeostatic plasticity [3, 4]. In recent studies, it has been shown that numerous molecules and genes are involved in the complex regulatory process of synaptic plasticity, through which the function of nervous system is coordinated and maintained.

MicroRNA (miRNA), an extensive class of evolutionarily conserved noncoding RNA, contains approximate 22 nucleotides and is involved in post-transcriptional modulation of gene expression. They function collectively to direct mRNA translational inhibition and degradation and to coordinate many physiological and pathophysiological signaling pathways [5]. More than half of those detectable miRNAs are abundant in mammalian nervous system, and accumulating evidence points to a widespread involvement of miRNA in neural development and function [6–8]. Notably, individual miRNAs are particularly enriched in presynaptic and postsynaptic compartments, where they serve to regulate synaptic plasticity and activity by coordinating the intricate genetic circuitries [9, 10]. In this review, we aim to analyze the current data regarding the function of individual miRNAs in synaptic plasticity and, in particular, to understand their regulatory role in synapse morphological and functional plasticity, as well as their implications in plasticity-related neurological diseases.

2. Overview of miRNA Biogenesis and Action

The general biogenesis and diverse functions of miRNA are increasingly becoming clear (Figure 1). There is a series of precise and consecutive processing steps in *Drosha*-dependent pathways of miRNA biogenesis. Initially, the transcription of primary miRNA (pri-miRNA) is mediated by RNA polymerase II in nucleus. Secondly, in the RNase

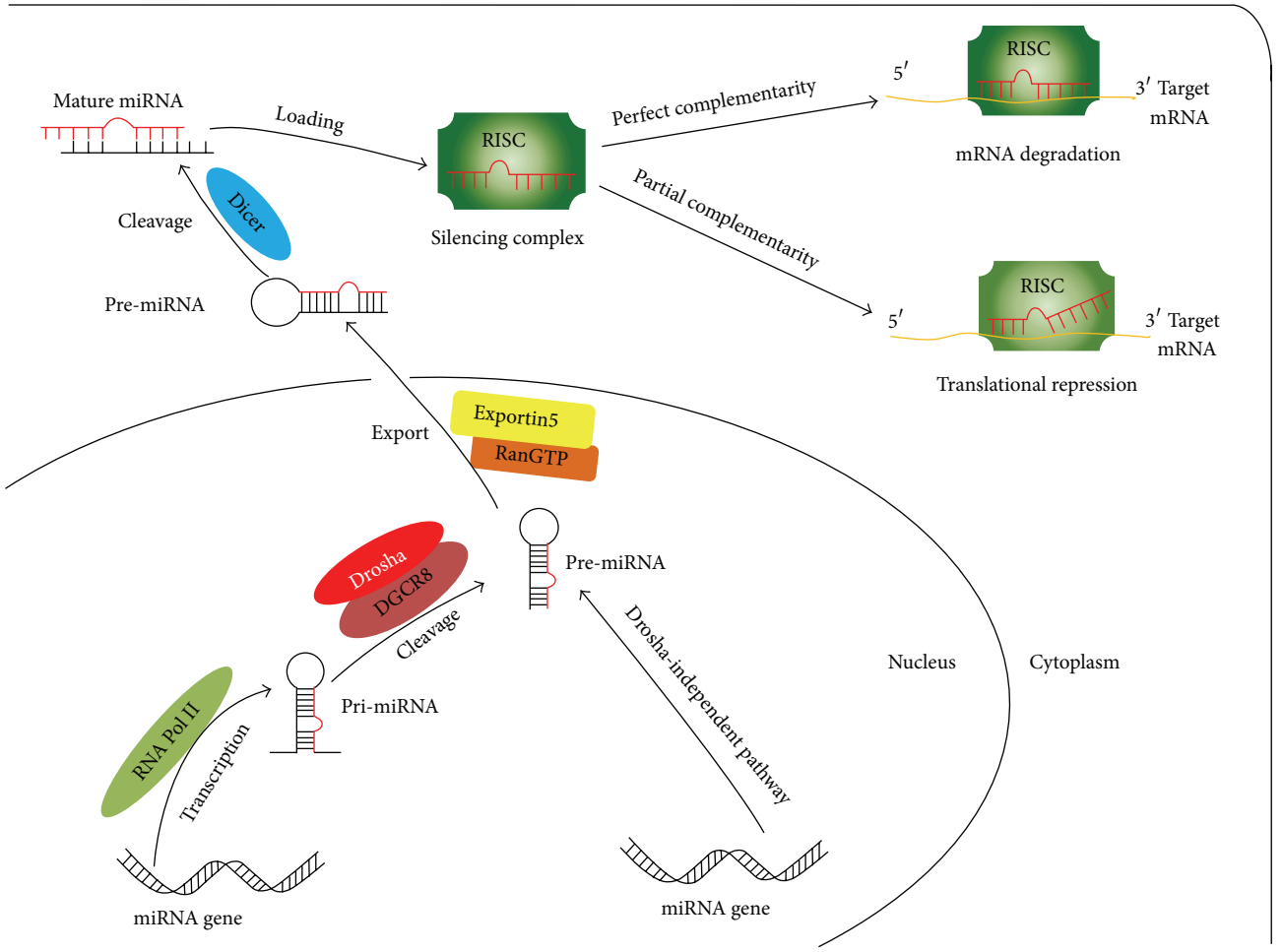

Figure 1: Biogenesis and action of miRNA.

III-family endonuclease *Drosha*/*DiGeorge* syndrome critical region 8 (DGCR8) dependent pathway, the pri-miRNA is cleaved into characteristic precursor miRNA (pre-miRNA), which has a hairpin-like long stem-loop structure containing about 70 nucleotides [11]. Next, pre-miRNA is exported from nucleus into cytoplasm via Exportin5/RanGTP machinery. Then, a second round of processing is mediated by the enzyme Dicer, which cleaves the pre-miRNA into a miRNA duplex of 22 nucleotides in cytoplasm; after that, the duplex is unwound by a helicase. One strand of the duplex interacts with its partner proteins such as argonaute family proteins (AGO2 in *Drosophila* and eIF2C in human) before they are processed into the RNA-induced silencing complex (RISC) [12]. Afterwards, the RISC complex incorporates with mature miRNA to form dissymmetric ribonucleoproteins complex, which will bind to target mRNA in 3′ untranslated region (UTR) through the complementary sequence including 6 to 8 nucleotides and thereby act on mRNA degradation or translational repression [7, 13]. In addition, miRNA is able to prevent circularization and inhibit translational initialing of m7G-capped mRNAs by targeting its 5′ cap region [14, 15].

However, besides the canonical mechanism for biogenesis of most miRNAs, alternative *Drosha*-independent pathways are involved in the synthesis and maturation of some specific miRNA populations [16–18]. One of the widely studied pathways is splicing-mediated pathway in the biogenesis of introns-derived miRNA (known as "miRtron"), which is originally identified in *Drosophila* and *Caenorhabditis elegans* [17, 18]. Following encoding in the introns of protein coding genes, miRtron is spliced and debranched, respectively, by spliceosome and lariat debranching enzyme, after which it is endowed with the features resembling those of pre-miRNA and turns into the main stream miRNA biogenesis pathway to produce functional miRNA *in vivo* [18, 19]. miRtrons are not only identified in invertebrate but also recognized recently in mammal such as mouse and human [17, 20, 21]. Interestingly, Havens et al. reported that two presumable human miRtrons did not rely on the splicing-mediated pathway and thereby termed them as splicing-independent miRtrons (simtrons), but the maturation of the two simtrons was inhibited by dominant negative form of *Drosha* in canonical pathway *in vitro* [17]. Hence, it can be inferred that the underlying cross talk among different pathways may exist and collectively act on the biogenesis of these distinct miRNAs *in vivo*; further exploration is required to elucidate it.

Both canonical and noncanonical pathways of miRNA biogenesis lay foundation for uncovering the interactions between miRNAs and synaptic plasticity. Although the notion that involvement of miRNAs in synaptic plasticity is quite recently coming up, the multiple role and mechanism have been investigated by extensive studies. Most recently, growing investigations have shed light on the sophisticated roles of specific miRNAs in modification of plasticity-related proteins within postsynaptic density, which benefits us to understand the influencing factors and underlying mechanism of synaptic plasticity [9, 22]. Based on the previous studies, it is possible that individual miRNAs are versatile processors in governing synapse morphological and functional plasticity, as stated below.

3. Regulation of miRNA-132 in Synaptic Plasticity

3.1. miRNA-132 and cAMP-Response Element Binding Protein (CREB). miRNA-132 is the most studied plasticity-related miRNA with diverse functions in the processing of synapse plasticity. The CREB induced miRNA-132 is capable of regulating neuronal morphogenesis and synaptic protein synthesis in response to neurotrophin *in vitro* [23, 24]. The fact that activation of neural networks in olfactory bulb, hippocampus, and striatum induced a rapid and significant rise of CREB-regulated miRNA-132 *in vivo* was reported for the first time by Nudelman et al. in 2010 [25]. Accordingly, both *in vitro* and *in vivo* determinations implicate that miRNA-132 is an activity-dependent miRNA and thereby contributes to experience-induced synapse proteomic expression that is regarded as necessary for synaptic plasticity [23–25]. Similarly, the findings are further confirmed and extended by detection of miRNA-132/phosphorylated-CREB (p-CREB) signaling chain in animals and patients with temporal lobe epilepsy (TLE). Compared with sham, the levels of p-CREB and miRNA-132 in epilepsy were significantly upregulated at 24 h after seizure that was characterized with excitatory synaptic activity, new synaptic connections, and LTP in hippocampus [26]. Correspondingly, microRNA-132 silencing inhibits the mossy fiber sprouting (MFS) and dendritic morphology in hippocampal CA3 region, which results in suppression of spontaneous recurrent seizures [27]. Therefore, it is possible that miRNA-132 plays a pathogenic role in epilepsy by processing the synapse activity-dependent plasticity, and intervention of the plasticity will be a novel therapeutic target for epilepsy. In addition, the CREB-regulated miRNA-132 also serves as a dynamic activity-dependent processor of cognition capacity; the level of miRNA-132 *in vivo* is fine-tuned within a suitable range to improve synaptic plasticity for learning and memory [28, 29].

3.2. miRNA-132 and Brain-Derived Neurotrophic Factor (BDNF). It is extensively characterized that BDNF, a critical member of the neurotrophin family, exerts multiple effects on synapse via activation of various intracellular signaling pathways such as phosphoinositide-3-kinase (PI3K), phospholipase C-γ (PLC-γ), mitogen-activated protein kinase/extracellular signal regulated protein kinase (MAPK/ERK), and CREB [24, 30–33]. However, the presumable involvement of miRNAs in BDNF-regulated synaptic function is less well revealed. The interplay between miRNA-132 and BDNF is a focus of recent interests. miRNA-132 is upregulated dose-dependently by BDNF to promote synaptic formation and plasticity [24, 30]. Kawashima and associates demonstrate that BDNF affects miRNA-132 level through MAPK/ERK1/2 pathway to influence synthesis of postsynaptic protein. Glucocorticoid exposure also results in a decrease in BDNF-induced synaptic function via inhibiting expression of miRNA-132 [30]. Furthermore, CREB is available for positive modulation of memory performance and consolidation by regulating the expression of BDNF [23]. In addition, new insight into miRNA-132 action has been verified in the development of retinal ganglion cell (RGC) axon. In this study, BDNF treatment gives rise to significant upregulation of miRNA-132 in RGC, which results in promotion of axon sprouting and growth [34].

3.3. miRNA-132 and p250 GTPase Activating Protein (p250GAP). As a downstream target of miRNA-132, p250GAP knockdown not only enhances hippocampal activity-dependent neuronal morphogenesis and the frequency of miniature excitatory postsynaptic currents (mEPSCs) but also promotes dendritic spine formation and the prevalence of glutamate receptor 1 (GluR1) positive spines. Yet upregulation of p250GAP by inhibiting the expression of miRNA-132 can give rise to a converse effect [35, 36]. Moreover, p250GAP is responsible for the activation of Rac1/Pak cascade, which has been identified as another downstream of miRNA-132 and specifically contributes to dendritic spine formation [36]. Shaltiel et al. provided further evidences that extended miRNA-132 to inhibit the level of hippocampal acetylcholinesterase (AChE), which played an important role in stressful experience-induced neurite extension and cognitive function [37]. In another example, cultured hippocampal HT22 cells suffering from ionizing radiation enabled a reduction of miRNA-132 and Rac1 in miRNA-132/p250GAP/Rac1/Cofilin signaling pathway, which was closely related to synaptic actin-remodeling and spine morphological alterations that enabled correct processing of learning and memory. In line with the *in vitro* result, the *in vivo* detection further confirmed the effect of miRNA-132 on irradiated mice brain [38]. Intriguingly, the powerful regulator of energy homeostasis, leptin, can act in hippocampus to promote the formation of stable dendritic spines and functional synapses by inducing CREB transcription and increasing miRNA-132-mediated suppression of p250GAP activity, which eventually improve cognitive function and attenuate depression or anxiety [39]. Additionally, in the neurotoxicity of polychlorinated biphenyls (PCB95), the sensitized ryanodine receptors (RyR) can upregulate miRNA-132 expression via CREB-dependent mechanism and subsequently inhibit the translation of p250GAP, resulting in abnormal enhancement of neuronal connectivity, aberrant synaptogenesis, incorrect synaptic network, and neuropsychological dysfunction [40]. Therefore, it can be concluded that miRNA-132/p250GAP pathway and its cross talk with other cascades play

a significant role in the regulation of synapse plasticity and that inhibiting this pathway may be beneficial to plasticity-related neurological diseases.

3.4. miRNA-132 and Methyl CpG-Binding Protein 2 (MeCP2). Another negative-regulated target of miRNA-132 is MeCP2, which is enriched in developing central nervous system (CNS) and highly correlated with activity-induced synaptic plasticity and axonal and dendritic development [41]. In the hippocampus of miRNA-132 overexpressed mice, significantly decreased MeCP2 level and increased dendritic spine density were observed, while the novel object recognition memory of these mice was impaired [42]. Meanwhile, the expression of MeCP2 and the functions of spatial learning and memory were also affected in miRNA-132/212 knockout mice [43]. Indeed, MeCP2 mutation restricts synaptogenesis, dendritic spine maturation, and neural circuits development, which is characterized in the pathogenesis of most Rett syndrome (RTT) cases and is closely linked to the mental abnormalities of RTT [44, 45]. Genome-wide screening showed that the expressions of miRNA-132 and BDNF were significantly decreased in a mouse model of RTT, suggesting that dysregulation of miRNA-132 was involved in the progression of RTT and boosting the level of miRNA-132 might be a valuable strategy for RTT therapy [46].

Most recently, the study by Zhang et al. stated that 2.5-fold overexpression of MeCP2 was available for attenuating both acute pain transduction and chronic pain formation in spinal cord via miR-132/CREB pathway, but excessive high level of MeCP2 would cause abnormal axonal arborization and had no analgesic role in pain transmission [47]. Therefore, this data indicates that intervention of miRNA-132/MeCP2 cascade to maintain MeCP2 within a proper and narrow range may be a promising therapeutic option for spinal cord pain. Further study revealed a modulatory feed loop for the homeostatic regulation of MeCP2 and miRNA-132 *in vivo* [48]. In the loop circuit, besides the known negative regulation of MeCP2 by miRNA-132, MeCP2 also plays a feedback control role in the transcription of miRNA-132 [46, 48].

3.5. miRNA-132 and Fragile X Mental Retardation Protein (FMRP). It has been showed that miRNA-132 and the proteins (e.g., Dicer and AGO1) of RISC could biochemically interact with FMRP, which was involved in regulation of synaptic plasticity by repressing translation of its mRNA ligands and synthesis of proteins at the synapse [49, 50]. Deletion of FMRP could result in pronounced overgrowth of dendritic spine and abnormal synthesis of synaptic protein at the larval neuromuscular junction (NMJ) [49]. Additionally, in the regulation of dendritic spine morphology by miRNA-132 and miRNA-125b, the downstream targets of the two miRNAs are tightly associated with FMRP to encode plasticity-related proteins involved in synaptic function [51]. Another recent study identified that FMRP along with the candidate RNA-binding protein Ataxin-2 modulated long-term plasticity via common presynaptic and postsynaptic target mRNA [52]. Since the abnormalities of synaptic plasticity resulting from FMRP dysfunction are known pathogenesis of fragile X syndrome (FXS) [53], therefore, it could be hypothesized that FXS might be, at least in part, related to the dysfunction of miRNA-132, yet the definite mechanism remains to be clarified.

3.6. miRNA-132 and miRNA-212. As miRNA-132 and miRNA-212 derive from the same intron of a small noncoding gene, they are capable of sharing the same targets and act in a common manner on synaptic plasticity [54]. It has been demonstrated that the expression pattern of pri-miRNA-132/212 and pre-miRNA-132/212 are affected in parallel during the process of dentate gyrus LTP [55]. Ablation of miRNA-132/212 can inhibit the neocortical θ burst-induced LTP and hippocampal synaptic transmission, which is possibly ascribed to the decreased postsynaptic α-amino-3-hydroxy-5-methyl-4-isoxazolepropionic acid receptor (AMPAR) [56]. With the analysis of bidirectional ratio metric miRNA sensors in hippocampus, Magill and colleagues also revealed that deletion of the miRNA-132/212 locus led to a dramatic decrease in dendritic length, arborization, and spine density of hippocampal newborn neurons [57]. Moreover, in the processing of hippocampal functional synapse formation, miRNA-132 is the key functional generation of the miRNA-132/212 locus to mediate the integration of newborn neurons into the dentate gyrus and contributes to the dendritic phenotype [57, 58]. In addition, the repressor element sites in promoter regions of miRNA-132 can be functionally targeted by repressor element 1 silencing transcription factor/neuron-restrictive silencing factor (REST/NRSF), and this interaction is essential for hippocampal newborn neurons activity and structural remodeling [59].

Interestingly, miRNA-132/212 also act on the synaptic plasticity of visual cortex [60–62]. It has been found that monocular deprivation would be in a position to hinder the modification of miRNA-132/212 locus and subsequently decreased the miRNA-132/212 cluster transcription in developing visual cortex [60]. Likewise, parallel findings revealed that the expression of miRNA-132 in the visual cortex was upregulated by light stimulation and delayed in response to dark-rearing. Inhibition of miRNA-132 can prevent dendritic spine maturation, ocular dominance plasticity, and formation of synaptic connectivity *in vivo* [61, 62].

4. Regulation of miRNA-134 in Synaptic Plasticity

4.1. miRNA-134 and Sirtuin1 (SIRT1). Another brain-enriched miRNA that has been found to be involved in the regulation of synaptic plasticity is miRNA-134. In the processing of miRNA-134 transport to dendrites, Bicker et al. showed that DEAH-box helicase DHX36 was responsible for the dendritic localization of miRNA-134 and the modification of miRNA-134 in dendritic spine size [63]. Furthermore, Gao and associates found that deacetylase SIRT1 was able to suppress the expression of miRNA-134 via cooperating with the transcription factor Yin Yang 1 (YY1) and additional proteins [64]. In their study, overexpression of miRNA-134 in hippocampal CA1 region following SIRT1 deficiency led to

a decreased level of CREB and BDNF and thereby impairing LTP and long-term memory formation in contextual fear conditioning [64]. Conversely, activation of SIRT1 could rescue the damaged synaptic plasticity by inhibiting the expression and posttranscriptional regulation of miRNA-134 [64]. In addition, miRNA-134 has also been implicated in the regulation of activity-induced dendritic excitability and outgrowth, as well as the number of excitatory synapses in hippocampus [65].

4.2. miRNA-134 and Lim Kinase 1 (Limk1). Overexpression of miRNA-134 causes a marked reduction in the dendritic spine volume and synaptic strength of hippocampal neurons *in vitro*, whereas silencing of endogenous miRNA-134 results in an increased spine width and enhanced synaptic transmission [66]. Another cortical morphometric observation revealed that overexpression of miRNA-134 in brain could reduce the dendritic arborization of cortical layer V pyramidal neurons *in vivo* [67]. Further mechanic analysis identified that these effects were mediated by the repression of miRNA-134 on Limk1 translation, which was critical to the regulation of Cofilin phosphorylation and actin dynamics for synaptic function and plasticity [66, 68, 69]. Accordingly, it might raise the possibility that miRNA-134 worked as a negative modulator of dendritic spine development, synaptic formation, and plasticity. Moreover, it has been demonstrated that BDNF has the potential to relieve miRNA-134 inhibition of Limk1 through activation of the TrkB/mTOR pathway and thereby results in the reversible effect [66, 70, 71]. However, some studies indicated that miRNA-134 activity was restricted to specific neurons such as inhibitory GABAergic interneurons rather than other types of cortical neurons including pyramidal neurons. In these interneurons, the palmitoylation enzyme DHHC9 serves as a putative target of miRNA-134 and is critical for the modification of H-Ras, which displays a pivotal role in neuronal membrane trafficking and LTP modification [72, 73].

Studies focusing on the association between miRNA and epilepsy revealed that hippocampal miRNA-134 level was significantly upregulated in TLE [74, 75]. Silencing of miRNA-134 is able to decrease the expression of Limk1 and leads to unexpectedly reduced pyramidal neuron spine density and improved seizures, but no alteration in dendritic spine size [74]. However, a subsequent study identified that miRNA-134 remained at a low level while the expressions of CREB and p-CREB were significantly increased in hippocampus of epileptic rats [76]. Taken together, these data suggest that miRNA-134 is implicated in regulation of synaptic plasticity in epilepsy through diverse downstream targets such as Limk1 and CREB. However, further investigations are expected to clarify the possible cross talk and collective effect of different signaling cascades.

5. Regulation of miRNA-138 in Synaptic Plasticity

5.1. miRNA-138 and Acyl Protein Thioesterase1 (APT1). miRNA-138 is ubiquitous with high expression in the dendrites of hippocampal neurons and contributes to regulation of dendritic spine size and structure [77, 78]. Functional screening demonstrates that APT1-induced palmitoylation of G protein α13 (Gα13) is important for the regulatory function of miRNA-138 during dendritic spine development [77]. High level of miRNA-138 leads to a significant decrease in APT1 level and subsequently increases Gα13 palmitoylation and membrane localization, which can activate the Rho-dependent signaling cascade and thereby induce dendritic spine shrinkage with a concomitant reduction in synaptic transmission [77].

Recently, a panel of studies focusing on miRNA-138 function during the process of learning and memory showed a close association with local plasticity-related protein synthesis [79, 80]. According to the detection of human postmortem brain tissue, miRNA-138 and decapping mRNA 1B (DCP1B) were identified to express in hippocampus and frontal cortex. Furthermore, Schröder et al. found that a human memory-associated single nucleotide polymorphism could interfere with miRNA-138 binding to the transcripts of DCP1B, implying that miRNA-138 might be a modulator of human memory performance [79]. In another determination, high level of miRNA-138 and its suppression on downstream target APT1 mRNA translation in the CA1 and DG give rise to better performance on novel object recognition task that reflects the short-term recognition memory [80]. Intriguingly, the hippocampal APT1 mRNA is dramatically increased in aged mice, but no alteration occurs in the status of impaired memory. And, in particular, the expression of APT1 protein presents location-specific pattern; its level in neuropil is evidently higher than that in cell body of neurons [80].

5.2. miRNA-138 and Sirtuin1 (SIRT1). miRNA-138 binding directly to the 3′ UTR of SIRT1 mRNA results in a marked decrease in the expression of SIRT1 and a significant inhibition of axon extension in DRG neurons, whereas overexpression of SIRT1 can dramatically promote axon growth [81]. This result indicates that SIRT1 serves as a downstream functional target of miRNA-138 in the modification of intrinsic axon growth capacity. In addition, SIRT1 is capable of acting as a feedback inhibitory factor to repress the level of miRNA-138 *in vivo*, suggesting that the interplay of miRNA-138 and SIRT1 is likely to be an effective intervening target to enhance axon regeneration [81].

6. Regulation of miRNA-9 in Synaptic Plasticity

miRNA-9 is one of the synapse-enriched miRNAs regulating gene expression. Using the miRNA sponge technique to silence the miRNA-9 conditionally in mice, Giusti et al. discovered that hippocampal dendrites growth and synaptic transmission were disturbed and concomitant with strong upregulation of transcriptional repressor REST. Further determination revealed that shRNAs against REST could rescue the dendritic growth deficit and impair synaptic transmission caused by miRNA-9 depletion [82]. Hence, it is possible that miRNA-9 is essential for synaptic formation and plasticity by targeting REST *in vivo*. Moreover, another study defined a novel role of miRNA-9 and its predictable target

forkhead box G 1 (FOXG1) in olfactory receptor neurons differentiation, axon elongation, and synaptic connectivity [83]. Meanwhile, the expression of miRNA-9 and miRNA-200 was regulated by transcriptional factor distal-less homeobox5 (DLX5) [83]. Additionally, two FMRP homologous fragile X related (FXR) proteins, FXR1P and FXR2P, are believed to participate in RNA metabolism [84]. Indeed, the level of miRNA-9 and miRNA-124 decreased in the brain of FXR1P knockout mouse, and overexpression of FXR1P led to significantly increased expression of miRNA-9 and miRNA-124. However, absence of either FXR2P or FMRP does not affect level of the two brain-specific miRNAs [85]. Accordingly, the data indicated that both miRNA-9 and miRNA-124 might not be responsible for FXS that mainly resulted from the loss of FMRP.

Amyloid β42- (Aβ42-) dependent downregulation of miRNA-9 provides novel insight into amyloidogenesis in the pathological process of Alzheimer's disease (AD) [86]. It has been documented that Aβ42 oligomers induce dendritic spine loss and microtubule-associated protein tau hyperphosphorylation by the calcium/calmodulin-dependent protein kinase kinase 2, adenosine monophosphate-activated protein kinase (CAMKK2-AMPK) signaling cascade, which is tightly associated with synaptic plasticity alteration in AD progression [87, 88]. Overexpression of miRNA-9 could attenuate the Aβ-induced synaptotoxic effect via inhibition of CAMKK2 level, implying that CAMKK2 emerged as an additional target of miRNA-9 in the abnormal synaptic plasticity of AD [89]. In addition, tau hyperphosphorylation in the progression of AD is also promoted by upregulated miRNA-138 via retinoic acid receptor alpha/glycogen synthase kinase-3β (RARA/GSK-3β) pathway [90]. However, whether or not and how synaptic plasticity responds to the increased tau phosphorylation in AD have not been identified, and future investigation is required to elucidate it.

7. Regulation of miRNA-124 in Synaptic Plasticity

Another highly and specifically expressed miRNA in nervous system is miRNA-124, which contributes to a multitude of biological processes such as neurogenesis, synapse morphology, and synaptosome transmission [91, 92]. Recently, miRNA-124 is reported to play an extending role in inhibiting the expression of RhoG [93]. This interaction is further involved in regulating the actin cytoskeleton in plasticity of synapse connections, which refers to dual modes: on one hand, RhoG is available to inhibit dendritic tree complexity via the small GTPase Cdc42 in hippocampal neuron; on the other hand, RhoG is pointed out to repress axonal branching and targeting dependent on the ELMO/Dock180/Rac1 signaling pathway [93–95]. Several groups have identified that the intelligence quotient motif containing GTPase activating protein 1 (IQGAP1), a broadly expressed scaffold protein in brain, acted as a suppressed target of miRNA-124 to regulate hippocampal LTP, long-term memory formation, and cognitive performance [96, 97]. Moreover, in cultured neurons of *Aplysia* sensorimotor synapses, miRNA-124 is localized exclusively to the presynaptic sensory neuron but found deficiently in motor neuron. Overexpression of miRNA-124 inhibits the serotonin-triggered synaptic long-term facilitation (LTF) by targeting CREB, and downregulation of miRNA-124 reversely gives rise to significant enhancement of LTF in learning-related synaptic plasticity [92]. In addition, high expression of miRNA-124 and decreased level of AMPAR are tightly associated with hippocampal demyelination and memory impairment in mice. And remyelination could restore the memory dysfunction and altered expression of miRNA-124 and AMPAR. Accordingly, it is possible that intervention of the potential miRNA-124/AMPA signaling may be a novel clue to improve memory performance in neurodegenerative diseases [98]. More importantly, miRNA-124 and miR-181a were engaged in cocaine-responsive plasticity through BDNF and downstream target, which played an important role in synaptic plasticity and addiction [99]. This data implies a promising possibility that a novel layer of miRNA-124 could be applied to drug rehabilitation in future.

8. Regulation of miRNA-125a and miRNA-125b in Synaptic Plasticity

Compared to other miRNAs at the synapse, miRNA-125a is abundant in the dendrites of hippocampal CA1 region and highly expressed in synaptoneurosomal fractions [66]. It has been showed that miRNA-125a is responsible for the translation of postsynaptic density (PSD-95), a core member of postsynaptic scaffold proteins with the function of managing synaptic strength and dendritic spine stabilization [100, 101]. Transfection of anti-miRNA-125a results in an upregulation of endogenous PSD-95 protein in the distal dendrites of hippocampal neurons, accompanied by significantly increased spine density and branching. And interfering with PSD-95 mRNA by specific siRNAs could reverse the altered spine morphology [101]. Further evidence reveals that the inhibition of miRNA-125a on PSD-95 is mediated by alternate G-quadruplex RNA conformations, which assist miRNA-125a to access into the binding site (G-rich region within 3′ UTR) of PSD-95 mRNA and form stable complex for interaction [22]. More intriguingly, the binding site of PSD-95 mRNA has been also shown to be directly recognized by FMRP, and phosphorylation of FMRP contributed to reinforcing the translational repression of PSD-95 induced by miRNA-125a [101, 102]. In addition, miRNA-125a is also involved in mGluR-mediated translation of local protein synthesis to modulate dendritic spine structure [101, 103].

The other homologous member of miRNA-125 family is miRNA-125b, which is also involved in synaptic plasticity [104–106]. It has been characterized that overexpression of miRNA-125b led to a significant increase in hyperphosphorylation of microtubule-associated protein tau and caused impairment of learning and memory. The activity was possibly mediated by the predicted targets of miRNA-125b including Bcl-2-like protein 2 (Bcl-W), dual specific phosphatase 6 (DUSP6), and protein phosphatase 1 catalytic subunit alpha isoform (PPP1CA) [105]. In addition, miRNA-125b induced downregulation of the essential synaptic glycoprotein synapsin-2 (SYN-2) is engaged in synaptic vesicles

activity and synaptic transmitters trafficking in neuronal circuitry [104, 106].

9. Regulation of miRNA-188 in Synaptic Plasticity

Neuropilin-2 (Nrp-2), a receptor of semaphorin 3F, is capable of disturbing dendritic spine development and synaptic structure [107]. Lee et al. have reported that miRNA-188 served as an important modulator for synaptic plasticity by negatively targeting Nrp-2. In the study, induction of LTP led to decreased expression of Nrp-2 and increased level of synaptic activity-regulated miRNA-188, which could improve abnormal synaptic morphology and promote mEPSCs in hippocampus [108]. In addition, studies of neurodegenerative processes emphasized that miRNA-188-3p played a crucial role in the interaction of 2-arachidonoylglycerol (2-AG) metabolism and β-site amyloid precursor protein cleaving enzyme 1 (BACE1) expression in AD. On one hand, miRNA-188-3p expression was identified to be significantly reduced in APP transgenic mice, but it could be upregulated by 2-AG via peroxisome proliferator-activated receptor-γ (PPARγ) and NF-κB signaling pathway. On the other hand, high level of miRNA-188-3p in hippocampus gave rise to a set of biochemical and cognitive changes, including suppressions in BACE1 expression, Aβ synthesis and promotions in LTP, synaptic transmission, and spatial learning and memory. Moreover, validation of functional binding of miRNA-188-3p seed region in the 3′ UTR of BACE1 indicates that BACE1 acts as a downstream target of miRNA-188-3p governing synaptic plasticity and cognitive function [109].

10. Regulation of Other Specific miRNAs in Synaptic Plasticity

In addition to the above well-studied miRNAs, recent investigations show that other synapse-specific miRNAs are emerging to take a share in the process of plasticity modulation. miRNA-8 along with its multiple downstream target genes plays a critical role in neuromuscular synapse maturation at diverse stages in *Drosophila* [110, 111]. Synaptic cell adhesion molecules fasciclin III (FasIII) and neuroglian (Nrg) depend on miRNA-8 for accurate motor axon extension, suggesting that miRNA-8 has the capacity of regulating synaptic sites assembly at early stages of synaptic formation [110]. Besides, the regulation of miRNA-8 on enabled/vasodilator-stimulated phosphoprotein (Ena/VASP) family is essential for the presynaptic morphological modification required to match the substantial growth of postsynaptic targets at late stages of synaptic maturation [111].

Most recently, the study by Gao et al. reveals that miRNA-15a induced MeCP2 has a significant impact on the expression of BDNF, which subsequently plays a critical role in hippocampal dendritic branching and complexity [112]. The role of miRNA-19b in dendritic development and synaptic protein synthesis is correlated to the phosphoinositide-3-kinase/mammalian target of rapamycin (PI3K/mTOR) signaling that is triggered by phosphatase and tensin homolog (PTEN) [113]. Notably, miRNA-22 is suppressed by serotonin to mediate the regulation of cytoplasmic polyadenylating element binding (CPEB) genes in synaptic protein synthesis, which contributes to the maintenance of memory-related long-term synaptic plasticity [114]. Furthermore, miRNA-26a and miRNA-384-5p are consistently required for the maintenance of LTP and dendritic spine growth in CA1 region by targeting endogenous ribosomal S6 kinase 3 (RSK3) [115]. Inhibition of miRNA-26a can attenuate neurite outgrowth and neuronal morphogenesis via activation of PTEN [116]. In addition, Lippi et al. found that Arpc3 (subunit 3 in the actin-related protein 2/3 complex), which was targeted by miRNA-29a/b, modulated synapse structural plasticity via spine actin cytoskeleton remodeling [117].

Tap73, a transcription factor of p53 family, is shown to control the expression of miRNA-34a in hippocampal neurons, and this action is involved in the manipulation of synaptic proteins such as synaptotagmin-1 (Syt-1) and syntaxin-1A (Stx-1A) to regulate dendritic spine morphology and function [118, 119]. Meanwhile, miRNA-34a together with miRNA-193a and miRNA-326 synergistically drives the expression of activity-regulated cytoskeleton (Arc) associated protein in the processing of adaptive synaptic plasticity in response to external stimulation [120].

In addition, miRNA-128 regulates the dendritic arborization and intrinsic excitability of upper layer cortical neurons mediated by plant homeodomain finger 6 (PHF6) genes [121]. miRNA-137 manages dendritic spine patterning and plasticity-related protein synthesis in hippocampus via translational modulation of mind bomb 1 (Mib1) [122]. More importantly, miRNA-182 acts through cortactin and Rac1 to regulate synaptic protein synthesis in long-lasting plasticity which is the first characterization of miRNA-182 in lateral amygdala and provides a novel mechanism for modulating synaptic plasticity [123]. miRNA-191 and miRNA-135 contribute to the N-methyl-D-aspartate (NMDA) receptor-induced LTD, respectively, by targeting tropomodulin 2 (Tmod2) and complexin-1/2 [124].

11. Discussion

The abundant evidence uncovers powerful regulatory role and mechanism of miRNA in various aspects of synaptic plasticity ranges from dendritic spine morphology and synaptic formation to plasticity-related protein synthesis (Table 1). The widespread miRNA-mediated regulation of synaptic plasticity is not only essential for neural development and physiological function but also involved in the pathogenesis and progression of multiple neurological disorders, such as AD, FXS, and epilepsy [27, 85, 89]. Furthermore, these findings lay favorable foundations for diagnosis and therapy of plasticity-related diseases. Actually, the identification of AD-related miRNAs in cerebrospinal fluid indicates that individual miRNAs may serve as promising biomarkers for AD diagnosis [86]. The regulation of miRNA-124 in cocaine-induced synaptic plasticity suggests that miRNA can be considered as a target for addiction therapy [99]. In addition, recent studies have showed that plasma miRNA-134 levels in mania patients treated with mood stabilizer lithium were significantly decreased, which was closely associated with

Table 1: Involvement of miRNA in synaptic plasticity.

miRNA	Target	Plasticity paradigm	References
miRNA-132		Regulated by CREB in activity-induced synaptic morphology, protein synthesis, and plasticity	[24, 25]
	p-CREB	Dendritic plasticity in TLE	[26]
	MFS	Dendrites morphology of CA3 region in spontaneous recurrent seizures	[27]
		Regulated by CREB in dendritic spine density and structure adaptation required for cognition capacity	[23, 28, 29]
	GR	Modulated by BDNF in synaptic formation and postsynaptic protein	[24, 30]
		Maturation of neuron and synapse in developing hippocampus	[31]
	p250GAP	RGC axonal sprouting and growth	[34]
	p250GAP	Activity-induced hippocampal dendrite spine morphogenesis and mEPSC and GluR1 positive spines	[35, 36]
	AChE	Stressful experiences induced neurite extension in cognitive and locomotion impairments	[37]
	Rac1	Synaptic actin-remodeling and spine morphological alteration in ionizing radiation	[38]
	p250GAP	Abnormal synaptogenesis and incorrect synaptic connectivity and function in PCB95 neurotoxicity	[40]
	p250GAP	Formation of stable dendritic spines and functional synapses in hippocampus	[39]
	MeCP2	Synaptic density and maturation in novel object recognition and memory retention	[42–44]
	MeCP2	Synaptic plasticity in RTT	[46, 48]
	MeCP2	Synaptic function in acute pain transduction and chronic pain formation	[47]
		Synaptic protein synthesis and dendritic spine structure related to FMRP	[49, 51]
	AMPAR	Neocortical θ burst-induced LTP and hippocampal synaptic transmission and plasticity	[56]
	IL-6, TSLP	Dendritic phenotype and synaptic formation in newborn neurons activity	[57, 58]
		Ocular dominance and visual cortex plasticity	[60–62]
		Modulated by REST/NRSF in synaptic plasticity and structural remodeling	[59]
miRNA-134		Regulated by SIRT1 in hippocampal LTP and long-term memory formation required for fear conditioning	[64]
		Regulated by DHX36 in plasticity-related genes and modification of dendritic spine size	[63]
	Pumilio2	Activity-induced hippocampal dendritic growth and excitatory synapse number	[65]
	Limk1	Dendritic spine size of neuron *in vitro* and dendritic arborization of cortical layer V pyramidal neurons *in vivo*	[66, 67]
	Limk1	Pyramidal neuron spine density in TLE	[74]
	DHHC9	Neuronal membrane trafficking and synaptic LTP and structure in specific interneurons by modification of H-Ras	[72]
	CREB	Synaptic plasticity in epileptic rat	[76]
miRNA-138	APT1	Dendritic spine size and synaptic transmission	[77]
		Episodic memory performance	[79]
	APT1	Synaptic protein synthesis in short-term recognition memory	[80]
	SIRT1	Axon growth in development and regeneration	[81]
miRNA-9	REST	Dendrites growth and synaptic transmission	[82]
	FOXG1	Affected by DLX5 in axon elongation and synaptic connectivity	[83]
	CAMKK2	Synaptotoxicity and dendritic spine loss in AD	[89]
	RhoG	Dendritic tree complexity and axonal branching	[93, 94]
miRNA-124	CREB	LTF in learning-related synaptic plasticity	[92]
	IQGAP1	Hippocampal LTP, long-term memory, and cognitive performance	[96, 97]
	AMPAR	Hippocampal demyelination and memory performance	[98]
	BDNF	Cocaine-induced plasticity and addiction	[99]
miRNA-125a	PSD-95	Synaptic strength and dendritic spine stabilization	[100, 101]
	GluR	Synaptic plasticity-related protein synthesis	[101, 103]

Table 1: Continued.

miRNA	Target	Plasticity paradigm	References
miRNA-125b	Tau	LTD and cognitive performance in AD	[105]
	SYN-2	Synaptic vesicles trafficking in neuronal circuitry	[104]
miRNA-188	Nrp-2	Dendritic spine development, synaptic structure, and mEPSC frequency	[108]
	BACE1	Regulated by 2-AG in hippocampal LTP, synaptic transmission, and cognitive function	[109]
miRNA-8	FasIII, Nrg	Assembly of synaptic sites at early stages of synaptic formation	[110]
	Ena/VASP	Presynaptic morphological modification at late stages of synaptic development	[111]
miRNA-15a	BDNF	Regulated by MeCP2 in hippocampal dendritic branching and complexity	[112]
miRNA-19b	PTEN	Synaptic development and synaptic protein synthesis	[113]
miRNA-22	CPEB	Memory-related long-term synaptic plasticity	[114]
miRNA-26a	PTEN	Synaptic plasticity and neuronal morphogenesis	[116]
	RSK3	Long-lasting synaptic and spine plasticity	[115]
miRNA-29a/b	Arpc3	Dendritic spine actin cytoskeleton remodeling and synaptic connectivity	[117]
miRNA-34a	Stx-1A, Syt-1	Regulated by Tap73 in dendritic spine morphology and synaptic function and plasticity	[118, 119]
	Arc	LTP, LTD, and adaptive synaptic plasticity	[120]
miRNA-128	PHF6	Dendritic arborization and intrinsic excitability of upper layer cortical neurons	[121]
miRNA-137	Mib1	Dendritic patterning and spine morphogenesis	[122]
miRNA-182	Rac1, cortactin	Long-lasting functional and structural plasticity	[123]
miRNA-191	Tmod2	Actin depolymerization in long-lasting dendritic spine remodeling	[124]
miRNA-135	Complexin-1/2	AMPAR exocytosis in prolonged spine structuring	[124]

Abbreviations in the table were illustrated in the text.

synaptic pathology and clinical symptoms of manic [125]. These investigations expand our knowledge about miRNA contribution to the pathophysiology of neural plasticity and further improve the likelihood of applying miRNA-related strategies in clinical neurological diseases management. Currently, interfering with disease-related miRNAs and genes in miRNA cascade seems to be a promising miRNA-based therapeutic strategy. However, there is a great deal of problems that remain unsolved, one of which is lack of feasible targeted-delivery system to transport miRNA mimics or antagonists to specific miRNA in CNS *in vivo*. Recently, Hwang et al. reported that rabies virus glycoprotein-disulfide linked polyethylene imine could be used as a carrier to deliver neurogenic miRNA-124a across the blood brain barrier and make it accumulated in brain, but there was hardly any functional effect due to the degradation of miRNA in the processing of transportation [126]. As a result, improving the stability of transporter is another critical factor for excellent miRNA targeted-delivery system.

In conclusion, miRNA is a crucial regulator in synaptic plasticity. Combining high-throughput identification with functional assay of the interconnected miRNA network enables us to understand more information about the global effect of miRNAs from synaptic plasticity regulation to neurological diseases treatment. A deep insight into the mechanism through which the miRNA works for synaptic plasticity is significantly necessary before miRNA is applied to novel therapeutic intervention for neurological disorders. Thus, establishment of the entire framework of plasticity-related miRNAs will be a challenge in the near future.

Conflict of Interests

The authors declare that there is no conflict of interests regarding the publication of this paper.

Authors' Contribution

Yuqin Ye, Hongyu Xu, and Xinhong Su contributed equally to this work.

Acknowledgment

The present work was supported by grants from the National Natural Science Foundation of China (ID: 81171155 and 81471264, obtained by Xiaosheng He).

References

[1] J. Wondolowski and D. Dickman, "Emerging links between homeostatic synaptic plasticity and neurological disease," *Frontiers in Cellular Neuroscience*, vol. 7, article 223, 2013.

[2] G. Turrigiano, "Homeostatic synaptic plasticity: local and global mechanisms for stabilizing neuronal function," *Cold Spring Harbor Perspectives in Biology*, vol. 4, no. 1, Article ID a5736, 2012.

[3] J. D. Richter, "RNA and the synapse," *RNA*, vol. 21, no. 4, pp. 716–717, 2015.

[4] C. Straub and B. L. Sabatini, "How to grow a synapse," *Neuron*, vol. 82, no. 2, pp. 256–257, 2014.

[5] E. Huntzinger and E. Izaurralde, "Gene silencing by microRNAs: contributions of translational repression and mRNA decay," *Nature Reviews Genetics*, vol. 12, no. 2, pp. 99–110, 2011.

[6] C. E. Holt and E. M. Schuman, "The central dogma decentralized: new perspectives on RNA function and local translation in neurons," *Neuron*, vol. 80, no. 3, pp. 648–657, 2013.

[7] D. Lenkala, E. R. Gamazon, B. LaCroix, H. K. Im, and R. S. Huang, "MicroRNA biogenesis and cellular proliferation," *Translational Research*, vol. 166, no. 2, pp. 145–151, 2015.

[8] E. M. Jobe, A. L. McQuate, and X. Zhao, "Crosstalk among epigenetic pathways regulates neurogenesis," *Frontiers in Neuroscience*, vol. 6, article 59, 2012.

[9] J. E. Cohen, P. R. Lee, S. Chen, W. Li, and R. D. Fields, "MicroRNA regulation of homeostatic synaptic plasticity," *Proceedings of the National Academy of Sciences of the United States of America*, vol. 108, no. 28, pp. 11650–11655, 2011.

[10] R. Fiore, G. Siegel, and G. Schratt, "MicroRNA function in neuronal development, plasticity and disease," *Biochimica et Biophysica Acta (BBA)—Gene Regulatory Mechanisms*, vol. 1779, no. 8, pp. 471–478, 2008.

[11] Y. Lee, C. Ahn, J. Han et al., "The nuclear RNase III *Drosha* initiates microRNA processing," *Nature*, vol. 425, no. 6956, pp. 415–419, 2003.

[12] P. J. Kenny, H. Zhou, M. Kim et al., "MOV10 and FMRP regulate AGO2 association with microRNA recognition elements," *Cell Reports*, vol. 9, no. 5, pp. 1729–1742, 2014.

[13] W. Filipowicz, S. N. Bhattacharyya, and N. Sonenberg, "Mechanisms of post-transcriptional regulation by microRNAs: are the answers in sight?" *Nature Reviews Genetics*, vol. 9, no. 2, pp. 102–114, 2008.

[14] A. Wilczynska and M. Bushell, "The complexity of miRNA-mediated repression," *Cell Death and Differentiation*, vol. 22, no. 1, pp. 22–33, 2015.

[15] G. Mathonnet, M. R. Fabian, Y. V. Svitkin et al., "MicroRNA inhibition of translation initiation *in vitro* by targeting the cap-binding complex eIF4F," *Science*, vol. 317, no. 5845, pp. 1764–1767, 2007.

[16] M. Xie and J. A. Steitz, "Versatile microRNA biogenesis in animals and their viruses," *RNA Biology*, vol. 11, no. 6, pp. 673–681, 2014.

[17] M. A. Havens, A. A. Reich, D. M. Duelli, and M. L. Hastings, "Biogenesis of mammalian microRNAs by a non-canonical processing pathway," *Nucleic Acids Research*, vol. 40, no. 10, pp. 4626–4640, 2012.

[18] J. G. Ruby, C. H. Jan, and D. P. Bartel, "Intronic microRNA precursors that bypass *Drosha* processing," *Nature*, vol. 448, no. 7149, pp. 83–86, 2007.

[19] R. Martin, P. Smibert, A. Yalcin et al., "A drosophila pasha mutant distinguishes the canonical microRNA and mirtron pathways," *Molecular and Cellular Biology*, vol. 29, no. 3, pp. 861–870, 2009.

[20] E. Ladewig, K. Okamura, A. S. Flynt, J. O. Westholm, and E. C. Lai, "Discovery of hundreds of mirtrons in mouse and human small RNA data," *Genome Research*, vol. 22, no. 9, pp. 1634–1645, 2012.

[21] C. R. Sibley, Y. Seow, S. Saayman et al., "The biogenesis and characterization of mammalian microRNAs of mirtron origin," *Nucleic Acids Research*, vol. 40, no. 1, pp. 438–448, 2012.

[22] S. Stefanovic, G. J. Bassell, and M. R. Mihailescu, "G quadruplex RNA structures in PSD-95 mRNA: potential regulators of miR-125a seed binding site accessibility," *RNA*, vol. 21, no. 1, pp. 48–60, 2015.

[23] A. Suzuki, H. Fukushima, T. Mukawa et al., "Upregulation of CREB-mediated transcription enhances both short- and long-term memory," *The Journal of Neuroscience*, vol. 31, no. 24, pp. 8786–8802, 2011.

[24] N. Vo, M. E. Klein, O. Varlamova et al., "A cAMP-response element binding protein-induced microRNA regulates neuronal morphogenesis," *Proceedings of the National Academy of Sciences of the United States of America*, vol. 102, no. 45, pp. 16426–16431, 2005.

[25] A. S. Nudelman, D. P. Dirocco, T. J. Lambert et al., "Neuronal activity rapidly induces transcription of the CREB-regulated microRNA-132, *in vivo*," *Hippocampus*, vol. 20, no. 4, pp. 492–498, 2010.

[26] J. Guo, H. Wang, Q. Wang, Y. Chen, and S. Chen, "Expression of p-CREB and activity-dependent miR-132 in temporal lobe epilepsy," *International Journal of Clinical and Experimental Medicine*, vol. 7, no. 5, pp. 1297–1306, 2014.

[27] Y. Huang, J. Guo, Q. Wang, and Y. Chen, "MicroRNA-132 silencing decreases the spontaneous recurrent seizures," *International Journal of Clinical and Experimental Medicine*, vol. 7, no. 7, pp. 1639–1649, 2014.

[28] K. F. Hansen, K. Karelina, K. Sakamoto, G. A. Wayman, S. Impey, and K. Obrietan, "miRNA-132: a dynamic regulator of cognitive capacity," *Brain Structure and Function*, vol. 218, no. 3, pp. 817–831, 2013.

[29] H. L. Scott, F. Tamagnini, K. E. Narduzzo et al., "MicroRNA-132 regulates recognition memory and synaptic plasticity in the perirhinal cortex," *European Journal of Neuroscience*, vol. 36, no. 7, pp. 2941–2948, 2012.

[30] H. Kawashima, T. Numakawa, E. Kumamaru et al., "Glucocorticoid attenuates brain-derived neurotrophic factor-dependent upregulation of glutamate receptors via the suppression of microRNA-132 expression," *Neuroscience*, vol. 165, no. 4, pp. 1301–1311, 2010.

[31] E. Kumamaru, T. Numakawa, N. Adachi et al., "Glucocorticoid prevents brain-derived neurotrophic factor-mediated maturation of synaptic function in developing hippocampal neurons through reduction in the activity of mitogen-activated protein kinase," *Molecular Endocrinology*, vol. 22, no. 3, pp. 546–558, 2008.

[32] T. Numakawa, E. Kumamaru, N. Adachi, Y. Yagasaki, A. Izumi, and H. Kunugi, "Glucocorticoid receptor interaction with TrkB promotes BDNF-triggered PLC-γ signaling for glutamate release via a glutamate transporter," *Proceedings of the National Academy of Sciences of the United States of America*, vol. 106, no. 2, pp. 647–652, 2009.

[33] S. Vaynman, Z. Ying, and F. Gomez-Pinilla, "Hippocampal BDNF mediates the efficacy of exercise on synaptic plasticity and cognition," *European Journal of Neuroscience*, vol. 20, no. 10, pp. 2580–2590, 2004.

[34] K. J. Marler, P. Suetterlin, A. Dopplapudi et al., "BDNF promotes axon branching of retinal ganglion cells via miRNA-132 and p250GAP," *The Journal of Neuroscience*, vol. 34, no. 3, pp. 969–979, 2014.

[35] G. A. Wayman, M. Davare, H. Ando et al., "An activity-regulated microRNA controls dendritic plasticity by down-regulating p250GAP," *Proceedings of the National Academy of Sciences of the United States of America*, vol. 105, no. 26, pp. 9093–9098, 2008.

[36] S. Impey, M. Davare, A. Lasiek et al., "An activity-induced microRNA controls dendritic spine formation by regulating

Rac1-PAK signaling," *Molecular and Cellular Neuroscience*, vol. 43, no. 1, pp. 146–156, 2010.

[37] G. Shaltiel, M. Hanan, Y. Wolf et al., "Hippocampal microRNA-132 mediates stress-inducible cognitive deficits through its acetylcholinesterase target," *Brain Structure and Function*, vol. 218, no. 1, pp. 59–72, 2013.

[38] S. J. Kempf, S. Buratovic, C. von Toerne et al., "Ionising radiation immediately impairs synaptic plasticity-associated cytoskeletal signalling pathways in HT22 cells and in mouse brain: an *in vitro/in vivo* comparison study," *PLoS ONE*, vol. 9, no. 10, Article ID e110464, 2014.

[39] M. Dhar, M. Zhu, S. Impey et al., "Leptin induces hippocampal synaptogenesis via CREB-regulated MicroRNA-132 suppression of p250GAP," *Molecular Endocrinology*, vol. 28, no. 7, pp. 1073–1087, 2014.

[40] A. Lesiak, M. Zhu, H. Chen et al., "The environmental neurotoxicant PCB 95 promotes synaptogenesis via ryanodine receptor-dependent miR132 upregulation," *Journal of Neuroscience*, vol. 34, no. 3, pp. 717–725, 2014.

[41] A. L. Degano, M. J. Park, J. Penati, Q. Li, and G. V. Ronnett, "MeCP2 is required for activity-dependent refinement of olfactory circuits," *Molecular and Cellular Neuroscience*, vol. 59, pp. 63–75, 2014.

[42] K. F. Hansen, K. Sakamoto, G. A. Wayman, S. Impey, and K. Obrietan, "Transgenic miR132 alters neuronal spine density and impairs novel object recognition memory," *PLoS ONE*, vol. 5, no. 11, Article ID e15497, 2010.

[43] J. Hernandez-Rapp, P. Y. Smith, M. Filali et al., "Memory formation and retention are affected in adult miR-132/212 knockout mice," *Behavioural Brain Research*, vol. 287, pp. 15–26, 2015.

[44] T. Fukuda, M. Itoh, T. Ichikawa, K. Washiyama, and Y.-I. Goto, "Delayed maturation of neuronal architecture and synaptogenesis in cerebral cortex of Mecp2-deficient mice," *Journal of Neuropathology and Experimental Neurology*, vol. 64, no. 6, pp. 537–544, 2005.

[45] Q. Chang, G. Khare, V. Dani, S. Nelson, and R. Jaenisch, "The disease progression of Mecp2 mutant mice is affected by the level of BDNF expression," *Neuron*, vol. 49, no. 3, pp. 341–348, 2006.

[46] H. Wu, J. Tao, P. J. Chen et al., "Genome-wide analysis reveals methyl-CpG-binding protein 2-dependent regulation of microRNAs in a mouse model of Rett syndrome," *Proceedings of the National Academy of Sciences of the United States of America*, vol. 107, no. 42, pp. 18161–18166, 2010.

[47] R. Zhang, M. Huang, Z. Cao, J. Qi, Z. Qiu, and L. Chiang, "MeCP2 plays an analgesic role in pain transmission through regulating CREB/miR-132 pathway," *Molecular Pain*, vol. 11, no. 1, article 19, 2015.

[48] M. E. Klein, D. T. Lioy, L. Ma, S. Impey, G. Mandel, and R. H. Goodman, "Homeostatic regulation of MeCP2 expression by a CREB-induced microRNA," *Nature Neuroscience*, vol. 10, no. 12, pp. 1513–1514, 2007.

[49] P. Jin, D. C. Zarnescu, S. Ceman et al., "Biochemical and genetic interaction between the fragile X mental retardation protein and the microRNA pathway," *Nature Neuroscience*, vol. 7, no. 2, pp. 113–117, 2004.

[50] I. Napoli, V. Mercaldo, P. P. Boyl et al., "The fragile X syndrome protein represses activity-dependent translation through CYFIP1, a new 4E-BP," *Cell*, vol. 134, no. 6, pp. 1042–1054, 2008.

[51] D. Edbauer, J. R. Neilson, K. A. Foster et al., "Regulation of synaptic structure and function by FMRP-associated microRNAs miR-125b and miR-132," *Neuron*, vol. 65, no. 3, pp. 373–384, 2010.

[52] I. P. Sudhakaran, J. Hillebrand, A. Dervan et al., "FMRP and Ataxin-2 function together in long-term olfactory habituation and neuronal translational control," *Proceedings of the National Academy of Sciences of the United States of America*, vol. 111, no. 1, pp. E99–E108, 2014.

[53] F. Sethna, C. Moon, and H. Wang, "From FMRP function to potential therapies for fragile X syndrome," *Neurochemical Research*, vol. 39, no. 6, pp. 1016–1031, 2014.

[54] P. Tognini and T. Pizzorusso, "MicroRNA212/132 family: molecular transducer of neuronal function and plasticity," *International Journal of Biochemistry & Cell Biology*, vol. 44, no. 1, pp. 6–10, 2012.

[55] K. Wibrand, D. Panja, A. Tiron et al., "Differential regulation of mature and precursor microRNA expression by NMDA and metabotropic glutamate receptor activation during LTP in the adult dentate gyrus *in vivo*," *European Journal of Neuroscience*, vol. 31, no. 4, pp. 636–645, 2010.

[56] J. Remenyi, M. W. M. van den Bosch, O. Palygin et al., "MiR-132/212 knockout mice reveal roles for these miRNAs in regulating cortical synaptic transmission and plasticity," *PLoS ONE*, vol. 8, no. 4, Article ID e62509, 2013.

[57] S. T. Magill, X. A. Cambronne, B. W. Luikart et al., "MicroRNA-132 regulates dendritic growth and arborization of newborn neurons in the adult hippocampus," *Proceedings of the National Academy of Sciences of the United States of America*, vol. 107, no. 47, pp. 20382–20387, 2010.

[58] B. W. Luikart, A. L. Bensen, E. K. Washburn et al., "MiR-132 mediates the integration of newborn neurons into the adult dentate gyrus," *PLoS ONE*, vol. 6, no. 5, Article ID e19077, 2011.

[59] J.-Y. Hwang, N. Kaneko, K.-M. Noh, F. Pontarelli, and R. S. Zukin, "The gene silencing transcription factor rest represses miR-132 expression in hippocampal neurons destined to die," *Journal of Molecular Biology*, vol. 426, no. 20, pp. 3454–3466, 2014.

[60] P. Tognini, E. Putignano, A. Coatti, and T. Pizzorusso, "Experience-dependent expression of miR-132 regulates ocular dominance plasticity," *Nature Neuroscience*, vol. 14, no. 10, pp. 1237–1239, 2011.

[61] N. Mellios, H. Sugihara, J. Castro et al., "MiR-132, an experience-dependent microRNA, is essential for visual cortex plasticity," *Nature Neuroscience*, vol. 14, no. 10, pp. 1240–1242, 2011.

[62] J. F. Maya-Vetencourt and T. Pizzorusso, "Molecular mechanisms at the basis of plasticity in the developing visual cortex: epigenetic processes and gene programs," *Journal of Experimental Neuroscience*, vol. 7, pp. 75–83, 2013.

[63] S. Bicker, S. Khudayberdiev, K. Weiß, K. Zocher, S. Baumeister, and G. Schratt, "The DEAH-box helicase DHX36 mediates dendritic localization of the neuronal precursor-microRNA-134," *Genes & Development*, vol. 27, no. 9, pp. 991–996, 2013.

[64] J. Gao, W.-Y. Wang, Y.-W. Mao et al., "A novel pathway regulates memory and plasticity via SIRT1 and miR-134," *Nature*, vol. 466, no. 7310, pp. 1105–1109, 2010.

[65] H. Siemen, D. Colas, H. C. Heller, O. Brüstle, and R. A. Pera, "Pumilio-2 function in the mouse nervous system," *PLoS ONE*, vol. 6, no. 10, Article ID e25932, 2011.

[66] G. M. Schratt, F. Tuebing, E. A. Nigh et al., "A brain-specific microRNA regulates dendritic spine development," *Nature*, vol. 439, no. 7074, pp. 283–289, 2006.

[67] M. Christensen, L. A. Larsen, S. Kauppinen, and G. Schratt, "Recombinant adeno-associated virus-mediated microRNA delivery into the postnatal mouse brain reveals a role for miR-134 in dendritogenesis *in vivo*," *Frontiers in Neural Circuits*, vol. 3, article no. 16, 2010.

[68] O. Bernard, "Lim kinases, regulators of actin dynamics," *The International Journal of Biochemistry & Cell Biology*, vol. 39, no. 6, pp. 1071–1076, 2007.

[69] Y. Meng, Y. Zhang, V. Tregoubov, D. L. Falls, and Z. Jia, "Regulation of spine morphology and synaptic function by LIMK and the actin cytoskeleton," *Reviews in the Neurosciences*, vol. 14, no. 3, pp. 233–240, 2003.

[70] Q. Dong, Y.-S. Ji, C. Cai, and Z.-Y. Chen, "LIM Kinase 1 (LIMK1) interacts with Tropomyosin-related Kinase B (TrkB) and mediates Brain-Derived Neurotrophic Factor (BDNF)-induced axonal elongation," *Journal of Biological Chemistry*, vol. 287, no. 50, pp. 41720–41731, 2012.

[71] G. Leal, D. Comprido, and C. B. Duarte, "BDNF-induced local protein synthesis and synaptic plasticity," *Neuropharmacology*, vol. 76, pp. 639–656, 2014.

[72] S. Chai, X. A. Cambronne, S. W. Eichhorn, and R. H. Goodman, "MicroRNA-134 activity in somatostatin interneurons regulates H-Ras localization by repressing the palmitoylation enzyme, DHHC9," *Proceedings of the National Academy of Sciences of the United States of America*, vol. 110, no. 44, pp. 17898–17903, 2013.

[73] T. Arendt, U. Gärtner, G. Seeger et al., "Neuronal activation of Ras regulates synaptic connectivity," *European Journal of Neuroscience*, vol. 19, no. 11, pp. 2953–2966, 2004.

[74] E. M. Jimenez-Mateos, T. Engel, P. Merino-Serrais et al., "Silencing microRNA-134 produces neuroprotective and prolonged seizure-suppressive effects," *Nature Medicine*, vol. 18, no. 7, pp. 1087–1094, 2012.

[75] J. Peng, A. Omran, M. U. Ashhab et al., "Expression patterns of miR-124, miR-134, miR-132, and miR-21 in an immature rat model and children with mesial temporal lobe epilepsy," *Journal of Molecular Neuroscience*, vol. 50, no. 2, pp. 291–297, 2013.

[76] Y. Zhu, C. Li, Y. Wang, and S. Zhou, "Change of MicroRNA-134, CREB and p-CREB expression in epileptic rat," *Asian Pacific Journal of Tropical Medicine*, vol. 8, no. 4, pp. 292–298, 2015.

[77] G. Siegel, G. Obernosterer, R. Fiore et al., "A functional screen implicates microRNA-138-dependent regulation of the depalmitoylation enzyme APT1 in dendritic spine morphogenesis," *Nature Cell Biology*, vol. 11, no. 6, pp. 705–716, 2009.

[78] M. Bak, A. Silahtaroglu, M. Møller et al., "MicroRNA expression in the adult mouse central nervous system," *RNA*, vol. 14, no. 3, pp. 432–444, 2008.

[79] J. Schröder, S. Ansaloni, M. Schilling et al., "MicroRNA-138 is a potential regulator of memory performance in humans," *Frontiers in Human Neuroscience*, vol. 8, article 501, 2014.

[80] E. T. Tatro, V. Risbrough, B. Soontornniyomkij et al., "Short-term recognition memory correlates with regional CNS expression of microRNA-138 in mice," *The American Journal of Geriatric Psychiatry*, vol. 21, no. 5, pp. 461–473, 2013.

[81] C.-M. Liu, R.-Y. Wang, Saijilafu, Z.-X. Jiao, B.-Y. Zhang, and F.-Q. Zhou, "MicroRNA-138 and SIRT1 form a mutual negative feedback loop to regulate mammalian axon regeneration," *Genes & Development*, vol. 27, no. 13, pp. 1473–1483, 2013.

[82] S. A. Giusti, A. M. Vogl, M. M. Brockmann et al., "MicroRNA-9 controls dendritic development by targeting REST," *eLife*, vol. 3, Article ID e02755, 2014.

[83] G. Garaffo, D. Conte, P. Provero et al., "The Dlx5 and Foxg1 transcription factors, linked via miRNA-9 and -200, are required for the development of the olfactory and GnRH system," *Molecular and Cellular Neuroscience*, vol. 68, pp. 103–119, 2015.

[84] M. C. Siomi, H. Siomi, W. H. Sauer, S. Srinivasan, R. L. Nussbaum, and G. Dreyfuss, "FXR1, an autosomal homolog of the fragile X mental retardation gene," *The EMBO Journal*, vol. 14, no. 11, pp. 2401–2408, 1995.

[85] X.-L. Xu, R. Zong, Z. Li et al., "Fxr1p but not fmrp regulates the levels of mammalian brain-specific microrna-9 and microrna-124," *Journal of Neuroscience*, vol. 31, no. 39, pp. 13705–13709, 2011.

[86] J. P. Cogswell, J. Ward, I. A. Taylor et al., "Identification of miRNA changes in Alzheimer's disease brain and CSF yields putative biomarkers and insights into disease pathways," *Journal of Alzheimer's Disease*, vol. 14, no. 1, pp. 27–41, 2008.

[87] G. Mairet-Coello, J. Courchet, S. Pieraut, V. Courchet, A. Maximov, and F. Polleux, "The CAMKK2-AMPK kinase pathway mediates the synaptotoxic effects of Aβ oligomers through Tau phosphorylation," *Neuron*, vol. 78, no. 1, pp. 94–108, 2013.

[88] A. Nakano and S. Takashima, "LKB1 and AMP-activated protein kinase: regulators of cell polarity," *Genes to Cells*, vol. 17, no. 9, pp. 737–747, 2012.

[89] F. Chang, L.-H. Zhang, W. U.-P. Xu, P. Jing, and P.-Y. Zhan, "microRNA-9 attenuates amyloidβ-induced synaptotoxicity by targeting calcium/calmodulin-dependent protein kinase kinase 2," *Molecular Medicine Reports*, vol. 9, no. 5, pp. 1917–1922, 2014.

[90] X. Wang, L. Tan, Y. Lu et al., "MicroRNA-138 promotes tau phosphorylation by targeting retinoic acid receptor alpha," *FEBS Letters*, vol. 589, no. 6, pp. 726–729, 2015.

[91] H. Soreq and Y. Wolf, "NeurimmiRs: microRNAs in the neuroimmune interface," *Trends in Molecular Medicine*, vol. 17, no. 10, pp. 548–555, 2011.

[92] P. Rajasethupathy, F. Fiumara, R. Sheridan et al., "Characterization of small RNAs in aplysia reveals a role for miR-124 in constraining synaptic plasticity through CREB," *Neuron*, vol. 63, no. 6, pp. 803–817, 2009.

[93] S. Schumacher and K. Franke, "miR-124-regulated RhoG: a conductor of neuronal process complexity," *Small GTPases*, vol. 4, no. 1, pp. 42–46, 2013.

[94] K. Franke, W. Otto, S. Johannes, J. Baumgart, R. Nitsch, and S. Schumacher, "miR-124-regulated RhoG reduces neuronal process complexity via ELMO/Dock180/Rac1 and Cdc42 signalling," *The EMBO Journal*, vol. 31, no. 13, pp. 2908–2921, 2012.

[95] H. Katoh and M. Negishi, "RhoG activates Rac1 by direct interaction with the Dock180-binding protein Elmo," *Nature*, vol. 424, no. 6947, pp. 461–464, 2003.

[96] L. Yang, R. Zhang, M. Li et al., "A functional MiR-124 binding-site polymorphism in IQGAP1 affects human cognitive performance," *PLoS ONE*, vol. 9, no. 9, Article ID e107065, 2014.

[97] C. Gao, S. F. Frausto, A. L. Guedea et al., "IQGAP1 regulates NR2A signaling, spine density, and cognitive processes," *Journal of Neuroscience*, vol. 31, no. 23, pp. 8533–8542, 2011.

[98] R. Dutta, A. M. Chomyk, A. Chang et al., "Hippocampal demyelination and memory dysfunction are associated with increased levels of the neuronal microRNA miR-124 and reduced AMPA receptors," *Annals of Neurology*, vol. 73, no. 5, pp. 637–645, 2013.

[99] V. Chandrasekar and J.-L. Dreyer, "microRNAs miR-124, let-7d and miR-181a regulate Cocaine-induced Plasticity," *Molecular and Cellular Neuroscience*, vol. 42, no. 4, pp. 350–362, 2009.

[100] W. Xu, O. M. Schlüter, P. Steiner, B. L. Czervionke, B. Sabatini, and R. C. Malenka, "Molecular dissociation of the role of PSD-95 in regulating synaptic strength and LTD," *Neuron*, vol. 57, no. 2, pp. 248–262, 2008.

[101] R. S. Muddashetty, V. C. Nalavadi, C. Gross et al., "Reversible inhibition of PSD-95 mRNA translation by miR-125a, FMRP phosphorylation, and mGluR signaling," *Molecular Cell*, vol. 42, no. 5, pp. 673–688, 2011.

[102] F. Zalfa, B. Eleuteri, K. S. Dickson et al., "A new function for the fragile X mental retardation protein in regulation of PSD-95 mRNA stability," *Nature Neuroscience*, vol. 10, no. 5, pp. 578–587, 2007.

[103] R. Anwyl, "Metabotropic glutamate receptor-dependent long-term potentiation," *Neuropharmacology*, vol. 56, no. 4, pp. 735–740, 2009.

[104] P. J. Yao, M. Zhu, E. I. Pyun et al., "Defects in expression of genes related to synaptic vesicle trafficking in frontal cortex of Alzheimer's disease," *Neurobiology of Disease*, vol. 12, no. 2, pp. 97–109, 2003.

[105] J. Banzhaf-Strathmann, E. Benito, S. May et al., "MicroRNA-125b induces tau hyperphosphorylation and cognitive deficits in Alzheimer's disease," *EMBO Journal*, vol. 33, no. 15, pp. 1667–1680, 2014.

[106] W. J. Lukiw and P. N. Alexandrov, "Regulation of complement factor H (CFH) by multiple miRNAs in Alzheimer's disease (AD) brain," *Molecular Neurobiology*, vol. 46, no. 1, pp. 11–19, 2012.

[107] R. P. Kruger, J. Aurandt, and K.-L. Guan, "Semaphorins command cells to move," *Nature Reviews Molecular Cell Biology*, vol. 6, no. 10, pp. 789–800, 2005.

[108] K. Lee, J.-H. Kim, O.-B. Kwon et al., "An activity-regulated microRNA, miR-188, controls dendritic plasticity and synaptic transmission by downregulating neuropilin-2," *The Journal of Neuroscience*, vol. 32, no. 16, pp. 5678–5687, 2012.

[109] J. Zhang, M. Hu, Z. Teng, Y.-P. Tang, and C. Chen, "Synaptic and cognitive improvements by inhibition of 2-AG metabolism are through upregulation of microRNA-188-3p in a mouse model of Alzheimer's disease," *Journal of Neuroscience*, vol. 34, no. 45, pp. 14919–14933, 2014.

[110] C. S. Lu, B. Zhai, A. Mauss, M. Landgraf, S. Gygi, and D. Van Vactor, "MicroRNA-8 promotes robust motor axon targeting by coordinate regulation of cell adhesion molecules during synapse development," *Philosophical Transactions of the Royal Society B: Biological Sciences*, vol. 369, no. 1652, article 517, 2014.

[111] C. M. Loya, E. M. McNeill, H. Bao, B. Zhang, and D. Van Vactor, "miR-8 controls synapse structure by repression of the actin regulator Enabled," *Development*, vol. 141, no. 9, pp. 1864–1874, 2014.

[112] Y. Gao, J. Su, W. Guo et al., "Inhibition of miR-15a promotes BDNF expression and rescues dendritic maturation deficits in MeCP2-deficient neurons," *Stem Cells*, vol. 33, no. 5, pp. 1618–1629, 2015.

[113] M. J. Kye, P. Neveu, Y.-S. Lee et al., "NMDA mediated contextual conditioning changes miRNA expression," *PLoS ONE*, vol. 6, no. 9, Article ID e24682, 2011.

[114] F. Fiumara, P. Rajasethupathy, I. Antonov, S. Kosmidis, W. S. Sossin, and E. R. Kandel, "MicroRNA-22 gates long-term heterosynaptic plasticity in aplysia through presynaptic regulation of CPEB and downstream targets," *Cell Reports*, vol. 11, no. 12, pp. 1866–1875, 2015.

[115] Q. Gu, D. Yu, Z. Hu et al., "miR-26a and miR-384-5p are required for LTP maintenance and spine enlargement," *Nature Communications*, vol. 6, article 6789, 2015.

[116] B. Li and H. Sun, "MiR-26a promotes neurite outgrowth by repressing PTEN expression," *Molecular Medicine Reports*, vol. 8, no. 2, pp. 676–680, 2013.

[117] G. Lippi, J. R. Steinert, E. L. Marczylo et al., "Targeting of the Arpc3 actin nucleation factor by miR-29a/b regulates dendritic spine morphology," *The Journal of Cell Biology*, vol. 194, no. 6, pp. 889–904, 2011.

[118] V. O. Pustylnyak, P. D. Lisachev, and M. B. Shtark, "Expression of p53 target genes in the early phase of long-term potentiation in the rat hippocampal CA1 area," *Neural Plasticity*, vol. 2015, Article ID 242158, 12 pages, 2015.

[119] M. Agostini, P. Tucci, J. R. Steinert et al., "microRNA-34a regulates neurite outgrowth, spinal morphology, and function," *Proceedings of the National Academy of Sciences of the United States of America*, vol. 108, no. 52, pp. 21099–21104, 2011.

[120] K. Wibrand, B. Pai, T. Siripornmongcolchai et al., "MicroRNA regulation of the synaptic plasticity-related gene Arc," *PLoS ONE*, vol. 7, no. 7, Article ID e41688, 2012.

[121] E. Franzoni, S. A. Booker, S. Parthasarathy et al., "miR-128 regulates neuronal migration, outgrowth and intrinsic excitability via the intellectual disability gene *Phf6*," *ELife*, vol. 4, Article ID e04263, 2015.

[122] R. D. Smrt, K. E. Szulwach, R. L. Pfeiffer et al., "MicroRNA miR-137 regulates neuronal maturation by targeting ubiquitin ligase mind bomb-1," *Stem Cells*, vol. 28, no. 6, pp. 1060–1070, 2010.

[123] E. M. Griggs, E. J. Young, G. Rumbaugh, and C. A. Miller, "MicroRNA-182 regulates amygdala-dependent memory formation," *The Journal of Neuroscience*, vol. 33, no. 4, pp. 1734–1740, 2013.

[124] Z. Hu, D. Yu, Q.-H. Gu et al., "MiR-191 and miR-135 are required for long-lasting spine remodelling associated with synaptic long-term depression," *Nature Communications*, vol. 5, article 3263, 2014.

[125] H. Rong, T. B. Liu, K. J. Yang et al., "MicroRNA-134 plasma levels before and after treatment for bipolar mania," *Journal of Psychiatric Research*, vol. 45, no. 1, pp. 92–95, 2011.

[126] D. W. Hwang, S. Son, J. Jang et al., "A brain-targeted rabies virus glycoprotein-disulfide linked PEI nanocarrier for delivery of neurogenic microRNA," *Biomaterials*, vol. 32, no. 21, pp. 4968–4975, 2011.

Hindawi Publishing Corporation
Neural Plasticity
Volume 2016, Article ID 3928726, 11 pages
http://dx.doi.org/10.1155/2016/3928726

Research Article

Housing Complexity Alters GFAP-Immunoreactive Astrocyte Morphology in the Rat Dentate Gyrus

Garrick Salois and Jeffrey S. Smith

The Brain Research Laboratory, Saginaw Valley State University, University Center, MI 48710, USA

Correspondence should be addressed to Jeffrey S. Smith; jsmith12@svsu.edu

Received 9 October 2015; Revised 10 January 2016; Accepted 28 January 2016

Academic Editor: Alfredo Pereira Jr.

Rats used in research are typically housed singly in cages with limited sensory stimulation. There is substantial evidence that housing rats in these conditions lead to numerous neuroanatomical and behavioral abnormalities. Alternatively, rats can be housed in an enriched environment in which rats are housed in groups and given room for exercise and exploration. Enriched environments result in considerable neuroplasticity in the rodent brain. In the dentate gyrus of the hippocampus, enriched environments evoke especially profound neural changes, including increases in the number of neurons and the number of dendritic spines. However, whether changes in astrocytes, a type of glia increasingly implicated in mediating neuroplasticity, are concurrent with these neural changes remains to be investigated. In order to assess morphological changes among astrocytes of the rat dentate gyrus, piSeeDB was used to optically clear 250 μm sections of tissue labeled using GFAP immunohistochemistry. Confocal imaging and image analysis were then used to measure astrocyte morphology. Astrocytes from animals housed in EE demonstrated a reduced distance between filament branch points. Furthermore, the most complex astrocytes were significantly more complex among animals housed in EE compared to standard environments.

1. Introduction

Studies in neuroscience often employ animal models because of the similarity in structure and function between human nervous systems and the nervous systems of other animals. Furthermore, animal models allow changes in behavior to be compared directly to changes in neurophysiology, an ability that cannot be accomplished through any other means. For this reason, animal models are critical for our understanding of human nervous system function and disease. Despite the utility of animal models, results obtained from their use do not always translate to the human nervous system. This problem is exemplified by the near universal failure of clinical trials of treatments for numerous neurological diseases, including traumatic brain injury [1] and stroke [2], despite demonstrated efficacy in animal models. While many of the differences between humans and other animals are unavoidable, researchers must be careful to ensure their animal models are valid.

One of the most commonly used animal models in neuroscience is the rat. Rat nervous systems, like all other nervous systems, are capable of responding to changes in their environment by altering neurophysiology and, in turn, behavior [3]. This feat is accomplished through a process called neuroplasticity. Rodent nervous systems evolved to interact with a chaotic and complex natural ecological niche. Animal models used in the lab, like their wild counterparts, exhibit neurological adaptation to their environments [4]. However, rats used in research experience an environment dramatically different from the one to which their nervous systems have adapted. The standard housing environment (SE) used for rats in the laboratory involves a small plastic cage in which one or two rats can be housed [5]. This housing environment provides extremely limited sensory stimulation, little or no social interaction, and no opportunity for exercise. There is substantial evidence that these conditions profoundly affect the brain and behavior of animals, leading to abnormal neuroplasticity and pathological functioning [6, 7].

In contrast to the SE, enriched environments (EE) consist of a significantly larger enclosure with room for rats to be housed in groups [3]. As social animals, rats demonstrate increased species-normative behavior in the presence of other rats [8]. In addition to social stimulation, rats in enriched environments are exposed to novel stimuli in the form of regularly introduced species-appropriate toys and changes in the location of food sources [5]. Furthermore, the larger enclosure substantially increases the ability of the rat to explore and exercise [5]. In sum, enriched environments allow rats to experience a constantly changing environment that more closely approximates their natural environment.

Numerous studies have demonstrated significant differences in the behavior of animals housed in EE compared to SE housing. The different components of enriched environments, a larger enclosure, social interaction, and novel toys, have each been shown to be beneficial in isolation but provide synergistic benefits when combined [8]. Housing rodents in enriched environments have been demonstrated to reduce the abnormal stereotyping behaviors that frequently occur as a result of housing in SE [6]. Furthermore, studies have shown significantly improved performance among rats housed in EE on tests of learning and memory such as the Morris water maze and Barnes maze [9–11], tests of gross motor function such as the Rotor Rod [9, 10], and tests of anxiety and depression such as the Open Field Test, Elevated Plus Maze, and the Forced Swim Task [9, 10, 12].

Studies have also demonstrated significant changes in the neuroanatomy of animals housed in EE which may underlie the observed changes in behavior. Early studies of EE identified numerous changes in the brain following housing in EE, including changes in cortical depth and glia number [13, 14], brain weight [15, 16], and total DNA content [16]. A brain region which undergoes significant structural remodeling in response to EE is the hippocampus [17]. The hippocampus is critically involved in learning and memory [18] and in maintaining a neural representation of extrapersonal space [19]. Studies of hippocampal plasticity in response to EE have generally focused on mechanisms of neural adaptation. For example, studies have demonstrated that the hippocampus responds to EE with changes in patterns of neurotransmitter receptor expression [20], as well as increasing dendritic complexity [21], spine density [22], and neurogenesis [11, 23].

Evidence suggests that glia are a fundamental factor in modulating neural plasticity. The most numerous cell in the brain [24], the astrocyte, is a glial cell critical in mediating central nervous system homeostasis through several mechanisms. Astrocytes are known to make contacts with both synapses and vasculature [25–27]. Astrocytic end-feet engulf the gaps between endothelial cells of the vasculature and alter their permeability, thus forming an integral component of the blood brain barrier [28, 29]. The ability of astrocytes to junction neural activity with vascular glucose influx is the basis for BOLD (blood oxygenation level dependent) signal used by fMRI [26]. Astrocytes are also critically involved in the brain's response to insult, such as stroke or traumatic brain injury. Following injury, astrocytes migrate to the site of injury and become hypertrophic, forming a glial scar which limits the spread of inflammation and apoptosis to surrounding intact tissue but also impedes the ability of axons to reinnervate damaged tissue [30–34]. Furthermore, astrocytes are capable of dynamically altering the properties of neurons in both the short and long term. In the short term, astrocytes are capable of altering concentrations of ions and neurotransmitter at the synapse [26], as well as metabolizing glucose to lactate, the primary energy source used by neurons [35]. In the long term, astrocytes may influence neural plasticity through control of spine dynamics [36–39] and neurotransmitter receptor expression at the synapse [20, 40, 41]. Recent studies have also demonstrated that release of the NMDA receptor coagonist D-serine by astrocytes is required for long-term potentiation in the hippocampus and prefrontal cortex [42–46]. In the dentate gyrus of the hippocampus, astrocytes actively modulate the differentiation, growth, survival, and integration of newborn neurons [47, 48]. Astrocytes have also shown to be structurally dynamic, with their processes demonstrating surprising motility in response to synaptic activity within their domains [36, 49]. In the visual cortex, GFAP-immunoreactive astrocytes demonstrated significant increases in number and GFAP expression in response to EE [50]. Thus, physiological changes in astrocytes in response to EE are likely to be coincident with changes in neurons.

Differences in neurophysiology that occur due to housing environment may confound animal studies of nervous system function. In the case of astrocytes, significant alterations in physiology have been observed in all disease models in which they have been studied, including Alzheimer's Disease, Parkinson's Disease, and epilepsy [51–61]. For this reason, it is critical to understand the physiological changes that occur in the brain in response to the housing environment of the animal model used. The present study was designed to determine whether hippocampal astrocytes undergo gross morphological changes in response to rearing in enriched environments. Measures of morphological complexity, such as number of filament branches, total filament length, number of terminal points, and number of Sholl intersections, were used to assess the possibility that astrocytes may be altered in an experience-dependent manner. It was hypothesized that, due to the crucial role of astrocytes in neural function, EE would result in an overall increase in the number and complexity of astrocytes in the dentate gyrus.

2. Methods

All brain samples used in this study were pseudorandomly selected from sham animals used in a study conducted by Jacqmain, Nudi, Fluharty, and Smith, 2014, on the effects of environmental enrichment on recovery from medial frontal cortex contusion. Eight samples were used, with four samples from animals housed in standard environments and four samples from animals housed in enriched environments. All procedures were approved prior to experimentation by the Saginaw Valley State University Institutional Animal Care and Use Committee.

2.1. Previous Study Procedures

2.1.1. Animals. Samples were selected from a cohort of 113 male Long-Evans rats (Charles River, Portage, MI) received

on PND 25 weighing from 51 g to 75 g. On arrival animals were randomly assigned to either an individual standard laboratory cage (SE) or an enriched environment (EE) with a total of 10 rats per cage. Animals housed in the EE condition were transferred to EE cages with a total of 6 rats at PND 115.

2.1.2. Housing Conditions. In each housing condition, animals were provided *ad libitum* access to food and water and were kept on a 12-hour reverse day/night cycle. Handling and behavior testing were conducted during the dark cycle. All rats were handled daily for 5 minutes per rat to acclimate them to human contact. Cell-sorb (Fangman Specialties, OH) was used as bedding for all cages and all rats were fed with rodent chow (Zeigler Bros, Inc., PN).

The SE condition consisted of a standard plastic laboratory cage (Alternative Design, Siloam Springs, AR) measuring 26.0 cm wide, 47.0 cm long, and 20.3 cm high. Rats were permanently given water and rodent chow through the top of the cage. One rat was housed per SE cage.

The EE condition consisted of a large plastic bin (Freedom Breeders #44, California) measuring 152.5 cm wide, 61 cm long, and 21.5 cm tall. Rodent chow was provided by a well placed along the width of the cage. Species-appropriate toys were added to EE cages, including PVC pipes, cardboard tubes, plastic shelters, wooden blocks, and chew toys. The toys were rearranged daily during handling and were changed during cleaning every three days. 10 animals were housed per cage until PND 115, at which point rats were housed in groups of six per EE enclosure.

2.1.3. Euthanization and Tissue Handling. On postsurgery day 28 (PND 143) rats were deeply anesthetized with 5% isoflurane. Following absent eye-blink and tail pinch reflexes, rats were intraperitoneally injected with Euthasol (pentobarbital, 392 mg/kg). Rats were then transcardially perfused with 500 mL 0.9% phosphate buffered saline, followed by 500 mL 10% buffered formalin. The rats were decapitated and the brains were extracted. The left hemisphere from each brain was placed in 25 mL of 10% formalin overnight. The brains were then dehydrated and embedded in paraffin wax on plastic cartridges using a Tissue-Tek III vacuum infiltration tissue processor (IMEB Inc., San Marco, CA) and a paraffin-embedding console (Miles Scientific, Fergus Falls, MN). Samples were then stored at RT until they were used in the present study.

2.2. piSeeDB. Fluorescent immunohistochemistry and optical clearing techniques were used to allow imaging of cellular morphology in the dentate gyrus. SeeDB [62], a recent optical clearing technique, uses Fructose in PBS to match the refractive index of scatter of cellular membranes, enhancing tissue transparency. However, SeeDB has been reported to be ineffective with immunohistochemistry because it does not facilitate antibody penetrance [62]. Furthermore, SeeDB was not designed for use with paraffinized samples. The SeeDB procedure was modified in order to facilitate effective immunohistological labeling in paraffinized samples, resulting in a new procedure called piSeeDB. Our results indicate that a relatively simple modification to the SeeDB protocol whereby samples were exposed to a freeze/thaw cycle increased antibody penetrance and allowed imaging to depths of up to 2 mm [10].

2.2.1. Deparaffinization. Paraffin-embedded left hemispheres were placed in a 40°C water bath for fifteen minutes prior to sectioning. The first 250 μm section from each sample was collected and placed in a vacuum oven (Sheldon Manufacturing, Cornelius, OR). Samples were heated to 60°C with 15 inches' Hg vacuum for 8 hours. Tissue samples were then placed in a Tissue-Tek III tissue processor which was used to alternate pressure and vacuum with 50°C xylene for 1 hour. Sections were then dehydrated using ascending concentrations of ethanol.

2.2.2. Freeze/Thaw. Recent work has established a method of freeze/thaw cycling that significantly improves immunostaining compared to other methods such as antigen retrieval when used with thick tissue samples [63]. Samples were placed in a sealed conical tube following dehydration. Samples were then placed in a freezer at −80°C for 30 minutes. Samples were then brought to room temperature for 30 minutes. This procedure was repeated four times for a total of four hours. Tissue was then rehydrated using descending concentrations of ethanol. Tissue was then rotated in a conical tube with 50 mL of 10% PBS and 1% Triton X-100 (PBS-T) at 36°C overnight.

2.2.3. Immunohistochemistry. Tissue was placed in a twelve-well plate with 1.25 mL of DaVinci Green (Biocare Medical, Concord, CA) with 1% Triton X-100 (12.5 μL) and incubated at 36°C for 24 hours. Tissue was then rinsed with PBS-T for 15 minutes. In order to block binding of endogenous IgG, samples were then incubated at 36°C in 1.25 mL of Rodent Block Rat (Biocare Medical, Concord, CA) for 24 hours. Tissue was then rotated in a 50 mL conical tube of PBS-T for three 30-minute washes with fresh PBS-T used for each wash.

Antibodies were added to 1.25 mL of DaVinci Green. Newborn neurons were labeled using 3.12 μL of guinea pig polyclonal anti-doublecortin (1 : 100; Bioss Inc., Woburn, MA), astrocyte filaments were labeled using 12.5 μL mouse monoclonal anti-GFAP conjugated with Cy3 (1 : 100; Abcam, Cambridge, MA), and neural cell bodies were labeled using 12.5 μL rabbit monoclonal anti-NeuN conjugated with AlexaFluor 647 (1 : 100; Abcam, Cambridge, MA). Tissue samples were then incubated at 36°C in the primary antibody solution for 24 hours. Tissue was flipped after 12 hours had elapsed. Tissue was then rotated again in a 50 mL conical tube of PBS-T for three 30-minute washes. Tissue was then incubated at 36°C in DAPI solution (Biocare Medical, Concord, CA) for 6 hours. The tissue was then rinsed a final time with three PBS-T washes.

2.2.4. SeeDB. SeeDB was prepared utilizing procedures from Ke et al. [62]. Ascending concentrations of D-Fructose in PBS were prepared in the following w/v concentrations of D-Fructose in PBS: 20%, 40%, 60%, 80%, and 100%. The final solution of SeeDB was produced using 60.75 g of D-Fructose and 15 mL of distilled water. Solutions were heated

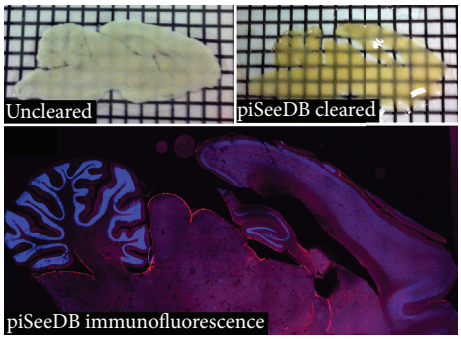

Figure 1: A comparison of the transparency of uncleared and piSeeDB cleared samples.

to 60°C and stirred periodically until fully dissolved. After the solution reached RT, 300 μL of α-thioglycerol was added in order to inhibit tissue browning from the Maillard reaction [62]. Tissue was then rotated in 20%, 40%, and 60% solutions for 8 hours each; 80% and 100% solutions for 12 hours each; and then SeeDB solution for 24 hours (Figure 1).

2.3. Imaging and Analysis

2.3.1. Confocal Imaging. Tissue sections were placed in a SeeDB-filled imaging chamber composed of a pair of square cover slips with a 250 μm silicon spacer placed between them. The sample was placed in its SeeDB solution in the interior of the imaging chamber with the most medial surface facing up. Confocal imaging was conducted with an Olympus Fluoview FV10i microscope in z-stack time-lapse mode. While piSeeDB was effective in clearing samples up to 2 mm in unparaffinized samples, and up to 250 μm in deparaffinized samples, the working distance of the FV10i 60x oil-objective limited imaging to depths of roughly 100 μm. This objective was used despite these limitations because high magnification is necessary to resolve the fine detail of astrocyte filaments. Images were captured with a region of interest centered against the anteriormost point of the granule cell layer of the dentate gyrus and measuring approximately 600 μm (x), 400 μm (y), and 100 μm (z). Imaging duration was four days per sample. The sample was kept at 36°C during imaging.

2.3.2. Image Processing and Analysis. Microscope images were produced as a z-series which was then stitched into z-stacks using XuvStitch 1.8.099. No compression was used. z-stacks were then visualized with Bitplane Imaris 7 (Bitplane, Concord, MA). z-stacks were normalized in order to maintain a consistent signal intensity through the depth of the sample.

Astrocytes within the granule layer and the hilus of the dentate gyrus were analyzed. Imaris FilamentTracer was used with the AutoPath (no loops) algorithm to trace, segment, and statistically analyze astrocyte morphology (Figure 2). GFAP$^+$ cells were counted automatically using a detection threshold value that was held constant between samples. An average of 171.88 GFAP$^+$ cells was analyzed per sample. GFAP$^+$ filaments were segmented and the length between branches, as well as the total length, was measured. Filament terminal points were then detected based on intensity thresholding. The number of branch points was also counted per cell. In addition, full branch depth, which measures the maximum number of branches between the starting point (nucleus) of the cell and a terminal point, was recorded. Finally, 3-dimensional Sholl analysis was used to measure filament complexity. The minimum, maximum, mean, and standard deviation per sample were analyzed for each measure of astrocyte morphology.

2.3.3. Data Analysis. All data were analyzed with t-tests using SPSS 21.0 for Windows (IBM, Armonk, NY). Homogeneity of variance was verified using Levine's test. A p value of $<.05$ was considered significant for all statistical tests.

3. Results

The total number of GFAP$^+$ cells within the granule cell layer and the hilus of the dentate gyrus were counted and analyzed. No significant differences were found in the number of GFAP$^+$ cells between animals housed in EE (M = 200.25, SEM = ±14.56) and those housed in SE (M = 143.50, SEM = ±45.49) (p = .280). GFAP$^+$ filament morphology was then analyzed to assess potential cellular differences between groups.

The total filament length was determined per cell and then averaged across samples. The mean total filament length was not significantly different between EE (M = 502.64, SEM = ±73.04) and SE (M = 361.00, SEM = ±23.10) (p = .146). The cell with the minimum total filament length was measured per sample and then averaged between groups. The mean minimum total filament length was not significantly different between EE (M = 38.2, SEM = ±19.10) and SE (M = 7.86, SEM = ±6.04) (p = .181). This analysis was repeated for cells with the maximum total filament length per sample and was also found to not be significant between EE (M = 1839.79, SEM = ±223.36) and SE (M = 1772.95, SEM = ±186.69) (p = .826). The standard deviation in total filament length was not significantly different between EE (M = 315.11, SEM = ±34.66) and SE (M = 297.34, SEM = ±15.86) (p = .658).

Within each cell, the mean length of GFAP$^+$ individual filament segments was significantly shorter among EE (M = 5.71, SEM = ±0.31) than SE (M = 7.08, SEM = ±0.43) ($t(6) = -2.576$, p = .042, Figure 3(a)). In addition, the mean minimum length of individual GFAP$^+$ filaments was significantly shorter among EE (M = 0.08, SEM = ±0.01) than SE (M = 0.11, SEM = ±0.01) ($t(6) = -4.033$, p = .007, Figure 3(b)). The mean maximum filament segment length was not significantly different between EE (M = 60.64, SEM = ±6.57) and SE (M = 82.19, SEM = ±10.42) (p = .131). The standard deviation in filament segment length was also not significant between EE (M = 10.68, SEM = ±5.44) and SE (M = 7.37, SEM = ±0.57) (p = .587).

The number of filament terminal points was also analyzed. The mean number of terminal points was not significantly different between EE (M = 48.08, SEM = ±8.63) and SE (M = 27.97, SEM = ±2.34) (p = .099). The mean maximum number of terminal points was significantly greater among EE (M = 225.75, SEM = ±26.02) than SE

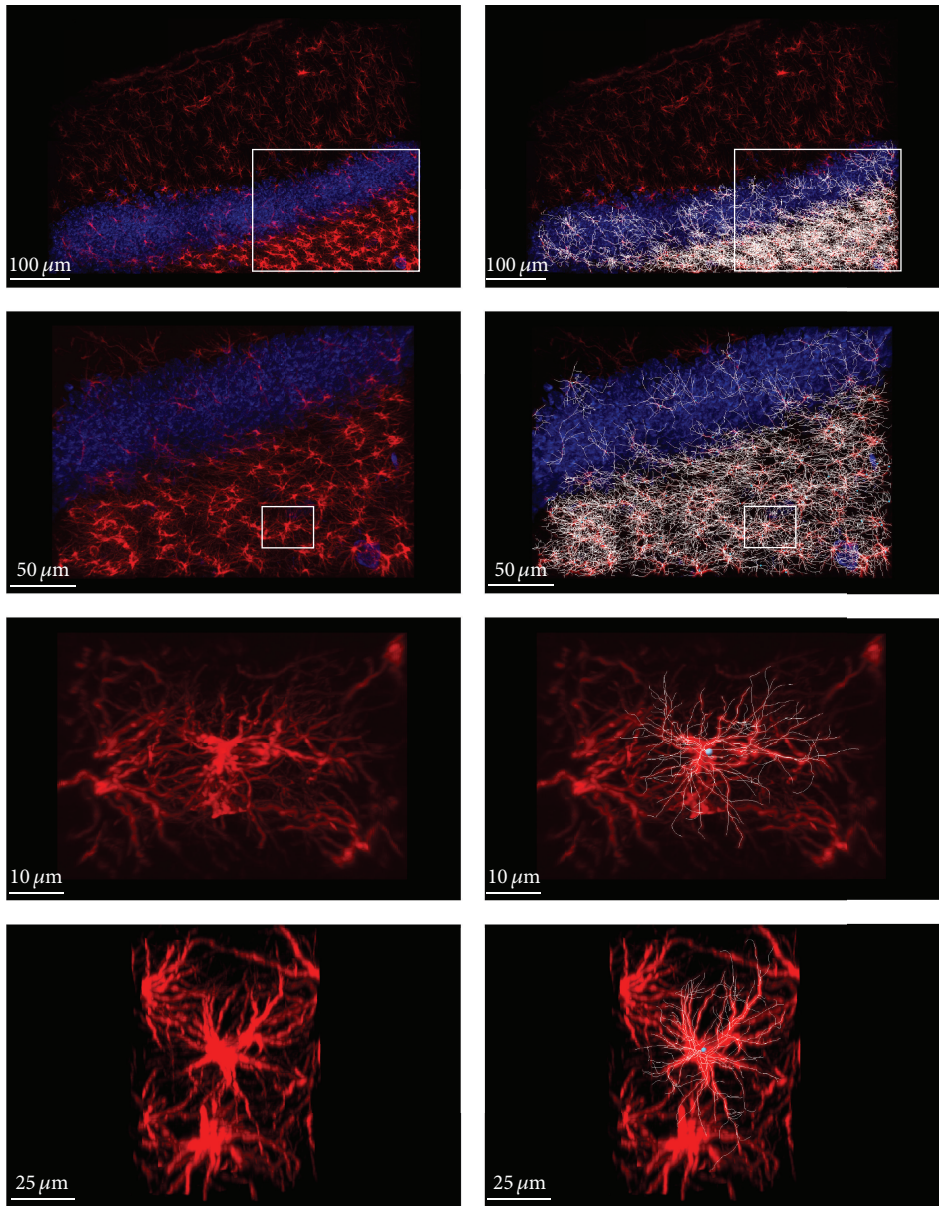

Figure 2: Astrocytes within the granule cell layer and hilus of the dentate gyrus were semiautomatically traced, segmented, and analyzed using Imaris FilamentTracer.

(M = 111.75, SEM = ±13.44) ($t(6) = 3.893$, $p = .008$, Figure 3(c)). The mean minimum number of terminal points was not significantly different between EE (M = 3.50, SEM = ±1.19) and SE (M = 0.75, SEM = ±0.48) ($p = .100$). The standard deviation in the number of terminal points was also not significantly different between EE (M = 26.95, SEM = ±9.18) and SE (M = 19.82, SEM = ±2.50) ($p = .501$).

The total number of branch points was calculated per cell. The mean total number of branch points per cell was not significantly different between EE (M = 42.00, SEM = ±8.26) and SE (M = 23.60, SEM = ±2.17) ($p = .109$). The minimum and maximum number of branch points per cell were averaged across samples and compared across groups. The maximum number of branch points was significantly greater among animals housed in EE (M = 200.50, SEM = ±20.52) than SE (M = 99.25, SEM = ±9.14) ($t(6) = 4.508$, $p = .004$, Figure 4(b)). The standard deviation in the number of branch points per cell was also calculated between groups and was significantly greater among EE animals (M = 30.38, SEM = ±3.92) compared to SE animals (M = 18.19, SEM = ±2.09) ($t(6) = 2.743$, $p = .045$, Figure 4(d)). The mean number of branches was not significantly different between EE (M = 11.41, SEM = ±1.88) and SE (M = 7.72, SEM = ±0.82) ($p = .109$). The maximum number of branches was significantly greater among samples from the EE group (M = 90.75, SEM = ±8.29) compared to the SE

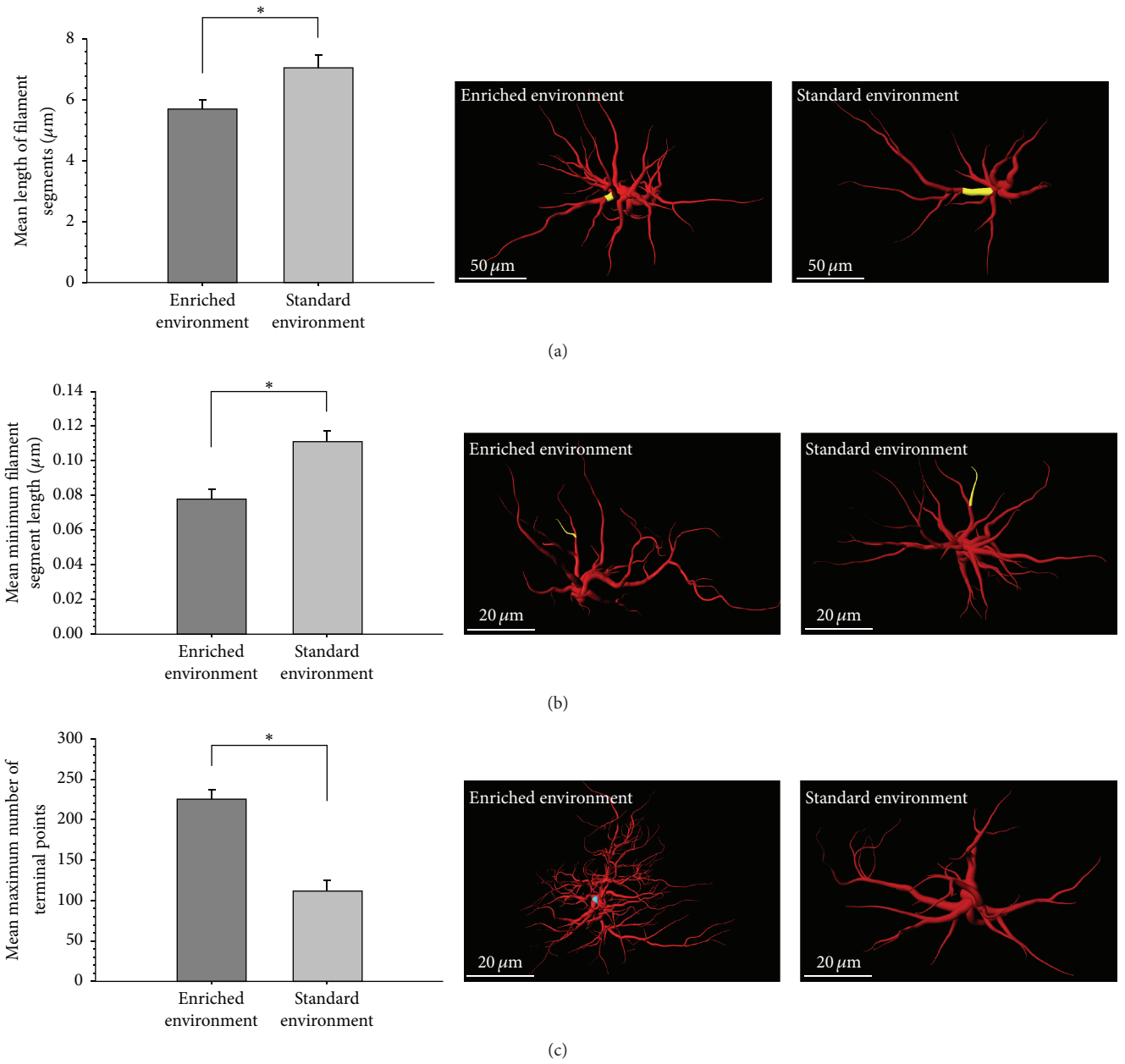

FIGURE 3: (a) Mean length of filament segments (regions between branch points), (b) mean minimum filament length, and (c) mean maximum number of terminal points. ∗ denotes a p value of <.05.

group (M = 40.50, SEM = ±4.79) ($t(6) = 5.249$, $p = .002$, Figure 4(c)).

The full branch depth (the greatest number of branches taken to reach a terminal point) was measured per cell and then averaged per sample and compared across groups. The value for the cell with the greatest full branch depth per sample was averaged across samples. Among the EE group, cells with the maximum branch depth had significantly more branches (M = 32.00, SEM = ±1.87) than those in the SE group (M = 22.75, SEM = ±2.72) ($t(6) = 2.802$, $p = .031$, Figure 4(a)). The cell with the lowest full branch depth per sample was also averaged across samples; however there were no significant differences when compared between EE (M = 1.50, SEM = ±0.87) and SE (M = 0.50, SEM = ±0.29) ($p = .315$). There were no significant differences in the mean full branch depth between EE (M = 9.47, SEM = ±1.55) and SE (M = 8.16, SEM = ±0.50) ($p = .453$). There were also no significant differences in standard deviation of full branch depth between EE (M = 4.19, SEM = ±0.23) and SE (M = 3.91, SEM = ±0.41) ($p = .573$).

Astrocyte filament complexity was further analyzed using three-dimensional Sholl analysis. The maximum number of Sholl intersections per sample was averaged across groups and found to be significantly greater among EE animals

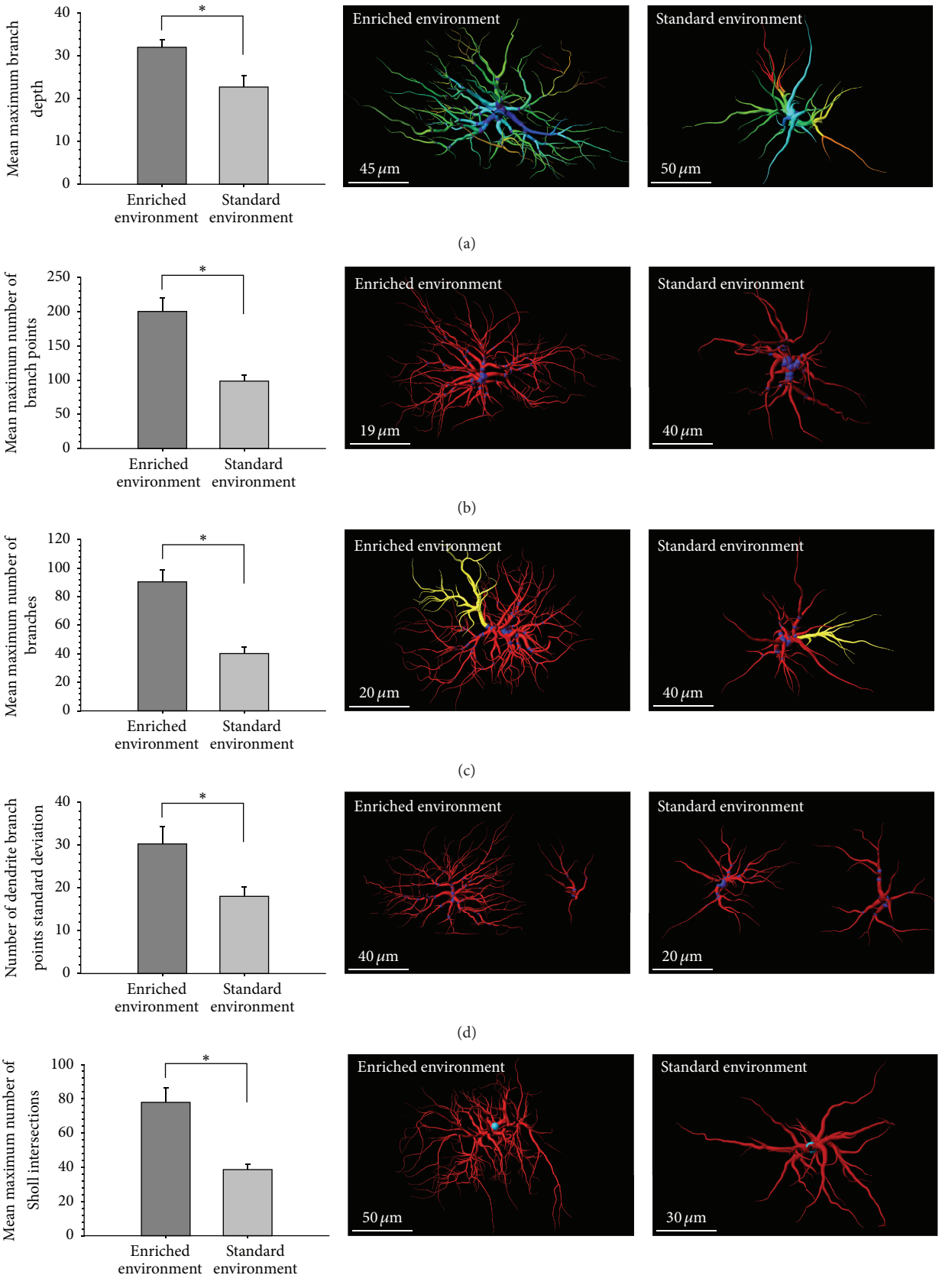

Figure 4: (a) Mean maximum branch depth. (b) Mean maximum number of branch points. (c) Mean maximum number of branches. (d) Standard deviation in the number of branch points. (e) Mean maximum number of Sholl intersections. $*$ denotes a p value of $<.05$.

(M = 78.00, SEM = ±8.33) compared to SE animals (M = 38.75, SEM = ±2.95) ($t(6) = 4.438$, $p = .004$, Figure 4(e)). There were no significant differences in the overall mean number of Sholl intersections between EE (M = 10.16, SEM = ±1.49) and SE (M = 7.11, SEM = ±0.67) ($p = .111$). In addition, the standard deviation of Sholl intersections was not significantly different between EE (M = 14.50, SEM = ±4.55) and SE (M = 6.41, SEM = ±0.58) ($p = .128$).

4. Discussion

It was hypothesized that enriched environments would induce an increase in the number and complexity of astrocytes in the rat dentate gyrus. However, evidence was not found for an increase in the number astrocytes, in contrast to results from other studies in different brain regions such as the visual cortex [50]. This may be due to a difference in the mechanisms mediating plasticity in different brain regions. The possibility that astrocytes respond to EE through changes in morphology rather than number of cells was also investigated. The results indicated a significantly shorter distance between branching points but no differences in the overall number of Sholl intersections, terminal points, branch number, or total filament length. However, a more detailed analysis demonstrated significant differences between cells with the most complex filaments when compared between EE and SE. The cells with the maximum value per sample for the number of Sholl intersections, number of terminal points, and number of branches per cell were significantly larger among astrocytes from EE animals. These data suggest that astrocytes of the dentate gyrus may not be uniformly affected by EE. Recent work has revealed that astrocyte populations are genetically and morphologically heterogeneous, even within individual brain regions [64, 65], a finding that may explain the differential effects of EE on astrocyte morphology. Furthermore, it is possible that the effect of EE on astrocytes is limited primarily to fully mature astrocytes, which are likely to exhibit a greater degree of filament complexity relative to more immature astrocytes.

An increase in astrocyte process complexity due to enriched housing environments may substantially alter the ability of affected astrocytes to influence neuronal properties within their domains. In response to EE, neurons form new dendritic spines as well as modulating the structure and function of existing spines [20–22]. As a critical regulator of spine dynamics, astrocytes are likely to be playing a key role in this process [36–41]. Increased astrocyte filament complexity in response to EE lends further support to this hypothesis. A more detailed understanding of how astrocytes affect plasticity will require further research of the interactions between newly formed astrocyte processes and the properties of the synapse in the context of environments of varying complexity.

It is possible that morphological changes in astrocytes in response to EE may not be fully evident by merely measuring changes in GFAP expression. Recent studies have demonstrated that as much as 85% of astrocyte volume is not shown by GFAP labeling [27]. In addition, not all astrocytes express GFAP at significant levels, despite meeting the other qualifications for astrocyte identity [66]. Thus, GFAP labeling may fail to capture smaller scale changes in astrocyte complexity. Nevertheless, these results suggest the possibility that EE invokes an increase in GFAP filament complexity among a subset of dentate gyrus astrocytes. New advances in molecular identification of astrocytes will be an important step in understanding the heterogeneous plasticity of astrocytes observed in this study.

Alteration of astrocyte structure and function is a hallmark feature of numerous neurological diseases including neurodegenerative diseases such as Alzheimer's Disease [56–59] and Parkinson's Disease [60, 61], as well as traumatic brain injury [67–69], stroke [70–73], and epilepsy [52–55, 74–76]. Activated astrocytes in these diseases undergo reactive gliosis, which involves the upregulation of astrocyte GFAP, as well as breakdown of domain specificity [64]. In TBI, serum levels of GFAP have been proposed as a potential biomarker of disease severity [68, 69]. As the results from this study indicate that astrocytes from animal models housed in SE may exhibit pathologic GFAP filament morphology, it is crucial to understand what effect housing environment may have on disease recovery processes and on the results of studies using animal models in general.

Despite these results, the potential role of astrocytes in mediating the behavioral effects of EE remains unclear. Detailed analysis of astrocyte morphological, electrophysiological, and genetic dynamics in the context of EE is crucial for understanding how plasticity in the dentate gyrus and other brain regions is controlled. New optical clearing techniques such as piSeeDB will be critical in understanding these processes. Despite recent advances in histological methods which allow imaging of large three-dimensional sections of tissue, specialized software for the automated analysis of *in situ* morphology is limited, and analysis by hand is extremely time-consuming, especially when dealing with large samples. New advances in automatic three-dimensional morphology analysis as well as in processing and storage of large image data sets are thus critically needed for the study of complex brain anatomy and physiology.

Conflict of Interests

The authors have no conflicting financial interests in the outcome of this study.

Acknowledgments

This research was supported by a Saginaw Valley State University Student Research and Creativity Institute grant to Garrick Salois. The authors would like to thank Zack Bowers, Jake Dunkerson, Sarah Fluharty, Katalin Geeck, Ivy Hiatt, Justin Jacqmain, Evan Nudi, Nick Sanislo, and Madeleine Searles for their assistance throughout the study.

References

[1] D. M. Morales, N. Marklund, D. Lebold et al., "Experimental models of traumatic brain injury: do we really need to build a better mousetrap?" *Neuroscience*, vol. 136, no. 4, pp. 971–989, 2005.

[2] V. E. O'Collins, M. R. Macleod, G. A. Donnan, L. L. Horky, B. H. Van Der Worp, and D. W. Howells, "1,026 Experimental treatments in acute stroke," *Annals of Neurology*, vol. 59, no. 3, pp. 467–477, 2006.

[3] M. R. Rosenzweig, D. Krech, E. L. Bennett, and J. F. Zolman, "Variation in environmental complexity and brain measures," *Journal of Comparative and Physiological Psychology*, vol. 55, no. 6, pp. 1092–1095, 1962.

[4] M. S. Landers, G. W. Knott, H. P. Lipp, I. Poletaeva, and E. Welker, "Synapse formation in adult barrel cortex following naturalistic environmental enrichment," *Neuroscience*, vol. 199, pp. 143–152, 2011.

[5] H. Van Praag, G. Kempermann, and F. H. Gage, "Neural consequences of environmental enrichment," *Nature Reviews Neuroscience*, vol. 1, no. 3, pp. 191–198, 2000.

[6] A. N. Gross, S. H. Richter, A. K. J. Engel, and H. Würbel, "Cage-induced stereotypies, perseveration and the effects of environmental enrichment in laboratory mice," *Behavioural Brain Research*, vol. 234, no. 1, pp. 61–68, 2012.

[7] G. B. Varty, M. P. Paulus, D. L. Braff, and M. A. Geyer, "Environmental enrichment and isolation rearing in the rat: effects on locomotor behavior and startle response plasticity," *Biological Psychiatry*, vol. 47, no. 10, pp. 864–873, 2000.

[8] C. N. Sozda, A. N. Hoffman, A. S. Olsen, J. P. Cheng, R. D. Zafonte, and A. E. Kline, "Empirical comparison of typical and atypical environmental enrichment paradigms on functional and histological outcome after experimental traumatic brain injury," *Journal of Neurotrauma*, vol. 27, no. 6, pp. 1047–1057, 2010.

[9] J. Jacqmain, E. T. Nudi, S. Fluharty, and J. S. Smith, "Pre and post-injury environmental enrichment effects functional recovery following medial frontal cortical contusion injury in rats," *Behavioural Brain Research*, vol. 275, pp. 201–211, 2014.

[10] E. T. Nudi, J. Jacqmain, K. Dubbs et al., "Combining enriched environment, progesterone, and embryonic neural stem cell therapy improves recovery after brain injury," *Journal of Neurotrauma*, vol. 32, no. 14, pp. 1117–1129, 2015.

[11] M. Nilsson, E. Perfilieva, U. Johansson, O. Orwar, and P. S. Eriksson, "Enriched environment increases neurogenesis in the adult rat dentate gyrus and improves spatial memory," *Journal of Neurobiology*, vol. 39, no. 4, pp. 569–578, 1999.

[12] J. Dunkerson, K. E. Moritz, J. Young et al., "Combining enriched environment and induced pluripotent stem cell therapy results in improved cognitive and motor function following traumatic brain injury," *Restorative Neurology and Neuroscience*, vol. 32, no. 5, pp. 675–687, 2014.

[13] M. C. Diamond, C. A. Ingham, R. E. Johnson, E. L. Bennett, and M. R. Rosenzweig, "Effects of environment on morphology of rat cerebral cortex and hippocampus," *Journal of Neurobiology*, vol. 7, no. 1, pp. 75–85, 1976.

[14] M. C. Diamond, F. Law, H. Rhodes et al., "Increases in cortical depth and glia numbers in rats subjected to enriched environment," *Journal of Comparative Neurology*, vol. 128, no. 1, pp. 117–126, 1966.

[15] E. L. Bennett, M. R. Rosenzweig, and M. C. Diamond, "Rat brain: effects of environmental enrichment on wet and dry weights," *Science*, vol. 163, no. 3869, pp. 825–826, 1969.

[16] M. R. Rosenzweig and E. L. Bennett, "Effects of differential environments on brain weights and enzyme activities in gerbils, rats, and mice," *Developmental Psychobiology*, vol. 2, no. 2, pp. 87–95, 1969.

[17] G. Kempermann, H. G. Kuhn, and F. H. Gage, "More hippocampal neurons in adult mice living in an enriched environment," *Nature*, vol. 386, no. 6624, pp. 493–495, 1997.

[18] S. Nabavi, R. Fox, C. D. Proulx, J. Y. Lin, R. Y. Tsien, and R. Malinow, "Engineering a memory with LTD and LTP," *Nature*, vol. 511, no. 7509, pp. 348–352, 2014.

[19] J. O'Keefe, "Place units in the hippocampus of the freely moving rat," *Experimental Neurology*, vol. 51, no. 1, pp. 78–109, 1976.

[20] T. C. Foster, H. N. Fugger, and S. G. Cunningham, "Receptor blockade reveals a correspondence between hippocampal-dependent behavior and experience-dependent synaptic enhancement," *Brain Research*, vol. 871, no. 1, pp. 39–43, 2000.

[21] J. Beauquis, P. Roig, A. F. de Nicola, and F. Saravia, "Short-term environmental enrichment enhances adult neurogenesis, vascular network and dendritic complexity in the hippocampus of type 1 diabetic mice," *PLoS ONE*, vol. 5, no. 11, Article ID e13993, 2010.

[22] B. B. Johansson and P. V. Belichenko, "Neuronal plasticity and dendritic spines: effect of environmental enrichment on intact and postischemic rat brain," *Journal of Cerebral Blood Flow & Metabolism*, vol. 22, no. 1, pp. 89–96, 2002.

[23] H. Song, C. F. Stevens, and F. H. Gage, "Astroglia induce neurogenesis from adult neural stem cells," *Nature*, vol. 417, no. 6884, pp. 39–44, 2002.

[24] C. C. Sherwood, C. D. Stimpson, M. A. Raghanti et al., "Evolution of increased glia–neuron ratios in the human frontal cortex," *Proceedings of the National Academy of Sciences of the United States of America*, vol. 103, no. 37, pp. 13606–13611, 2006.

[25] J. H. McCarty, "Cell adhesion and signaling networks in brain neurovascular units," *Current Opinion in Hematology*, vol. 16, no. 3, pp. 209–214, 2009.

[26] T. Takano, G.-F. Tian, W. Peng et al., "Astrocyte-mediated control of cerebral blood flow," *Nature Neuroscience*, vol. 9, no. 2, pp. 260–267, 2006.

[27] E. A. Bushong, M. E. Martone, Y. Z. Jones, and M. H. Ellisman, "Protoplasmic astrocytes in CA1 stratum radiatum occupy separate anatomical domains," *The Journal of Neuroscience*, vol. 22, no. 1, pp. 183–192, 2002.

[28] M. L. Schroeter, K. Mertsch, H. Giese et al., "Astrocytes enhance radical defence in capillary endothelial cells constituting the blood-brain barrier," *FEBS Letters*, vol. 449, no. 2-3, pp. 241–244, 1999.

[29] Y. Hayashi, M. Nomura, S. Yamagishi, S. Harada, J. Yamashita, and H. Yamamoto, "Induction of various blood-brain barrier properties in non-neural endothelial cells by close apposition to co-cultured astrocytes," *Glia*, vol. 19, no. 1, pp. 13–26, 1997.

[30] I. B. Wanner, A. Deik, M. Torres et al., "A new in vitro model of the glial scar inhibits axon growth," *Glia*, vol. 56, no. 15, pp. 1691–1709, 2008.

[31] T. G. Bush, N. Puvanachandra, C. H. Horner et al., "Leukocyte infiltration, neuronal degeneration, and neurite outgrowth after ablation of scar-forming, reactive astrocytes in adult transgenic mice," *Neuron*, vol. 23, no. 2, pp. 297–308, 1999.

[32] J. R. Faulkner, J. E. Herrmann, M. J. Woo, K. E. Tansey, N. B. Doan, and M. V. Sofroniew, "Reactive astrocytes protect tissue and preserve function after spinal cord injury," *The Journal of Neuroscience*, vol. 24, no. 9, pp. 2143–2155, 2004.

[33] I. B. Wanner, M. A. Anderson, B. Song et al., "Glial scar borders are formed by newly proliferated, elongated astrocytes that interact to corral inflammatory and fibrotic cells via STAT3-dependent mechanisms after spinal cord injury," *The Journal of Neuroscience*, vol. 33, no. 31, pp. 12870–12886, 2013.

[34] S. Okada, M. Nakamura, H. Katoh et al., "Conditional ablation of Stat3 or Socs3 discloses a dual role for reactive astrocytes after spinal cord injury," *Nature Medicine*, vol. 12, no. 7, pp. 829–834, 2006.

[35] T. Çakır, S. Alsan, H. Saybaşili, A. Akin, and K. Ö. Ülgen, "Reconstruction and flux analysis of coupling between metabolic pathways of astrocytes and neurons: application to cerebral hypoxia," *Theoretical Biology & Medical Modelling*, vol. 4, article 48, 2007.

[36] M. Haber, L. Zhou, and K. K. Murai, "Cooperative astrocyte and dendritic spine dynamics at hippocampal excitatory synapses," *The Journal of Neuroscience*, vol. 26, no. 35, pp. 8881–8891, 2006.

[37] K. S. Christopherson, E. M. Ullian, C. C. A. Stokes et al., "Thrombospondins are astrocyte-secreted proteins that promote CNS synaptogenesis," *Cell*, vol. 120, no. 3, pp. 421–433, 2005.

[38] E. M. Ullian, S. K. Sapperstein, K. S. Christopherson, and B. A. Barres, "Control of synapse number by glia," *Science*, vol. 291, no. 5504, pp. 657–661, 2001.

[39] T. A. Jones and W. T. Greenough, "Ultrastructural evidence for increased contact between astrocytes and synapses in rats reared in a complex environment," *Neurobiology of Learning and Memory*, vol. 65, no. 1, pp. 48–56, 1996.

[40] E. J. Green and W. T. Greenough, "Altered synaptic transmission in dentate gyrus of rats reared in complex environments: evidence from hippocampal slices maintained in vitro," *Journal of Neurophysiology*, vol. 55, no. 4, pp. 739–750, 1986.

[41] M. Navarrete, G. Perea, D. F. de Sevilla et al., "Astrocytes mediate in vivo cholinergic-induced synaptic plasticity," *PLoS Biology*, vol. 10, no. 2, Article ID e1001259, 2012.

[42] C. Henneberger, T. Papouin, S. H. R. Oliet, and D. A. Rusakov, "Long-term potentiation depends on release of D-serine from astrocytes," *Nature*, vol. 463, no. 7278, pp. 232–236, 2010.

[43] P. Fossat, F. R. Turpin, S. Sacchi et al., "Glial D-serine gates NMDA receptors at excitatory synapses in prefrontal cortex," *Cerebral Cortex*, vol. 22, no. 3, pp. 595–606, 2012.

[44] Y. Yang, W. Ge, Y. Chen et al., "Contribution of astrocytes to hippocampal long-term potentiation through release of D-serine," *Proceedings of the National Academy of Sciences of the United States of America*, vol. 100, no. 25, pp. 15194–15199, 2003.

[45] M. Martineau, T. Shi, J. Puyal et al., "Storage and uptake of D-serine into astrocytic synaptic-like vesicles specify gliotransmission," *The Journal of Neuroscience*, vol. 33, no. 8, pp. 3413–3423, 2013.

[46] M. Le Bail, M. Martineau, S. Sacchi et al., "Identity of the NMDA receptor coagonist is synapse specific and developmentally regulated in the hippocampus," *Proceedings of the National Academy of Sciences of the United States of America*, vol. 112, no. 2, pp. E204–E213, 2015.

[47] R. S. Ashton, A. Conway, C. Pangarkar et al., "Astrocytes regulate adult hippocampal neurogenesis through ephrin-B signaling," *Nature Neuroscience*, vol. 15, no. 10, pp. 1399–1406, 2012.

[48] S. Sultan, L. Li, J. Moss et al., "Synaptic integration of adult-born hippocampal neurons is locally controlled by astrocytes," *Neuron*, vol. 88, no. 5, pp. 957–972, 2015.

[49] J. Hirrlinger, S. Hülsmann, and F. Kirchhoff, "Astroglial processes show spontaneous motility at active synaptic terminals in situ," *European Journal of Neuroscience*, vol. 20, no. 8, pp. 2235–2239, 2004.

[50] A. M. Sirevaag and W. T. Greenough, "Plasticity of GFAP-immunoreactive astrocyte size and number in visual cortex of rats reared in complex environments," *Brain Research*, vol. 540, no. 1-2, pp. 273–278, 1991.

[51] H. Kettenmann and A. Verkhratsky, "Neuroglia: the 150 years after," *Trends in Neurosciences*, vol. 31, no. 12, pp. 653–659, 2008.

[52] C. G. Fonseca, C. R. Green, and L. F. B. Nicholson, "Upregulation in astrocytic connexin 43 gap junction levels may exacerbate generalized seizures in mesial temporal lobe epilepsy," *Brain Research*, vol. 929, no. 1, pp. 105–116, 2002.

[53] G. Seifert, G. Carmignoto, and C. Steinhäuser, "Astrocyte dysfunction in epilepsy," *Brain Research Reviews*, vol. 63, no. 1-2, pp. 212–221, 2010.

[54] E. Aronica, E. A. Van Vliet, O. A. Mayboroda, D. Troost, F. H. Lopes Da Silva, and J. A. Gorter, "Upregulation of metabotropic glutamate receptor subtype mGluR3 and mGluR5 in reactive astrocytes in a rat model of mesial temporal lobe epilepsy," *European Journal of Neuroscience*, vol. 12, no. 7, pp. 2333–2344, 2000.

[55] S. Hinterkeuser, W. Schröder, G. Hager et al., "Astrocytes in the hippocampus of patients with temporal lobe epilepsy display changes in potassium conductances," *European Journal of Neuroscience*, vol. 12, no. 6, pp. 2087–2096, 2000.

[56] A. Minagar, P. Shapshak, R. Fujimura, R. Ownby, M. Heyes, and C. Eisdorfer, "The role of macrophage/microglia and astrocytes in the pathogenesis of three neurologic disorders: HIV-associated dementia, Alzheimer disease, and multiple sclerosis," *Journal of the Neurological Sciences*, vol. 202, no. 1-2, pp. 13–23, 2002.

[57] A. Delekate, M. Füchtemeier, T. Schumacher, C. Ulbrich, M. Foddis, and G. C. Petzold, "Metabotropic P2Y1 receptor signalling mediates astrocytic hyperactivity in vivo in an Alzheimer's disease mouse model," *Nature Communications*, vol. 5, article 5422, 2014.

[58] J. L. Furman, D. M. Sama, J. C. Gant et al., "Targeting astrocytes ameliorates neurologic changes in a mouse model of Alzheimer's disease," *The Journal of Neuroscience*, vol. 32, no. 46, pp. 16129–16140, 2012.

[59] E. Alberdi, A. Wyssenbach, M. Alberdi et al., "Ca^{2+}-dependent endoplasmic reticulum stress correlates with astrogliosis in oligomeric amyloid β-treated astrocytes and in a model of Alzheimer's disease," *Aging Cell*, vol. 12, no. 2, pp. 292–302, 2013.

[60] S. K. Bae, C. H. Heo, D. J. Choi et al., "A ratiometric two-photon fluorescent probe reveals reduction in mitochondrial H_2S production in Parkinson's disease gene knockout astrocytes," *Journal of the American Chemical Society*, vol. 135, no. 26, pp. 9915–9923, 2013.

[61] R. Niranjan, "The role of inflammatory and oxidative stress mechanisms in the pathogenesis of Parkinson's disease: focus on astrocytes," *Molecular Neurobiology*, vol. 49, no. 1, pp. 28–38, 2014.

[62] M.-T. Ke, S. Fujimoto, and T. Imai, "SeeDB: a simple and morphology-preserving optical clearing agent for neuronal circuit reconstruction," *Nature Neuroscience*, vol. 16, no. 8, pp. 1154–1161, 2013.

[63] J. A. Gleave, J. P. Lerch, R. M. Henkelman, and B. J. Nieman, "A method for 3D immunostaining and optical imaging of the mouse brain demonstrated in neural progenitor cells," *PLoS ONE*, vol. 8, no. 8, Article ID e72039, 2013.

[64] N. A. Oberheim, S. A. Goldman, and M. Nedergaard, "Heterogeneity of astrocytic form and function," in *Astrocytes*, R. Milner, Ed., vol. 814 of *Methods in Molecular Biology*, pp. 23–45, Springer, 2012.

[65] V. Matyash and H. Kettenmann, "Heterogeneity in astrocyte morphology and physiology," *Brain Research Reviews*, vol. 63, no. 1-2, pp. 2–10, 2010.

[66] H. K. Kimelberg, "The problem of astrocyte identity," *Neurochemistry International*, vol. 45, no. 2-3, pp. 191–202, 2004.

[67] J. Silver and J. H. Miller, "Regeneration beyond the glial scar," *Nature Reviews Neuroscience*, vol. 5, no. 2, pp. 146–156, 2004.

[68] P. E. Vos, B. Jacobs, T. M. J. C. Andriessen et al., "GFAP and S100B are biomarkers of traumatic brain injury. An observational cohort study," *Neurology*, vol. 75, no. 20, pp. 1786–1793, 2010.

[69] L. E. Pelika, A. Kroepfl, M. Leixnering, W. Buchinger, A. Raabe, and H. Redl, "GFAP versus S100B in serum after traumatic brain injury: relationship to brain damage and outcome," *Journal of Neurotrauma*, vol. 21, no. 11, pp. 1553–1561, 2004.

[70] D.-C. Wagner, J. Scheibe, I. Glocke et al., "Object-based analysis of astroglial reaction and astrocyte subtype morphology after ischemic brain injury," *Acta Neurobiologiae Experimentalis*, vol. 73, no. 1, pp. 79–87, 2013.

[71] M. V. Sofroniew, "Molecular dissection of reactive astrogliosis and glial scar formation," *Trends in Neurosciences*, vol. 32, no. 12, pp. 638–647, 2009.

[72] G. Barreto, R. E. White, Y. Ouyang, L. Xu, and R. G. Giffard, "Astrocytes: targets for neuroprotection in stroke," *Central Nervous System Agents in Medicinal Chemistry*, vol. 11, no. 2, pp. 164–173, 2011.

[73] Y. Zhao and D. A. Rempe, "Targeting astrocytes for stroke therapy," *Neurotherapeutics*, vol. 7, no. 4, pp. 439–451, 2010.

[74] J. H. Kim, "Pathology of epilepsy," *Experimental and Molecular Pathology*, vol. 70, no. 3, pp. 345–367, 2001.

[75] W. Schröder, S. Hinterkeuser, G. Seifert et al., "Functional and molecular properties of human astrocytes in acute hippocampal slices obtained from patients with temporal lobe epilepsy," *Epilepsia*, vol. 41, supplement 6, pp. S181–S184, 2000.

[76] A. Bordey and H. Sontheimer, "Properties of human glial cells associated with epileptic seizure foci," *Epilepsy Research*, vol. 32, no. 1-2, pp. 286–303, 1998.

Hindawi Publishing Corporation
Neural Plasticity
Volume 2016, Article ID 8941327, 8 pages
http://dx.doi.org/10.1155/2016/8941327

Review Article

Recent Advance in the Relationship between Excitatory Amino Acid Transporters and Parkinson's Disease

Yunlong Zhang,[1,2] Feng Tan,[3] Pingyi Xu,[4] and Shaogang Qu[1]

[1] *Department of Blood Transfusion, The Fifth Affiliated Hospital, Southern Medical University, Guangzhou, Guangdong 510900, China*
[2] *Department of Traditional Chinese Medicine, College of Medicine, Xiamen University, Xiamen, Fujian 361102, China*
[3] *Department of Neurology, Foshan Hospital of Traditional Chinese Medicine, Guangzhou University of Chinese Medicine, Foshan, Guangdong 528000, China*
[4] *Department of Neurology, The First Affiliated Hospital of Guangzhou Medical University, Guangzhou, Guangdong 510080, China*

Correspondence should be addressed to Pingyi Xu; pingyixu@sina.com and Shaogang Qu; sgq9528@163.com

Received 21 October 2015; Revised 5 January 2016; Accepted 18 January 2016

Academic Editor: Jason H. Huang

Parkinson's disease (PD) is the most common movement disorder disease in the elderly and is characterized by degeneration of dopamine neurons and formation of Lewy bodies. Glutamate is the major excitatory neurotransmitter in the central nervous system (CNS). If glutamate is not removed promptly in the synaptic cleft, it will excessively stimulate the glutamate receptors and induce excitotoxic effects on the CNS. With lack of extracellular enzyme to decompose glutamate, glutamate uptake in the synaptic cleft is mainly achieved by the excitatory amino acid transporters (EAATs, also known as high-affinity glutamate transporters). Current studies have confirmed that decreased expression and function of EAATs appear in PD animal models. Moreover, single unilateral administration of EAATs inhibitor in the substantia nigra mimics several PD features and this is a solid evidence supporting that decreased EAATs contribute to the process of PD. Drugs or treatments promoting the expression and function of EAATs are shown to attenuate dopamine neurons death in the substantia nigra and striatum, ameliorate the behavior disorder, and improve cognitive abilities in PD animal models. EAATs are potential effective drug targets in treatment of PD and thus study of relationship between EAATs and PD has predominant medical significance currently.

1. Introduction

Glutamate is the predominant excitatory neurotransmitter in the central nervous system (CNS). It is released from presynaptic glutamatergic neurons and activates the ionotropic and metabotropic glutamate receptors located on the postsynaptic neurons. Glutamate in the synaptic cleft is kept in a low concentration, while excessive glutamate will overstimulate the glutamate receptors and mediate the excitotoxic effects on the CNS [1, 2]. Previous studies have revealed that glutamate excitotoxicity induces the dopamine (DA) neurons death, movement disorder, and cognitive impairment, and thus glutamate excitotoxicity plays an important role in the pathogenesis of Parkinson's disease (PD) [3, 4]. Glutamatez uptake in the synaptic cleft is performed by the excitatory amino acid transporters (EAATs, also known as high-affinity glutamate transporters). Five mammalian EAATs have been characterized: GLAST (glutamate/aspartate transporter, also called EAAT1), GLT-1 (glutamate transporter-1, also called EAAT2), EAAC1 (excitatory amino acid carrier-1, also called EAAT3), EAAT4, and EAAT5 [5–10]. Among these, astrocytic GLT-1 and, to a lesser extent, GLAST are mainly responsible for the glutamate uptake and mitigate excitotoxicity. Increasing evidences suggest that dysfunctional EAATs expressions are found in PD patients and models [11–14], and, moreover, DA neurons expressing EAAC1 are preferentially affected by EAATs dysfunction and *in vitro* studies show that application of EAATs substrate inhibitor is preferentially toxic for DA neurons by lowering their resistance threshold to glutamate excitotoxicity [15]. However, it is unclear whether decreased EAATs expression is the consequence or the cause of PD. Recently Assous et al. report that single unilateral administration of EAATs inhibitor in the substantia nigra mimics several PD features, as they find DA neurons death

and axons dystrophy in the substantia nigra and striatum, and the motor disorder appears when DA neurons loss exceeds 50% [16]. Thus far this is a solid evidence which supports that dysfunctional EAATs are linked to the pathogenesis of PD.

In this review, we outline the recent advance of structure, function, and distribution of EAATs in the CNS, we also highlight the glutamate excitotoxicity in the pathogenesis of PD and the role of dysfunctional EAATs in the excitotoxicity, and we show the related finding in treatment of PD by upregulating EAATs in recent years.

2. Structure and Function of EAATs

As stated previously, these five mammalian EAATs have been cloned and characterized [5–10], and they share nearly 50–60% of homologous sequences [17]. In 2004, Yernool et al. revealed the crystal structure of prokaryotic aspartate transporter Glt_{Ph} from *Pyrococcus horikoshii*, which is the homologue of the glutamate transporters [18]. The transport domain for each Glt_{Ph} subunit is composed of eight transmembrane (TM) domains TM1–TM8 and two opposite-facing helical hairpins HP1 and HP2 [18]. Glutamate or aspartate transport process is operated via an "alternate access mechanism"; the mode of EAATs action is shown in Figure 1. Currently, the crystal structures of Glt_{Ph} at several different phases have been revealed. Briefly, these phases contain the substrate binding phase (PDB ID 1XFH), Glt_{Ph} binding with TBOA (PBD 2NWW), and Glt_{Ph} is trapped in the inward facing state (PDB ID 3KBC), Glt_{Ph} with two protomers in an inward facing state and the third in an intermediate conformation between the outward and inward facing states (PDB ID 3V8G), and also the newly reported Glt_{Ph} in the cation-only bound site (PDB ID 4P1A) [18–22]. These different phases are significant for further study of the structure and function of eukaryotic glutamate transporter.

EAATs terminate the glutamate excitatory synaptic transmission via uptake of glutamate in the synaptic cleft. In addition, through clearing the excessive glutamate in the synaptic cleft, EAATs could modulate the location of metabotropic glutamate receptor within the synapse, maintain the most effective distribution of glutamate, and keep the accurate neurotransmission in the synapse [23, 24]. Furthermore, EAATs can promote the astrocytes near the glutamatergic synapse releasing glutamine rapidly and provide the neurons with glutamine for synthesis of glutamate and γ-aminobutyric acid (γ-GABA) [23–25]. Glutamate transporters are also involved in regulating learning, memory, and the motor behavior [25–29]. Moreover, EAATs also provide cysteine or glutamate for the synthesis of glutathione and some other proteins [30].

Among these five subtypes, GLAST is abundantly expressed in the Bergmann glial cells in the molecular layer of the cerebellum, and it is also expressed in the spinal cord, forebrain, inner ear, and retina [31]. GLT-1 is widely distributed in the CNS and is mainly expressed in astrocytes in the forebrain, cerebral cortex, hippocampus, and other regions. Besides, GLT-1 is also expressed in the neurons in the development stage [7, 32, 33]. Recently, C-terminal splice variants of GLT-1 are found and among these splice variants GLT-1a, GLT-1b (also called GLT-1v), and GLT-1c are

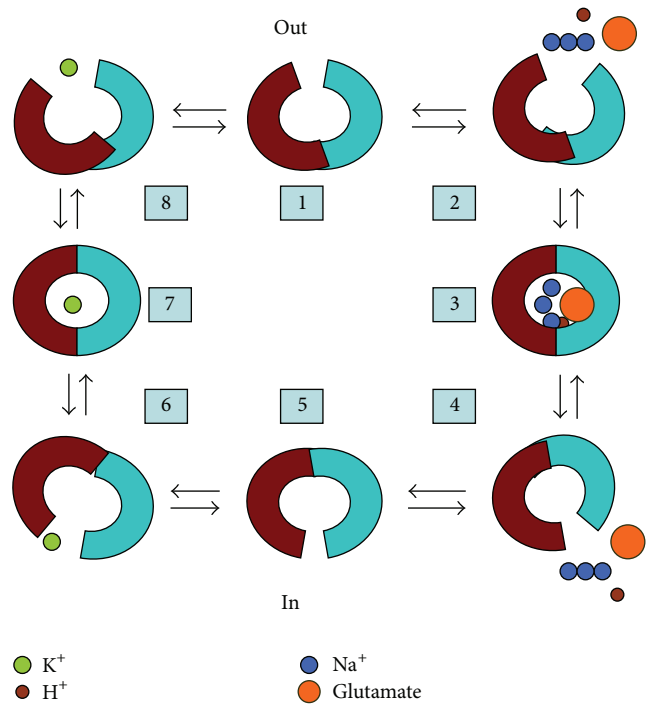

Figure 1: The mode of EAATs action. In the normal condition, the outward facing empty glutamate transporter (1) binds with glutamate, H^+, and 3 Na^+ (2) and turns into the fully loaded carrier state (3). Followed by releasing the substrates at the intracellular face (4), the transporter turns into the inward facing empty state (5). Thereafter, K^+ binds to the inward facing transporter (6) and turns into the K^+ loaded transporter state (7). Afterwards, the transporter releases K^+ at the extracellular face (8) and translocates back into the outward facing empty glutamate transporter state (1).

closely related to the neurodegenerative diseases [34]. They are mainly expressed in the neurons and also in astrocytes and microglia, and their distribution in different cell types is complementary [34]. GLT-1 is responsible for clearing nearly 90% of glutamate in the synaptic cleft. Using conditional knockout model, Petr et al. find that when astrocytic GLT-1 is eliminated, glutamate uptake in the forebrain synaptosomes shows no significant changes [35]. However, when GLT-1 is deleted in neurons, the glutamate uptake in the synaptosomes is decreased significantly [35]. This study reveals that lowly expressed GLT-1 in the neurons is responsible for the most of glutamate uptake in the forebrain synaptosomes; in addition, astrocytic and neuronal GLT-1 possibly take on different roles in the synaptic excitatory neurotransmission [35].

EAAC1 is mainly expressed in the postsynaptic membrane of neurons and is abundantly distributed in the hippocampal CA1–CA4 region and cortical pyramidal cell layers. Studies showed that EAAC1 is highly expressed in the hippocampus of young adult rat and per gram of tissue containing about 0.013 mg of EAAC1 [36]. EAAT4 is limitedly expressed in the Purkinje cells in the cerebellar molecular layer and EAAT5 is limitedly expressed in the neurons and astrocytes in the retina, and it is also expressed in the photoreceptors, bipolar cells, and amacrine cells [10, 37].

Recent studies also show that EAAT4 and EAAT5 are also expressed in type I and II vestibular hair cells [38].

3. Excitotoxicity in the Pathogenesis of Parkinson's Disease

3.1. Mechanism of Excitotoxicity in PD. PD is a common chronic neurodegenerative disease in elderly and is characterized by the progressive degeneration of DA neurons in the pars compacta of substantia nigra (SNpc) and the formation of Lewy bodies. Besides, glutamate excitotoxicity also participates in the pathogenesis of PD. Impaired motor coordination and dyskinesias in PD have been shown to be closely linked to the increase of glutamate levels within the basal ganglia [39–43]. Dopaminergic denervation also induces dysfunctional corticostriatal glutamate release, and this circuitry imbalance contributes to further DA neurons loss in substantia nigra [44]. In addition, depression, dementia, and the nonmotor symptoms in the pathogenesis of PD attract much more attention nowadays [45–49]. Dysfunction of glutamate metabolism is also involved in the cognitive impairment in PD [26, 27].

Excessive glutamate in the synaptic cleft overstimulates the ionotropic and metabotropic glutamate receptors in the postsynaptic membrane and mediates excitotoxicity. Through overactivating the N-methyl-D-aspartate (NMDA) receptor, glutamate can induce intracellular Ca^{2+} overload, production of reactive oxygen species, and reactive nitrogen radicals, result in mitochondrial dysfunction, and thus lead to the neuronal death; through overactivating α-amino-3-hydroxy-5-methyl-4-isoxazole-propionic acid (AMPA) receptor and kainic acid (KA) receptor, glutamate can induce Na^{+} influx and acute osmotic swelling of nerve cells and mediate neuronal death [50–55]. Current studies also show that, except glutamate, other factors also could induce excitotoxicity in PD. Alpha-synuclein could downregulate the expression and function of NR2B-containing NMDA receptors [56]. Knockout of α-synuclein can weaken the decreased expression of NR2B-containing NMDA receptors mediated by rotenone and reduce the cortical neurons death [56]. Moreover, glutamate also stimulates group I metabotropic glutamate receptors (mGluR), activates the intracellular phospholipase C (PLC), and induces the hydrolysis of PLC into inositol triphosphate (IP3) and diacylglycerol (DAG), wherein IP3 can induce intracellular Ca^{2+} release and DAG can activate protein kinase C (PKC) and strengthen the calcium influx mediated by NMDA receptor and thus these effects induce neuronal death [57–59].

Thus, accumulation of glutamate in the synaptic cleft and other pathological productions contribute to the pathogenesis of PD via different pathways and excitotoxicity is a key link in the process of PD (Figure 2).

3.2. Malfunction of EAATs Contributes to the Excitotoxicity in PD. Previously Ferrarese et al. study the glutamate uptake in platelet in PD patients and normal control, and they find that glutamate uptake in platelet in PD patients is reduced by 50% compared with control [60]. Moreover, the glutamate uptake

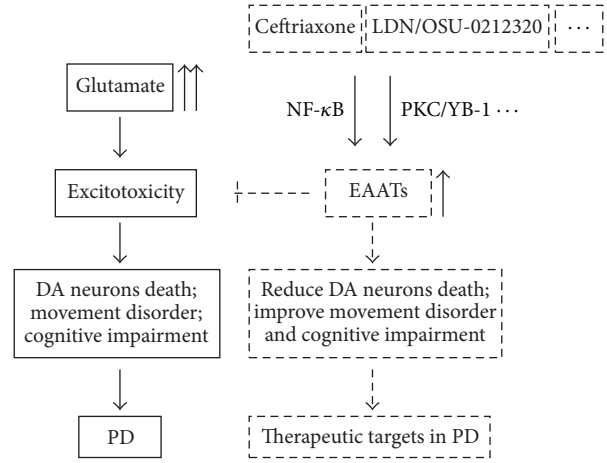

Figure 2: EAATs are therapeutic targets in PD. Excessive glutamate in the synaptic cleft overstimulates glutamate receptors in the postsynaptic membrane and mediates excitotoxicity. Glutamate excitotoxicity can induce the dopamine neurons death, movement disorder, and cognitive impairment, and thus it contributes to the pathogenesis of PD. Through upregulation of EAATs, ceftriaxone, LDN/OSU-0212320, and other drugs can reduce the DA neuron death in SNpc and striatum, improve the movement disorder and cognitive impairment in PD, and thus improve the PD progression. Thus, EAATs are therapeutic targets in PD.

reduction is related to the severity of PD [60]. Generally, dysfunction of glutamate transporters reduces the glutamate uptake, mediates the glutamate excitotoxicity and oxidative stress, damages the DA neurons in substantia nigra, and thus contributes to the pathogenesis of PD. We stated the relationship between EAATs and PD as follows.

3.2.1. GLAST and PD. Some studies reported that GLAST protein expression is significantly decreased in the striatum at 1 week and 2 weeks after 6-hydroxydopamine (6-OHDA) lesion [11, 61]. Besides, GLAST mRNA expression is also decreased in the 6-OHDA lesion rats [41]. Considering that GLAST plays a lesser important role in the glutamate uptake, decreased GLAST expression possibly is a product in the pathogenesis of PD. Salvatore et al. use a novel GLAST inhibitor UCPH-101 ((2-amino-5,6,7,8-tetrahydro-4-(4-methoxyphenyl)-7-naphthalen-1-yl)-5-oxo-4H-chromene-3-carbonitrile) and GLT-1 inhibitor DHK to evaluate the role of GLAST and GLT-1 in PD. They find that GLAST-mediated reuptake component in striatum may be relatively minor, but it can be dramatically promoted when GLT-1 blockade increases extracellular glutamate levels [12]. Moreover, GLAST expression is also shown to be increased in striatum in 6-OHDA lesion rats [62]. As astrocytic GLT-1 is mainly responsible for glutamate reuptake, these studies reveal that GLAST may play a compensatory role when GLT-1 function is impaired in PD.

3.2.2. GLT-1 and PD. As GLT-1 is mainly responsible for the glutamate uptake in the CNS, increasing evidences indicate the role of GLT-1 in PD. Impaired glutamate uptake and reduced GLT-1 expression are found in

PD animal models constructed by 6-OHDA, 1-methyl-4-phenyl-1,2,3,6-tetrahydropyridine (MPTP), and 1-methyl-4-phenylpyridinium (MPP^+) [11–14]. Using GLT-1 inhibitor blocks the glutamate uptake and reduces the expression of phosphorylated tyrosine hydroxylase and the synthesis of DA [12]. Also, DA denervation may trigger modulations in GLT-1 [63]. Thus, these results indicate that GLT-1 dysfunction plays a role in PD progression. To further explore the role of GLT-1 in PD, recently Assous et al. used the inhibitor of glutamate transporter PDC to inject in the unilateral SNpc of rats [16]. They find DA neurons death and axons dystrophy in the SNpc and striatum [16]. When the DA neurons loss exceeds 50%, the motor disorder appears in rats [16]. This study confirms that reduced glutamate uptake using glutamate transporter inhibitor leads to the DA neurons death and progressive parkinsonism symptoms, and this is a solid evidence which supports that reduced expression and function of glutamate transporter are involved in PD.

GLT-1 expression is also found to be increased in response to injury or excitotoxic insult [64, 65]. Besides, Massie et al. find that GLT-1 expression is increased in the striatum at 3 weeks and 12 weeks after 6-OHDA lesion [62]. Chronic inflammation is confirmed to contribute to the pathogenesis of PD [66]; Brothers et al. construct a PD model of chronic inflammation using lipopolysaccharide (LPS) and find reduced tyrosine hydroxylase expression in the substantia nigra and locus coeruleus and also the microglial activation [67]. Meanwhile, chronic inflammation increases extracellular glutamate concentration and GLT-1 expression in the hippocampal CA3 and the dentate gyrus regions [67]. GLT-1 expression and glutamate uptake are found obviously altered in PD models, and some studies report the related regulatory mechanism. Since DA neurons loss is the classical mechanism of PD, Vollbrecht et al. find that partial prefrontal cortex (PFC) dopamine depletion increases GLT-1 protein expression in the membrane and glutamate uptake, but dopamine depletion does not change the expressions of GLAST and EAAC1 [68]. These results suggest that dopamine depletion possibly promotes PFC astrocytic GLT-1 expression and activity via posttranslational modification [68]. It is clear that nuclear factor-κB (NF-κB) could bind with the GLT-1 promoter, and activation of NF-κB signaling pathway is demonstrated to elevate GLT-1 transcription upon ceftriaxone treatment [69]. Our previous *in vitro* study indicates that neurotoxin MPP^+ decreases GLT-1 expression in the membrane and induces astrocytic death via activation of NF-κB/c-Jun N-terminal kinase (JNK)/c-Jun pathway [70].

3.2.3. EAAC1 and PD. As mentioned previously, neuronal glutamate transporter EAAC1 is responsible for the glutamate uptake and cysteine uptake, and the latter is used to synthesize glutathione. As neuronal EAAC1 does not contribute to bulk glutamate uptake in the synaptic cleft, increasing studies focus on the antioxidative effects of EAAC1 in the pathogenesis of PD. EAAC1 deficiency mice show age-dependent loss of DA neurons in the SNpc, and nearly 40% of DA neurons are lost at 12 months' age [71]. Meanwhile, DA neurons loss is accompanied by increased nitrotyrosine formation, nitrosylated α-synuclein, and microglial activation [71]. Moreover, Kinoshita et al. find that cysteine in the mesencephalon is expressed in a diurnal variation manner and is accompanied by the diurnal fluctuations of EAAC1 protein expression [72]. MicroRNA-96-5p can downregulate EAAC1 expression, and intracerebroventricular administration of microRNA-96-5p inhibitor increases the levels of glutathione and EAAC1 expression in the substantia nigra, suggesting that suppressing microRNA-96-5p shows benefit in the progress of PD [72].

However, EAAC1 expression is also reported to be increased in PD patients and models. The *in situ* hybridization results performed by Plaitakis and Shashidharan in the brain in PD patients suggest that EAAC1 expression is increased in DA neurons and EAAC1 has a close correlation with PD [73]. Increased expression and function of EAAC1 are also found in PD animal models [11, 62]. GLT-1 blockade increased EAAC1 expression, suggesting the reciprocal regulation within different EAATs subtypes in PD progression [12]. Besides participating in glutathione homeostasis, the glutamate transported by EAAC1 also contributes to the neuronal metabolism and motor function. EAAC1 may participate in normal GABA neurosynthesis and plays a role in epilepsy [74].

As EAAT4 is limitedly expressed in the Purkinje cells in the cerebellum and EAAT5 is limitedly expressed in the retina, recently there is still lack of evidence on their contributions in PD.

These studies suggest that, in the process of PD, reduced EAATs expression induces the excessive extracellular glutamate and glutamate can damage the DA neurons via overstimulating the ionotropic and metabotropic glutamate receptors, while increased EAATs expression is involved in the compensation mechanism to reduce the glutamate excitotoxicity. The related regulatory mechanism of EAATs in PD still needs further study.

4. EAATs Are Potential Therapeutic Targets in PD

Upregulation of EAATs can weaken the excitotoxic damage to the CNS. Studies have shown that ceftriaxone can improve GLT-1 expression by activation of NF-κB and reduce glutamate concentration in the synaptic cleft [69, 75, 76]. Through upregulation of GLT-1, ceftriaxone can reduce the DA neuron death in the SNpc and striatum and ceftriaxone can also improve the movement disorder and cognitive impairment in PD models (Figure 2) [77–80]. Besides, ceftriaxone can also improve the levodopa-induced dyskinesia via upregulation of GLT-1 [81]. In addition, ATP-sensitive potassium channel (KATP) opener iptakalim (IPT) can enhance the glutamate transporter function in astrocytes and reduce the extracellular glutamate, and thus IPT is also a prospective drug in treatment of PD [82]. The improvement of behavioral disorder and cognitive impairment by ceftriaxone and other drugs is closely linked to EAATs, because EAATs are also reported to participate in modulating learning,

memory, and also motor function in human being and animal models [26–29]. MicroRNAs are a novel type of 19- to 22-nucleotide noncoding RNAs that modulate gene expression primarily at the posttranscriptional level. As stated previously, suppressing microRNA-96-5p can increase the levels of glutathione via promoting EAAC1 expression in PD [72]. Neuronal exosomes containing microRNA-124a and astrocyte-enriched microRNA-181 antagomir can increase GLT-1 expression and show benefit in forebrain ischemia and amyotrophic lateral sclerosis (ALS) animal models [83, 84]. These results suggest that microRNAs targeting EAATs are also possible therapeutic targets in PD. In addition to ceftriaxone, recently compound LDN/OSU-0212320 is also shown to promote GLT-1 expression and activity at the translational level via activation of PKC and subsequent Y-box-binding protein 1 (YB-1) specially [85] (Figure 2). N-acetylcysteine administration restores DA neurons loss, nitrosylated α-synuclein aggregation, and microglial activation in SNpc in EAAC1 deficiency mice [70]. Thus, N-acetylcysteine shows benefit via evaluation of glutathione in treatment of PD. The locomotor impairment is a common symptom in PD progression; Arnold and Salvatore indicate that short-term exercise can attenuate the locomotor impairment in aging rats via increasing nigral glial cell line-derived neurotrophic factor (GDNF) receptor, GFR-α1, and EAAC1 expression in conjunction with increased nigral tyrosine hydroxylase expression [86]. We previously found that ceftriaxone can improve the cell viability, glutamate uptake, and GLT-1 expression in the membrane in neurotoxin MPP^+-treated astrocytes [70]. Furthermore, we explore the related mechanism and we find that, by inhibiting NF-κB/JNK/c-Jun pathway, ceftriaxone enhances the astrocytes viability and attenuates the apoptosis mediated by neurotoxin MPP^+, and ceftriaxone promotes the GLT-1 expression in the membrane and the glutamate uptake and thus reduces the glutamate excitotoxicity effects in MPP^+-treated astrocytes [70].

In this review we indicate the structural and functional characters of EAATs and their distribution in the CNS, we also show that glutamate and other factors can mediate the excitotoxicity in PD, and we point out the related mechanism, respectively. Within these, decreased expression and function of EAATs play a predominant role in the excitotoxic damage in PD. According to previous studies and our work, we show that EAATs are novel therapeutic targets in PD and reveal that the structure, function, and regulation mechanism of EAATs will be a prospective research area in the clinical practice of PD.

Conflict of Interests

The authors declare no conflict of interests regarding the publication of this paper.

Authors' Contribution

Yunlong Zhang and Feng Tan contributed equally to this work.

Acknowledgments

This work was supported by grants from the National Natural Science Foundation of China (31170734 and 31570716), the Science and Technology Planning Project of Guangdong Province (2012B050200003 and 2013B021800305), the Science and Technology Planning Project of Guangzhou (2013J4500018), and the Scientific and Technological Innovation Programs of Higher Education Institution in Guangdong (2013KJCX0041).

References

[1] D. A. Rusakov, L. P. Savtchenko, K. Zheng, and J. M. Henley, "Shaping the synaptic signal: molecular mobility inside and outside the cleft," *Trends in Neurosciences*, vol. 34, no. 7, pp. 359–369, 2011.

[2] D. Shan, S. Yates, R. C. Roberts, and R. E. McCullumsmith, "Update on the neurobiology of schizophrenia: a role for extracellular microdomains," *Minerva Psichiatrica*, vol. 53, no. 3, pp. 233–249, 2012.

[3] P. K. Sonsalla, D. S. Albers, and G. D. Zeevalk, "Role of glutamate in neurodegeneration of dopamine neurons in several animal models of parkinsonism," *Amino Acids*, vol. 14, no. 1–3, pp. 69–74, 1998.

[4] G. E. Meredith, S. Totterdell, M. Beales, and C. K. Meshul, "Impaired glutamate homeostasis and programmed cell death in a chronic MPTP mouse model of Parkinson's disease," *Experimental Neurology*, vol. 219, no. 1, pp. 334–340, 2009.

[5] T. Storck, S. Schulte, K. Hofmann, and W. Stoffel, "Structure, expression, and functional analysis of a Na^+-dependent glutamate/aspartate transporter from rat brain," *Proceedings of the National Academy of Sciences of the United States of America*, vol. 89, no. 22, pp. 10955–10959, 1992.

[6] Y. Kanai and M. A. Hediger, "Primary structure and functional characterization of a high-affinity glutamate transporter," *Nature*, vol. 360, no. 6403, pp. 467–471, 1992.

[7] G. Pines, N. C. Danbolt, M. Bjørås et al., "Cloning and expression of a rat brain L-glutamate transporter," *Nature*, vol. 360, no. 6403, pp. 464–467, 1992.

[8] J. L. Arriza, W. A. Fairman, J. I. Wadiche, G. H. Murdoch, M. P. Kavanaugh, and S. G. Amara, "Functional comparisons of three glutamate transporter subtypes cloned from human motor cortex," *Journal of Neuroscience*, vol. 14, no. 9, pp. 5559–5569, 1994.

[9] W. A. Fairman, R. J. Vandenberg, J. L. Arriza, M. P. Kavanaugh, and S. G. Amara, "An excitatory amino-acid transporter with properties of a ligand-gated chloride channel," *Nature*, vol. 375, no. 6532, pp. 599–603, 1995.

[10] J. L. Arriza, S. Eliasof, M. P. Kavanaugh, and S. G. Amara, "Excitatory amino acid transporter 5, a retinal glutamate transporter coupled to a chloride conductance," *Proceedings of the National Academy of Sciences of the United States of America*, vol. 94, no. 8, pp. 4155–4160, 1997.

[11] E. K. Y. Chung, L. W. Chen, Y. S. Chan, and K. K. L. Yung, "Downregulation of glial glutamate transporters after dopamine denervation in the striatum of 6-hydroxydopamine-lesioned rats," *Journal of Comparative Neurology*, vol. 511, no. 4, pp. 421–437, 2008.

[12] M. F. Salvatore, R. W. Davis, J. C. Arnold, and T. Chotibut, "Transient striatal GLT-1 blockade increases EAAC1 expression, glutamate reuptake, and decreases tyrosine hydroxylase phosphorylation at ser[19]," *Experimental Neurology*, vol. 234, no. 2, pp. 428–436, 2012.

[13] J.-Y. Wu, F.-N. Niu, R. Huang, and Y. Xu, "Enhancement of glutamate uptake in 1-methyl-4-phenylpyridinium-treated astrocytes by trichostatin A," *NeuroReport*, vol. 19, no. 12, pp. 1209–1212, 2008.

[14] H. K. Holmer, M. Keyghobadi, C. Moore, and C. K. Meshul, "L-dopa-induced reversal in striatal glutamate following partial depletion of nigrostriatal dopamine with 1-methyl-4-phenyl-1,2,3,6-tetrahydropyridine," *Neuroscience*, vol. 136, no. 1, pp. 333–341, 2005.

[15] I. Nafia, D. B. Re, F. Masmejean et al., "Preferential vulnerability of mesencephalic dopamine neurons to glutamate transporter dysfunction," *Journal of Neurochemistry*, vol. 105, no. 2, pp. 484–496, 2008.

[16] M. Assous, L. Had-Aissouni, P. Gubellini et al., "Progressive Parkinsonism by acute dysfunction of excitatory amino acid transporters in the rat substantia nigra," *Neurobiology of Disease*, vol. 65, pp. 69–81, 2014.

[17] D. J. Slotboom, W. N. Konings, and J. S. Lolkema, "Structural features of the glutamate transporter family," *Microbiology and Molecular Biology Reviews*, vol. 63, no. 2, pp. 293–307, 1999.

[18] D. Yernool, O. Boudker, Y. Jin, and E. Gouaux, "Structure of a glutamate transporter homologue from *Pyrococcus horikoshii*," *Nature*, vol. 431, no. 7010, pp. 811–818, 2004.

[19] O. Boudker, R. M. Ryan, D. Yernool, K. Shimamoto, and E. Gouaux, "Coupling substrate and ion binding to extracellular gate of a sodium-dependent aspartate transporter," *Nature*, vol. 445, no. 7126, pp. 387–393, 2007.

[20] N. Reyes, C. Ginter, and O. Boudker, "Transport mechanism of a bacterial homologue of glutamate transporters," *Nature*, vol. 462, no. 7275, pp. 880–885, 2009.

[21] G. Verdon and O. Boudker, "Crystal structure of an asymmetric trimer of a bacterial glutamate transporter homolog," *Nature Structural and Molecular Biology*, vol. 19, no. 3, pp. 355–357, 2012.

[22] G. Vendon, S. Oh, R. N. Serio, and O. Boudker, "Coupled ion binding and structural transitions along the transport cycle of glutamate transporters," *eLife*, vol. 3, Article ID e02283, 2014.

[23] C. Murphy-Royal, J. P. Dupuis, J. A. Varela et al., "Surface diffusion of astrocytic glutamate transporters shapes synaptic transmission," *Nature Neuroscience*, vol. 18, no. 2, pp. 219–226, 2015.

[24] A. Scimemi, H. Tian, and J. S. Diamond, "Neuronal transporters regulate glutamate clearance, NMDA receptor activation, and synaptic plasticity in the hippocampus," *Journal of Neuroscience*, vol. 29, no. 46, pp. 14581–14595, 2009.

[25] T. Aida, J. Yoshida, M. Nomura et al., "Astroglial glutamate transporter deficiency increases synaptic excitability and leads to pathological repetitive behaviors in mice," *Neuropsychopharmacology*, vol. 40, no. 7, pp. 1569–1579, 2015.

[26] J. D. Pita-Almenar, S. Zou, C. M. Colbert, and A. Eskin, "Relationship between increase in astrocytic GLT-1 glutamate transport and late-LTP," *Learning and Memory*, vol. 19, no. 12, pp. 615–626, 2012.

[27] X. Qu, C. Xu, H. Wang et al., "Hippocampal glutamate level and glutamate aspartate transporter (GLAST) are up-regulated in senior rat associated with isoflurane-induced spatial learning/memory impairment," *Neurochemical Research*, vol. 38, no. 1, pp. 59–73, 2013.

[28] K. Aoyama, N. Matsumura, M. Watabe, and T. Nakaki, "Oxidative stress on EAAC1 is involved in MPTP-induced glutathione depletion and motor dysfunction," *European Journal of Neuroscience*, vol. 27, no. 1, pp. 20–30, 2008.

[29] K. A. McKeown, R. Moreno, V. L. Hall, A. B. Ribera, and G. B. Downes, "Disruption of Eaat2b, a glutamate transporter, results in abnormal motor behaviors in developing zebrafish," *Developmental Biology*, vol. 362, no. 2, pp. 162–171, 2012.

[30] C. Escartin, S. J. Won, C. Malgorn et al., "Nuclear factor erythroid 2-related factor 2 facilitates neuronal glutathione synthesis by upregulating neuronal excitatory amino acid transporter 3 expression," *Journal of Neuroscience*, vol. 31, no. 20, pp. 7392–7401, 2011.

[31] R. J. Vandenberg and R. M. Ryan, "Mechanisms of glutamate transport," *Physiological Reviews*, vol. 93, no. 4, pp. 1621–1657, 2013.

[32] J. D. Rothstein, M. Dykes-Hoberg, C. A. Pardo et al., "Knockout of glutamate transporters reveals a major role for astroglial transport in excitotoxicity and clearance of glutamate," *Neuron*, vol. 16, no. 3, pp. 675–686, 1996.

[33] Ø. Haugeto, K. Ullensvang, L. M. Levy et al., "Brain glutamate transporter proteins form homomultimers," *The Journal of Biological Chemistry*, vol. 271, no. 44, pp. 27715–27722, 1996.

[34] U. V. Berger, T. M. DeSilva, W. Chen, and P. A. Rosenberg, "Cellular and subcellular mRNA localization of glutamate transporter isoforms GLT1A and GLT1B in rat brain by in situ hybridization," *Journal of Comparative Neurology*, vol. 492, no. 1, pp. 78–89, 2005.

[35] G. T. Petr, Y. Sun, N. M. Frederick et al., "Conditional deletion of the glutamate transporter GLT-1 reveals that astrocytic GLT-1 protects against fatal epilepsy while neuronal GLT-1 contributes significantly to glutamate uptake into synaptosomes," *The Journal of Neuroscience*, vol. 35, no. 13, pp. 5187–5201, 2015.

[36] S. Holmseth, Y. Dehnes, Y. H. Huang et al., "The density of EAAC1 (EAAT3) glutamate transporters expressed by neurons in the mammalian CNS," *Journal of Neuroscience*, vol. 32, no. 17, pp. 6000–6013, 2012.

[37] A. V. Tzingounis and J. I. Wadiche, "Glutamate transporters: confining runaway excitation by shaping synaptic transmission," *Nature Reviews Neuroscience*, vol. 8, no. 12, pp. 935–947, 2007.

[38] A. Dalet, J. Bonsacquet, S. Gaboyard-Niay et al., "Glutamate transporters EAAT4 and EAAT5 are expressed in vestibular hair cells and calyx endings," *PLoS ONE*, vol. 7, no. 9, Article ID e46261, 2012.

[39] V. G. Kucheryanu and G. N. Kryzhanovskii, "Effect of glutamate and antagonists of N-methyl-D-aspartate receptors on experimental parkinsonian syndrome in rats," *Bulletin of Experimental Biology and Medicine*, vol. 130, no. 7, pp. 629–632, 2000.

[40] M. S. Nandhu, J. Paul, K. P. Kuruvila, P. M. Abraham, S. Antony, and C. S. Paulose, "Glutamate and NMDA receptors activation leads to cerebellar dysfunction and impaired motor coordination in unilateral 6-hydroxydopamine lesioned Parkinson's rat: functional recovery with bone marrow cells, serotonin and GABA," *Molecular and Cellular Biochemistry*, vol. 353, no. 1-2, pp. 47–57, 2011.

[41] T. N. Chase, J. D. Oh, and S. Konitsiotis, "Antiparkinsonian and antidyskinetic activity of drugs targeting central glutamatergic mechanisms," *Journal of Neurology*, vol. 247, supplement 2, pp. II36–II42, 2000.

[42] V. Sgambato-Faure and M. A. Cenci, "Glutamatergic mechanisms in the dyskinesias induced by pharmacological dopamine replacement and deep brain stimulation for the treatment of Parkinson's disease," *Progress in Neurobiology*, vol. 96, no. 1, pp. 69–86, 2012.

[43] M. A. Cenci, "Glutamatergic pathways as a target for the treatment of dyskinesias in Parkinson's disease," *Biochemical Society Transactions*, vol. 42, no. 2, pp. 600–604, 2014.

[44] B. G. Garcia, M. D. Neely, and A. Y. Deutch, "Cortical regulation of striatal medium spiny neuron dendritic remodeling in parkinsonism: modulation of glutamate release reverses dopamine depletion-induced dendritic spine loss," *Cerebral Cortex*, vol. 20, no. 10, pp. 2423–2432, 2010.

[45] T. A. Hughes, H. F. Ross, R. H. S. Mindham, and E. G. S. Spokes, "Mortality in Parkinson's disease and its association with dementia and depression," *Acta Neurologica Scandinavica*, vol. 110, no. 2, pp. 118–123, 2004.

[46] I. Leroi, H. Pantula, K. McDonald, and V. Harbishettar, "Neuropsychiatric symptoms in Parkinson's disease with mild cognitive impairment and dementia," *Parkinson's Disease*, vol. 2012, Article ID 308097, 10 pages, 2012.

[47] C. H. Lin, J. W. Lin, Y. C. Liu, C. H. Chang, and R. M. Wu, "Risk of Parkinson's disease following anxiety disorders: a nationwide population-based cohort study," *European Journal of Neurology*, vol. 22, no. 9, pp. 1280–1287, 2015.

[48] Y. S. Oh, J. S. Kim, and P. H. Lee, "Effect of rivastigmine on behavioral and psychiatric symptoms of Parkinson's disease dementia," *Journal of Movement Disorders*, vol. 8, no. 2, pp. 98–102, 2015.

[49] D. J. McCarthy, R. Alexander, M. A. Smith et al., "Glutamate-based depression GBD," *Medical Hypotheses*, vol. 78, no. 5, pp. 675–681, 2012.

[50] E. Berdichevsky, N. Riveros, S. Sánchez-Armáss, and F. Orrego, "Kainate, N-methylaspartate and other excitatory amino acids increase calcium influx into rat brain cortex cells in vitro," *Neuroscience Letters*, vol. 36, no. 1, pp. 75–80, 1983.

[51] D. W. Choi, J. Y. Koh, and S. Peters, "Pharmacology of glutamate neurotoxicity in cortical cell culture: attenuation by NMDA antagonists," *Journal of Neuroscience*, vol. 8, no. 1, pp. 185–196, 1988.

[52] T. Farooqui and A. A. Farooqui, "Aging: an important factor for the pathogenesis of neurodegenerative diseases," *Mechanisms of Ageing and Development*, vol. 130, no. 4, pp. 203–215, 2009.

[53] G. Ambrosi, S. Cerri, and F. Blandini, "A further update on the role of excitotoxicity in the pathogenesis of Parkinson's disease," *Journal of Neural Transmission*, vol. 121, no. 8, pp. 849–859, 2014.

[54] F. Gardoni and M. Di Luca, "Targeting glutamatergic synapses in Parkinson's disease," *Current Opinion in Pharmacology*, vol. 20, pp. 24–28, 2015.

[55] A. Mehta, M. Prabhakar, P. Kumar, R. Deshmukh, and P. L. Sharma, "Excitotoxicity: bridge to various triggers in neurodegenerative disorders," *European Journal of Pharmacology*, vol. 698, no. 1–3, pp. 6–18, 2013.

[56] L. Navarria, M. Zaltieri, F. Longhena et al., "Alpha-synuclein modulates NR2B-containing NMDA receptors and decreases their levels after rotenone exposure," *Neurochemistry International*, vol. 85-86, pp. 14–23, 2015.

[57] J.-P. Pin, T. Galvez, and L. Prézeau, "Evolution, structure, and activation mechanism of family 3/C G-protein-coupled receptors," *Pharmacology and Therapeutics*, vol. 98, no. 3, pp. 325–354, 2003.

[58] E. Hermans and R. A. J. Challiss, "Structural, signalling and regulatory properties of the group I metabotropic glutamate receptors: prototypic family C G-protein-coupled receptors," *Biochemical Journal*, vol. 359, no. 3, pp. 465–484, 2001.

[59] M. Nandhu, J. Paul, K. P. Kuruvilla, A. Malat, C. Romeo, and C. S. Paulose, "Enhanced glutamate, IP3 and cAMP activity in the cerebral cortex of unilateral 6-hydroxydopamine induced Parkinson's rats: effect of 5-HT, GABA and bone marrow cell supplementation," *Journal of Biomedical Science*, vol. 18, no. 1, article 5, 2011.

[60] C. Ferrarese, L. Tremolizzo, M. Rigoldi et al., "Decreased platelet glutamate uptake and genetic risk factors in patients with Parkinson's disease," *Neurological Sciences*, vol. 22, no. 1, pp. 65–66, 2001.

[61] A. El Arfani, G. Albertini, E. Bentea et al., "Alterations in the motor cortical and striatal glutamatergic system and d-serine levels in the bilateral 6-hydroxydopamine rat model for Parkinson's disease," *Neurochemistry International*, vol. 88, pp. 88–96, 2015.

[62] A. Massie, S. Goursaud, A. Schallier et al., "Time-dependent changes in GLT-1 functioning in striatum of hemi-Parkinson rats," *Neurochemistry International*, vol. 57, no. 5, pp. 572–578, 2010.

[63] A. G. Dervan, C. K. Meshul, M. Beales et al., "Astroglial plasticity and glutamate function in a chronic mouse model of Parkinson's disease," *Experimental Neurology*, vol. 190, no. 1, pp. 145–156, 2004.

[64] B. D. Schlag, J. R. Vondrasek, M. Munir et al., "Regulation of the glial Na+-dependent glutamate transporters by cyclic AMP analogs and neurons," *Molecular Pharmacology*, vol. 53, no. 3, pp. 355–369, 1998.

[65] G. Tian, L. Lai, H. Guo et al., "Translational control of glial glutamate transporter EAAT2 expression," *The Journal of Biological Chemistry*, vol. 282, no. 3, pp. 1727–1737, 2007.

[66] J. Yan, Q. Fu, L. Cheng et al., "Inflammatory response in Parkinson's disease (Review)," *Molecular Medicine Reports*, vol. 10, no. 5, pp. 2223–2233, 2014.

[67] H. M. Brothers, I. Bardou, S. C. Hopp et al., "Time-dependent compensatory responses to chronic neuroinflammation in hippocampus and brainstem: the potential role of glutamate neurotransmission," *Journal of Alzheimer's Disease & Parkinsonism*, vol. 3, article 110, 2013.

[68] P. J. Vollbrecht, L. D. Simmler, R. D. Blakely, and A. Y. Deutch, "Dopamine denervation of the prefrontal cortex increases expression of the astrocytic glutamate transporter GLT-1," *Journal of Neurochemistry*, vol. 130, no. 1, pp. 109–114, 2014.

[69] S.-G. Lee, Z.-Z. Su, L. Emdad et al., "Mechanism of ceftriaxone induction of excitatory amino acid transporter-2 expression and glutamate uptake in primary human astrocytes," *The Journal of Biological Chemistry*, vol. 283, no. 19, pp. 13116–13123, 2008.

[70] Y. Zhang, X. Zhang, and S. Qu, "Ceftriaxone protects astrocytes from MPP^+ via suppression of NF-κB/JNK/c-Jun signaling," *Molecular Neurobiology*, vol. 52, no. 1, pp. 78–92, 2015.

[71] A. E. Berman, W. Y. Chan, A. M. Brennan et al., "N-acetylcysteine prevents loss of dopaminergic neurons in the EAAC1$^{-/-}$ mouse," *Annals of Neurology*, vol. 69, no. 3, pp. 509–520, 2011.

[72] C. Kinoshita, K. Aoyama, N. Matsumura, K. Kikuchi-Utsumi, M. Watabe, and T. Nakaki, "Rhythmic oscillations of the microRNA miR-96-5p play a neuroprotective role by indirectly regulating glutathione levels," *Nature Communications*, vol. 5, article 3823, 2014.

[73] A. Plaitakis and P. Shashidharan, "Glutamate transport and metabolism in dopaminergic neurons of substantia nigra: implications for the pathogenesis of Parkinson's disease," *Journal of Neurology*, vol. 247, supplement 2, pp. II25–II35, 2000.

[74] J. P. Sepkuty, A. S. Cohen, C. Eccles et al., "A neuronal glutamate transporter contributes to neurotransmitter GABA synthesis and epilepsy," *The Journal of Neuroscience*, vol. 22, no. 15, pp. 6372–6379, 2002.

[75] J. D. Rothstein, S. Patel, M. R. Regan et al., "β-Lactam antibiotics offer neuroprotection by increasing glutamate transporter expression," *Nature*, vol. 433, no. 7021, pp. 73–77, 2005.

[76] J. E. Kelsey and C. Neville, "The effects of the β-lactam antibiotic, ceftriaxone, on forepaw stepping and l-DOPA-induced dyskinesia in a rodent model of Parkinson's disease," *Psychopharmacology*, vol. 231, no. 12, pp. 2405–2415, 2014.

[77] T. C. H. Leung, C. N. P. Lui, L. W. Chen, W. H. Yung, Y. S. Chan, and K. K. L. Yung, "Ceftriaxone ameliorates motor deficits and protects dopaminergic neurons in 6-hydroxydopamine-lesioned rats," *ACS Chemical Neuroscience*, vol. 3, no. 1, pp. 22–30, 2012.

[78] T. Chotibut, R. W. Davis, J. C. Arnold et al., "Ceftriaxone increases glutamate uptake and reduces striatal tyrosine hydroxylase loss in 6-OHDA Parkinson's model," *Molecular Neurobiology*, vol. 49, no. 3, pp. 1282–1292, 2014.

[79] S.-C. Ho, C.-C. Hsu, C. R. Pawlak et al., "Effects of ceftriaxone on the behavioral and neuronal changes in an MPTP-induced Parkinson's disease rat model," *Behavioural Brain Research*, vol. 268, pp. 177–184, 2014.

[80] C.-Y. Hsu, C.-S. Hung, H.-M. Chang, W.-C. Liao, S.-C. Ho, and Y.-J. Ho, "Ceftriaxone prevents and reverses behavioral and neuronal deficits in an MPTP-induced animal model of Parkinson's disease dementia," *Neuropharmacology*, vol. 91, pp. 43–56, 2015.

[81] J. E. Kelsey and C. Neville, "The effects of the β-lactam antibiotic, ceftriaxone, on forepaw stepping and l-DOPA-induced dyskinesia in a rodent model of Parkinson's disease," *Psychopharmacology*, vol. 231, no. 12, pp. 2405–2415, 2014.

[82] X.-L. Sun, X.-N. Zeng, F. Zhou, C.-P. Dai, J.-H. Ding, and G. Hu, "KATP channel openers facilitate glutamate uptake by GluTs in rat primary cultured astrocytes," *Neuropsychopharmacology*, vol. 33, no. 6, pp. 1336–1342, 2008.

[83] Y.-B. Ouyang, L. Xu, S. Liu, and R. G. Giffard, "Role of astrocytes in delayed neuronal death: GLT-1 and its novel regulation by MicroRNAs," in *Glutamate and ATP at the Interface of Metabolism and Signaling in the Brain*, vol. 11 of *Advances in Neurobiology*, pp. 171–188, Springer, Basel, Switzerland, 2014.

[84] J.-M. Moon, L. Xu, and R. G. Giffard, "Inhibition of microRNA-181 reduces forebrain ischemia-induced neuronal loss," *Journal of Cerebral Blood Flow and Metabolism*, vol. 33, no. 12, pp. 1976–1982, 2013.

[85] Q. Kong, L.-C. Chang, K. Takahashi et al., "Small-molecule activator of glutamate transporter EAAT2 translation provides neuroprotection," *The Journal of Clinical Investigation*, vol. 124, no. 3, pp. 1255–1267, 2014.

[86] J. C. Arnold and M. F. Salvatore, "Exercise-mediated increase in nigral tyrosine hydroxylase is accompanied by increased nigral GFR-α1 and EAAC1 expression in aging rats," *ACS ChemicalNeuroscience*, 2015.

Hindawi Publishing Corporation
Neural Plasticity
Volume 2016, Article ID 4129015, 12 pages
http://dx.doi.org/10.1155/2016/4129015

Research Article

Anger Emotional Stress Influences VEGF/VEGFR2 and Its Induced PI3K/AKT/mTOR Signaling Pathway

Peng Sun,[1] Sheng Wei,[2] Xia Wei,[3] Jieqiong Wang,[1] Yuanyuan Zhang,[1] Mingqi Qiao,[4] and Jibiao Wu[4]

[1]*College of Pharmacy, Shandong University of Traditional Chinese Medicine, Jinan, Shandong 250355, China*
[2]*Experiment Center, Shandong University of Traditional Chinese Medicine, Jinan, Shandong 250355, China*
[3]*Technical Office of Pharmacology, Shandong Institute for Food and Drug Control, Jinan 250351, China*
[4]*School of Preclinical Medicine, Shandong University of Traditional Chinese Medicine, Jinan, Shandong 250355, China*

Correspondence should be addressed to Mingqi Qiao; qmingqi@163.com and Jibiao Wu; wujibiao1963@163.com

Received 30 October 2015; Revised 6 January 2016; Accepted 11 January 2016

Academic Editor: Alexei Verkhratsky

Objective. We discuss the influence of anger emotional stress upon VEGF/VEGFR2 and its induced PI3K/AKT/mTOR signal pathway. *Methods.* We created a rat model of induced anger (anger-out and anger-in) emotional response using social isolation and resident-intruder paradigms and assessed changes in hippocampus' VEGF content, neuroplasticity, and the PI3K/AKT/mTOR signaling pathway. *Results.* The resident-intruder method successfully generated anger-out and anger-in models that differed significantly in composite aggression score, aggression incubation, open field behavior, sucrose preference, and weight gain. Anger emotional stress decreased synaptic connections and VEGFR2 expression. Anger emotional stress led to abnormal expression of VEGF/VEGFR2 mRNA and protein and disorderly expression of key factors in the PI3K/AKT/mTOR signal pathway. Fluoxetine administration ameliorated behavioral abnormalities and damage to hippocampal neurons caused by anger emotional stress, as well as abnormal expression of some proteins in VEGF/VEGFR2 and its induced PI3K/AKT/mTOR signal pathway. *Conclusion.* This research provides a detailed classification of anger emotion and verifies its influence upon VEGF and the VEGF-induced signaling pathway, thus providing circumstantial evidence of mechanisms by which anger emotion damages neurogenesis. As VEGFR2 can promote neurogenesis and vasculogenesis in the hippocampus and frontal lobe, these results suggest that anger emotional stress can result in decreased neurogenesis.

1. Introduction

Research has shown that anger is one of the negative, most influential emotional responses in interpersonal relationships and social harmony; it is also the most stressful response and is comorbid with pathogenesis. Anger is closely linked with cardiovascular and cerebrovascular diseases, digestive system diseases, and cancer, as well as psychological disorders and related behaviors, such as depression and suicide. As anger serves as a disease-inducing factor, it is important to study the biological foundation of this emotion [1, 2].

At present, the state of research on the biological mechanism of anger emotion is relatively limited. As the core expression of anger, aggressive behavior has been used as a measure of anger across the literature. The substrate of aggressive action is a physiological cascade that involves GABA and 5-HT, as well as neurosteroids [3–5]. This results in overactivation of the amygdaloid nucleus, which is in charge of impulse control, causing the prefrontal cortex to malfunction [6–11]. Hormones also play an important role in human aggression. Moderate levels of progesterone, high levels of testosterone, and a lowered level of corticosterone appear to be key factors mediating aggressiveness [12–16]. Furthermore, allosteric modification of $GABA_AR$ is closely related to aggressive behavior. Moderate levels of allopregnanolone, high levels of androstenediol, and a positive endogenous modifier of $GABA_AR$ can increase aggressiveness [17–20]. Decreased 5-HT can also lead to aggressive behavior. Decreased expression of $5\text{-}HT_{1A}$ receptors in

the prefrontal cortex and increased raphe nucleus density are also relevant to aggression [21].

Contemporary research focuses on the cellular and molecular foundation of mental diseases on trophic factors, with relevant cell types covering neurons and endothelial cells. These cells, with highly varied functions, interact with each other through common signaling molecules. Disorders of cell signaling pathways can influence cerebral function and behavioral expression. Multifunction trophic factors, such as vascular endothelial growth factor (VEGF), can ameliorate defects in vessel and nerve growth to affect emotional expression and psychodynamic cognition processes. Understanding the behavior and cellular and molecular function of multifunction trophic factors like VEGF may elucidate novel therapeutic targets [22]. VEGF also promotes angiogenesis, vascular endothelial growth, and vascular permeability.

In recent years, VEGF has been found to promote hippocampal neuron growth. Research has confirmed that this VEGF-induced stimulation of neurogenesis plays an important role in neuropsychological diseases and stress responses. VEGF participates in the stress response to relevant diseases, particularly depression, and it also plays a role in the activity of antidepression drugs through serotonin selective reuptake inhibitor (SSRI) and interacts with the 5-HT system [23]. We predict that VEGF may participate in the expression of anger emotion caused by a psychological stress response. We investigated the influence of this process on VEGF and the possible regulating mechanisms. An understanding of the influence of anger emotion stress response abnormality upon VEGF and its regulating processes may inform the biological foundation of anger emotion.

The current research was designed to create rat models of anger-out and anger-in expression induced by the resident-intruder paradigm. By measuring the compound influence of stress response and fluoxetine intervention upon aggressive behavior, open field behavior, and sucrose preference level, the behavioral features of anger-out and anger-in rats with different responses induced by the resident-intruder paradigm were revealed. We used electron microscopy to observe the microstructure of hippocampal synapse of model rats and explore the influence of anger emotional stress upon the microstructure morphology of hippocampus; immunofluorescent staining was used to further probe the influence of anger emotional stress upon neuron expression of VEGFR2. Real-time PCR and Western blot assays were used to analyze mRNA and protein expression of hippocampal VEGF and VEGFR2, as well as the signal pathway changes of PI3K/AKT/mTOR induced by VEGFR2, in order to explore relevant biological foundation of VEGF in anger emotional stress expression. Our research further revealed the function of VEGF, with anger as the chronic psychological stress damage disease-inducing factor, and the function of VEGF and the relevant signal pathway in relation to psychological stress damage. Taken together, these results may provide a scientific foundation for researching and developing intervening drugs for treating anger-related pathology.

2. Materials and Methods

2.1. Experiment Animals and Drugs. SPF-grade healthy Wistar rats, weighing 250–270 g, and SD rats, weighing 180–200 g, were used (production permit number SCXK (Beijing) 2012-0001, Beijing Vital River Experiment Animal Co., Ltd.). Wistar rats were used as experimental animals and were randomly divided into groups. SD male rats were designated as intruders, eliciting the emotion and behavior of experiment rats. Each group of experimental rats was weighed at key time points during the study to assess weight gain.

Laboratory animals were provided by the *Laboratory Animal Center of Shandong Traditional Chinese Medicine University* (license number: SCXK (LU) 2011-0003). Laboratory animals were cared for according to "The Care and Use of Laboratory Animals" by the *Laboratory Animal Center of Shandong Traditional Chinese Medicine University*.

Fluoxetine capsules were used (Suzhou Chung-Hwa Pharmaceutical Co., Ltd., approval number: 53513004). Based on clinical equivalence conversion, an intragastric dose of 0.267 mg/100 g/d was administered to rats according to product manual.

2.2. Macro Behavioral Experiment

2.2.1. Open Field Test. An open field test chamber, made of opaque materials and measuring 100 cm × 100 cm × 40 cm, was used. The inside wall and floor were gray, and the bottom was divided into 25 equal zones. The entire field was recorded from above using a camera. During the test, each rat was gently placed into the middle grid of the open field chamber, and its general movement path during 3 min was recorded (Panlab Smart-15 software). The experiment was conducted in a quiet environment. To account for circadian movement changes, all studies were conducted at the same time of day. Before each experiment, ethyl alcohol was used to clean the floor of the chamber [24, 25].

2.2.2. Sucrose Preference Experiment. The sucrose preference experiment [26, 27] included 48 h sucrose drinking training and 1 h test after 24 h of training. 48 h before the experiment, rats were habituated to drinking water with sucrose. Two bottles of water, with equivalent weights, were given to animals, one containing 1% sucrose solution and the other containing common tap water. Every 12 h, the position of the two bottles was shifted so as to avoid the positional effect of rats in drinking behavior. After the training, rats were provided with tap water for 6 h. After 18 h of providing no water or food, each rat was given two bottles of water (one containing 1% sucrose solution and the other containing common tap water) for them to drink for 1 h. Consumption of each liquid was calculated from the weights of the bottles. Sucrose preference was calculated as follows: sucrose preference rate = sucrose consumption (g)/[sucrose consumption (g) + water consumption (g)] × 100%.

2.2.3. Resident-Intruder Anger Emotional Stress Model and Its Subtype. Animals were placed on a reverse light cycle to habituate to the environment for one week and bred in isolation for one more week. Then, they were sent into the

Table 1: Primers and probes which were used in real-time PCR.

Primer ID	Sequence
VEGFR2-forward	5′-CCA CAT GGT CTC TCT GGT TG-3′
VEGFR2-reverse	5′-GGA GGG TTG GCA TAG ACT GT-3′
VEGFR2-probe	5′-TGG CAC CAT GCA GAC GCT GA-3′
VEGF-forward	5′-TAT CTT CAA GCC GTC CTG TG-3′
VEGF-reverse	5′-GAT CCG CAT GAT CTG CAT AG-3′
VEGF-probe	5′-ATC ATT GCA GCA GCC CGC AC-3′
GADPH-forward	5′-GTT ACC AGG GCT GCC TTC TC-3′
GADPH-reverse	5′-GGG TTT CCC GTT GAT GAC C-3′
GADPH-probe	5′-AAC GGC ACA GTC AAG GCT GAG AAT G-3′

resident-intruder experiment. After one week in resident-intruder experiment, the score of composite aggressive behavior was calculated. Experimental rats were divided into two groups based on the median method as follows: High Aggressive (HA) described the anger-out group, while Low Aggressive (LA) described the anger-in group [28]. Composite aggression was calculated using the following formula: composite aggression = [(number of attacks) + 0.2 × (attack duration) + (number of bites) + 0.2 × (on-top duration) + (piloerection)].

2.3. Transmission Electron Microscopy (TEM). On the day following drug administration, 40 mg/kg pentobarbital sodium (Sigma-Aldrich) was used for intraperitoneal anesthesia. The specific steps were as follows: opened the chest to expose the heart, inserted the tube through ascending aorta of the left ventricle, and then used scissors to cut open the auricula dextra; used precooled 0.9% NaCl solution (provided by Qilu Hospital, Jinan) followed by 4°C 4% paraformaldehyde, 0.1 mol/L PBS (Beyotime Institute of Biotechnology, pH7.4) for perfusion, then opened the skull after hardening to take out the cerebral tissues to be fixed with 2.5% glutaraldehyde (Sigma-Aldrich). In reference to the stereotaxic atlas of brain, took 3 parts of brain tissues, measuring 2 mm × 2 mm × 2 mm, out of hippocampus to be rinsed 8 times for a duration of 48 h with 0.1 M phosphate buffer; used 2% osmic acid (Sigma-Aldrich) to fix for 1.5 h and rinsed with PBS 5 times; dehydrated with 50%, 70%, 80%, 90%, 95%, and 100% acetone I for 10 min and with 100% acetone II and III for 40 min, respectively; used 812 epoxy resin and acetone (Sigma-Aldrich) 1 : 1 mixed liquor for embedding and saturation for 1.5 h. Pure resin was embedded and polymerized for 3 h at room temperature, 12 h at 37°C, 12 h at 45°C, and 48 h at 60°C; trimmed the embedding end; sliced and double stained with uranium lead; and then observed [29] them under TEM (JEOL, JEM-1400).

2.4. Fluorescent Immunohistochemistry. Sections of hippocampus and frontal lobes were selected based on the stereotaxic atlas of the rat brain. The distribution of VEGFR2 in lobes and hippocampal brains was observed with a laser scanning confocal microscope (LSM510, ZEISS, Germany). Three different angles were chosen from each target brain area in each slice for imaging [30, 31]. The primary antibody used was anti-VEGFR2 (Abcam, ab131441, dilution ratio: 1 : 1000), and the secondary antibody was IgG marked with FITC (Wuhan Boster Biological Engineering Co., Ltd., BA1105, dilution ratio: 1 : 50).

Table 2: Primary antibodies which were used in Western blotting.

Antibody	Supplier	Cat. number	Dilution ratio
anti-PI3K	Cell Signaling Technology	#4257	1 : 1000
anti-pPI3K	Cell Signaling Technology	#4228	1 : 500
anti-pAKT	Cell Signaling Technology	#4060	1 : 1000
anti-AKT	Cell Signaling Technology	#4691	1 : 1000
anti-pmTOR	Cell Signaling Technology	#5536	1 : 1000
anti-mTOR	Cell Signaling Technology	#2983	1 : 1000

2.5. Real-Time qPCR. After the splitting decomposition of samples, total RNAs (RNA Lyzol, Shanghai ExCell Biology Co., Ltd., MB000-0012) were extracted and reverse transcription (Thermo Scientific RevertAid First Strand cDNA Synthesis Kit, Thermo Scientific Co., Ltd., K1622) was performed according to the manufacturer's instructions. The prepared cDNA samples were used for fluorescent quantification via RT-PCR (Real-time PCR Master Mix, Toyobo Co., Ltd., QPK-101T). There were 3 duplication wells for each sample; 7500 Fast system software was used for analysis [32]. The primer and sequence used were as shown in Table 1.

2.6. Western Blotting. The Western blotting experiment was conducted according to standard procedures [33]. The primary antibodies used and their dilution ratios are shown in Table 2. The second antibody was horseradish peroxidase- (HRP-) conjugated goat anti-mouse IgG (Jackson ImmunoResearch, 115-035-166) or HRP-conjugated goat anti-rabbit IgG (Jackson ImmunoResearch, 111-035-144), with a dilution ratio of 1 : 5000.

2.7. Statistics. All data were analyzed with GraphPad Prism 5 statistical software and are shown as mean ± SEM. One-way ANOVA was used for analysis and processing, and $P < 0.05$ indicated statistical significance.

3. Results

3.1. Anger-Out and Anger-In Stress Rat Modeling and Behavior Evaluation. We mainly referred to the anger stress model

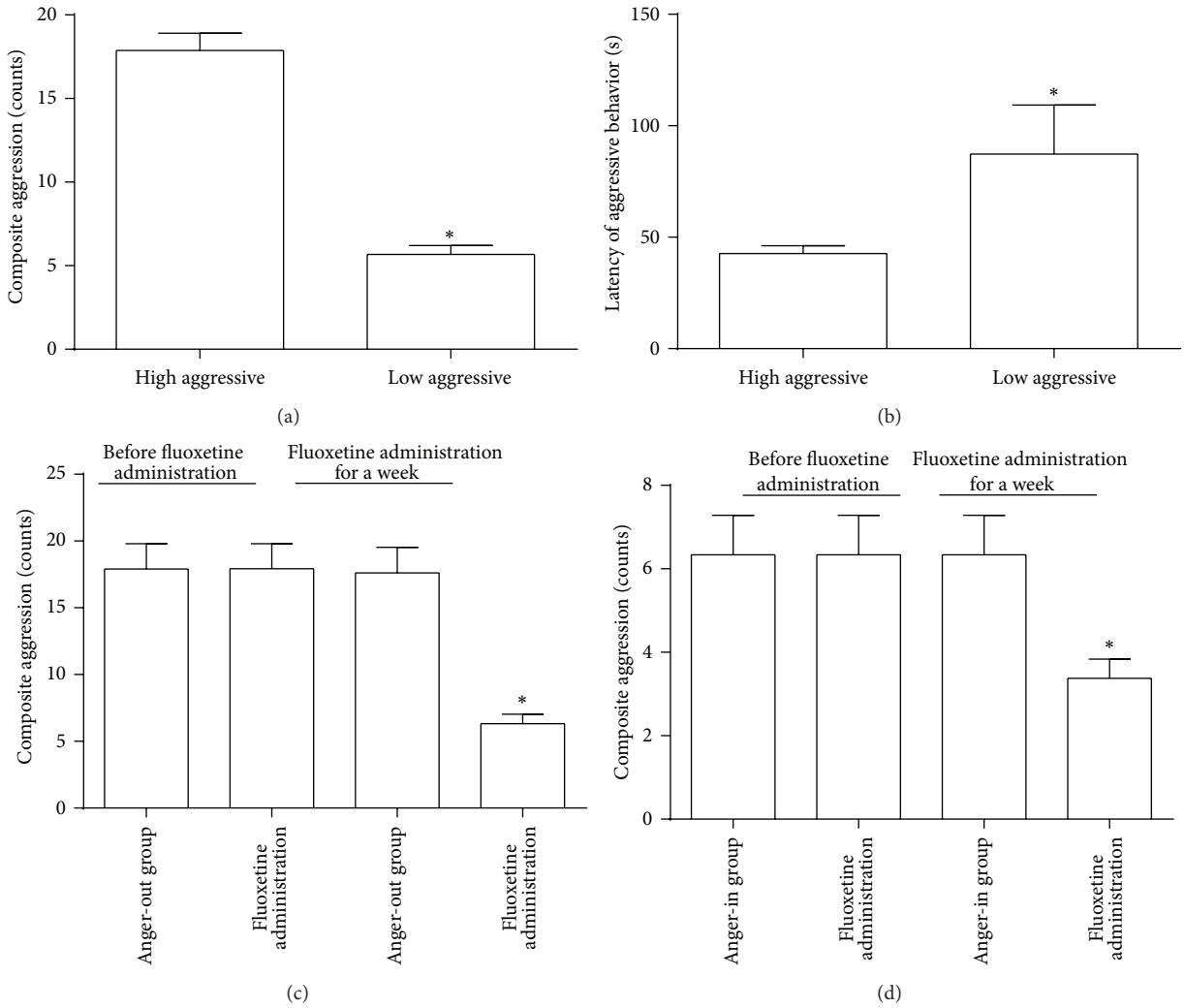

Figure 1: (a) Composite aggression scores of HA group and LA group ($n = 36$, $^{*}P < 0.05$). (b) Latency of aggressive behavior of HA group and LA group ($n = 36$, $^{*}P < 0.05$). (c) Composite aggression scores of anger-out group before and after fluoxetine administration ($n = 12$, $^{*}P < 0.05$). (d) Composite aggression scores of anger-in group before and after fluoxetine administration ($n = 12$, $^{*}P < 0.05$).

based on resident-intruder paradigm out of territory awareness proposed by Prof. Sieste F. de Boer. After one week in the resident-intruder mode, the scores of composite aggression were tested and calculated, and the resident rats were divided into two groups according to the median method. HA rats were assigned to the anger-out group (Figure 1(a)) and LA rats were assigned to the anger-in group (Figure 1(a)). We also measured the latency of aggression. The HA group showed shorter latency (Figure 1(b)) and the LA group showed longer latency (Figure 1(b)). Division into HA and LA groups based on the median method of composite aggression score was practically feasible.

We randomly divided the anger-out group, namely, the HA group, into two groups, including anger-out model group and anger-out model group with administration of fluoxetine (Figure 1(c)). We also divided the anger-in group into two groups randomly, namely, anger-in model group and anger-in model group with administration of fluoxetine (Figure 1(d)). It has been shown that fluoxetine can effectively ease depression, anxiety, and anger emotions induced by various factors, so fluoxetine serves as an important tool in studying anger emotion model. After one week of drug administration, fluoxetine was able to effectively cut down the aggression scores of both anger-out and anger-in groups (Figures 1(c) and 1(d)).

Before model making, we tested the body weights for all groups as the baseline. The body weights were statistically the same among groups. At key times in modeling, we analyzed weight gain. After one week in the resident-intruder mode, the added weight of each group (including model group and group of fluoxetine administration) significantly decreased when compared with the control group (Figures 2(a) and 2(c)). After one week of drug administration, the added weight of model group still decreased when compared with the control group. Meanwhile, the added weight of the group with drug administration had returned to the level of the control group (Figures 2(b) and 2(d)). It is worth noting that, after one week in the resident-intruder mode, although we

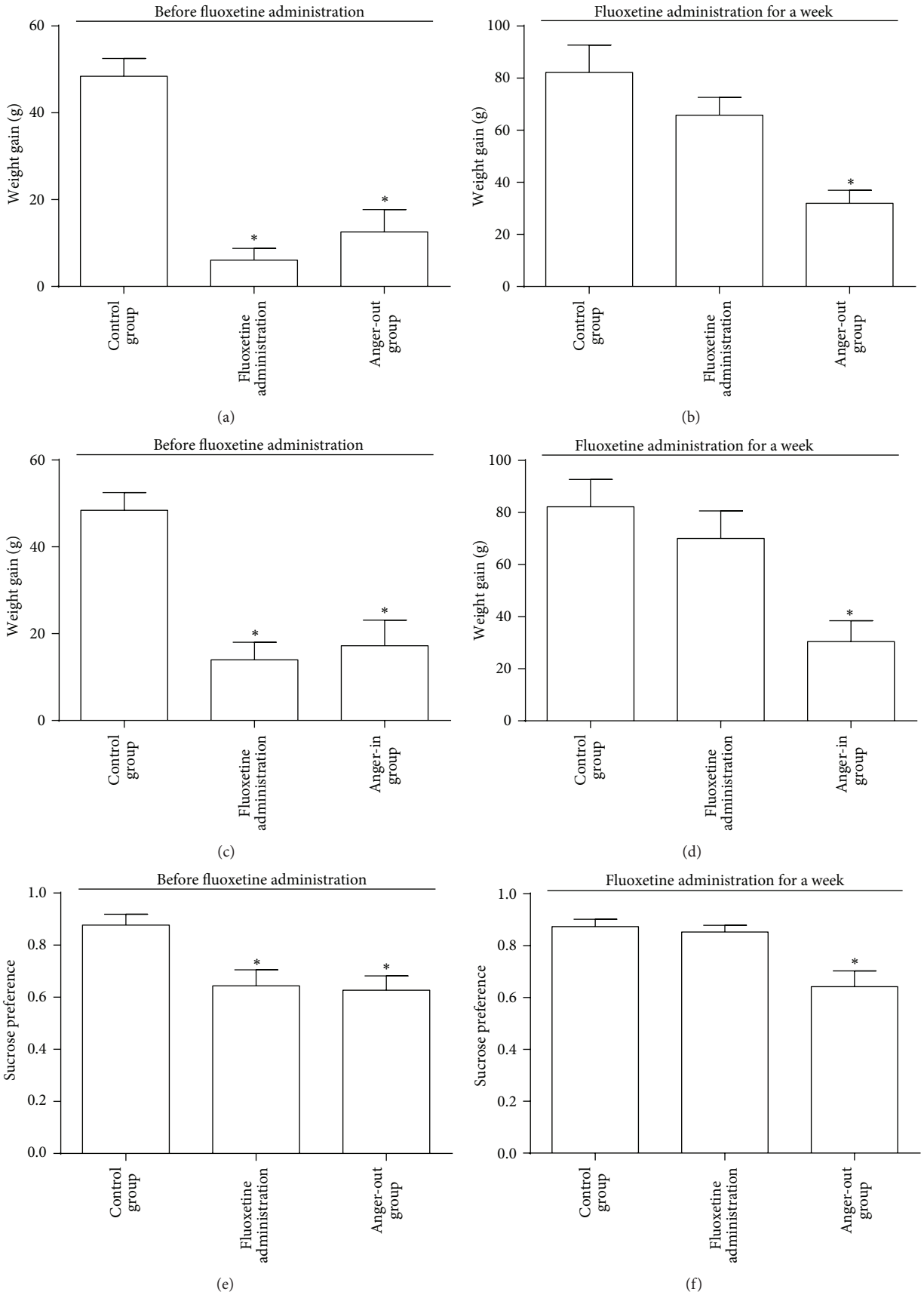

Figure 2: Continued.

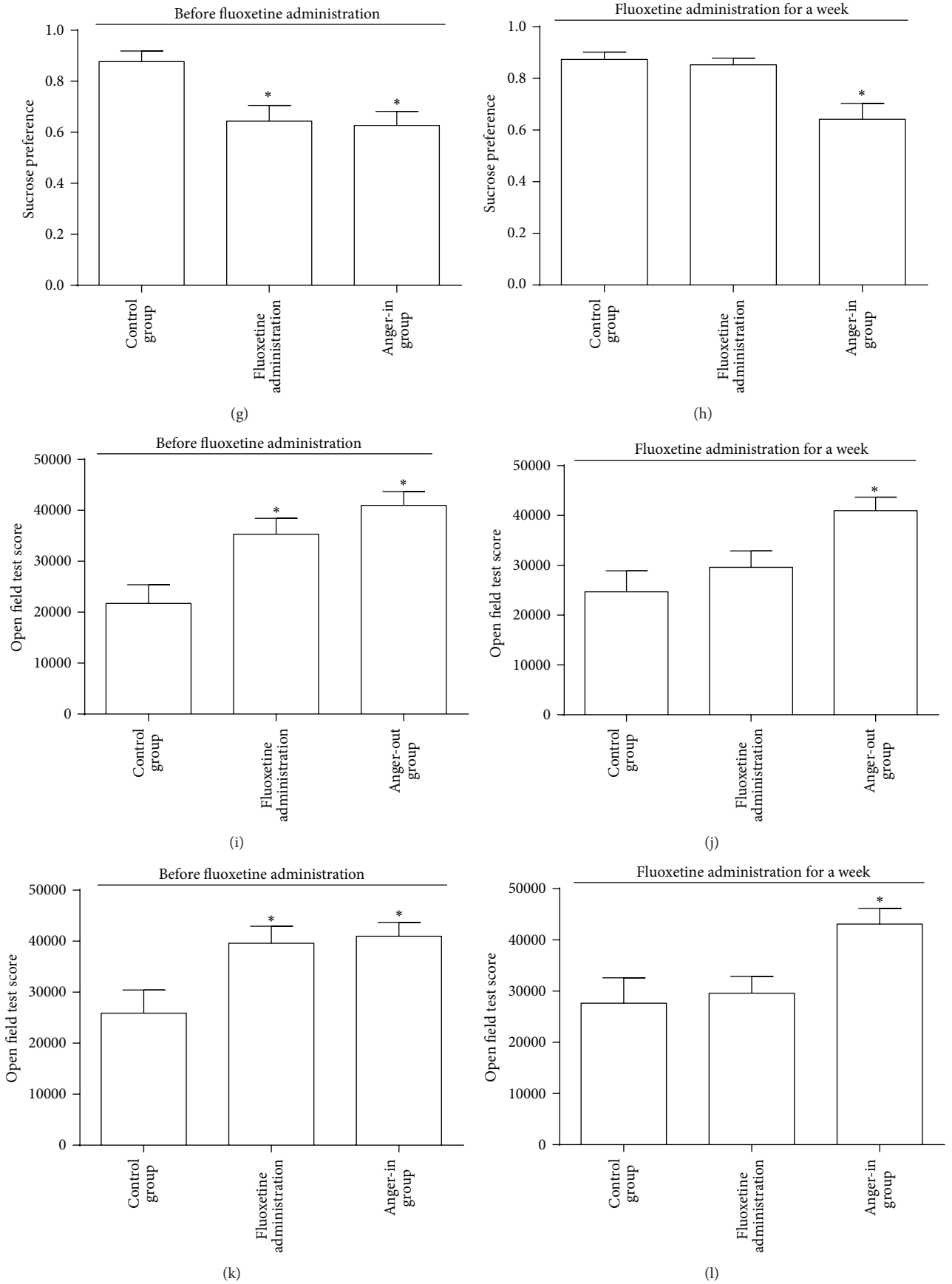

FIGURE 2: Quantitative analysis ($n = 12$) in weight gain (a, b, c, d), sucrose preference (e, f, g, h), and open field test (i, j, k, l) of anger-out (a, b, e, f, i, j) and anger-in (c, d, g, h, k, l) groups before (a, c, e, g, i, k) and after (b, d, f, h, j, l) fluoxetine administration ($^*P < 0.05$).

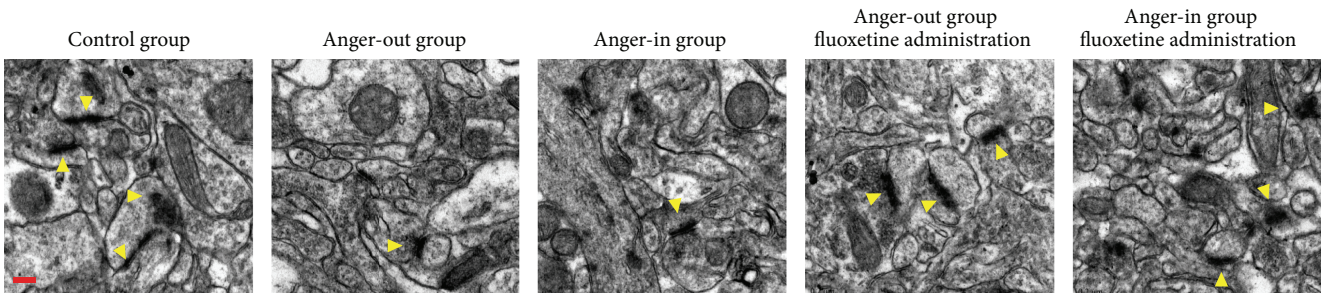

Figure 3: Synaptic ultrastructure in hippocampal CA3 of control, anger-out, anger-in, fluoxetine treated anger-out, and fluoxetine treated anger-in groups. Arrow heads were used to highlight synapses. Scale bar: 0.2 μm.

conducted statistics and analysis of the weight gains of each group, drug had not been administered. In other words, after two weeks in the resident-intruder mode, the group with drug administration had only received the drug for one week.

We also conducted the sucrose preference test and open field test. The results of the sucrose preference experiment showed that after one week in the resident-intruder mode the sucrose preference level of each group dropped significantly (Figures 2(e) and 2(g)); after one week of drug administration, the sucrose preference level of the model group registered a significant decrease when compared with the control group, while the group with drug administration returned to the level of the control group (Figures 2(f) and 2(h)). On the other hand, open field test results showed that after one week in the resident-intruder mode the open field score for each group increased significantly (Figures 2(i) and 2(k)); after one week of drug administration, the open field score of the model group improved when compared with the control group, while the group with drug administration returned to the level of the control group (Figures 2(j) and 2(l)).

3.2. Influence of Anger Stress upon the Microstructure of Hippocampal Synapse of Rats as well as the Distribution and Number of VEGFR2 Positive Cells in Hippocampus and Lobe. Hippocampal neurons in the control group were complete and clear in structure, with structurally complete mitochondria, clear mitochondria ridge, full and rich postsynaptic density, and clearly visible synaptic vesicles, as well as increasing synaptic connections (Figure 3). Mitochondrial structure in the model group was normal, with spindle-shaped neurons, increased ribosomes, and decreased numbers of other cells, as well as decreased synaptic connections. Administration of fluoxetine was able to improve these deficits to some extent (Figure 3).

Immunofluorescence results showed that there were a large number of VEGFR2 positive cells in the hippocampus and CA3 area, with closely arrayed pyramidal cells (Figure 4). In addition, the number of VEGFR2 positive cells in the hippocampus and CA3 area of rats subjected to the resident-intruder paradigm decreased, with loose array and irregularity (Figure 4). Moreover, both anger-in and anger-out groups exhibited decreased number of VEGFR2 positive cells. These deficits were attenuated after administration of fluoxetine (Figure 4).

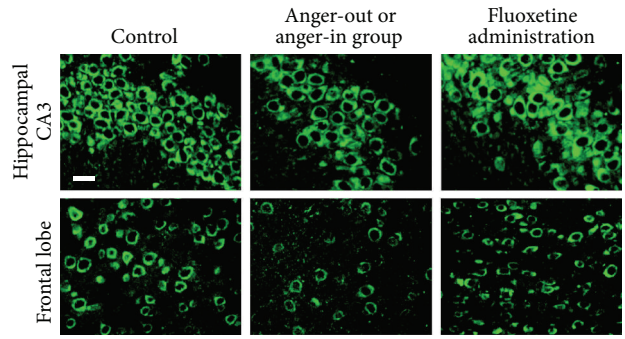

Figure 4: Hippocampal CA3 and frontal lobe (of control, anger-in/anger-out, and fluoxetine administration groups) were stained with anti-VEGFR2 antibody. Scale bar: 100 μm.

3.3. Influence of Anger-Out and Anger-In Stress upon VEGF and VEGFR2 in Rat's Hippocampus and Lobe, as well as the Induced PI3k/AKT/mTOR. We used fluorescent quantitative PCR to detect VEGF and VEGFR2 mRNA levels in rat's hippocampus and frontal lobe. The results showed that, when compared to the control group, the mRNA expression of VEGF in hippocampus and lobe decreased in the model group (Figure 5(a)) and that fluoxetine administration could significantly attenuate decreases caused by anger emotional stress (Figure 5(a)). However, there was no significant difference between the two brain regions of VEGFR2 mRNA in each group (Figure 5(b)).

We then used Western blotting to detect expression changes of relevant proteins in the PI3k/AKT/mTOR signal pathway induced by VEGF and VEGFR2 (Figure 6(a)). The results showed that the anger-out group registered decreased pmTOR protein expression compared to the control group (Figure 6(b)) and that administration of fluoxetine could improve the situation significantly (Figure 6(b)). When compared with the control group, pmTOR expression in the anger-in group decreased, and fluoxetine administration failed to improve it (Figure 6(b)).

The tmTOR expression of the anger-out group had no significant changes when compared with the other groups, including the control group (Figure 6(c)). The tmTOR expression of the anger-in group decreased significantly when compared with the control group, and fluoxetine administration failed to improve it (Figure 6(c)).

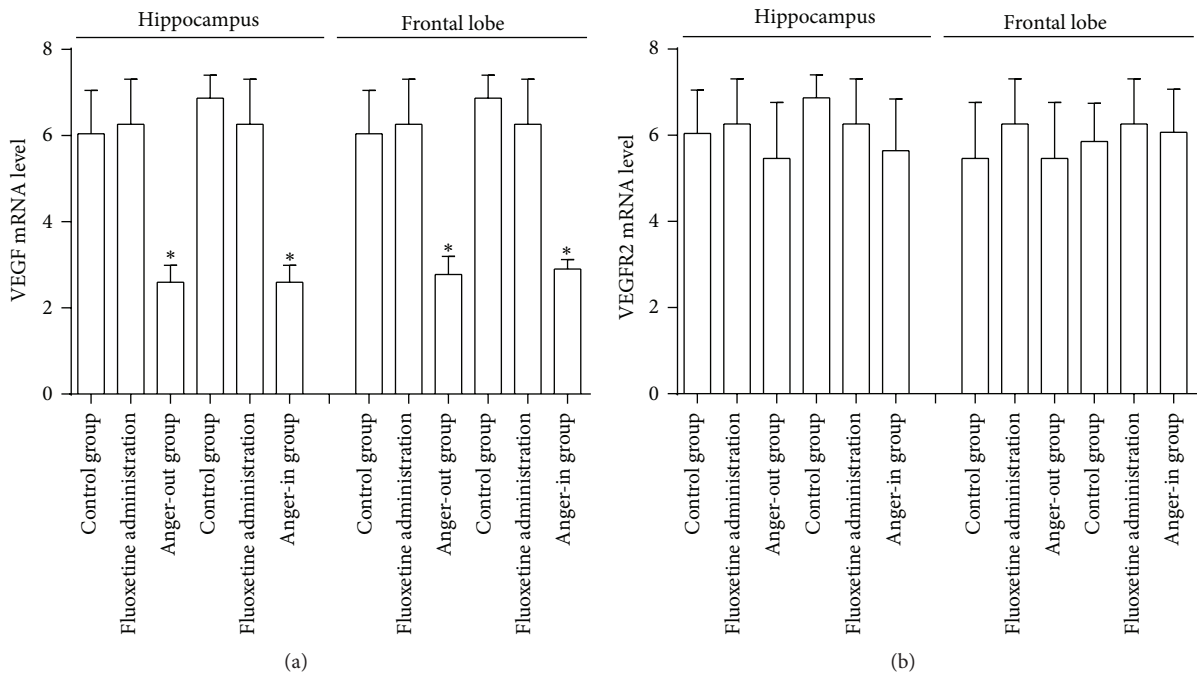

Figure 5: Quantitative analysis ($n = 5$) in VEGF mRNA (a) and VEGFR2 mRNA (b) of hippocampus and frontal lobe. Control, anger-out, anger-in, fluoxetine treated anger-out, and fluoxetine treated anger-in groups were tested ($^*P < 0.05$).

As for pPI3Kp85 level, its expression in the anger-out group registered greater improvement than the control group (Figure 6(d)), and fluoxetine administration greatly improved the expression of pPI3Kp85 level in the anger-out group (Figure 6(d)). The expression of pPI3Kp85 in the anger-in group registered a greater decrease than the control group (Figure 6(d)), and fluoxetine administration could greatly improve the situation (Figure 6(d)). The tPI3Kp85 expression of all experimental groups (including anger-out group, anger-in group, and both fluoxetine administration groups) had no significant changes when compared with control group (Figure 6(e)).

Moreover, the pAKT expression at the anger-out group showed greater improvement than the control group (Figure 6(f)), and fluoxetine administration significantly increased pAKT expression in the anger-out group (Figure 6(f)). The expression of pAKT in the anger-in group registered a greater improvement than the control group, and fluoxetine administration significantly increased pAKT expression among anger-in rats (Figure 6(f)).

Finally, we discovered that tAKT expression in the anger-out group registered a greater improvement than the control group (Figure 6(g)) and that fluoxetine administration failed to improve it (Figure 6(g)). The expression of tAKT in the anger-in group also registered a greater improvement than the control group, and fluoxetine administration had no statistically significant effect in improving the expression (Figure 6(g)).

4. Discussion

This research takes advantage of the resident-intruder paradigm to establish the anger emotional model, further divides anger into two groups, anger-out and anger-in, and then explores the biological mechanisms of anger in living creatures. Behavioral changes induced by the resident-intruder paradigm are considered to be similar to human aggression. Although aggressive behavior is not defined as anger, the anger neuroendocrine mechanism is very similar to the human emotion of anger [34] and it is widely believed that aggressive behavior is caused by anger [35].

As a result of population research, scientists have divided anger into anger-out and anger-in groups. Twice, they have developed and revised the state-trait anger inventory (STAXI) to distinguish anger into two different modes of expression [36]. Present research distinguishes anger-out group from anger-in group according to the median method of aggression scores. After one week of the resident-intruder mode, we observed decreased weight gain in each group when compared with the control group. This demonstrates the same effect of inhibiting weight gain through emotional stress, as observed with chronic unpredictable mild stress (CUMS) [37]. After one week of fluoxetine administration (second week of resident-intruder paradigm), there was no significant difference of weight gain between anger emotional stress groups and the control group. On the other hand, after one week in the resident-intruder mode, the anger-out group had a higher score in composite aggression than the control group, and anger-out group exhibited a shorter latency of aggression than the anger-in group. After fluoxetine administration, the score of composite aggression in each anger emotional stress group dropped significantly, compared to groups without administration. The above-described information indicates that the modeling is successful in setting up the major evaluation indexes.

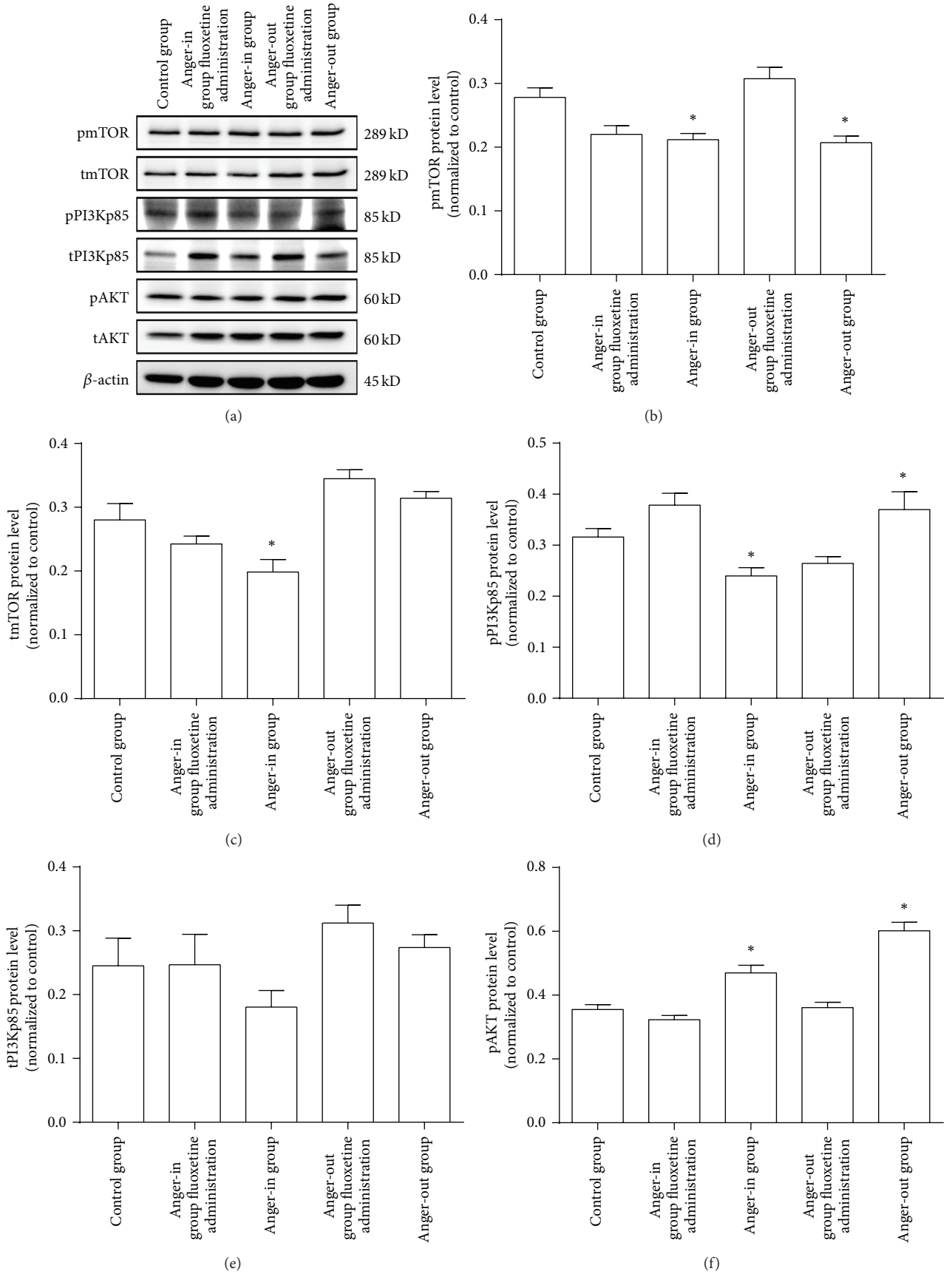

Figure 6: Continued.

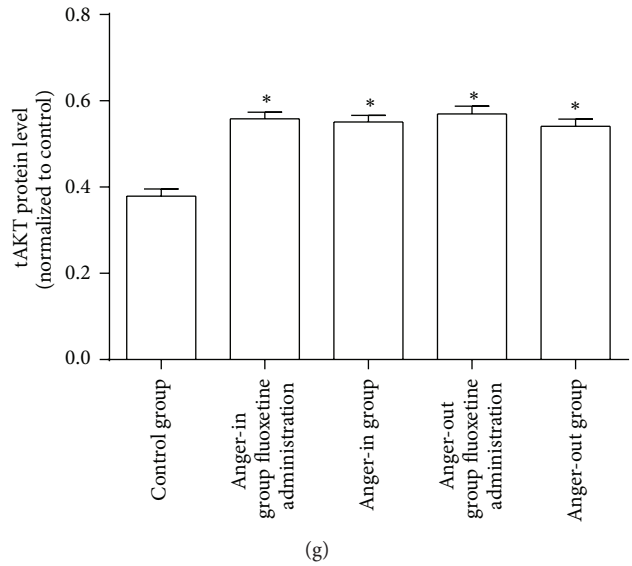

(g)

Figure 6: (a) Western blotting was performed with hippocampus' samples of control, anger-out, anger-in, fluoxetine treated anger-out, and fluoxetine treated anger-in groups. (b) Quantitative analysis ($n = 8$) in pmTOR protein level ($^*P < 0.05$). (c) Quantitative analysis ($n = 8$) in tmTOR protein level ($^*P < 0.05$). (d) Quantitative analysis ($n = 8$) in pPI3Kp85 protein level ($^*P < 0.05$). (e) Quantitative analysis ($n = 8$) in tPI3Kp85 protein level. (f) Quantitative analysis ($n = 8$) in pAKT protein level ($^*P < 0.05$). (g) Quantitative analysis ($n = 8$) in tAKT protein level ($^*P < 0.05$).

Rodents are very sensitive to sweet solutions (common sugar water), so sucrose drinking amount and sucrose preference level are often used to evaluate the degree of anhedonia. They are more frequently used in depression and anxiety models and serve as an important sensitive index for evaluation [38]. This is the first study to link anhedonia to anger emotion. After one week in the resident-intruder mode, the sucrose preference level significantly decreased at each group when compared with the control group, but after fluoxetine administration the level of the model group still dropped greatly, while the level at the group with administration returned to the level of the control group, revealing the presence of anhedonia during expression of the emotion of anger. The open field test is designed to assess cognition of, anxiety-like behavior towards, and interest in the outside world and assesses behavioral inhibition and increased fear, as well as decreased social behavior, through the activity level of subjects [39]. The open field behavior can be measured using several parameters, among which horizontal score reflects the excitement of animals and vertical score reflects the uncertainty and exploration trend of animals against the surroundings. The total score in open field test is a general reflection of the exploratory behaviors and motivation of animals. After one week in the resident-intruder model, the total score of open field test of each group improved significantly when compared with the control group; fluoxetine administration produced control-like behavior in the open field test. This indicates that the motivation of rats was increased following the resident-intruder test and that fluoxetine was able to regulate this emotionality.

Although aggressive behavior is not defined as anger, this research modeled valid subtypes for anger based on composite aggression scores and obtained valid results from subsequent behavioral tests. As a result, we believe that aggressive behavior plays an important role in the generation and development of anger emotion, which, to some degree, prompts us to connect the research on anger and the research on aggression. Research shows that disorders of the 5-HT system can lead to impulsive aggressive behavior [40–44]. In addition, activation and distribution of different 5-HT receptors are related to aggression [45]. 5-HT1A receptors are distributed in presynaptic membranes of the raphe nucleus, prefrontal cortex, and amygdala and postsynaptic membranes of 5-HT neurons in the hippocampus. Our work shows that rats with anger stress had more spindle-shaped hippocampal neurons, more ribosomes, less organelles, and fewer synaptic connections (Figure 3) and that, after fluoxetine administration, these deficits could be improved to some extent (Figure 3). These results provide evidence for a relationship between aggression and anger.

Synaptic plasticity serves as important means for message transfer and processing among neurons. Here we show evidence of damage to microstructures in the hippocampal CA3 area among anger-out and anger-in rats. The decrease in synapse number and structural damage can influence the release of neurotransmitters, hence hindering message transfer in the central nervous system. The damage to the neurons in the hippocampal CA3 area and microstructure of synapse indicates that anger emotional stress harms the plasticity of central nervous system. Meanwhile, chronic stress, caused by emotional stress exceeding the bearing capacity of the living body, will cause disorders in many aspects like mood, nerve, internal secretion and immunity, and changes in brain structure, as well as learning and memory.

There have been multiple studies concerning the role of VEGF in depression, with a focus on the PI3K/AKT/mTOR signal pathway influencing the process of pathogenesis [46] and neurogenesis [47]. As emotional stress abnormality, after discovering the influence of anger emotion upon hippocampal structure, this research further explored the effects of anger on the PI3K/AKT/mTOR signal pathway induced by VEGF and its receptor VEGFR2. It was found out that the content of hippocampal VEGF dropped during anger emotional stress. The expression of mRNA of VEGF in hippocampus and lobes decreased, while there was no significant change to the mRNA expression of VEGFR2. The reason may lie in the fact that VEGFR2 plays its role mainly through protein expression levels. The mode of anger expression not only is connected with external stress but also is related to individual physiological and psychological features, which determines different responses of organisms to external stress. The expression level of key proteins in PI3K/AKT/mTOR signaling pathway is in disorder, pmTOR, pPI3Kp85, and pAKT in particular. Protein phosphorylation is called the "door to life," as a protein will be activated after phosphorylation, giving way to its biological function. This complexity of change may be related to the complexity and networking nature of signal pathway. Further research will be required to assess these effects.

In summary, this research provides a detailed classification of anger emotion and provides evidence of the influence of anger emotion upon VEGF and its signal pathway. This may provide a mechanism by which anger impairs neurogenesis through influencing VEGF/VEGFR2 and its induced PI3k/AKT/mTOR signal pathway.

Conflict of Interests

The authors declare that there is no conflict of interests regarding the publication of this paper.

Authors' Contribution

Peng Sun and Sheng Wei contributed equally to this work.

Acknowledgments

This research was supported by the National Natural Science Foundation of China (NSFC, Grant no. 81102537) and by Taishan Scholar Program.

References

[1] A. L. Chapman and K. L. Dixon-Gordon, "Emotional antecedents and consequences of deliberate self-harm and suicide attempts," *Suicide and Life-Threatening Behavior*, vol. 37, no. 5, pp. 543–552, 2007.

[2] K. B. Koh and J. K. Park, "The relation between anger management style and organ system-related somatic symptoms in patients with depressive disorders and somatoform disorders," *Yonsei Medical Journal*, vol. 49, no. 1, pp. 46–52, 2008.

[3] D. S. Reddy and K. H. Jian, "The testosterone-derived neurosteroid androstanediol is a positive allosteric modulator of GABAA receptors," *Journal of Pharmacology and Experimental Therapeutics*, vol. 334, no. 3, pp. 1031–1041, 2010.

[4] J. L. Aikey, J. G. Nyby, D. M. Anmuth, and P. J. James, "Testosterone rapidly reduces anxiety in male house mice (*Mus musculus*)," *Hormones and Behavior*, vol. 42, no. 4, pp. 448–460, 2002.

[5] V. Michopoulos, M. Checchi, D. Sharpe, and M. E. Wilson, "Estradiol effects on behavior and serum oxytocin are modified by social status and polymorphisms in the serotonin transporter gene in female rhesus monkeys," *Hormones and Behavior*, vol. 59, no. 4, pp. 528–535, 2011.

[6] G. Ambar and S. Chiavegatto, "Anabolic-androgenic steroid treatment induces behavioral disinhibition and downregulation of serotonin receptor messenger RNA in the prefrontal cortex and amygdala of male mice," *Genes, Brain and Behavior*, vol. 8, no. 2, pp. 161–173, 2009.

[7] E. F. Coccaro, M. S. McCloskey, D. A. Fitzgerald, and K. L. Phan, "Amygdala and orbitofrontal reactivity to social threat in individuals with impulsive aggression," *Biological Psychiatry*, vol. 62, no. 2, pp. 168–178, 2007.

[8] R. J. R. Blair, "The amygdala and ventromedial prefrontal cortex in morality and psychopathy," *Trends in Cognitive Sciences*, vol. 11, no. 9, pp. 387–392, 2007.

[9] B. Derntl, C. Windischberger, S. Robinson et al., "Amygdala activity to fear and anger in healthy young males is associated with testosterone," *Psychoneuroendocrinology*, vol. 34, no. 5, pp. 687–693, 2009.

[10] S. J. Stanton, M. M. Wirth, C. E. Waugh, and O. C. Schultheiss, "Endogenous testosterone levels are associated with amygdala and ventromedial prefrontal cortex responses to anger faces in men but not women," *Biological Psychology*, vol. 81, no. 2, pp. 118–122, 2009.

[11] A. S. New, E. A. Hazlett, M. S. Buchsbaum et al., "Amygdala-prefrontal disconnection in borderline personality disorder," *Neuropsychopharmacology*, vol. 32, no. 7, pp. 1629–1640, 2007.

[12] M. A. de Souza Silva, B. Topic, J. P. Huston, and C. Mattern, "Intranasal administration of progesterone increases dopaminergic activity in amygdala and neostriatum of male rats," *Neuroscience*, vol. 157, no. 1, pp. 196–203, 2008.

[13] M. Giammanco, G. Tabacchi, S. Giammanco, D. Di Majo, and M. La Guardia, "Testosterone and aggressiveness," *Medical Science Monitor*, vol. 11, no. 4, pp. RA136–RA145, 2005.

[14] J. Archer, "The influence of testosterone on human aggression," *British Journal of Psychology*, vol. 82, no. 1, pp. 1–28, 1991.

[15] C. C. C. Cohen-Bendahan, J. K. Buitelaar, S. H. M. van Goozen, J. F. Orlebeke, and P. T. Cohen-Kettenis, "Is there an effect of prenatal testosterone on aggression and other behavioral traits? A study comparing same-sex and opposite-sex twin girls," *Hormones and Behavior*, vol. 47, no. 2, pp. 230–237, 2005.

[16] E. W. Fish, J. F. DeBold, and K. A. Miczek, "Escalated aggression as a reward: corticosterone and $GABA_A$ receptor positive modulators in mice," *Psychopharmacology*, vol. 182, no. 1, pp. 116–127, 2005.

[17] E. W. Fish, S. Faccidomo, J. F. DeBold, and K. A. Miczek, "Alcohol, allopregnanolone and aggression in mice," *Psychopharmacology*, vol. 153, no. 4, pp. 473–483, 2001.

[18] B. Segebladh, E. Bannbers, L. Moby et al., "Allopregnanolone serum concentrations and diurnal cortisol secretion in women with premenstrual dysphoric disorder," *Archives of Women's Mental Health*, vol. 16, no. 2, pp. 131–137, 2013.

[19] P. Monteleone, S. Luisi, A. Tonetti et al., "Allopregnanolone concentrations and premenstrual syndrome," *European Journal of Endocrinology*, vol. 142, no. 3, pp. 269–273, 2000.

[20] S. S. Girdler, P. A. Straneva, K. C. Light, C. A. Pedersen, and A. L. Morrow, "Allopregnanolone levels and reactivity to mental stress in premenstrual dysphoric disorder," *Biological Psychiatry*, vol. 49, no. 9, pp. 788–797, 2001.

[21] P. R. Albert, F. Vahid-Ansari, and C. Luckhart, "Serotonin-prefrontal cortical circuitry in anxiety and depression phenotypes: pivotal role of pre- and post-synaptic 5-HT1A receptor expression," *Frontiers in Behavioral Neuroscience*, vol. 8, article 199, 2014.

[22] S. S. Newton, N. M. Fournier, and R. S. Duman, "Vascular growth factors in neuropsychiatry," *Cellular and Molecular Life Sciences*, vol. 70, no. 10, pp. 1739–1752, 2013.

[23] J. Greene, M. Banasr, B. Lee, J. Warner-Schmidt, and R. S. Duman, "Vascular endothelial growth factor signaling is required for the behavioral actions of antidepressant treatment: pharmacological and cellular characterization," *Neuropsychopharmacology*, vol. 34, no. 11, pp. 2459–2468, 2009.

[24] M. L. Seibenhener and M. C. Wooten, "Use of the Open Field Maze to measure locomotor and anxiety-like behavior in mice," *Journal of Visualized Experiments*, no. 96, Article ID e52434, 2015.

[25] X. Zhu, T. Li, S. Peng, X. Ma, X. Chen, and X. Zhang, "Maternal deprivation-caused behavioral abnormalities in adult rats relate to a non-methylation-regulated D2 receptor levels in the nucleus accumbens," *Behavioural Brain Research*, vol. 209, no. 2, pp. 281–288, 2010.

[26] M. Gross and A. Pinhasov, "Chronic mild stress in submissive mice: marked polydipsia and social avoidance without hedonic deficit in the sucrose preference test," *Behavioural Brain Research*, vol. 298, pp. 25–34, 2016.

[27] G. Dagyt, I. Crescente, F. Postema et al., "Agomelatine reverses the decrease in hippocampal cell survival induced by chronic mild stress," *Behavioural Brain Research*, vol. 218, no. 1, pp. 121–128, 2011.

[28] Y. Guo, H. Zhang, J. Gao et al., "Study of genes associated with the 'anger-in' and 'anger-out' emotions of humans using a rat model," *Experimental and Therapeutic Medicine*, vol. 9, no. 4, pp. 1448–1454, 2015.

[29] G. Gan, H. Lv, W. Xie, and R. Zhou, "Morphological identification and development of neurite in *Drosophila* ventral nerve cord neuropil," *PLoS ONE*, vol. 9, no. 8, Article ID e105497, 2014.

[30] C. Wang, T. Feng, Q. Wan, Y. Kong, and L. Yuan, "miR-124 controls *Drosophila* behavior and is required for neural development," *International Journal of Developmental Neuroscience*, vol. 38, pp. 105–112, 2014.

[31] J. Peng, C. Wang, C. Wan et al., "miR-184 is Critical for the motility-related PNS development in *Drosophila*," *International Journal of Developmental Neuroscience*, vol. 46, pp. 100–107, 2015.

[32] R. S. Tebbs, P. Balachandran, L. Y. Wong et al., "Evaluation of applied biosystems MicroSeq$^{\text{Ÿ}}$ real-time PCR system for detection of *Listeria monocytogenes* in food. Performance Tested Method 011002," *Journal of AOAC International*, vol. 94, no. 5, pp. 1481–1489, 2011.

[33] J. Kaur and A. K. Bachhawat, "A modified Western blot protocol for enhanced sensitivity in the detection of a membrane protein," *Analytical Biochemistry*, vol. 384, no. 2, pp. 348–349, 2009.

[34] H.-P. Ho, M. Olsson, L. Westberg, J. Melke, and E. Eriksson, "The serotonin reuptake inhibitor fluoxetine reduces sex steroid-related aggression in female rats: an animal model of premenstrual irritability?" *Neuropsychopharmacology*, vol. 24, no. 5, pp. 502–510, 2001.

[35] L. J. Siever, "Neurobiology of aggression and violence," *The American Journal of Psychiatry*, vol. 165, no. 4, pp. 429–442, 2008.

[36] S. Schamborg, R. J. Tully, and K. D. Browne, "The use of the state—trait anger expression inventory—II with forensic populations: a psychometric critique," *International Journal of Offender Therapy and Comparative Criminology*, 2015.

[37] X.-J. Liu, Z.-Y. Li, Z.-F. Li et al., "Urinary metabonomic study using a CUMS rat model of depression," *Magnetic Resonance in Chemistry*, vol. 50, no. 3, pp. 187–192, 2012.

[38] O. Berton, M. Durand, S. Aguerre, P. Mormède, and F. Chaouloff, "Behavioral, neuroendocrine and serotonergic consequences of single social defeat and repeated fluoxetine pretreatment in the Lewis rat strain," *Neuroscience*, vol. 92, no. 1, pp. 327–341, 1999.

[39] N. N. Kudryavtseva, "A sensory contact model for the study of aggressive and submissive behavior in male mice," *Aggressive Behavior*, vol. 17, no. 5, pp. 285–291, 1991.

[40] J. D. Higley, P. T. Mehlman, R. E. Poland et al., "CSF testosterone and 5-HIAA correlate with different types of aggressive behaviors," *Biological Psychiatry*, vol. 40, no. 11, pp. 1067–1082, 1996.

[41] M. Virkkunen, R. Rawlings, R. Tokola et al., "CSF biochemistries, glucose metabolism, and diurnal activity rhythms in alcoholic, violent offenders, fire setters, and healthy volunteers," *Archives of General Psychiatry*, vol. 51, no. 1, pp. 20–27, 1994.

[42] P. H. Soloff, T. M. Kelly, S. J. Strotmeyer, K. M. Malone, and J. J. Mann, "Impulsivity, gender, and response to fenfluramine challenge in borderline personality disorder," *Psychiatry Research*, vol. 119, no. 1-2, pp. 11–24, 2003.

[43] E. F. Coccaro, J. M. Silverman, H. M. Klar, T. B. Horvath, and L. J. Siever, "Familial correlates of reduced central serotonergic system function in patients with personality disorders," *Archives of General Psychiatry*, vol. 51, no. 4, pp. 318–324, 1994.

[44] A. S. Unis, E. H. Cook, J. G. Vincent et al., "Platelet serotonin measures in adolescents with conduct disorder," *Biological Psychiatry*, vol. 42, no. 7, pp. 553–559, 1997.

[45] M. Nomura and Y. Nomura, "Psychological, neuroimaging, and biochemical studies on functional association between impulsive behavior and the 5-HT2A receptor gene polymorphism in humans," *Annals of the New York Academy of Sciences*, vol. 1086, pp. 134–143, 2006.

[46] G. K. Boora, R. Kanwar, A. A. Kulkarni et al., "Exome-level comparison of primary well-differentiated neuroendocrine tumors and their cell lines," *Cancer Genetics*, vol. 208, no. 7-8, pp. 374–381, 2015.

[47] T.-J. Liu, D. Koul, T. LaFortune et al., "NVP-BEZ235, a novel dual phosphatidylinositol 3-kinase/mammalian target of rapamycin inhibitor, elicits multifaceted antitumor activities in human gliomas," *Molecular Cancer Therapeutics*, vol. 8, no. 8, pp. 2204–2210, 2009.

Hindawi Publishing Corporation
Neural Plasticity
Volume 2016, Article ID 7192427, 20 pages
http://dx.doi.org/10.1155/2016/7192427

Review Article

The Plastic Glial-Synaptic Dynamics within the Neuropil: A Self-Organizing System Composed of Polyelectrolytes in Phase Transition

Vera Maura Fernandes de Lima[1] and Alfredo Pereira Jr.[2]

[1]*Centro de Biotecnologia, IPEN-CNEN/SP, Avenida Prof. Lineu Prestes 2242, Butantã, 05508-000 São Paulo, SP, Brazil*
[2]*Institute of Biosciences of Botucatu, São Paulo State University (UNESP), Campus Rubião Jr., 18618-970 Botucatu, SP, Brazil*

Correspondence should be addressed to Alfredo Pereira Jr.; alfredo.pereira@gmail.com

Received 25 September 2015; Accepted 27 December 2015

Academic Editor: Bruno Poucet

Several explanations have been proposed to account for the mechanisms of neuroglial interactions involved in neural plasticity. We review experimental results addressing plastic nonlinear interactions between glial membranes and synaptic terminals. These results indicate the necessity of elaborating on a model based on the dynamics of hydroionic waves within the neuropil. These waves have been detected in a small scale experimental model of the central nervous system, the *in vitro* retina. We suggest that the brain, as the heart and kidney, is a system for which the state of water is functional. The use of nonlinear thermodynamics supports experiments at convenient biological spatiotemporal scales, while an understanding of the properties of ions and their interactions with water requires explanations based on quantum theories. In our approach, neural plasticity is seen as part of a larger process that encompasses higher brain functions; in this regard, hydroionic waves within the neuropil are considered to carry both physiological and cognitive functions.

1. Introduction

We discuss the plastic nonlinear interactions between glial membranes and synaptic terminals, using physical-chemical (electrochemical) concepts to describe the basic brain dynamics that carry psychophysical processes. In our approach, the Hodgkin-Huxley membrane model was not relevant for the explanation of experimental results. Instead, Ichigi Tasaki's membrane model [1–4] and Katchalsky's [5–7] proposed synapse model are the foundations of the interpretation of our electrophysiological and optical data obtained from experiments with *in vitro* retinas.

The spreading depression is a general central grey matter phenomenon predicted by Lashley in 1941 [8]. There is an aphorism in this field of research that "to understand spreading depression is to understand the brain." Based on the evolution of his own scotomas preceding a full-fledged migraine attack, Lashley predicted an excitation/inhibition wave spreading in the primary visual cortex and correctly estimated its velocity at 3 mm/min. The distortion of perception that accompanies the wave made him interpret it as a psychophysical phenomenon, as expressed in the paper's title [8].

This model of brain activity advanced by Lashley has not been hegemonic within the neurosciences community but was kept alive by a minority of researchers. For example, just two years after Tasaki and Chang's paper on cortical glial cells slow potentials [9] and its implicit contribution to the EEG, Galambos [10] published an enthusiastic review of the role of glia in the brain. The role of polyelectrolytes (in this case polyanions) in synapses and their role in the brain self-organization were clearly stated by Katchalsky [6, 7] in the late sixties and early seventies of the XX century.

The explanatory value of a scientific conjecture can be confirmed if it permits clear predictions and these predictions are supported by experimental results. We quote directly Neumann and Katchalsky [11]: "Controlled changes in the environment of metastable macromols or subcellular

macromol. organizations such as membranes by high elec. fields or by ion gradients can induce conformational changes which could serve as reproducible imprints of a memory nature." Note that the supramolecular structure of biological polyanionic gels creates electromagnetic fields that in turn influence the metastable state of these gels (a case of "circular causation," a concept that plays a central role in synergetics and systems control theories). Estimations of these fields range in the order of 300,000 V/cm^2 [6]. Shortly after this prediction, in 1977, a type of long-term memory (with a duration of two weeks) was demonstrated in the basement membrane of striated muscles [12]. This finding has been confirmed many times over (see, e.g., [13–15]). These results led to the suggestion that information could be embodied not in special molecules, but in the energy pattern generated by the macroscopic supramolecular structure.

A second vantage of the electrochemical approach to the neuropil is that it is a unifying explanation for apparently disparate research results: for instance, the effects of lithium on the heart and its usage in psychiatry to control bipolar disorder; the effects of cationic proteins in both tissues; the physical-chemical (i.e., the solvent and not the isotope) effects of deuterium in the retina model, as well as in psychiatry (explaining the reported increase of depression in populations submitted to high concentration of deuterium in drinking water; see [16]).

All the above results are discussed in the following sections. We begin with deuterium as solvent in two electrochemical systems; then, we discuss the role of the basement membrane in the emergence of dynamic structures and proceed to discuss the limitations of electrophysiological recordings within the neuropil, when these dynamic patterns are studied. The presence of remarkable intrinsic optic signals (IOS) in retinal grey matter adds a new dimension to these studies. Two recent publications give a detailed description of the retinal IOS and how to use it in research [17, 18].

2. The Deuterium Experimental Results and the Fourth State of Water

The deuterium solvent experiments series complemented a long series of experiments aimed at comparing the behavior of two very convenient excitable media systems: the excitation states in *in vitro* retinas and the Belousov-Zhabotinsky reaction system (B-Z; for the definition and history of this chemical system, see Zhabotinsky's article in Scholarpedia [19]). Both are well-known excitable media and share the same descriptive mathematical dynamics. Zykov [20] states the mathematical identity between the biological equations of FitzHug Nagumo and Brusselator [21] of Ilya Prigogine chemical equations systems. In addition, there is a very good definition of excitable media in the chapter.

We have analyzed dynamical waves in retinas as a two-dimensional electrochemical pattern. In Brazil, the first set of comparative experiments in biological and chemical system was made in 1980: a circling B-Z system in analogy with the circling retinal waves created by Martins-Ferreira in 1974 [22, 23]. Later on, one of the authors was part of a research group that proceeded to compare the two systems' behavior using modulation of physical fields, electromagnetic and gravitational [24–26]. The similarity in response was uncanny. For example, at similar temperature, the circling retinal waves and B-Z waves spread at very close velocities, and the retina and the B-Z system in gel react to increases of gravitational forces and to microgravity in the same qualitative way.

Deuterium solutions have different physical properties than water solutions, as shown by Katz in 1960 [27]. The use of liquid deuterium as solvent interferes with the global coupling observed in excitable media [28, 29]. Liquid deuterium and water have similar dielectric constant and surface tension. By contrast, the viscosity of deuterium at 25°C is 25% greater than that of water. Also significant is the temperature of maximum density (g/cc): 3.98°C for water and 11.2°C for deuterium. This difference made researchers speculate that some effects of liquid deuterium would mimic temperature effects [27, 30, 31]. However, the greater difference (except for mass) between the isotopes is in self-ionization: liquid deuterium dissociation is five times smaller than that of water.

Previous experimental research with deuterium gave a 20% lower flow within aquaporins [32] for deuterium compared to water. Based on earlier reports that the deuterium effect was equal to a temperature difference of 4 degrees [30, 31], we expected a milder effect on retinas and a larger effect on the B-Z reaction system. Zhabotinsky remarked that "the *Belousov-Zhabotinsky (BZ) reaction* is a family of oscillating chemical reactions. During these reactions, transition-metal ions catalyze oxidation of various, usually organic, reductants by bromic acid in acidic water solution. ... The BZ reaction can generate up to several thousand oscillatory cycles in a closed system, which permits studying chemical waves and patterns without constant replenishment of reactants" [19].

In spite of the expectation, retinal excitation waves and B-Z systems responded in the same way, with complete collapse of excitability in a short time. This was a very powerful change in both systems. The role of self-ionization of water in spreading depression was unclear until we learned about the work of Pollack and Bunkin with interfacial water close to polyelectrolytes [33–38]. To summarize these results, we can say that when water is close to hydrophilic polyanions (or cations), it assumes a state that has the properties of *quasi*-liquid crystals! [39]. For example, the Bunkin group found that its refractive index is 1.46 (while water has 1.332) and that the interface is anisotropically sharing the optical properties of photonic crystals. This structure is very dynamic and fragile and disrupted by ultrasound. Therefore, when liquid deuterium substitutes water, the diminished capacity for self-ionization impairs the formation and increases the fragility of these crystals and the system excitability collapses.

A very important point to be made for the structured interfacial water is that it stores electrical energy and a negative potential surges at the interface. At the interface with the synthetic Nafion, this structure has a range of more than 100 μm and a negative potential of 120 mV. This negative interfacial potential can explain the three-to-four mV potential drop one measures in electrophysiological recordings when one electrode enters the tissue.

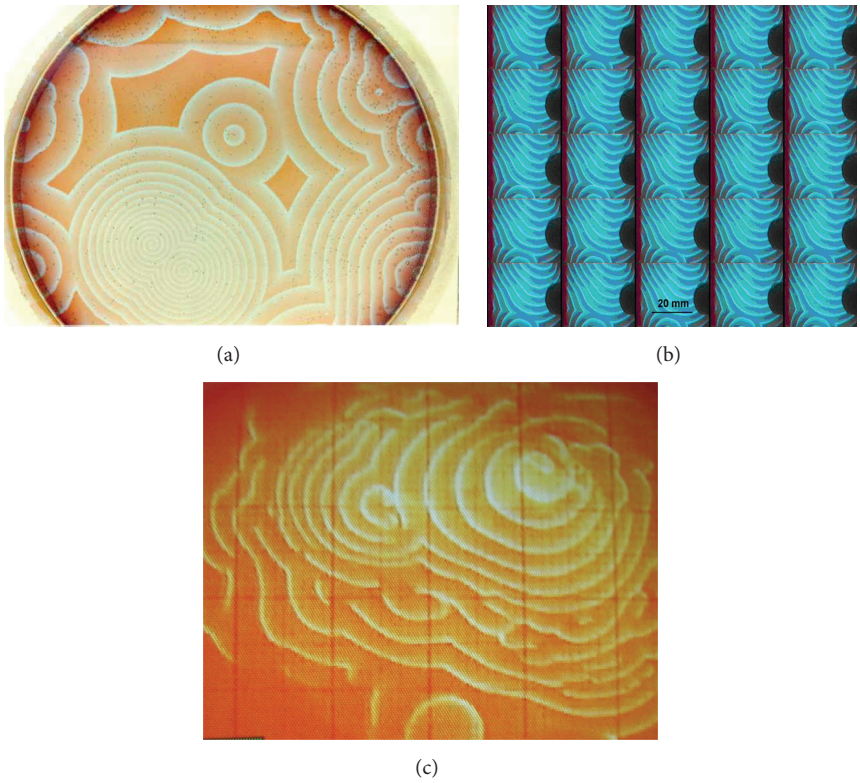

Figure 1: Experiment with the B-Z system. Clockwise: (a) the catalyzer ferroin was fixed in silica gel. One hour after covering the gel with the reactants, several centers begin to create propagating circular waves that cause annihilation of each other upon collision. The whole Petri dish (10 cm diameter) is filled with the self-organized spatiotemporal pattern; (b) detail of another experiment showing the temporal evolution of the B-Z system using water as solvent; (c) experiment of B-Z in gel in which deuterium was used as solvent. Only about one-third of the Petri dish is occupied by the propagating waves. The grid overlaying the dish has 2.0 cm spacing. A few reactive centers send waves that died out long before reaching the border of the Petri dish. The waves become "fuzzy" and disappear. The propagation velocity was five times slower than the ones in the water gel. The deuterium systems also were short-lived compared to the water systems. The results suggest the importance of dissociated water in the B-Z system (figure modified from [28]).

In Figures 1(a) and 1(c), we show two self-organized wave patterns of B-Z reaction in gel using water (a) and deuterium as solvent (c). The spatial scale of the pattern shown in (c) is four times amplified compared to (a).

In water, B-Z waves occupy the whole Petri dish within the first hour of the experiment. In deuterium, only a fraction of the dish showed waves and these waves had blurred endings and died before travelling to the border.

Out of seven retinas submitted to liquid deuterium, two (from the same animal) were dead within the hour. Both displayed the typical excitotoxic optical profile before tissue death (see [18]). The other five became unstable and developed "spontaneous" activity [29], in which the optical profiles also changed from wave to wave. Some of these optical profiles had resemblance to waves recorded at 20°C [40], whereas others had the absence of the second peak one finds in low glucose conditions leading to tissue exhaustion [41]. After one hour or so of such activity, the retinas were unexcitable for the next two hours of washing off the deuterium, when the experiments were finished.

Experimental results at the extracellular matrix of the inner plexiform layer of chick retinas showed a fast (in the order of seconds) pH shift in the alkaline direction at the wave onset [42]. Similar records made intracellularly in astrocytes [43] showed a similar pH shift during spreading depression. It is tempting to interpret this early alkaline shift as the loss of the self-ionized hydronium ions around the polyanions. The Glial Fibrillary Acidic Protein appears to be the ideal candidate for inducing the formation of *quasi*-liquid crystals inside the cells. Thus, the depolarization of spreading depression could well be dominated by the transient loss of this structure intra- and extracellularly and therefore the loss of transparency.

We learned from the liquid deuterium experiments the crucial role of hydronium ions in the brain. The next important question was as follows: what is the brain doing with the energy of the interfacial water?

3. The Basement Membrane/Glial Endfeet CNS Interface and Its Interactions with Complex Molecules

The experiments presented in this section have in common complex molecules that did not easily penetrate the tissue

and hence had to interact with the basement membrane glial endfeet. They showed a powerful transducer role for the tissue interface.

The glycoside ouabain is a large hydrophilic molecule and as such it is poorly permeable in lipid membranes. On the other hand, it is a well-known blocker of the Na/K ATPase activity. The putative place of the blockade is an extracellular loop close to the lipid bilayer. Therefore, in order to reach the loop, ouabain has to negotiate a pathway through the 200 μm thick layer of polyanions continuous to the lipid bilayer. We applied ouabain to *in vitro* chick retinas, first in circling experiments and later with exogenous pulses or slow perfusion [44].

In this avascular retina, the metabolism depends one hundred percent on anaerobic glycolysis performed in the glia [45]. Moreover, there is tight coupling between the rate of ion transport and the production of lactate by glia (for details and relevant literature, see [18, 45]). The consequence of stopping ion transport is a halt in metabolism and subsequent change in the ATP/ADP ratio. We used short pulses as well as slow perfusion to apply ouabain from 1 mM to 10 nM concentration [44]. All 10 retinas were dead within one to two hours of exposition to ouabain. In this series of experiments, we could distinguish two pathways to tissue death: an acute cell lysis that has the appearance of a macroscopic edema [18, 45] and a second type of evolution to death (apoptosis?) without the edema.

At the lowest concentration of 10 nM, the onset of the excitotoxic response had a latency of 30 minutes whereas the onset was 20–30 seconds with 1 mM. The nanomolar concentration range is the hormonal range and indeed the hypothalamus and suprarenal glands produce cardiac glycosides (see references at [18, 44]). It happens that the β subunit of the glia ATPase is an adhesion molecule [46, 47]. In epithelium, adhesion molecules are closely linked to apoptosis. Therefore, the tissue death induced by nanomolar concentration of ouabain could be a consequence of subunit interaction mechanisms rather than ion transport blockade. It was in the lowest concentration that we observed slow death without the macroscopic edema of acute cell lysis. All in all, these experiments showed a dominant role of the glial network in the control of the tissue state.

The ubiquitous Na/K ATPase exemplified the transducer role of the glia. Phase transitions also have an important role in the spread of excitation. Gyroxin (28 KD) is a toxin of the Brazilian rattlesnake venom (2% of the proteins), which caused seizures in rats and mice, but did not have explanatory mechanisms for its CNS action until we applied it to *in vitro* retinas [48]. It has enzymatic activity as a serinoprotease like the thrombin, and up to 30% of its weight is carbohydrate. It is one unlikely candidate to cross the blood brain barrier and yet it produces seizures in rats and mice.

At high concentration short pulses (0.500 μg/500 μL), the rise of the excitotoxic response was so fast that it precluded the toxin entering the tissue. The change had to be at the basement membrane endfeet interface. The change in optical properties was five to six times larger than that measured at the peak of the first optical component of the retinal spreading depression waves. The change in the optical signal was in the millisecond range. For comparison, a similar large pulse of glutamate (1 mM/500 μL) elicits excitotoxicity with a latency of 4 seconds. With the large volume pulse, the IOS of the whole central retina changed at once. In order to see propagation of this change, we used micro pulses with only 50 μL volume aspersed close to the retina surface. In this case, we could see propagation of the excitation with speed also up to five times the spread of retinal circular waves.

Serinoproteases like thrombin cause platelet aggregation and this aggregation is in itself an abrupt change akin to phase transitions. Essays made to compare gyroxin and thrombin produced similar activity for both [48]. This action is due to PAR (Protein Activated Receptors members of the 7TM receptor family). These receptors have a prominent extracellular loop that is cut by the activating enzyme in an irreversible faction. That apparently was the trigger for the gyroxin excitotoxic response. *A conformational change that spreads through the basement membrane* is a clear example of phase transition in polyelectrolytes that abruptly changes the glia neural dynamics. In mammalian CNS, PAR were localized in glia membrane and endothelial basement membrane. Glia PAR activation leads to neuronal activation [49]. The retinal gyroxin results confirmed the interpretation of neural glial dynamics in slices. Because chicken retina is avascular, no vascular component of the basement membrane was present at the vitreal retina interface; only the glia basement membrane contacted the gyroxin. To explain the seizures in rats and mice, either gyroxin acted at the AV3V system in which the blood brain barrier does not exist or gyroxin could cause breakdown of the barrier. Essays confirmed that it did cause this breakdown [48]. This mechanism of triggering seizures could only be proposed due to the added dimension of the strong intrinsic optical signal present in retinal experiments.

The membrane model that assigns a prominent role for phase transition in polyelectrolytes is the Tasaki model [2, 3]. The phase transitions of interest are "volume phase transitions" of polyelectrolytes. A change in electrical field or of ion activity can bring about abrupt changes in polyanions. Once started, they spread through the network. Within this model, the action potential is an electrochemical wave propagating at one dimension, while a retinal spreading depression wave is a wave in two dimensions, and a heartbeat is a propagating pattern in three dimensions. At least for the *in vitro* retina, it is long known that glia and extracellular matrix are sufficient to maintain propagation of a wave without changes in the optical signal and at the same velocity of the neuropil spread. This is due to the optical nerve papilla, a place where only exiting axons and glia are present. It covers a relatively large area continuous to the pecten. Waves invade this area without changes in the optical signal. The Müller cells of chicken retina also do not have gap junctions and have only very few mitochondria. These are located close to the receptor layer far away from the inner plexiform layer, the place where all wave concomitants are at maximum value [17, 18]. Thus, theories assigning important roles for gap junctions or mitochondria in spreading depression do not agree with results of retina experiments. The propagation within the papilla shows that the glial network is necessary and sufficient for maintaining

propagation, while the gyroxin experiments showed that the endfeet layer can initiate excitotoxic responses that propagate in the system.

In the previous section, we described a pathway toward tissue excitability collapse in the presence of deuterium. The tissue lost transparency and hence functionality. In here, we describe another pathway toward excitability collapse in which transparency increased and the tissue appeared in very good shape. We refer to the experiments with protamine, a small (32 amino acids), cationic, naturally occurring protein. In medicine, the avidity of protamine for heparan sulfate (heparin) is used in patients being weaned off anticoagulant treatment. The protein is a polyarginine that in acid pH can acquire a charge of +11. Heparan sulfate is a constituent of glycocalyx and basement membranes (indeed, it is very hard to decide when glycocalyx ends and the basement membrane begins). Essays *in vitro* [50] with heparinized human plasma showed that protamine made stable (up to 4 hours), large (100 nm) heteropolymers complexes with heparin in plasma.

In retinas, the results were just fascinating [51]: protamine induced excitability collapse in 32–34 minutes at concentrations of 0.625 and 1.25 nM [51]. Several waves were observed in this interval. A video recorded the passage of waves in central retina, and optical profiles were acquired at two spatial dimensions, a macro profile obtained from a photomultiplier sampling a circular area of 1 mm diameter and a 50 μm square matrix of pixels obtained from a camera signal. This micro optical signal recorded as close as possible to an electrode tip that measured the potential drop associated with the retinal waves. The photomultiplier counted the amount of scattered light by the retina and its baseline quantified the shifts in transparency. The retinas just became more and more transparent with time, and the observed waves became split with larger and larger areas not invaded by the waves. With 22.7 nM, the excitability collapse occurred in three minutes. More interestingly, the wave optical profiles just became smaller such that if one compares the profile obtained before the protamine application with the last obtained before complete collapse of excitability, the later looks like a miniature version of the first, suggesting that membrane mechanisms and tissue metabolism were not affected by the protein. It appeared that the heteropolymers created by the cationic peptide were far away from the endfeet membrane and the effect was purely physical, a type of mechanical clamping of the basement membrane that prevents wave propagation.

Two facts support this interpretation: first, a functional retina is a transparent one and the degree of transparency is extremely sensitive to membrane states and tissue metabolic state; second, mechanical stimuli did irritate the tissue and with strong mechanical touch that can create large lesions, we could see initial propagation that died out after 250–300 μm. With these results, we could predict a similar effect on heart and axons. Indeed, protamine blocks action potentials in axons [51]. In the heart, we found a report of blockade of a *transplanted* human heart by protamine. This precluded neural mechanisms and the effect could only be intrinsic [52]. *We see the same effect of basement membranes on the propagation of electrochemical patterns at one, two, and three spatial dimensions of biological systems*, in all cases caused by the same agent. At vessels and epithelium, respectively, protamine blocked the rolling over of leucocytes and was found to alter the structure of the epithelial basement membrane while not affecting gap junctions [53, 54]. Neither had any effect on the membrane apical potential.

Another cationic protein applied to retinas was crotamine [51]. It is also small (42 amino acids in the primary chain of which 9 are lysines and 2 arginines). In acid pH, it acquires a charge of +9. It is also a Brazilian rattlesnake toxin that belongs to a class of small basic toxins. Its primary chain is identical to the *Naja naja* P6 toxin. Like gyroxin, it produces a complex sequence of stereotyped behavior in mice (for details, see [51]).

With 9 lysines in the primary chain, crotamine is a naturally occurring polylysine. Polylysines adsorb on red blood cells membranes and red cell "ghosts" [6]. They raise the surface potential of the cells and at a critical potential promote agglutination of the cells or membranes "ghosts." This critical potential lies well below the maximum potential. The critical potential measured with potentiometers was ~ −10 mV and with increasing adsorption of the peptide surface potential reached more than +20 mV [6].

We applied crotamine with short pulses of 500 μg/500 μL (206 nM) with pipettes. The perfusion was stopped for a short time and then resumed. The baseline transparency shifted with a latency too short to be measurable and reached a plateau after 5 to 6 minutes. Waves elicited after 12 minutes of crotamine exposure had an altered profile with a small first optical peak, slow recovery, and a high amplitude long duration second peak. The altered parameters of the profiles indicate that all membrane mechanisms, from the dissipation of the electrochemical gradients at wave onset and its recovery, were disturbed. Upon resumption of perfusion, the transparency baseline recovered and the profiles reverted to the typical pattern in 15 minutes, suggesting an electrostatic effect and a weak interaction with the endfeet membrane. The wave profile pattern recorded in the presence of crotamine suggested modulation of the rate of the Na/K ATPase ion transfer.

In Figure 2, we show the photomicrograph under UV illumination of characteristic microvilli of the outer segment of an intensely labelled Müller cell. Fresh retinal slices incubated with fluorescent crotamine (see [51]) under UV illumination showed intense fluorescence associated with the glial membrane, compared with the inner segment of the adjacent cone receptor cell that also shows some fluorescence. In these experiments, one could see bright spots inside the Müller cells indicating fast internalization of the protein by glia. It appears that the adsorption of crotamine induces endocytosis of membrane patches. In additional experiments, we showed that crotamine is easily incorporated into lipid monolayers and bilayers and that the protein itself forms oligomers in aqueous solution due to its amphiphilic nature [55].

The crotamine effect on muscle cells is depolarization and cell death. The place of crotamine action was first supposed to be sodium channels, while the cell death effect of a similar basic toxin, the P6 toxin, with the same 9 lysines and 2

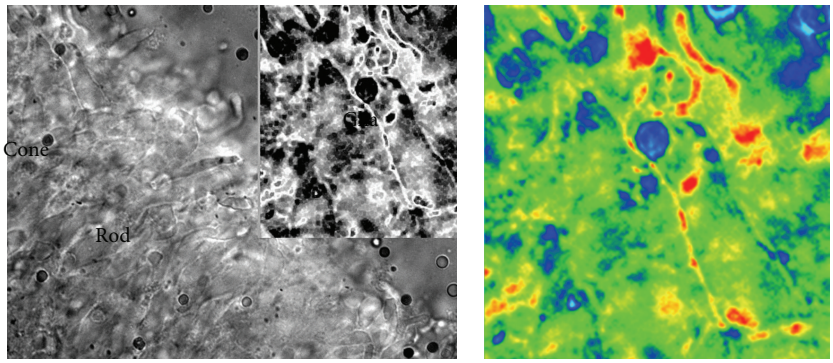

(a) (b)

Figure 2: Fluorescence in Müller cell. (a) Fresh thin slice of retina under UV illumination. The slice was previously incubated with fluorescent crotamine [51]. The outer retina receptor layer has strong fluorescence. Part of the fluorescence is intrinsic, due to oil droplets (blue, green, and red) found in the inner segment of cones. A rod outer segment and a cone inner segment can easily be seen. Close to the cone, the inner segment microvilli of the outer retina portion are very bright. (b) False color display of the inset. Note that all the fluorescence in glia is extrinsic or due to the close association (adsorption) of the basic protein with glial membrane.

arginines in the primary chain, was attributed to the Na/K ATPase [56–59]. More recently, research in molecular biology did not confirm sodium channel interaction with crotamine [60]. Why would the adsorption of crotamine kill muscle and spare retinas? The pump subunits assembled in muscle and glia are different enough to change their physiology: muscle pump is driven by sodium inside cells, whereas glia pump is driven by potassium outside [61]. Not only the distribution of α subunits but also their associated β subunits (the glycosylated subunits) differ in CNS and heart. Irrespective of the subunits expressed, all of the membrane ATPases have several functions besides ion transport, including the apoptotic and acute cell lysis pathways [62].

Ouabain promotes acute cell lysis and apoptosis in the central gray matter of cortex [63] and retina [44], and in muscle it modulates ion transport without killing the tissue. While crotamine modulates ion transport in central gray matter and depolarizes the glial network without further harm, it kills muscle and tumors cells either with acute cell lysis or with apoptosis [56, 57]. The depolarization of the glial network in mice initiates stereotyped behavior that ends in a frozen characteristic posture followed by death [51].

If the results described by Katchalsky [6] for polylysines on red blood cells membranes are taken into account, then the crotamine effects are not classical lock-and-key effects on specific receptors, but a physical change in the membrane electrical field that changes the state of intrinsic and associated membrane proteins. The glial membrane network depolarization changes the tissue dynamics expressed in the tissue baseline transparency and parameters of the optical profiles of propagating waves.

The ouabain experiments merely reproduced in the retina the cortical effects of the glycoside [63], just showing one more time that the inner retina is part of the CNS and not just a model of it. The experiments reinforced the transducer role of the Na/K ATPase of the endfeet membrane. With gyroxin, we learned how fast the change in neural and glial dynamics can happen and spread after a trigger that promoted conformational changes in the basement membrane. The appropriate name for this is *phase transition*. Protamine and crotamine experiments suggest the adaptability of polyelectrolytes to the surrounding medium. If one thinks in very simple terms of stick-and-ball configuration, both proteins that are thought to be compact (disulfide bonds) can unfold under the influence of the electrical fields at the membrane interface. The stick configuration of the amphiphilic crotamine inserts itself in the membrane the same way that it does in bilayers and monolayers, while the more hydrophilic protamine repelled by the hydronium ions at the interface and in the basement membrane finds heparan sulfates and then makes stable heteropolymers that clamp pieces of the basement membrane, thus impairing polyelectrolytes conformational changes crucial for spread of excitation.

Last but not least, the remarkable IOS of retinas permit the observation not only of the velocity of spread of excitation, but also of the manner of spread. Excitotoxic responses spread very differently from circular waves. Also, we observed that there are several ways of tissue death. Acute cell lysis is observed while it is happening in retinas, instead of hours to days later which is the rule in cortex [44, 48, 63, 64]. The cause is the macroscopic tissue edema associated with acute cell lysis while the apoptotic pathway produces final states without the edema [44, 48, 62, 63].

4. The Potassium and Calcium Activities within the Neuropil during Spread of Excitation and within Dynamic Electrochemical Patterns

In this section, we apply the model to the neuropil, approaching the mechanisms involved in neural plasticity. We begin by describing results of measured activity with ion-sensitive electrodes inserted in the neuropil and the related extrinsic fluorescence. The layered structure of vertebrate retinas, in

which cell bodies and synaptic terminals are completely segregated, gives rise to sharp potential profiles that can be better identified than in the hippocampus cell bodies' *stratum radiatum*. In the inner plexiform layer, there are only two types of membrane: glial and synaptic terminals. The microglia of this avascular retina is situated at the border of the ganglion cell layer and inner plexiform layer [45].

The ion activities changes during excitation waves are related to lyotropic effects of ions (or the Hofmeister series). The first researchers to do a systematic investigation of the lyotropic effect of ions on neural excitability were Tasaki et al. in 1965 [65]. A classical study in the field of stereochemical properties of ions is the review by Williams in 1970 [66]; more recent ones are by Collins in 2004 [67] and Zhang and Cremer in 2006 [68]. Ions with the same charge interact very differently with polyelectrolytes. For example, magnesium can only make special spatial configurations (octahedral) in electrostatic interactions with polyanions, while calcium has no spatial exigencies [66]. Katchalsky [6] cites a report of ionic interactions with polyacid alginate. The result showed that only 1% of calcium was free and 99% bound in complexes, while 15% of magnesium was free. One ion electrostatically immobilized had no detected activity. In the same study, 40% of sodium and 35% of potassium were free.

Ion concentration and activity are equivalent only in diluted solutions. At the synaptic space between membranes, a layer of 50 nm of polyelectrolytes creates enormous electric fields (300,000 V/cm^2). The behavior of ions in this environment is simply different from their behavior in diluted solutions. Ionic activity can rise and fall according to ionization of the polyanions and their screening capacity to immobilize counterions.

High sodium solutions (120–140 mEq/L from the standard 100 mEq/L) on retinas had a negative effect on tissue excitability: the amplitude of the potential drop was to 40% of controls, its time derivative 23%, and propagation velocity 66%. The retina loses transparency in high sodium and the optical profiles become inverted: transparency increases when the potential drops [69]. Based on these results on retinal waves and the Hofmeister series position (Jones-Doyle viscosity B coefficient [67]) of lithium and sodium, we could predict pronounced lithium effects on excitable tissue. These effects have been reported [70–72]. Dietary lithium changed spread velocity of cortical spreading depressions. We have reports of negative effects on excitability in the single axon, as well as systemic effects in the heart and CNS. Therefore, we have an explanation for the general effect of lithium salts on mood swings. The probability of metastable states of the polyanions just changes decreasing excitability of axons, heart, and CNS.

4.1. The Extracellular Potassium Component of Circling Waves Experiments and Exogeneous Pulses. This type of self-sustained wave activity was created by Martins-Ferreira et al. in 1974 [23] (for its history, see [18]). The other type of self-sustained wave activity in retinas is the sequence of spiral waves [73].

A metal ring cut a circle of tissue in central retina, separating it from the rest of the tissue. A wave elicited on the outer ring had one wavefront killed by aspersion of magnesium chloride (4 mEq/L). The other front will keep circling for several hours (typically 3 to 4 hours). In most retinas, the inner circle remains quiescent but sometimes a region of it will start "spontaneous" (not deliberately elicited) waves. When the inner circle wave reaches the border, in the gap between the inner and outer circles, extracellular potassium activity increases. This gap is filled by the perfusion solution, set at 6 mEq/L of potassium (in this gap, concentration and activity are about the same). If the recording electrode in the outer circle position is at 0.5 mm or closer to the border, extracellular potassium activity transients are recorded associated with the inner circle wave. If the position is farther than 0.5 mm, no transient extracellular potassium appears in the recording. This observation shows the tissue long-range correlations for ion activities in the neuropil.

Figure 3 shows two extracellular potassium transients associated with inner circle "spontaneous" waves (arrows). The numbers on the side of the potassium and potential records show the peak value for each successive circling wave. These values are typical of spreading depression waves recorded in neuropil. The kinetics of both wave concomitants are of the more usual shape: an abrupt rise and long-lasting relaxation to prewave values.

The first inner circle wave alters the recovery of the extracellular potassium wave recorded in the outer circle. The second produces a potassium activity transient typical of exogenous potassium application. In the extracellular potential recording, there is no visible alteration caused by both extracellular potassium transients. Therefore, there is no simple relation between the kinetics of ion activity and extracellular potential recorded nearby (double barrel pipettes). Moreover, there is no linear rise in potassium preceding the abrupt rise that signals the wave onset, nor a potential rise within the neuropil associated with the second potassium transient.

What changes in the record of Figure 3 is the baseline potassium activity, which was 4 mEq/L at the end of the record. At the beginning, the value was 6 mEq/L, the same as the perfusion solution. The potassium baseline value at the end of the record is 4 mEq/L. This retina is maintaining extracellular potassium level below 6 mEq/L used in the perfusion solution for about 30 minutes. This is possible only if potassium is being pumped by glia and accumulated intracellularly or if the potassium activity is being checked by electrostatic screening.

The active transport of potassium is attributed to the Na/K ATPase. Reichenbach et al. [61] showed that the glial pump is driven by extracellular potassium and that its work is adaptive (the rate of transport adjusting to the potassium level). At 2 mEq/L or below, the pumping stops. At 12 mEq/L, it reaches the maximum rate. This maximum rate was estimated at billions of ATP cleavages (3×10^9) per cell per minute. Glial Na/K ATPases can change the stoichiometric ratio of 3 Na for 2 K in situations of low Na, high K, or high depolarization. In these situations, potassium will be transported even in the absence of sodium. There must exist a synergic action between the kinetics of potassium channels and glial pumping rates; otherwise, the

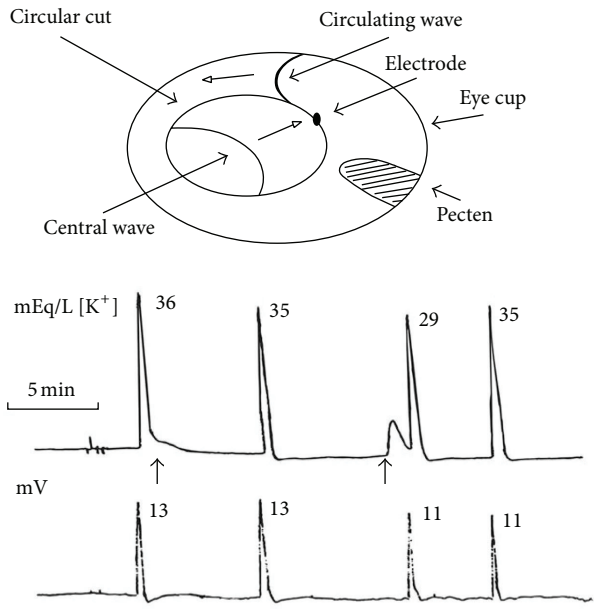

Figure 3: Schema of circling wave experiment with a potassium sensitive electrode inserted in the inner plexiform layer. A circular cut created an inner circular area separating the outer ring and the inner circle. The gap is filled with the perfusion solution. A wave is elicited in the outer ring and one wavefront is killed by aspersion with a high $MgCl_2$ (4 mEq/L) solution. The perfusion rate is transiently increased such that the remaining wavefront is kept propagating. The electrode was positioned within 0.5 mm of the border of the circular cut. The potassium activity and the extracellular local potential are recorded simultaneously. At the side of each potassium activity wave and extracellular potential drop, the peak values are shown in mEq/L and mV. The values shown are typical of this type of experiment, as well as the shape of the potassium and potential wave concomitants. "Spontaneous" waves appeared at the inner circle and potassium activity increased in the solution gap and at the inner plexiform layer of the outer ring. Two potassium activity transients are shown (arrows). Note that both do not influence local extracellular potential, although the potassium activity waves were affected (expected in system with hysteresis). Note also that the relation between potential and potassium peaks is not linear (modified from [74]).

dissipation of potassium gradients would lead the glial cells toward potassium equilibrium in tens of seconds. We can see from the figure that the tissue maintains neuropil potassium activity not in equilibrium, with the perfusion solution at the inner limiting membrane being kept in this state for tens of minutes.

As shown in the figure, the interwave interval increases between the second and third wave and then decreases between the third and fourth ones. Usually, a retina maintains a uniform mean spread velocity for long periods (hours), if left undisturbed. The system can maintain the *metastable* state far from equilibrium for hours, with the circling wave still spreading during the relative refractory state. The shorter the absolute refractoriness, the higher the spread velocity in the relative refractory period (see [75, 76] for the details). Therefore, we can say that this retina had fluctuations on its absolute refractory *period* and was in a nonstationary state.

What did not change in the record shown in Figure 3 was the abrupt rise of potassium and the potential drop when the front wave invaded the region sampled by the electrode. In 74 circling waves, the peaks of the simultaneously measured time derivative of potassium activity and potential drop coincided [77], suggesting tight coupling between the two wave concomitants, although there is no linear causality between them. In a different series, the simultaneously recorded time derivative of potential and of the μIOS (the brightness of a 50 μm square pixel matrix overlaying the electrode tip inserted in the inner plexiform layer) of retinal waves also showed coincidence between the extracellular potential drop and the change in the optical signal [17]. In summary, the rate of fast changes at wave onset in potassium activity, potential drop, and optical properties are tightly coupled events.

The effects of exogenous potassium applied in retinas can be different from the ones shown in Figure 3 and reported previously for experiments with slow pulses [77]. If a very fast pulse of high concentration KCl (200 mEq/L and 200 μL) is asperged with pipettes very close to the inner limiting membrane, then the local potential and optical response can behave as shown in Figure 4.

The simultaneously recorded local potential and the μIOS time series were stored. Later, the time derivative was calculated [17]. Figure 4 shows the potential, the time derivative, and the μIOS time series. Note that the extracellular local potential rises with pulse and with no latency measurable with our slow sampling rate (10 Hz). The potential rise recovers exponentially in about 3 seconds. Then, the system is at a supracritical state for 10 seconds, when the usual potential drop signals the onset of excitation propagation. The potential drop has the usual abrupt onset and slow relaxation in one minute, but the recovery is not complete: a small negative shift persists for five minutes. The time derivative shows two components clearly separated and in different directions.

The μIOS shows an increase in tissue transparency with kinetics close to the potential rise and 10 seconds later the usual abrupt onset of light scatter at wave onset. The recovery of the tissue transparency stops at a plateau level (the duration of plateaus is 15–20 minutes in different retinas). The results show that the same agent elicits opposite electrical and optical responses, demonstrating that there is no simple relationship between ion activities and tissue transitions of states. However, "complex" does not mean "inscrutable," and an electrochemical interpretation of these results is possible.

With fast pulses close to the inner limiting membrane, KCl is pushed toward the endfeet layer. In solution, potassium and chloride have the same mobility and they occupy the same relative position in the Hofmeister series. They are both named *chaotropic*. The rise in potential means that more potassium than chloride reaches the endfeet membrane. In other words, electroneutrality does not hold. The negative charges of the polyanions in the gel and the lipids heads of the bilayer will repel chloride, and the endfeet membrane potential rises just as it rises in lipid bilayers in response to fast solutions changes [78]. The endfeet membrane area is a considerable part of the total area of the glial cells, and the membrane is continuous with the rest of the cell, so that the whole surface cell membrane potential rises. The recording

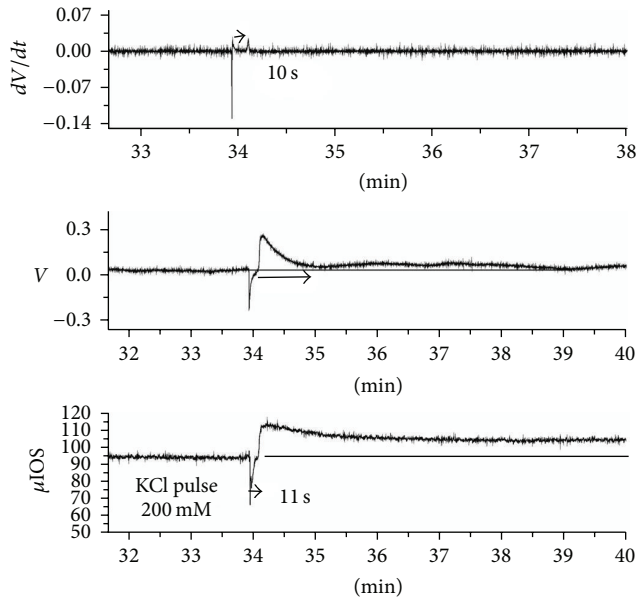

Figure 4: Experiment with fast high concentration KCl solution asperged over the inner limiting membrane (200 mEq/L and 200 μL) with an Eppendorf pipette. The local potential and local IOS (the average brightness of a 50 μm square matrix overlaying the electrode tip) were simultaneously recorded. In the upper row, the dV/dt time series, calculated from the potential time series, shows two separated peaks. The potential time series is in the middle row and the μIOS in the lower row. Note that, in this context, both the IOS and potential show two components: a potential rise at the inner plexiform layer coincides with transient hypertransparency. We interpret this component as the "passive" response of the endfeet bilayer responding to the sudden potassium increase. Note that electroneutrality is broken for three seconds. Ten seconds later, the typical potential drop of retinal waves coincides with the typical wave light scatter increase. We interpret this response as the "active" response of the glial network/synapses, corresponding to the cooperative conformational change in the polyelectrolyte gel. The μIOS time series recovery stops at a plateau level, as well as the potential time series, although the small negative potential only lasts 5 minutes. Note also that in the 10-second interval between the two components the system is at a supercritical state. Ten seconds separates the two dV/dt components and eleven seconds the two peaks of the μIOS. The potential drop has the typical one-minute duration of retinal waves recorded at the inner plexiform layer.

electrode inserted in the inner plexiform layer senses this potential.

There is a long held hypothesis that the Müller cells act as light guides. It is radial glia elongated from inner limiting membrane to outer limiting membrane, with its nuclei on the side of the body pushed out from the light pathway. Recently, experimental evidence appears to confirm this hypothesis (for a summary and relevant literature, see [45]). The endfeet shape acts as a lens and its refractive index matches the *humour vitreous*. The rise in surface potential of the endfeet changed the shape in favor of the light pathway through the retina, increasing transparency. This is one pathway of glial cells modulating retina activity, thus promoting functional plasticity.

The experiment shown in Figure 4 belongs to a series in which the macroscopic IOS also was recorded simultaneously with the time series displayed in the figure [17]. The hypertransparency was also recorded at macroscopic scale (1 mm diameter circular area of central retina). We estimated that about 15.000 Müller cells and 180.000 endfeet responded synchronously to the fast KCl pulse. It is possible that, inside the tubules of glia at the inner plexiform layer, the glial acidic protein filaments helped to create photonic crystals allowing more light to traverse the cell. After a few seconds, potential and transparency were back to baseline values; however, the excess potassium made the system unstable and a wave was triggered 10 seconds after the pulse. The potassium rise at the inner plexiform layer at the wave onset coincides with the second component of the dV/dt time series [77]. The potential drops and the tissue transparency falls abruptly. Again, a structural change in the glial network can explain the result: now conformation changes in the polyanionic gel liberate potassium from screening sites in a cooperative manner typical of "volume phase transitions" in these gels [3, 4]. The polyelectrolytes conformational changes change the membrane potential and ions activities. The loss of the structured interfacial water makes the hydronium ions associated with it disappear and pH shifts both intra- and extracellularly in the alkaline direction within the glial network [42, 43]. The loss of the photonic crystals decreases the tissue transparency (see section on deuterium).

4.2. The Extracellular Calcium Waves in Circling Waves Experiments and Intracellular Calcium Fluorescence in Solitary Circular Waves. The extracellular calcium activity was also recorded in circling waves experiments. Figure 5 shows three segments in our experiment with duration of 4 hours.

In the initial period shown in Figure 5, the circling wave passes the region sampled by the calcium sensitive electrode at regular intervals and with the local potential drop and calcium activity fall with similar amplitudes in the successive waves. The tissue is in a steady metastable state. Then, the calcium concentration in the perfusion solution was switched from 1 to 0.1 mEq/L for 10 minutes. For 3 minutes after the solution was equilibrated in the retinal chamber, calcium activity in the neuropil did not change; after that, it begins a slow fall reaching 0.6 mEq/L at the end of low calcium perfusion. The baseline calcium activity was back to control 10 minutes after the end of the low calcium perfusion. There was a small and slow negative shift of the local potential. The amplitudes of the electrochemical wave concomitants did not change but the recovery of the calcium transient was somewhat extended. It seems that immobilized calcium within the gel was being liberated in order to maintain homeostasis. Ionic exchanges at the membrane surface can explain the results.

The abrupt fall in calcium activity at wave onset begins at the peak of the local potential drop and potassium increase derivatives. The fall in activity is one to two log units in different retinas. The recovery to baseline apparently has a fast and a slow component. Waves with only a small amplitude and slow kinetics calcium activity have been occasionally

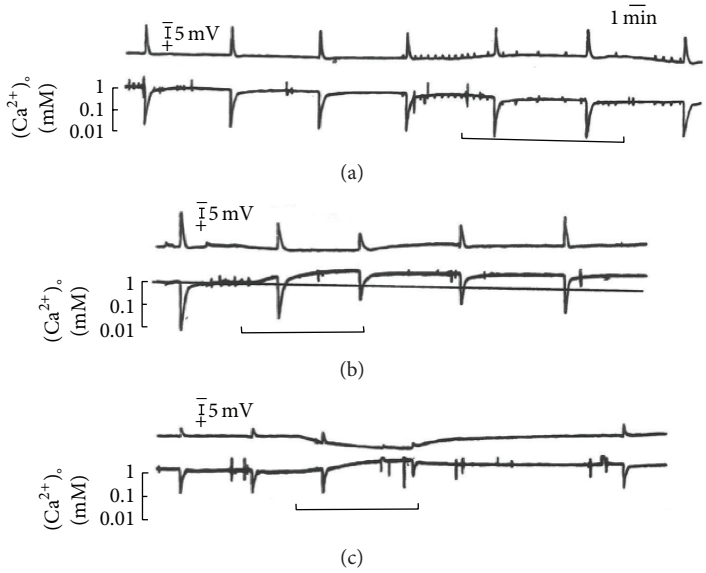

Figure 5: Circling wave experiment recording with calcium sensitive electrode and local potential glass electrodes inserted at the inner plexiform layer. (a) In the initial hour of the experiment, the circling wave spreads with uniform velocity. The extracellular calcium activity falls two log units from 1 to 0.01 mEq/L. The bar shows the change in the perfusion solution from 1 mEq/L to 0.1 mEq/L. Note that the fall in baseline calcium activity at the neuropil is very slow and reaches the value of 0.6 mEq/L at the end of the pulse. The wave transients do not change. Note the slower propagation velocity with low calcium. (b) 40 minutes later, the system returned to control values for the wave concomitants and propagation velocity. Flunarizin 2 μM was applied for 8 minutes. The baseline calcium activity increased to 3.2 mEq/L at the end of the pulse. The wave concomitants were smaller. Note the increase in propagation velocity under the influence of flunarizin. It took 40 minutes of flunarizin washing off for the baseline calcium activity to return to control level. (c) Third hour of circling wave recording, one hour after the last wave in (b). Barium chloride (4 mEq/L) was applied. Note the depression of potential and calcium transient during turning waves. Barium was the agent which could depress the potential drop to zero and slow propagation to a factor of 5 times slower. There was an increase in the baseline calcium and a positive shift in the baseline extracellular potential in the presence of barium (figure modified from [79]).

recorded (see [80]). However, more frequently, we recorded circling waves without changes in calcium activity (see the next section). Calcium differs from the monovalent cations and magnesium in the ability to make cross-links provoking conformational changes in polyelectrolytes (as we already commented in the results with alginic acids measurements of 99% bound calcium). All membrane receptors and channels are glycoproteins with the sugars shown as tree branches protruding into the extracellular gel. It is possible then that most of the fall in activity is due to the ion-polymer interaction and not to the transfer through channels from the extra- to the intracellular compartment. Calcium activity increases intracellularly in astrocytes at wave onset, but not always [43, 81]. Measurements with calcium sensitive dyes in *in vitro* retinas showed that even in one spreading wave calcium signal could be absent in large patches of the tissue; in [82], the scatter of red light and of exogenous calcium dye fluorescence is shown, in which a large patch of a spreading wave lacks both signals, while the scatter of green light was seen in the area. In [82, 83], it was shown that barium addition in the perfusion solution blocked the intracellular calcium signal and the red light scatter of a propagating retinal wave, without affecting the green light scatter of the wave.

Barium was also applied to circling waves. Figure 5(c) shows an example of barium application to a circling wave experiment. The bar shows the time when the barium added solution (4 mEq/L) reached equilibrium. The local potential rises slowly and the potential drop associated with the waves becomes smaller and smaller. The baseline activity of the calcium electrode shows an increase and a smaller calcium transient in the second wave recorded in the presence of barium. Barium also had profound effects on the kinetics of the extracellular potassium wave transients (see [80]). The peak amplitude was increased and the recovery slowed down. Also baseline potassium was maintained below 6 mEq/L for a prolonged period. However, the more pronounced effect of barium was in the spread velocity of circling waves. An effect on the absolute refractory period could explain the slower spread velocity of circling waves.

Barium does increase the absolute refractory period; it almost doubles it [76]. In two separate sets of mechanically elicited, solitary waves experiments [69, 83], barium had a marked effect on the amplitude of the local potential drop and the spread velocity of retinal waves. In one of the experimental series [69], from 10 out of the 17 waves elicited in the presence of barium, 7 had complete depletion of the potential amplitude. The other 10 waves appeared in (a mean of) 39% of controls with the peak of the derivative appearing in 31% of controls. However, barium did not change the shape of the dispersion relation curve but only shifted it to lower values

for all the interwave intervals tested [76]. The effect on the spread velocity thus appears to be independent of metabolic effects of barium. Physicochemical or lyotropic effects appear to dominate barium effects. For monovalent cations, the position in the Hofmeister series correlates well with the value of the Jones-Doyle viscosity B coefficient [67]. This coefficient is a direct measure of the ion-water interactions normalized for water-water interactions. The B coefficients for cations are magnesium 0.385, calcium 0.285, barium 0.220, lithium 0.150, and sodium 0.086. They are all said to be *kosmotropes*. Potassium −0.007 and cesium −0.045 are said to be *chaotropes*. For example, calcium is prone to promote aggregation of macromolecules (or even membranes), one of the mechanisms behind "volume phase transitions" of polyanions. These effects are apparently used in nature to form tight junctions and desmosomes. Lithium has 14 times the affinity for carboxylate side chains in peptides compared to magnesium [84]. Magnesium has spatial constraints for charge interaction [66].

Figure 5(b) shows the marked effect of flunarizine [79] on the baseline activity of calcium in the neuropil. It reached 3.2 mEq/L and persisted for more than 20 minutes after the pulse. After forty minutes, the baseline calcium was back to 1 mEq/L. Unlike barium, flunarizine increased the spread velocity of circling waves ($n = 4$ retinas and 6 pulses). Low calcium perfusion slows down propagation, but there is no simple relationship between high calcium activity and spread velocity in circling waves experiments.

A detailed study on the role of extracellular calcium and propagating retinal waves used zwitterionic (phosphatidylcholine, PC) and negatively charged phospholipids (phosphatidylserine), as well as sialic acid, to compare their effects with exogenous applied gangliosides [85]. Sialic acid (1 mM) was able to make the tissue unexcitable in about 2.5 hours. Its effect was washed off in 30 minutes. Gangliosides had a similar effect at 50 μM. The more glycosylated the side chains, the more pronounced the effect. Washing the tissue for two or more hours did not reverse the ganglioside effect. Spread velocity and the shape and intensity of the IOS also were depressed by sialic acid and gangliosides, either in solitary circular waves protocols or in circling waves. PC had no effect and PS smaller effects than gangliosides at 500 μM. EGTA at 800 μM had smaller effects than the gangliosides (at 50 μM).

Gangliosides are found exclusively at the outer leaflet of lipid bilayers of mammalian membranes. They form the nearest polyanion layer to the lipids and trap calcium ions. The depression of the IOS amplitude by gangliosides suggests that conformational changes at the endfeet membrane were responsible for the optical and spread velocity effect on the waves.

4.3. Wave Propagation with Nonstationary Glial-Neural Dynamics in the Neuropil. Circling waves experiments are especially suited to observe the conditions compatible with the spread of excitation waves within the neuropil. The absence of the local potential drop and of the calcium activity fall transients was the common absence recorded. Extracellular potassium increase in activity was always present but its shape and peak values could vary.

Figure 6 shows one circling wave experiment in which for 31 turns of the circling wave the local potential drop did not occur; then, from wave 32 to wave 42, a small amplitude potential drop appeared (around 2 mV). The circling stopped when a marked increase in extracellular potassium activity elicited a "spontaneous" wave that collided with the original circling one, annihilating each other. Two waves were recorded by the electrode within this potassium activity transient in which the activity reached 37 mEq/L.

The extracellular potassium transients had a low amplitude and variable shape in the first 10 turns and began to stabilize in the typical shape and grow in amplitude at turn 32. Note the two small oscillations in the baseline potassium activity, the second just before the prolonged high amplitude transient. The observed IOS of the circling waves ensures the existence of propagation.

Figure 7 shows a record of a solitary circular wave with zero potential drop. In this series, local potentials were recorded with the IOS at two spatial scales: 1 mm circular area sampled by a photomultiplier (labelled IOS in the figure) and the pixel brightness of a square matrix overlying the region of the inserted electrode tip calculated from digitized frames from a camera (labelled in the figure as μIOS). The local extracellular potential (labelled V) is the upper row time series. The three time series were simultaneously recorded. Note the abrupt rise of the IOS at the micro spatial scale and the smooth growth of the photomultiplier signal. The photomultiplier is integrating the light scatter of all μIOS within the circular area, such that the peak of the photomultiplier signal is set at the point when the wave covers half of the sampled circular area. The peak of time derivative of the μIOS and of the local potential matched in 44 circular waves of 34 retinas [17]. Therefore, in this wave, we found the peak of the time derivative of the μIOS and looked at the local potential time series to see what was happening. A very small (order of μV), sharp transient coincided with the maximum rate of change of the μIOS shown in the figure (marked by an asterisk). If the optical properties of the tissue depend to a large extent on the light guide role of glial cells, then this geometric change can happen and propagate without the local *synchronous* potential drop in the neuropil of the inner plexiform layer.

Figure 8 shows a circling wave experiment in which for 10 turns the ion-sensitive electrode did not show calcium transients. The local potential had the typical shape and amplitude and then lost amplitude, inverted to local potential rises in the next 20 turns, and inverted to potential drops again for the next 11 turns. Other examples of "positive potential" waves are shown in [80]. At turn 11, the recording electrode was changed to potassium sensitive and the extracellular potassium transients associated with the circling wave show variable kinetics and low amplitude until the end of the recording. These experiments show clearly the nonlinearities in the system. Just as there are several B-Z system "recipes," excitation in the neuropil propagates with the interacting glial-synaptic membranes at different states and these states can change within a circling wave experiment with 3 to 4 hours of recording time. In other words, it is a flexible dynamical system.

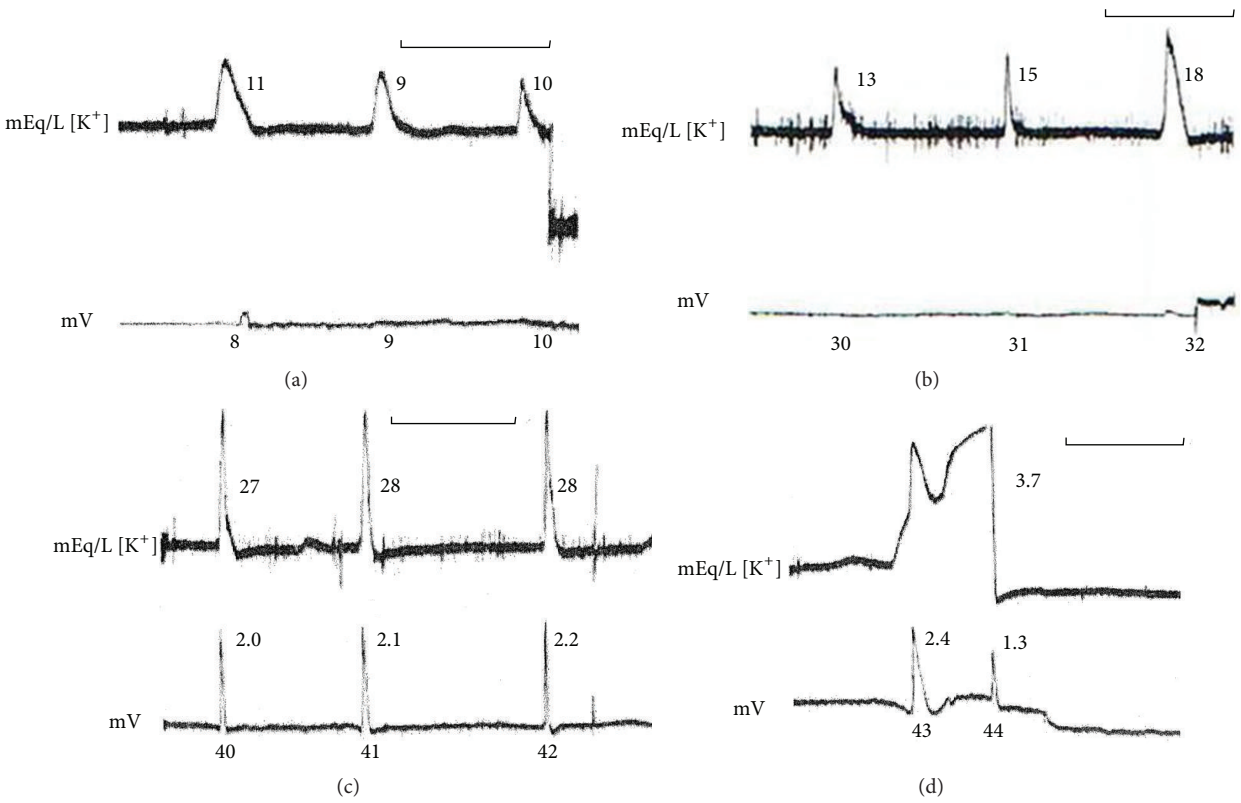

Figure 6: Plastic dynamics between the glia network and synaptic terminals in a circling wave experiment with 4-hour recording time. Potassium sensitive electrode and local potential recorded at the inner plexiform layer. The horizontal bars in each square show 7 minutes of time in the record. Below each wave is the number of the turns that reached the electrode tip. In the first 31 turns, the local potential did not show the "typical" potential drop and the extracellular potassium activity wave change showed low amplitude and changed shape (or kinetics). Then, at turn 32, a small potential drop appeared and the peak of the potassium waves increased to typical values. The potential waves also increased in amplitude but remained one order of magnitude smaller than the "typical" values (above 10 mV). Note the fast kinetics of the potential and ion activity waves at 40–42. Note also the small oscillations of potassium activity in (a) and (c) before the long (order of minutes) potassium increase that interacted with two propagating neuropil waves. The long potassium activity transient begins with a linear growth and potential rise within the neuropil; then, a second linear growth interacts with the turning wave invading the area and the extracellular potential drops. This second linear growth also had an IOS that showed a standing pattern that lasted for 24 minutes and faded without leaving lesions behind. The value of potassium activity reached 37 mEq/L. This value was maintained for 24 minutes and the return to baseline control levels took another 20 minutes. As usual, one wave was elicited at the border of the standing pattern and this wave killed the previous circling wave on collision. One hour after the circling stopped, the retina was readily excitable by mechanical touches and 8 waves were elicited with shape and amplitudes similar to the ones in 40–43 turns. This experiment illustrates well the plastic dynamics between glia and synaptic terminals membranes interactions and the nonlinear system response to any particular macroscopic wave concomitant precluding linear causality among these concomitants (modified from [79]).

5. Conceptual, Physical, and Mathematical Models

In this section, we apply some concepts derived from chemical and electrochemical excitable media to the brain. Some predictions derived from the field and from the physical-chemical properties of polyelectrolytes have been fulfilled and they help to understand the brain dynamics.

What is now termed the field of excitable media had, at its origin, the confluence of three factors: the fast increase in computer power for simulations, the discovery (by western researchers) of the chemical system created by Boris Belouzov in the fifties of the XX century [19, 86], and, almost simultaneously, the acceptance of the theoretical model of Ilya Prigogine for chemical self-organization [21]. The recognition of the spreading depression wave as a phenomenon akin to the B-Z system by one of the leaders of the spreading depression research, Bureš, led to the second prediction about these CNS waves: the existence of evolving sequences of spiral waves [73, 87].

Forty years later, the existing knowledge about these systems permits some generalizations. First, the system where they occur must be far from thermodynamical equilibrium (plenty of energy is available for dissipation); second, positive feedback of some kind is present at the wave onset (autocatalysis in chemical systems, interfacial electrical field at electrochemical systems [88]). There is slow inhibition following the explosive growth of a component of the system.

Mathematically, a nonlinear (quadratic or cubic) growth, followed by linear slow decay, is the minimum requirement

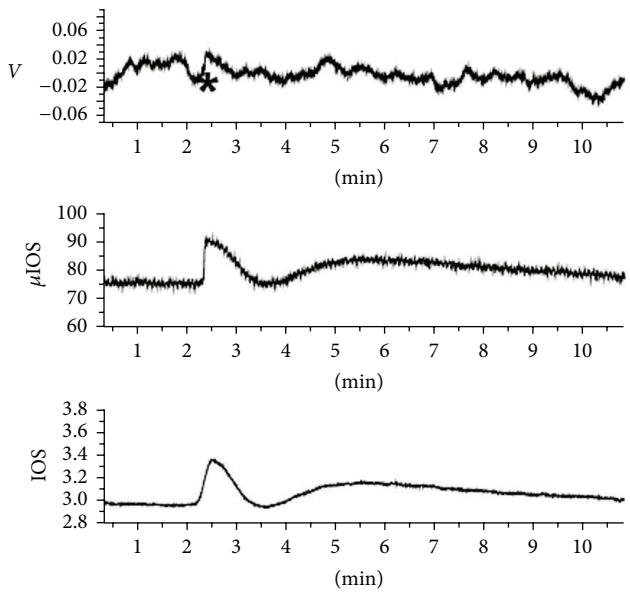

Figure 7: Extracellular potential recorded at the inner plexiform layer and the wave IOS recorded simultaneously. The IOS was recorded at two different spatial scales. μIOS time series depicts the mean brightness of the 50 μm square pixel matrix overlaying the electrode tip and IOS the photomultiplier output that samples the scattered photons of a circular area of central retina with a 1 mm diameter. The wave recorded was from a series of 44 isolated circular waves from 34 retinas [17]. This wave had a "zero potential" record at the usual amplification. However, when the time derivative of the μIOS was calculated, a small sharp transient (about 200 μV/100 ms) coincided with the peak of $d\mu$IOS/dt, suggesting that asynchronous small transients were present at the inner plexiform layer instead of the typical synchronous potential drop at wave onset. Note the sharp onset of the μIOS, whose peak coincided with the macroscopic IOS peak (the electrode tip is at the centre of the photomultiplier's sampled circle) and slow smooth growth of the IOS time series: the photomultiplier is integrating (summing up) many μIOS signals from a large area.

for self-organization. These systems exhibit a rich behavioral repertoire. The system has at least three states: quiescent but ready to be excited, excited, and refractory to excitation. The refractoriness goes from absolute to relative before the system is back to quiescence. For example, both computer simulations and experiments with bulk reactors showed that the temporal behavior of the B-Z system changed from a simple limit circle to complex periodic states to chaotic behavior, depending on the rate of pumping matter or chemical energy in the system. In two dimensions, waves appear in the form of either target patterns (Figure 1) or sequence of spirals [73].

The heart can be conceived as a machine designed to produce excitation waves in three dimensions, while the axons of neurons produce them in one dimension. This knowledge explains why the retina is such a good model for experiments with two-dimensional excitation waves: the CNS slice has an intact network in which only the output axons are cut behind the sclera. In the perfusion solution, glucose concentration (30 mM) is higher than the physiological 20 mM found in the avian liquor. Furthermore, the network is wired for transduction of electromagnetic energy; in order to observe the waves, illumination is used. This second source of energy in retinas is physiological. Only good shape retinas with plenty of energy to expend will display waves. The fact that the initial phase of the wave is very similar to the onset of excitotoxic responses brings about some confusion for experiments with other preparations. The complete optical profile of these two states makes them easily recognizable in retinas [44] and the recovery of excitability after an episode of excitotoxic response ensures the functionality of the network.

Both cortical and retinal neuropils display excitation waves, but with different probabilities and geometry of the wavefront, due to the differences in the geometry of the glial network [18]. The same structure will also display macroscopic oscillations (alpha and theta EEG cortical rhythms) and standing patterns (a good guess for *petit mal* seizures).

Katchalsky predicted that electrochemical patterns in the brain would happen at the suprasynaptic or macroscopic scale and that wave propagation would show coherent flow of matter or energy. An almost horizontal dipole standing around a mechanical stimulus zone (see Figure 19 of [83]) produces a pattern that shimmers and shifts in place, suggesting a dynamic pattern of space/time energy oscillations. The predicted coherent flow was demonstrated by Rovinsky and Menzinger [89] in a series of experiments with the B-Z system. They constructed an almost one-dimensional system, but one can also say that they created a system analogous to the neuropil: they filled a tube of 3.2 mm diameter and 25 cm length with 40 μm microspheres coated with cation exchanger resin (sulfate polyanion). Upon this coat, ferroin was loaded to act as catalyzer. The microspheres had 40 μm average diameter and they were packed to fill the maximum packing density, leaving 30% of the tube volume for the reactors solution. In other words, a convoluted space with a high surface-to-volume ratio separates facing reactive surfaces, in a similar fashion to the neuropil. Coherent flow was demonstrated beyond any doubt. The propagating wavelengths were in the order of centimeters. The authors called attention to the presence of the same organizing principle in electrolytes in the presence of energy fields, as predicted by Katchalsky.

Another significant result from excitable media is the almost perfect two-dimensional system of Flätgen et al. [88]. The authors recorded images of potentials drops and two-dimensional waves propagated at velocities of meters/second, the order of magnitude of action potential propagation. They stated that they did not interpret this as mere coincidence, and neither do we. If Tasaki's membrane model is used, then the action potential is a surface or interfacial electrochemical phenomenon: "The cortical gel layer of nerve fibers has the properties of a cation exchanger. Hence, this layer can, and actually does, undergo a reversible abrupt structural change when monovalent cations (e.g., Na^+) are substituted for the divalent counter-ions (e.g., Ca^{2+}). This structural change brings about a sudden rise in the water content of the layer, which in turn produces a large enhancement of cation mobilities accompanied by a shift of ion-selectivity in favor of hydrophilic cations" [4]. In the present interpretation,

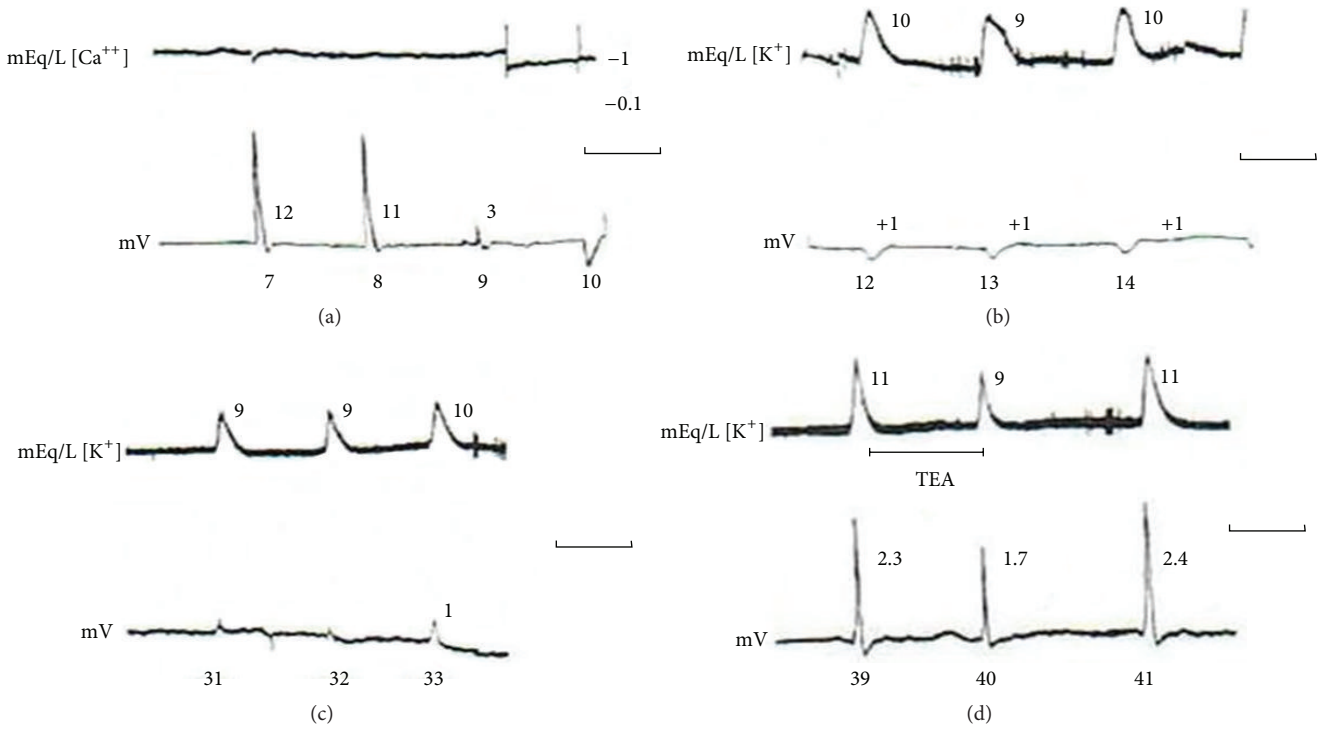

Figure 8: Circling experiment with 4-hour recording time and changing extracellular potential and ion activity concomitants. The horizontal bars show the recording length of 7 minutes. (a) First-hour recording time, waves 7–10, calcium sensitive electrode inserted at the inner plexiform layer. Only wave turn 7 has a small extracellular calcium transient. The extracellular potential drop looked typical for turns 7 and 8 and dropped markedly in amplitude for turn 9. The electrode was reinserted nearby (about 1 mm away) and the calcium transient was still zero with the extracellular potential changing direction from negative to positive for turns 10 to 20. (b) Second-hour recording time; the calcium electrode was replaced by a potassium sensitive electrode. Wave turns at 12–14. Low amplitude and variable shape of the potassium activity wave and potential rises in the extracellular inner plexiform layer occur. The "positive" potential waves were present from turns 10 to 20, and from 21 to 26 there were "zero potential" waves. (c) Third-hour recording time. Small potential drops reappear and persist from turns 33 to 39, when a pulse of 3 mM TEA was applied. TEA depressed the amplitude of potassium and potential waves and slowed down their propagation velocity (modified from [74]).

interfacial water also transiently changes states from the structured interfacial water to bulk liquid.

However, the most interesting model of excitable system, in the present context, was created by Wüssling and collaborators in 1999 [90–92]. They inserted fragments of sarcoplasmic reticulum membrane of muscle in the polyanionic gel of agarose and demonstrated optically the existence of calcium activity waves. All the requirements of excitable media were present (the first of their papers [90] is a good introduction to the field). Furthermore, these experiments show how the experimental context changes the behavior of the system: the addition of mitochondria to the gel and membrane increased the wave propagation velocity in the first publication; however, changing the distribution of the elements from aggregates to a more uniform one changed the response to mitochondrial activity. This excitable medium is probably the simplest model for biological relevant ion activity waves, and its constituents are a polyanionic gel with positive feedback on calcium release by ryanodine receptors. The slow kinetics of the transporters provide the negative feedback. Ryanodine receptors have been identified as a source of cytoplasmic calcium on astrocytes [93].

Katchalsky also predicted that what he called the mechanoelectric coupling of polyelectrolytes could be used in biology when phase transitions would produce mechanical work. This is exactly the case for the mechanical behavior of inner ear hair cells: the integral membrane protein prestin has a prominent intracellular loop and is expressed in assemblies of molecules. A change of monovalent anion to a divalent one at the intracellular loop triggers the cooperative conformational change (phase transition) that spreads through the assembly [94, 95].

The biological significance of the results with Nafion gels can be found by means of a description of exclusion zones (EZs) in microvessels. Venules and capillaries have 0.5 μm zone that excludes red blood cells and colloidal particles [96–98]. The structured water around the polyelectrolyte fixes the negative charges vibrating in place. The important points here reiterated are as follows: the structured water is a very dynamic and fragile structure that promotes charge separation, and charge separation is energy. The vessels use this energy to facilitate the flow. Nafion tubes submerged in water showed self-driven flow in the absence of pressure gradient [99]; furthermore, white and UV light increased the flow velocity.

6. Discussion

We have assumed an excitable media and polyelectrolytic approach to explain ionic oscillations and waves in neuropil. We also interpreted B-Z with deuterium experiments from an electrochemical point of view. Usually, B-Z is seen as a chemical self-organized system. However, the role of hydronium ions in organizing coherent flow is the simplest explanation for the excitability collapse of B-Z systems and retinas. There is little doubt now that water can store charge [35, 100, 101]. Therefore, interfacial water is not electroneutral, including the unstirred layer of bilayers and the hydration of polyanions of the extracellular and intracellular gels.

The structure of the neuropil membranes and interacting gel between them generates electrical fields; fields imply forces, and forces can direct a coherent flow of charges (e.g., in hydronium ions). A direct demonstration of this type of far-from-equilibrium flow has been published [99]. This effect was not fully taken into account [89]; although a residual flow due to gravitational field was recognized, the additional electrical field effect was not considered in the interpretation of the behavior of excitable media. The polyanionic gel was considered to be just a passive element [90–92], since the deuterium effects on retinas and B-Z were first presented [28, 29]. With hindsight, the intrinsic electrical field effects could be the unifying factor in all these excitable media.

Bunkin studied the optical properties of interfacial water and demonstrated its birefringence [37, 38]. It is long known as the birefringence of axons (e.g., [1]). He called attention to the similarity of the optical properties of interfacial water and quasi-liquid crystals [39] (photonic crystals behavior of this water). The first photonic crystals described were dielectrics. The pioneers of proposing the importance of the dielectric properties of brain and cells were Frölich and Adey [102–106]. The intrinsic electric field of the neuropil membranes and the polyelectrolytes between them compose a vibrating, self-organizing system. Macroscopic patterns can be formed, as we have seen with a large dipole (Figure 19 of [83]). These patterns can store information, as proposed by Neumann and Katchalsky [11]. The brain, heart, and kidney could be systems for which the state of water is functional.

The proposal of Hameroff and Penrose [107] of using quantum mechanical concepts to explain consciousness has one direct piece of experimental evidence: the resonant vibrations of energy found in a single *wet* microtubule (then promoted to a nanotubule status) [108]. However, *dry* microtubules did not show this energy. The authors probably were not aware of the work of Pollack and Bunkin showing that water interaction with microtubules is far from unique. The Nafion experiments and exclusion zones of microvessels suggest that the energy of interfacial water is ubiquitous in physiology. The brain, after all, could be a "smart gel" machine [109] in which some phase transitions are perceived as functional pathologies (epilepsies, migraine aura, and transient global amnesia).

The use of concepts from nonlinear thermodynamics has the additional advantage of permitting experiments at very convenient time and space scales, without the abstraction of the concepts derived from quantum mechanics, such as the famous "wave collapse" that has been the object of a long controversy among specialists. Focusing on these spatiotemporal scales does not imply complete abandonment of quantum-like concepts, since an understanding of the properties of ions and their biological milieu, as well as their interactions, demands explanations based on quantum theories.

The distortion in perception described in migraine aura, hallucinations in the onset of complex seizures, and the impairment of learning and memory described by experimenters with cortical spreading depressions show how electrochemical patterns are close to higher mental functions [8, 110, 111].

A question able to suggest further experiments concerns the little discussed aspect of the asymmetry of the biological membranes lipid bilayers and associated gels. The zwitterionic phosphatidyl choline predominates in the external leaflet of human red cells membranes, while the negatively charged phosphatidyl serine predominates at the internal leaflet. Computer simulations showed that this asymmetry creates electrical fields [112]. Furthermore, glycolipids (gangliosides) and glycoproteins are exclusive of the external leaflet. The polyanion of the associated gel has carboxyl and sulfate as the predominant fixed anions in the external face, while phosphates are found in the intracellular milieu. Volume phase transitions [113] appear to be the conformational change that spreads at the external gel, while polymerization is the main change in the intracellular gel. The significance of this asymmetry alone could sustain a research program. We have measured in the retina long-range correlations of the order of 300–500 μm (see Figure 3 in this paper and [114]). Another experimental result that is still in need of explanation is the fact that the light scatter of the retinal IOS has a red component that differs from the green light scatter in temporal and spatial distribution [83, 114–116]. The red scatter follows closely the potential drops and preceded propagation, displaying fluctuations, while the green scatter is the hallmark of propagation. Barium blocks the red scatter and glycerol predominantly the green part of the IOS. The second component of optical profiles has close coupling to metabolic acceleration [117, 118] and follows an acid shift in the extracellular compartment of the neuropil [42]. The kinetics of this component are independent of spatial scale [17] and its IOS spectrum has broad smooth appearance [115]. The green red preference found in the first component of the optical profile experimental manipulations is another issue for further investigation.

7. Concluding Remarks

Early interpretations of the function of astroglial ionic waves concentrated on neuroastroglial bidirectional glutamatergic mechanisms activating calcium waves. This interpretation was recently put into question by experiments with IP3 pathway knockout mice, revealing that blocking the release of calcium ions from the endoplasmatic reticulum mediated by the inositol pathway does not cause serious behavioral impairment in cognitive tasks [119]. While glutamatergic gliotransmission was questioned, new findings have suggested

important roles for the astroglial control of potassium homeostasis in brain function [120, 121]. The findings reviewed in this paper suggest an original interpretive hypothesis addressing the mechanisms of neuron-glia interactions and related cognitive functions: the movements of calcium and potassium ions inside astrocytes and from astrocytes to neurons compose *a coherent hydroionic wave* with essential roles in brain and mental functions [122–124].

The activity of extracellular potassium and calcium changes the structure and state of excitable membranes in both glia and neurons. The kinetics of the sodium pump as well as membrane channels are changed in both networks with consequent changes in the intracellular ionic environment and metabolism. The spread of such changes is continuous in brain tissue and depends on the integrity of extracellular polyanionic gel and its capacity for phase transitions. This capacity is not impaired in IP3R2 knocked out mice [119], since Ca^{2+} signaling in astrocytes relevant for the hydroionic wave and related phase transitions is dependent on the ryanodine.

Conflict of Interests

The authors declare that there is no conflict of interests regarding the publication of this paper.

Acknowledgment

FAPESP is acknowledged for financial support to Alfredo Pereira Jr.

References

[1] I. Tasaki, A. Watanabe, R. Sandlin, and L. Carnay, "Changes in fluorescence, turbidity, and birefringence associated with nerve excitation," *Proceedings of the National Academy of Sciences of the United States of America*, vol. 61, no. 3, pp. 883–888, 1968.

[2] I. Tasaki, "Rapid structural changes in nerve fibers and cells associated with their excitation processes," *Japanese Journal of Physiology*, vol. 49, no. 2, pp. 125–138, 1999.

[3] I. Tasaki, "Repetitive abrupt structural changes in polyanionic gels: a comparison with analogous processes in nerve fibers," *Journal of Theoretical Biology*, vol. 236, no. 1, pp. 2–11, 2005.

[4] I. Tasaki, "On the reversible abrupt structural changes in nerve fibers underlying their excitation and conduction processes," in *Phase Transitions in Cell Biology*, G. H. Pollack and W. C. Chin, Eds., pp. 1–21, Springer, Dordrecht, The Netherlands, 2008.

[5] A. Katchalsky, "Carriers and specificity in membranes. VI. Biological flow structure and their relation to chemodiffusion coupling," *Neurosciences Research Program Bulletin*, vol. 9, no. 3, pp. 397–413, 1971.

[6] A. Katchalsky, "Polyelectrolytes and their biological interactions," *Biophysical Journal*, vol. 4, no. 1, part 2, pp. 9–41, 1971.

[7] E. Neumann, D. Nachmansohn, and A. Katchalsky, "An attempt at an integral interpretation of nerve excitability," *Proceedings of the National Academy of Sciences of the United States of America*, vol. 70, no. 3, pp. 727–731, 1973.

[8] K. S. Lashley, "Patterns of cerebral integration indicated by the scotomas of migraine," *Archives of Neurology And Psychiatry*, vol. 46, no. 2, pp. 331–339, 1941.

[9] I. Tasaki and J. J. Chang, "Electric response of glia cells in cat brain," *Science*, vol. 128, no. 3333, pp. 1209–1210, 1958.

[10] R. Galambos, "A glia-neural theory of brain function," *Proceedings of the National Academy of Sciences of the United States of America*, vol. 47, no. 1, pp. 129–136, 1961.

[11] E. Neumann and A. Katchalsky, "Hysteretic conformational changes in biopolymers induced by high electric fields. Model for a physical record of biological memory," in *Proceedings of the 1st European Biophysics Congress*, E. Broda, Ed., vol. 6, pp. 91–96, Wiener Medizinische Akademie, Baden, Austria, September 1971, CODEN: 24KMAA, CAN 76:82256 AN 1972:82256 CAPLUS.

[12] L. M. Marshall, J. R. Sanes, and U. J. Mcmahan, "Reinnervation of original synaptic sites on muscle fiber basement membrane after disruption of the muscle cells," *Proceedings of the National Academy of Sciences of the United States of America*, vol. 74, no. 7, pp. 3073–3077, 1977.

[13] J. R. Sanes, L. M. Marshall, and U. J. McMahan, "Reinnervation of muscle fiber basal lamina after removal of myofibers. Differentiation of regenerating axons at original synaptic sites," *Journal of Cell Biology*, vol. 78, no. 1, pp. 176–198, 1978.

[14] C. Ide, K. Tohyama, R. Yokota, T. Nitatori, and S. Onodera, "Schwann cell basal lamina and nerve regeneration," *Brain Research*, vol. 288, no. 1-2, pp. 61–75, 1983.

[15] S. A. Jo and S. J. Burden, "Synaptic basal lamina contains a signal for synapse-specific transcription," *Development*, vol. 115, no. 3, pp. 673–680, 1992.

[16] T. Strekalova, M. Evans, A. Chernopiatko et al., "Deuterium content of water increases depression susceptibility: the potential role of a serotonin-related mechanism," *Behavioural Brain Research*, vol. 277, pp. 237–244, 2015.

[17] V. M. F. de Lima, J. R. C. Piqueira, and W. Hanke, "The tight coupling and non-linear relationship between the macroscopic electrical and optical concomitants of electrochemical CNS waves reflect the non-linear dynamics of neural glial propagation," *Open Journal of Biophysics*, vol. 5, pp. 1–20, 2014.

[18] V. M. W. Hanke and V. M. W. Fernandes de Lima, "Relevance of excitable media theory and retinal spreading depression experiments in preclinical pharmacological research," *Current Neuropharmacology*, vol. 12, no. 5, pp. 413–433, 2014.

[19] A. M. Zhabotinsky, "Belousov-Zhabotinsky reaction," *Scholarpedia*, vol. 2, no. 9, article 1435, 2007.

[20] V. Zykov, "Excitable media," *Scholarpedia*, vol. 3, no. 5, article 1834, 2008.

[21] I. Prigogine and R. Lefever, "Symmetry breaking instabilities in dissipative systems. II," *The Journal of Chemical Physics*, vol. 48, no. 4, pp. 1695–1700, 1968.

[22] M. A. F. Faria, *Depressão alastrante e reação de Belouzov-Zabotinsky [M.S. thesis]*, Instituto de Biofísica, Universidade Federal do Rio de Janeiro, Rio de Janeiro, Brazil, 1980.

[23] H. Martins-Ferreira, G. De Oliveira Castro, C. J. Struchiner, and P. S. Rodrigues, "Circling spreading depression in isolated chick retina," *Journal of Neurophysiology*, vol. 37, no. 4, pp. 773–784, 1974.

[24] W. Hanke, M. Wiedemann, and V. M. Fernandes de Lima, "Control of the excitability of neuronal tissue by weak external forces," *Faraday Discussions*, vol. 120, pp. 237–248, 2001.

[25] M. Wiedemann, V. M. Fernandes de Lima, and W. Hanke, "Gravity dependence of waves in the retinal spreading depression and in gel-type Belousov-Zhabotinsky systems," *Physical Chemistry Chemical Physics*, vol. 4, no. 8, pp. 1370–1373, 2002.

[26] M. Wiedemann, F. P. M. Khon, H. Roesner, and W. R. L. Hanke, *Self-Organization and Pattern-Formation in Neuronal Systems Under Conditions of Variable Gravity*, Springer, Berlin, Germany, 2011.

[27] J. J. Katz, "Chemical and biological studies with deuterium," *American Scientist*, vol. 48, no. 4, pp. 544–580, 1960.

[28] O. Klink, W. Hanke, E. Gebershagen, and V. M. Fernandes de Lima, "Influence of heavy water on waves and oscillations in the Belouzov-Zabotinsky reaction," in *Wave Propagation in Materials for Modern Applications*, A. Petrin, Ed., p. 21, InTech Books, Morn Hill, UK, 2010.

[29] V. M. F. de Lima and W. Hanke, "Modulation of CNS excitability by water movement. The D_2O effects on the non-linear neuron-glial dynamics," *Journal of Biophysical Chemistry*, vol. 2, no. 3, pp. 353–360, 2011.

[30] M. McDaniel, F. M. Sulzman, and J. W. Hastings, "Heavy water slows the *Gonyaulax* clock: a test of the hypothesis that D_2O affects circadian oscillations by diminishing the apparent temperature," *Proceedings of the National Academy of Sciences of the United States of America*, vol. 71, no. 11, pp. 4389–4391, 1974.

[31] D. Landowne, "D_2O and the sodium pump in squid nerve membrane," *The Journal of Membrane Biology*, vol. 96, no. 3, pp. 277–281, 1987.

[32] A. B. Mamonov, R. D. Coalson, M. L. Zeidel, and J. C. Mathai, "Water and deuterium oxide permeability through aquaporin 1: MD predictions and experimental verification," *Journal of General Physiology*, vol. 130, no. 1, pp. 111–116, 2007.

[33] J.-M. Zheng and G. H. Pollack, "Long-range forces extending from polymer-gel surfaces," *Physical Review E: Statistical, Nonlinear, and Soft Matter Physics*, vol. 68, no. 3, part 1, Article ID 031408, 2003.

[34] J.-M. Zheng, W.-C. Chin, E. Khijniak, E. Khijniak Jr., and G. H. Pollack, "Surfaces and interfacial water: evidence that hydrophilic surfaces have long-range impact," *Advances in Colloid and Interface Science*, vol. 127, no. 1, pp. 19–27, 2006.

[35] K. Ovchinnikova and G. H. Pollack, "Can water store charge?" *Langmuir*, vol. 25, no. 1, pp. 542–547, 2009.

[36] B. Chai and G. H. Pollack, "Solute-free interfacial zones in polar liquids," *The Journal of Physical Chemistry B*, vol. 114, no. 16, pp. 5371–5375, 2010.

[37] N. F. Bunkin, P. S. Ignatiev, V. A. Koslov, A. V. Shikirin, S. D. Zhakarov, and A. A. Zinchenko, "Study of the phase states of water close to nafion interface," *Water*, vol. 4, pp. 129–154, 2013.

[38] N. F. Bunkin, V. S. Gorelik, V. A. Kozlov, A. V. Shkirin, and N. V. Suyazov, "Colloidal crystal formation at the 'nafion-water' interface," *Journal of Physical Chemistry B*, vol. 118, no. 12, pp. 3372–3377, 2014.

[39] F. Shvartzman and V. Korngauz, "Quasi-liquid crystals," *Nature*, vol. 309, pp. 609–611, 1984.

[40] M. S. Weimer and W. Hanke, "Correlation between the durations of refractory period and intrinsic optical signals of retinal spreading depression during temperature variations," *Experimental Brain Research*, vol. 161, no. 2, pp. 201–208, 2005.

[41] A. Vercesi and H. Martins-Ferreira, "Oxygen and glucose requirements in chick spreading depression," *Anais da Academia Brasileira de Ciências*, vol. 55, no. 3, pp. 309–316, 1983.

[42] C. R. Ferreira Filho and H. Martins-Ferreira, "Interstitial fluid pH and its change during spreading depression in isolated chicken retina," in *Spreading Depression*, R. DoCarmo, Ed., pp. 75–88, Springer, Berlin, Germany, 1992.

[43] R. P. Kraig, "Interrelation of astrocytic pH and calcium changes during spreading depression," in *Migraine: Basic Mechanisms and Treatment*, A. Lehmenkueller, K. H. Grotemeyer, and F. Tegtmeyer, Eds., pp. 309–318, Urban & Schwarzenberg, Munich, Germany, 1993.

[44] V. M. F. de Lima and W. Hanke, "The kinetics of non-synaptically triggered acute excitotoxic responses in the central nervous system observed using intrinsic optical signals," *CNS & Neurological Disorders—Drug Targets*, vol. 11, no. 2, pp. 132–141, 2012.

[45] A. Reichenbach and A. Bringmann, *Müller Cells in the Healthy and Diseased Retina*, Springer, New York, NY, USA, 2010.

[46] S. Gloor, H. Antonicek, K. J. Sweadner et al., "The adhesion molecule on glia (AMOG) is a homologue of the beta subunit of the Na,K-ATPase," *The Journal of Cell Biology*, vol. 110, no. 1, pp. 165–174, 1990.

[47] G. Schmalzing, S. Kröner, M. Schachner, and S. Gloor, "The adhesion molecule on glia (AMOG/β_2) and α_1 subunits assemble to functional sodium pumps in *Xenopus oocytes*," *The Journal of Biological Chemistry*, vol. 267, no. 28, pp. 20212–20216, 1992.

[48] J. A. A. Silva, P. Spencer, M. A. Camillo, and V. M. F. Lima, "Gyroxin and its biological activity: effects on CNS basement membranes and endothelium and protease-activated receptors," *Current Medicinal Chemistry*, vol. 19, no. 2, pp. 281–291, 2012.

[49] G. E. Hermann, M. J. Van Meter, J. C. Rood, and R. C. Rogers, "Proteinase-activated receptors in the nucleus of the solitary tract: evidence for glial-neural interactions in autonomic control of the stomach," *Journal of Neuroscience*, vol. 29, no. 29, pp. 9292–9300, 2009.

[50] J. Maurer, S. Haselbach, O. Klein, D. Baykut, V. Vogel, and W. Mäntele, "Analysis of the complex formation of heparin with protamine by light scattering and analytical ultracentrifugation: implications for blood coagulation management," *Journal of the American Chemical Society*, vol. 133, no. 4, pp. 1134–1140, 2011.

[51] V. M. Fernandes de Lima, P. Spencer, and W. Hanke, "Interaction of small cationic peptides with intact basement membranes. A study using intrinsic optical signals of chick retinas," *Current Medicinal Chemistry*, vol. 21, no. 12, pp. 1458–1466, 2014.

[52] A. L. Lehninger, "The neuronal membrane," *Proceedings of the National Academy of Sciences of the United States of America*, vol. 60, no. 4, pp. 1069–1080, 1968.

[53] S. B. Backman, I. Gilron, and R. Robbins, "Protamine-induced hypotension and bradycardia in a cardiac transplant patient," *Canadian Journal of Anaesthesia*, vol. 44, no. 5, pp. 520–524, 1997.

[54] G. J. Tangelder and K.-E. Arfors, "Inhibition of leukocyte rolling in venules by protamine and sulfated polysaccharides," *Blood*, vol. 77, no. 7, pp. 1565–1571, 1991.

[55] M. Sieber, B. Bosh, W. Hanke, and V. M. F. de Lima, "Membrane-modifying properties of crotamine, a small peptide-toxin from *Crotalus durissus terrificus* venom," *Biochimica et Biophysica Acta—General Subjects*, vol. 1840, no. 3, pp. 945–950, 2014.

[56] A. Zaher, S. S. Iver, and B. M. Bragança, "Influence of charge on the inactivation of membrane bound Na-K ATPase of Yoshida sarcoma cells by inhibitor proteins from Cobra venoms," *Cancer Biochemistry Biophysics*, vol. 3, pp. 123–127, 1979.

[57] A. Zaheer, S. H. Noronha, A. V. Hospattankar, and B. M. Braganca, "Inactivation of (Na^+ + K^+)-stimulated ATPase by a cytotoxic protein from cobra venom in relation to its lytic effects on cells," *Biochimica et Biophysica Acta*, vol. 394, no. 2, pp. 293–303, 1975.

[58] C. C. Chang and K. H. Tseng, "Effect of crotamine, a toxin of South American rattlesnake venom, on the sodium channel of murine skeletal muscle," *British Journal of Pharmacology*, vol. 63, no. 3, pp. 551–559, 1978.

[59] A. C. S. Matavel, D. L. Ferreira-Alves, P. S. L. Beirão, and J. S. Cruz, "Tension generation and increase in voltage-activated Na^+ current by crotamine," *European Journal of Pharmacology*, vol. 348, no. 2-3, pp. 167–173, 1998.

[60] C. T. Rizzi, J. L. Carvalho-de-Souza, E. Schiavon, A. C. Cassola, E. Wanke, and L. R. P. Troncone, "Crotamine inhibits preferentially fast-twitching muscles but is inactive on sodium channels," *Toxicon*, vol. 50, no. 4, pp. 553–562, 2007.

[61] A. Reichenbach, A. Henke, W. Eberhardt, W. Reichelt, and D. Dettmer, "K^+ ion regulation in retina," *Canadian Journal of Physiology and Pharmacology*, vol. 70, pp. S239–S247, 1992.

[62] Z. Xie and T. Cai, "Na+-K+-ATPase mediated signal transduction: from protein interaction to cellular function," *Molecular Interventions*, vol. 3, no. 3, pp. 157–167, 2003.

[63] G. J. Lees, "Inhibition of sodium-potassium-ATPase: a potentially ubiquitous mechanism contributing to central nervous system neuropathology," *Brain Research Reviews*, vol. 16, no. 3, pp. 283–300, 1991.

[64] M. Wiedemann and W. Hanke, "The chicken retina as an experimental model for investigation of central nervous lesions," *Neuroscience Letters*, vol. 232, no. 2, pp. 99–102, 1997.

[65] I. Tasaki, I. Singer, and T. Takenaka, "Effects of internal and external ionic environment on excitability of squid giant axon. A macromolecular approach," *Journal of General Physiology*, vol. 48, no. 6, pp. 1095–1123, 1965.

[66] R. J. P. Williams, "Tilden Lecture. The biochemistry of sodium, potassium, magnesium, and calcium," *Quarterly Reviews, Chemical Society*, vol. 24, no. 3, pp. 331–365, 1970.

[67] K. D. Collins, "Ions from the Hofmeister series and osmolytes: effects on proteins in solution and in the crystallization process," *Methods*, vol. 34, no. 3, pp. 300–311, 2004.

[68] Y. Zhang and P. S. Cremer, "Interactions between macromolecules and ions: the Hofmeister series," *Current Opinion in Chemical Biology*, vol. 10, no. 6, pp. 658–663, 2006.

[69] N. L. V. Peixoto, *A depressão alastrante na retina [M.S. thesis]*, Graduate School of the Faculty of Electrical Engineering, University of Campinas (UNICAMP), 1997.

[70] G. Isenberg and W. Trautwein, "The effect of dihydro-ouabain and lithium-ions on the outward current in cardiac Purkinje fibers," *Pflügers Archiv*, vol. 350, no. 1, pp. 41–54, 1974.

[71] E. J. Ploeger, "The effects of lithium on excitable cell membranes. On the mechanism of inhibition of the sodium pump of non-myelinated nerve fibres of the rat," *European Journal of Pharmacology*, vol. 25, no. 3, pp. 316–321, 1974.

[72] R. C. A. Guedes, L. F. Amorim, M. C. Medeiros, A. T. Silva, and N. R. Teodosio, "Effect of dietary lithium on cortical spreading depression," *Brazilian Journal of Medical and Biological Research*, vol. 22, no. 7, pp. 923–925, 1989.

[73] M. A. Dahlem and S. C. Müller, "Self-induced splitting of spiral-shaped spreading depression waves in chicken retina," *Experimental Brain Research*, vol. 115, no. 2, pp. 319–324, 1997.

[74] V. M. Fernandes de Lima and W. R. L. Hanke, "Observations of non-stationarities in extracelular potassium dynamics within the gray matter neuropil during self-sustained SDs," *Journal of Brain Research*, vol. 37, no. 4, pp. 505–518, 1996.

[75] S. Brand, M. A. Dahlem, V. M. F. de Lima, S. C. Müller, and W. Hanke, "Dispersion relation of spreading depression waves in the chicken retina," *International Journal of Bifurcation and Chaos*, vol. 7, no. 6, pp. 1359–1365, 1997.

[76] S. Brand, V. M. Fernandes de Lima, and W. Hanke, "Pharmacological modulation of the refractory period of retinal spreading depression," *Naunyn-Schmiedeberg's Archives of Pharmacology*, vol. 357, no. 4, pp. 419–425, 1998.

[77] V. M. F. de Lima, J. R. C. Piqueira, and W. Hanke, "The synergetic modulation of the excitability of central gray matter by a neuropeptide: two protocols using excitation waves in chick retina," *Anais da Academia Brasileira de Ciências*, vol. 81, no. 1, pp. 1–11, 2009.

[78] D. R. Laver and B. A. Curtis, "Surface potentials measure ion concentrations near lipid bilayers during rapid solution changes," *Biophysical Journal*, vol. 71, no. 2, pp. 722–731, 1996.

[79] V. M. Fernandes de Lima, D. Scheller, W. Hanke, and W. R. Schlue, "Neuronal-glial interactions during 'en masse' propagating activity: the retinal spreading depression as a good pharmacological tool," in *Migraine: Basic Mechanisms and Treatment*, A. Lehmemkueller, K. H. Grotemeyer, and F. Tegtmeyer, Eds., pp. 547–562, Urban & Schwarzenberg, Munich, Germany, 1993.

[80] V. M. Fernandes de Lima, D. Scheller, F. Tegtemeir, W. Hanke, and W. R. Schlue, "Self-sustained spreading depression and short-term neuronal-glial interactions within the gray matter neuropil," *Brain Research*, vol. 614, pp. 45–51, 1993.

[81] T. A. Basarsky, S. N. Duffy, R. D. Andrew, and B. A. MacVicar, "Imaging spreading depression and associated intracellular calcium waves in brain slices," *Journal of Neuroscience*, vol. 18, no. 18, pp. 7189–7199, 1998.

[82] V. M. Fernandes de Lima and W. Hanke, "Excitation waves in central grey matter: the retinal spreading depression," *Progress in Retinal and Eye Research*, vol. 16, no. 4, pp. 657–690, 1997.

[83] V. M. F. de Lima, M. Goldermann, and W. R. L. Hanke, "Calcium waves in gray matter are due to voltage-sensitive glial membrane channels," *Brain Research*, vol. 663, no. 1, pp. 77–83, 1994.

[84] J. Kherb, S. C. Flores, and P. S. Cremer, "Role of carboxylate side chains in the cation hofmeister series," *Journal of Physical Chemistry B*, vol. 116, no. 25, pp. 7389–7397, 2012.

[85] V. M. F. de Lima, M. Wiedemann, H. Klotigg, H. Rahmann, and W. Hanke, "Exogenous application of gangliosides changes the state of excitability of retinal tissue as demonstrated by retinal spreading depression experiments," *Naunyn-Schmiedeberg's Archives of Pharmacology*, vol. 355, no. 4, pp. 507–514, 1997.

[86] A. N. Zaikin and A. M. Zhabotinsky, "Concentration wave propagation in two-dimensional liquid-phase self-oscillating system," *Nature*, vol. 225, no. 5232, pp. 535–537, 1970.

[87] N. A. Gorelova and J. Bureš, "Spiral waves of spreading depression in the isolated chicken retina," *Journal of Neurobiology*, vol. 14, no. 5, pp. 353–363, 1983.

[88] G. Flätgen, K. Krischer, B. Pettinger, K. Doblhofer, H. Junkes, and G. Ertl, "Two-dimensional imaging of potential waves in electrochemical systems by surface plasmon microscopy," *Science*, vol. 269, no. 5224, pp. 668–671, 1995.

[89] A. B. Rovinsky and M. Menzinger, "Self-organization induced by the differential flow of activator and inhibitor," *Physical Review Letters*, vol. 70, no. 6, pp. 778–781, 1993.

[90] M. H. P. Wüssling, K. Krannich, G. Landgraf et al., "Sarcoplasmic reticulum vesicles embedded in agarose gel exhibit propagating calcium waves," *FEBS Letters*, vol. 463, no. 1-2, pp. 103–109, 1999.

[91] M. H. P. Wussling, K. Krannich, V. Drygalla, and H. Podhaisky, "Calcium waves in agarose gel with cell organelles: implications of the velocity curvature relationship," *Biophysical Journal*, vol. 80, no. 6, pp. 2658–2666, 2001.

[92] H. H. Podhaisky and M. H. P. Wussling, "The velocity of calcium waves is expected to depend non-monotoneously on the density of the calcium release units," *Molecular and Cellular Biochemistry*, vol. 256-257, no. 1-2, pp. 387–390, 2004.

[93] D. Oppelt, R. Rodnight, J. Horn et al., "Role of intracellular calcium stores on the effect of metabotropic glutamate receptors on phosporylation of glial fibrillary acidic protein in hippocampal slices from immature rats," *Neurochemical Research*, vol. 29, no. 8, pp. 1541–1545, 2004.

[94] D. Oliver, D. Z. Z. He, N. Klöcker et al., "Intracellular anions as the voltage sensor of prestin, the outer hair cell motor protein," *Science*, vol. 292, no. 5525, pp. 2340–2343, 2001.

[95] J. Ashmore, "Cochlear outer hair cell motility," *Physiological Reviews*, vol. 88, no. 1, pp. 173–210, 2008.

[96] C. B. S. Henry and B. R. Duling, "Permeation of the luminal capillary glycocalyx is determined by hyaluronan," *The American Journal of Physiology—Heart and Circulatory Physiology*, vol. 277, no. 2, pp. H508–H514, 1999.

[97] A. R. Pries, T. W. Secomb, and P. Gaehtgens, "The endothelial surface layer," *Pflügers Archiv*, vol. 440, no. 5, pp. 653–666, 2000.

[98] K. P. Arkill, C. Knupp, C. C. Michel et al., "Similar endothelial glycocalyx structures in microvessels from a range of mammalian tissues: evidence for a common filtering mechanism?" *Biophysical Journal*, vol. 101, no. 5, pp. 1046–1056, 2011.

[99] M. Rohani and G. H. Pollack, "Flow through horizontal tubes submerged in water in the absence of a pressure gradient: mechanistic considerations," *Langmuir*, vol. 29, no. 22, pp. 6556–6561, 2013.

[100] R. F. Gouveia and F. Galembeck, "Electrostatic charging of hydrophilic particles due to water adsorption," *Journal of the American Chemical Society*, vol. 131, no. 32, pp. 11381–11386, 2009.

[101] L. P. Santos, T. R. D. Ducati, L. B. S. Balestrin, and F. Galembeck, "Water with excess electric charge," *Journal of Physical Chemistry C*, vol. 115, no. 22, pp. 11226–11232, 2011.

[102] H. Frölich, "The extraordinary dielectric properties of biological materials and the action of enzymes," *Proceedings of the National Academy of Sciences of the United States of America*, vol. 72, no. 11, pp. 4211–4215, 1975.

[103] H. Frölich, "Coherent electric vibrations in biological systems and the cancer problem," *IEEE Transactions on Microwave Theory and Techniques*, vol. 26, no. 8, pp. 613–617, 1978.

[104] S. M. Bawin and W. R. Adey, "Sensitivity of calcium binding in cerebral tissue to weak environmental electric fields oscillating at low frequency," *Proceedings of the National Academy of Sciences of the United States of America*, vol. 73, no. 6, pp. 1999–2003, 1976.

[105] S. M. Bawin, W. R. Adey, and I. M. Sabbot, "Ionic factors in release of 45Ca2+ from chicken cerebral tissue by electromagnetic fields," *Proceedings of the National Academy of Sciences of the United States of America*, vol. 75, no. 12, pp. 6314–6318, 1978.

[106] W. R. Adey, "Electromagnetic fields, the modulation of brain tissue functions—a possible paradigm shift in biology," in *International Encyclopedia of Neuroscience*, B. Smith and G. Adelmann, Eds., Elsevier, New York, NY, USA, 3rd edition, 2003.

[107] S. Hameroff and R. Penrose, "Consciousness in the universe: a review of the 'ORCH OR' theory," *Physics of Life Reviews*, vol. 11, no. 1, pp. 39–78, 2014.

[108] S. Sahu, S. Ghosh, B. Ghosh et al., "Atomic water channel controlling remarkable properties of a single brain microtubule: correlating single protein to its supramolecular assembly," *Biosensors and Bioelectronics*, vol. 47, pp. 141–148, 2013.

[109] A. Kumar, A. Srivastava, I. Y. Galaev, and B. Mattiasson, "Smart polymers: physical forms and bioengineering applications," *Progress in Polymer Science*, vol. 32, no. 10, pp. 1205–1237, 2007.

[110] I. S. Russel and S. Ochs, "One-trial interhemispheric transfer of a learning engram," *Science*, vol. 133, no. 3458, pp. 1077–1078, 1961.

[111] J. Bureš and O. Burešová, "Cortical spreading depression as a memory disturbing factor," *Journal of Comparative and Physiological Psychology*, vol. 56, no. 2, pp. 268–272, 1963.

[112] A. A. Gurtovenko and I. Vattulainen, "Membrane potential and electrostatics of phospholipid bilayers with asymmetric transmembrane distribution of anionic lipids," *Journal of Physical Chemistry B*, vol. 112, no. 15, pp. 4629–4634, 2008.

[113] T. Tanaka, D. Fillmore, S.-T. Sun, I. Nishio, G. Swislow, and A. Shah, "Phase transitions in ionic gels," *Physical Review Letters*, vol. 45, no. 20, pp. 1636–1639, 1980.

[114] M. Goldermann, W. Hanke, A. C. G. de Almeida, and V. M. de Lima, "Observations on the onset and propagation of excitation waves in neural tissue," *International Journal of Bifurcation and Chaos*, vol. 8, no. 7, pp. 1541–1549, 1998.

[115] V. M. Fernandes de Lima, M. Weimer, and W. Hanke, "Spectral dependence of the intrinsic optical signal of excited states of central gray matter and conformational changes at membrane interfaces," *Physical Chemistry Chemical Physics*, vol. 4, no. 8, pp. 1374–1379, 2002.

[116] V. M. Fernandes-de-Lima, J. E. Kogler, J. Bennaton, and W. Hanke, "Wave onset in central gray matter—its intrinsic optical signal and phase transitions in extracellular polymers," *Anais da Academia Brasileira de Ciencias*, vol. 73, no. 3, pp. 351–364, 2001.

[117] G. D. O. Castro, H. Martins-Ferreira, and P. F. Gardino, "Dual nature of the peaks of light scattered during spreading depression in chick retina," *Anais da Academia Brasileira de Ciências*, vol. 57, no. 1, pp. 95–103, 1985.

[118] Y. A. Dahlem and W. Hanke, "Intrinsic optical signal of retinal spreading depression: second phase depends on energy metabolism and nitric oxide," *Brain Research*, vol. 1049, no. 1, pp. 15–24, 2005.

[119] J. Petravicz, K. M. Boyt, and K. D. McCarthy, "Astrocyte IP3R2-dependent Ca^{2+} signaling is not a major modulator of neuronal pathways governing behavior," *Frontiers in Behavioral Neuroscience*, vol. 8, article 384, 2014.

[120] F. N. Quandt and B. A. MacVicar, "Calcium activated potassium channels in cultured astrocytes," *Neuroscience*, vol. 19, no. 1, pp. 29–41, 1986.

[121] F. Wang, N. A. Smith, Q. Xu et al., "Astrocytes modulate neural network activity by Ca^{2+}-dependent uptake of extracellular K^+," *Science Signaling*, vol. 5, no. 218, article ra26, 2012.

[122] A. Pereira Jr., "Perceptual information integration: hypothetical role of astrocytes," *Cognitive Computation*, vol. 4, no. 1, pp. 51–62, 2012.

[123] A. Pereira Jr. and F. A. Furlan, "Astrocytes and human cognition: modeling information integration and modulation of neuronal activity," *Progress in Neurobiology*, vol. 92, no. 3, pp. 405–420, 2010.

[124] A. Pereira Jr., R. P. dos Santos, and R. F. Barros, "The calcium wave model of the perception-action cycle: evidence from semantic relevance in memory experiments," *Frontiers in Psychology*, vol. 4, article 252, 4 pages, 2013.

Hindawi Publishing Corporation
Neural Plasticity
Volume 2016, Article ID 1680905, 7 pages
http://dx.doi.org/10.1155/2016/1680905

Review Article

Glia and TRPM2 Channels in Plasticity of Central Nervous System and Alzheimer's Diseases

Jing Wang,[1] Michael F. Jackson,[2,3] and Yu-Feng Xie[2,3,4]

[1]*Key Laboratory of Orthopedics of Gansu Province, The Second Hospital of Lanzhou University, No. 82 Cui Ying Men, Lanzhou, Gansu 730030, China*
[2]*Department of Pharmacology & Therapeutics, University of Manitoba, Canada*
[3]*Kleysen Institute for Advanced Medicine, University of Manitoba, 710 William Avenue, SR426 Winnipeg, MB, Canada R3E 0Z3*
[4]*Leslie Dan Faculty of Pharmacy, University of Toronto, 144 College Street, Toronto, ON, Canada M5S 3M2*

Correspondence should be addressed to Jing Wang; wang_jing@lzu.edu.cn, Michael F. Jackson; michael.jackson@umanitoba.ca, and Yu-Feng Xie; yufeng711@gmail.com

Received 11 October 2015; Revised 25 December 2015; Accepted 29 December 2015

Academic Editor: Jason H. Huang

Synaptic plasticity refers to the ability of neurons to strengthen or weaken synaptic efficacy in response to activity and is the basis for learning and memory. Glial cells communicate with neurons and in this way contribute in part to plasticity in the CNS and to the pathology of Alzheimer's disease (AD), a neurodegenerative disease in which impaired synaptic plasticity is causally implicated. The transient receptor potential melastatin member 2 (TRPM2) channel is a nonselective Ca^{2+}-permeable channel expressed in both glial cells (microglia and astrocytes) and neurons. Recent studies indicated that TRPM2 regulates synaptic plasticity as well as the activation of glial cells. TRPM2 also modulates oxidative stress and inflammation through interaction with glial cells. As both oxidative stress and inflammation have been implicated in AD pathology, this suggests a possible contribution of TRPM2 to disease processes. Through modulating the homeostasis of glutathione, TRPM2 is involved in the process of aging which is a risk factor of AD. These results potentially point TRPM2 channel to be involved in AD through glial cells. This review summarizes recent advances in studying the contribution of TRPM2 in health and in AD pathology, with a focus on contributions via glia cells.

1. Introduction

Inflammation, oxidative stress, and disturbance of intracellular Ca^{2+} ($[Ca^{2+}]_i$) homeostasis are the most common signaling pathways contributing to many neuropathological conditions and/or diseases, such as Alzheimer's disease (AD), prion-related diseases, parkinsonism-dementia, and chronic neuropathic/inflammatory pain [1–4]. These neuropathological changes are associated with not only the roles played by neurons but also the activation of glial cells (mainly including microglia and astrocytes) and the interaction between neurons and glial cells [1, 2]. Central sensitization is an enhanced state of excitatory synaptic transmission in nociceptive neurons and is a specific form of synaptic plasticity involving neurons and glial cells in the central nervous system (CNS) [5–8]. Synaptic plasticity is the ability of neurons to change the transmission efficacy at synapses to adapt to different conditions, involves glial cells, and is thought of as the mechanism of learning and memory [2, 9–12]. Alzheimer's disease (AD) is a neurodegenerative disease characterized by progressive decline of recognition with advanced age and involves the pathophysiological changes of N-methyl-D-aspartate (NMDA) receptor which is also involved in central sensitization and synaptic plasticity [13–15]. Therefore, through inflammation, glutamate receptor involvement, and neuron-glia communication [2, 6, 7, 16–18], both the central sensitization and synaptic plasticity may be involved in the pathology AD.

As a newly identified nonselective Ca^{2+}-permeable cation channel and the sensor of reactive oxygen species (ROS), transient receptor potential melastatin member 2 (TRPM2) channel has recently been indicated to be involved in

inflammatory/neuropathic pain, synaptic plasticity, oxidative stress, and neurodegenerative diseases through modulation of multiple signaling pathways [17–20]. In addition to being expressed in neurons, the TRPM2 channel is also found to be expressed in glial cells (microglia and astrocytes) and plays important role in pathophysiological conditions [21]. Therefore, TRPM2 channel is an important regulator of plasticity, not only in health but also in AD which is characterized by synapse loss and involves inflammation and oxidative stress [1, 13].

2. TRPM2 Channel Expression in Glial Cells

The glial cells in the CNS mainly include microglia, astrocytes, and oligodendrocytes. The microglia in the CNS function as quiescent immune cells that maintain the homeostasis of brain through surveying the environment and scavenging debris. The astrocytes regulate multiple aspects of neurons and synaptic functions throughout the lifetime, including synapse formation and uptake and recycling of neurotransmitters. Recent study indicates that glial cells also express the TRPM2 channel which plays an important role in immune and inflammatory responses [22, 23]. The protein and mRNA of TRPM2 channel are both confirmed to be expressed in spinal microglia [17, 21, 24, 25]. Consistently, TRPM2-mediated Ca^{2+} current can be detected in cultured microglia [24, 26] while inhibiting the expression of TRPM2 channel by introduction of small interfering RNA (siRNA) into the astrocytes can reduce the inflammation-induced oxidative stress [21]. These results suggest that TRPM2 channel is expressed in microglia and astrocytes in the CNS at both transcriptional and posttranscriptional levels and functions well in these cells.

In addition, the expression of TRPM2 channel in glial cells is affected by multiple stimulations and plays important role in behavior. For example, the expression of TRPM2 mRNA can be increased by cytokine interleukin-1β (IL-1β) in human C13 microglial cells [24]. Oxidative stress can enhance the expression of TRPM2 mRNA in astrocytes through influx of extracellular Ca^{2+} [27]. In carrageenan-induced inflammation and sciatic nerve injury, the expression of TRPM2 mRNA in the inflamed paw and areas around the injured sciatic nerve is increased [17]. In addition, the Ca^{2+} signaling induced by lipopolysaccharide and interferon gamma (LPS/IFNγ) in microglia is absent by pharmacological blockade or gene deletion of TRPM2 channel [28] while deletion of TRPM2 channel attenuates the activation of spinal microglia in the neuropathic pain model with peripheral nerve injury [22, 23]. These studies imply that glial TRPM2 channel may play an important role in the plasticity of the CNS and neurodegenerative diseases such as AD, since the Ca^{2+} signaling, oxidative stress, and inflammation/nerve injury are involved in the plasticity of the CNS and the pathology of AD.

3. Glia and TRPM2 Channel in Central Sensitization and Synaptic Plasticity in CNS

Central sensitization, is a specific use-dependent plasticity of nociceptive neurons in the CNS, can result in pain under normally innocuous stimulus after inflammation or injury, and is thought of as a crucial mechanism underlying the increased excitability of nociceptive pathways in the CNS [5]. Previous studies [6, 7, 29] indicate that inflammatory stimulation of the tooth pulp produces central sensitization of nociceptive neurons in the trigeminal subnucleus caudalis mediated by glutamate, ATP, and mitogen-activated protein kinase p38 (p38MAPK) signaling which are well-known to be involved in the synaptic plasticity [30–32]. In parallel, excitatory synaptic transmission in spinal cord slices, long-term potentiation (LTP, a form of synaptic plasticity to underlie the basic molecular mechanism of learning and memory) in the intact spinal cord, and the central sensitization-driven pain hypersensitivity are impaired in toll-like receptor knockout mice [33]. Astrocytes can release ATP, causing significant attenuation of synaptic inhibition in the pyramidal neurons and facilitating the induction of LTP through neuron-glia communication and action on cannabinoid receptor [34, 35]. Microglia can prune unnecessary synapses and axon terminals during postnatal development and adaptation to novel environments, which plays important role in synaptic remodeling [36, 37]. These studies imply that both central sensitization and synaptic plasticity are involved in learning and memory through the activities of glial cells. This hypothesis is further supported by the study finding that both anxiety and chronic pain are capable of blocking the presynaptic LTP [38].

The involvement of glial cells in sensitization and plasticity is suggested to be related with the TRPM2 channel expressed in glial cells. The TRPM2 channel in microglia and astrocyte is found to be involved in the neurotoxicity mediated by p38MAPK, c-Jun N-terminal kinase (c-JNK), and nuclear factor kappa-B (NFκB) signaling [21] while p38MAPK is involved in the central sensitization mediated by glial cells [7] and in the synaptic plasticity [30]. The Ca^{2+} signaling induced by inflammatory molecules, LPS/IFNγ, in microglia from wild-type mice is absent after pharmacological blockade or gene deletion of TRPM2 channel, while the Ca^{2+} signaling is a mechanism for activation of microglia [28]. Furthermore, the p38MAPK and JNK signaling is suggested to contribute to the LPS/IFNγ-induced activation of microglia mediated by TRPM2 channel [28]. In the neuropathic pain models induced by peripheral nerve injury, the deletion of TRPM2 channel attenuates the neutrophil infiltration through the activation of spinal microglia and the production of chemokine ligand-2 from macrophages around the damaged peripheral nerve [17, 22, 23]. Furthermore, it is found that TRPM2 knock-out mice demonstrate attenuation of nocifensive behaviors in formalin test, mechanical allodynia, and thermal hyperalgesia in carrageenan-induced inflammatory pain and sciatic nerve injury-induced neuropathic pain models [17]. The activation of microglia by nerve injury and the glial chemokines are suppressed by knock-out of TRPM2 channel [17]. Previous studies indicate that the TRPM2 knock-out mice also demonstrate decreased PSD95 and phosphorylation of glycogen synthase kinase-3β (GSK3β), impaired long-term depression (LTD, another form of synaptic plasticity) [39]. These results imply that the TRPM2 channel expressed in glial cells is involved in

the plasticity of CNS in neuropathic and inflammatory pain through aggravating pronociceptive response, which requires further elucidation using specific deletion of TRPM2 channel in glial cells.

4. Glia and TRPM2 Channel in Alzheimer's Diseases

There is increasing evidence suggesting that the pathophysiology of neurodegenerative disorders is related to the inflammatory responses and oxidative stress mediated by microglia through producing neurotoxic factors such as proinflammatory cytokines and nitric oxide that lead to neuronal degeneration [2]. It is found that microglia can be activated by transthyretin amyloid accumulation which in the CNS can cause a kind of fatal and untreatable genetic disease, oculoleptomeningeal amyloidosis, leading to the secretion of inflammatory molecules such as tumor necrosis factor-α (TNF-α), interleukin-6 (IL-6), and nitric oxide, and the neuronal damage [40]. The release of ATP from cortical astrocytes decreases following the age, which impairs the astrocytic modulation of synaptic transmission in neocortex and therefore contributes to the impairment of synaptic plasticity and the age-related decline of cognition [34, 35]. These studies suggest that the glial cells and the neuron-glia communication in the CNS are involved in the functions of brain and the pathology of AD.

AD, a neurodegenerative disorder exhibiting a gradual decline in cognitive function, is characterized by the presence of neuritic plaques composed of neurofibrillary tangles and amyloid beta (Aβ) peptide. Animals treated with Aβ show impaired ability of learning and memory, activated astrocytes and microglial cells, and disturbed activation of c-JNK and GSK3β [41], suggesting activation of glial cells in AD pathology. Astrocytes around the amyloid plaques are found to be activated to produce GABA by monoamine oxidase-B and release GABA through the bestrophin 1 channel. Through acting on presynaptic GABA receptors, the released GABA from astrocytes is capable of decreasing the spike probability of granule cells in the dentate gyrus of AD model mice, impairing the synaptic plasticity and learning and memory [42]. These results provide solid support for the proposal that glial cells are involved in AD. In AD, the neuropathological characteristics of the formation of senile plaques by Aβ is associated with the chronic inflammation involving reactivated astrocytes, microglia, and proinflammatory molecules such as IL-1β, TNF-α, human CCAAT/enhancer-binding protein (CEBP) delta (CEBPD), p38MAPK, and GSK3β. In amyloid precursor protein (APP) transgenic mice, astrocytic CEBPD is associated with the activation and migration of microglia [43]. Furthermore, Aβ derived from transgenic mice is found to be accumulated initially on neurite membranes with normal morphology, rapidly recognized by glial cells, and finally transferred to attenuated processes of microglia and astrocytes [44]. These results suggest that glial processes can recognize the misfolded monomeric or oligomeric membrane proteins accumulated in Aβ amyloidosis which contributes to the cell death and neurotoxicity during AD and prion disease through interaction with cellular prion protein and stress-inducible phosphoprotein-1 [45].

More and more studies suggest that the involvement of glial cells in AD is related with the TRPM2 channel and through inflammation and oxidative stress which are highly involved in the pathology of AD. It is found that TRPM2 channel contributes to the trauma-induced oxidative stress, neuronal apoptosis, mitochondria dysfunction, and $[Ca^{2+}]_i$ increase [46]; all these changes are related with the pathology of AD. As an antioxidant agent, glutathione is found to play an important role in neuronal oxidant defense and AD [47]. Following aging and during the pathology of AD, glutathione is decreased [47] while the increased current of TRPM2 channel in old culture neurons can be decreased by provision of glutathione [48]. Furthermore, depletion of glutathione can induce oxidative stress, disturbance of Ca^{2+} homeostasis, and apoptosis of hippocampal neurons through activation of TRPM2 channel [49]. The Ca^{2+} influx through TRPM2 channel is linked with the change of glutathione level in microglia and astrocytes [21]. ROS such as H_2O_2 can activate TRPM2 channel as plasma membrane channel or intracellular Ca^{2+}-release channel [50] to increase intracellular Ca^{2+} and subsequently to induce cell death via poly[ADP-ribose (ADPR)] polymerase (PARP) activation in macrophage cells [51] which are peripheral encounter part of glial cells in the CNS. It is found that ADPR and H_2O_2 can elicit a large Ca^{2+} influx, cation current in lipopolysaccharide (LPS) treated microglial cells, and activate the TRPM2 channel expressed in microglia [26]. In a rat stroke model by transient middle cerebral artery occlusion, Aβ, ADPR, and H_2O_2 can induce TRPM2 current in microglia [24, 52]. In transcriptional level, oxidative stress and traumatic injury of brain can result in Ca^{2+} influx and enhanced expression of TRPM2 mRNA [27, 53]. Furthermore, oxidative stress induced by inhibition of glutathione biosynthesis can induce human microglia and astrocytes to secrete toxic materials, stimulating them to release TNF-α, IL-6, and nitrite ions and to increase the concentration of intracellular Ca^{2+} ($[Ca^{2+}]_i$) in microglia and astrocytes. These effects are correlated with the activation of inflammatory signaling of p38MAPK, JNK, and NFκB and are reduced by pharmacological blockade of TRPM2 channel or genetic inhibition of TRPM2 channel expression in microglia and astrocytes [21]. These studies suggest that glial TRPM2 channel contributes to AD through inflammation and oxidative stress. Furthermore, recent study indicated that the TRPM2 current in cultured hippocampal neurons can be enhanced by Aβ treatment while TRPM2$^{-/-}$/APP/PS1 transgenic mice demonstrated blockades of increased endoplasmic reticulum stress, age-dependent spatial memory deficit, and reduction of microglial activation although TRPM2$^{-/-}$/APP/PS1 transgenic mice did not show significant change in plaque [20]. These results suggest that deletion of the TRPM2 channel shows protective effect in the AD pathology, which may be achieved through the activation of microglia servicing as the scavenger in the brain and remain to be further studied using specific deletion of TRPM2 channels in glial cells.

Table 1: Major references studying TRPM2 channel in plasticity and AD.

Experimental approach	Effects	Reference
TRPM2 KO hippocampal slice	Deficit in LTD, GSK3β inactivation	[39]
TRPM2 KO glia and neuron culture	Glutathione homeostasis loss, inflammation	[21, 48]
TRPM2 KO animal stroke	Neuroprotection, GSK3β inhibition	[54]
Expression of TRPM2 in striatal culture, Aβ/oxidative stress	Cell death	[52]
Human microglia culture, rat brain ischemia, inflammation/oxidative stress/electrophysiology	TRPM2 activated in microglia by ADPR	[24]
TRPM2 KO, ROS and inflammation in whole animal	Negative feedback	[19]
Neuropathic and inflammatory pain in TRPM2 KO animal	Inhibition of microglia and pain in KO mice	[17, 22]
Expression of TRPM2 in human glioblastoma, oxidative stress	Promoting cell death	[55]
Electrophysiology in microglia, ADPR/H_2O_2	Induction of Ca^{2+} influx and TRPM2 current	[26, 56]
Diabetic rat, brain and DRG	TRPM2 activity and oxidative stress enhanced	[50]
Pharmacological gene deletion of TRPM2 in microglia	TRPM2 mediates inflammation through p38MAPK/JNK	[28]
TRPM2/APP/PS1 KO mice	Absent microglia activation and memory impairment	[20]

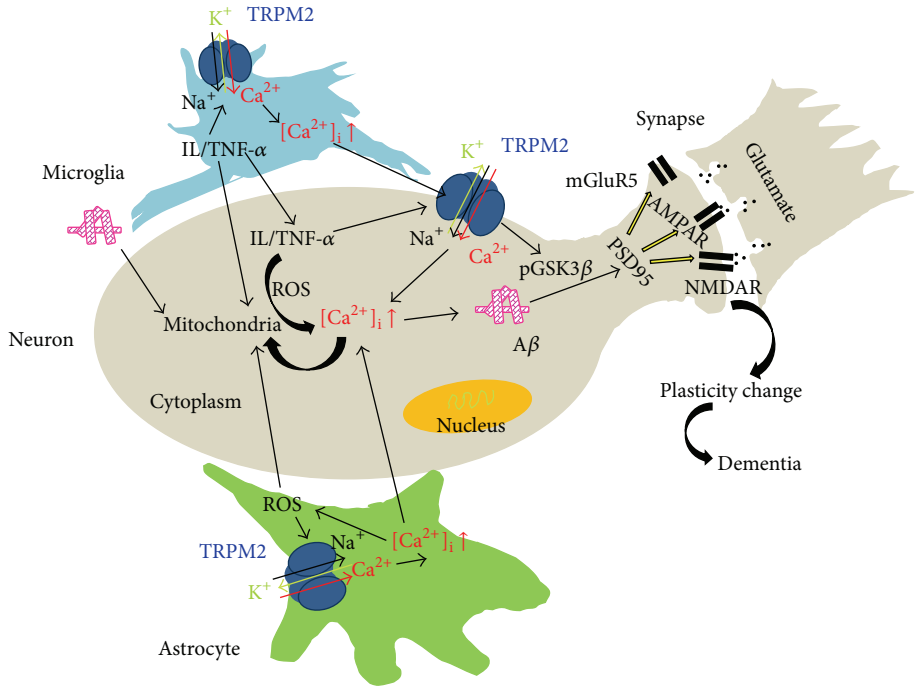

Figure 1: A schematic figure for the involvement of glial TRPM2 channel in plasticity of CNS and AD. We proposed that the activation of TRPM2 channels in microglia and astrocytes produces Ca^{2+} overload and subsequent inflammation and oxidative stress which results in mitochondrial dysfunctions, $[Ca^{2+}]_i$ increase, Aβ accumulation in neurons, PSD95 reduction, glutamate receptor dysfunction, and finally change of plasticity and dementia. On the other hand, extinct factors such as aging and diabetes can result in increase of extracellular Aβ, which activates the above pathways. The third pathway may be that activation of neuronal TRPM2 channel enhances $[Ca^{2+}]_i$ and phosphorylates GSK3β and subsequent pathway to change plasticity.

5. Conclusion

As a newly identified nonselective Ca^{2+}-permeable channel, the TRPM2 channel is expressed in both neurons and glial cells (mainly microglia and astrocytes). TRPM2 channel can be activated by Aβ and is involved in the synaptic plasticity through interaction with PSD95 and GSK3β signal pathway. TRPM2 channel is involved in the plasticity induced by neuropathic and inflammatory pain through glia cells and immune cells. These studies suggest that TRPM2 channel is highly involved in the plasticity of CNS and the pathology of AD through glial cells, as shown in Table 1. According to the schematic figure (Figure 1), we proposed that the activation of TRPM2 channels in microglia and astrocytes produces Ca^{2+} overload and subsequent inflammation and oxidative stress which results in mitochondrial dysfunctions, $[Ca^{2+}]_i$

increase, Aβ accumulation in neurons, PSD95 reduction, glutamate receptor dysfunction, and finally change of plasticity and dementia. On the other hand, distinct factors such as aging and diabetes can result in increase of extracellular Aβ, which activates the above pathways. The third pathway may be that activation of neuronal TRPM2 channel enhances $[Ca^{2+}]_i$ and phosphorylates GSK3β and subsequent pathway to change plasticity. However, there are still many further studies remaining to be performed to elucidate the detailed mechanism of glial TRPM2 channel in the plasticity of CNS and the pathology of neurodegenerative diseases such as AD, particularly using specific deletion of TRPM2 channel in glial cells. Following the elucidation of the features of the TRPM2 channel in glial cells, it will shed a light on the study of neurodegenerative diseases.

Highlights

TRPM2 channel is expressed in both neurons and glial cells.
Glial TRPM2 channel is involved in plasticity in CNS.
Glial TRPM2 channel is involved in Alzheimer's disease.

Conflict of Interests

The authors declare that there is no conflict of interests regarding the publication of this paper.

Acknowledgments

This study was supported by CIHR grant to Dr. Michael F. Jackson (no. R4321A07), NSFC (no. 81371230), and NSF for Distinguished Young Scholars of Gansu Province, China (no. 1210RJDA010) to Dr. Jing Wang.

References

[1] P. Agostinho, R. A. Cunha, and C. Oliveira, "Neuroinflammation, oxidative stress and the pathogenesis of Alzheimer's disease," *Current Pharmaceutical Design*, vol. 16, no. 25, pp. 2766–2778, 2010.

[2] W. S. Chung, C. A. Welsh, B. A. Barres, and B. Stevens, "Do glia drive synaptic and cognitive impairment in disease?," *Nature Neuroscience*, vol. 18, no. 11, pp. 1539–1545, 2015.

[3] V. A. Yürekli, S. Gürler, M. Naziroğlu, A. C. Uğuz, and H. R. Koyuncuoğlu, "Zonisamide attenuates MPP(+)-induced oxidative toxicity through modulation of Ca^{2+} signaling and caspase-3 activity in neuronal PC12 cells," *Cellular and Molecular Neurobiology*, vol. 33, no. 2, pp. 205–212, 2013.

[4] M. Nazıroğlu, "Molecular role of catalase on oxidative stress-induced Ca^{2+} signaling and TRP cation channel activation in nervous system," *Journal of Receptors and Signal Transduction*, vol. 32, no. 3, pp. 134–141, 2012.

[5] A. Latremoliere and C. J. Woolf, "Central sensitization: a generator of pain hypersensitivity by central neural plasticity," *Journal of Pain*, vol. 10, no. 9, pp. 895–926, 2009.

[6] C.-Y. Chiang, J. Wang, Y.-F. Xie et al., "Astroglial glutamate-glutamine shuttle is involved in central sensitization of nociceptive neurons in rat medullary dorsal horn," *The Journal of Neuroscience*, vol. 27, no. 34, pp. 9068–9076, 2007.

[7] Y. F. Xie, S. Zhang, C. Y. Chiang, J. W. Hu, J. O. Dostrovsky, and B. J. Sessle, "Involvement of glia in central sensitization in trigeminal subnucleus caudalis (medullary dorsal horn)," *Brain, Behavior, and Immunity*, vol. 21, no. 5, pp. 634–641, 2007.

[8] Y.-F. Xie, "Glial involvement in trigeminal central sensitization," *Acta Pharmacologica Sinica*, vol. 29, no. 6, pp. 641–645, 2008.

[9] F. Benfenati, "Synaptic plasticity and the neurobiology of learning and memory," *Acta Biomedica*, vol. 78, supplement 1, no. 1, pp. 58–66, 2007.

[10] L. Welberg, "Synaptic plasticity: a synaptic role for microglia," *Nature Reviews Neuroscience*, vol. 15, no. 2, p. 69, 2014.

[11] D. Yates, "Synaptic plasticity: microglial cell-mediated depression," *Nature Reviews Neuroscience*, vol. 15, no. 5, pp. 280–281, 2014.

[12] Y. Bernardinelli, D. Muller, and I. Nikonenko, "Astrocyte-synapse structural plasticity," *Neural Plasticity*, vol. 2014, Article ID 232105, 13 pages, 2014.

[13] J. Gonzalez, J. C. Jurado-Coronel, M. F. Ávila, A. Sabogal, F. Capani, and G. E. Barreto, "NMDARs in neurological diseases: a potential therapeutic target," *International Journal of Neuroscience*, vol. 125, no. 5, pp. 315–327, 2015.

[14] M. J. Kim, K. Futai, J. Jo, Y. Hayashi, K. Cho, and M. Sheng, "Synaptic accumulation of PSD-95 and synaptic function regulated by phosphorylation of serine-295 of PSD-95," *Neuron*, vol. 56, no. 3, pp. 488–502, 2007.

[15] S. E. Hoey, R. J. Williams, and M. S. Perkinton, "Synaptic NMDA receptor activation stimulates α-secretase amyloid precursor protein processing and inhibits amyloid-β Production," *Journal of Neuroscience*, vol. 29, no. 14, pp. 4442–4460, 2009.

[16] M. Nazıroğlu, "TRPM2 cation channels, oxidative stress and neurological diseases: where are we now?" *Neurochemical Research*, vol. 36, no. 3, pp. 355–366, 2011.

[17] K. Haraguchi, A. Kawamoto, K. Isami et al., "TRPM2 contributes to inflammatory and neuropathic pain through the aggravation of pronociceptive inflammatory responses in mice," *The Journal of Neuroscience*, vol. 32, no. 11, pp. 3931–3941, 2012.

[18] Y.-F. Xie, J. F. MacDonald, and M. F. Jackson, "TRPM2, calcium and neurodegenerative diseases," *International Journal of Physiology, Pathophysiology and Pharmacology*, vol. 2, no. 2, pp. 95–103, 2010.

[19] A. Di, X. P. Gao, F. Qian et al., "The redox-sensitive cation channel TRPM2 modulates phagocyte ROS production and inflammation," *Nature Immunology*, vol. 13, no. 1, pp. 29–34, 2012.

[20] V. G. Ostapchenko, M. Chen, M. S. Guzman et al., "The Transient Receptor Potential Melastatin 2 (TRPM2) channel contributes to β-amyloid oligomer-related neurotoxicity and memory impairment," *The Journal of Neuroscience*, vol. 35, no. 45, pp. 15157–15169, 2015.

[21] M. Lee, T. Cho, N. Jantaratnotai, Y. T. Wang, E. McGeer, and P. L. McGeer, "Depletion of GSH in glial cells induces neurotoxicity: relevance to aging and degenerative neurological diseases," *FASEB Journal*, vol. 24, no. 7, pp. 2533–2545, 2010.

[22] K. So, K. Haraguchi, K. Asakura et al., "Involvement of TRPM2 in a wide range of inflammatory and neuropathic pain mouse models," *Journal of Pharmacological Sciences*, vol. 127, no. 3, pp. 237–243, 2015.

[23] K. Isami, K. Haraguchi, K. So et al., "Involvement of TRPM2 in peripheral nerve injury-induced infiltration of peripheral immune cells into the spinal cord in mouse neuropathic pain model," *PLoS ONE*, vol. 8, no. 7, Article ID e66410, 2013.

[24] E. Fonfria, C. Mattei, K. Hill et al., "TRPM2 is elevated in the tMCAO stroke model, transcriptionally regulated, and functionally expressed in C13 microglia," *Journal of Receptors and Signal Transduction*, vol. 26, no. 3, pp. 179–198, 2006.

[25] L. Ohana, E. W. Newell, E. F. Stanley, and L. C. Schlichter, "The Ca^{2+} release-activated Ca^{2+} current (I_{CRAC}) mediates store-operated Ca^{2+} entry in rat microglia," *Channels*, vol. 3, no. 2, pp. 129–139, 2009.

[26] R. Kraft, C. Grimm, K. Grosse et al., "Hydrogen peroxide and ADP-ribose induce TRPM2-mediated calcium influx and cation currents in microglia," *The American Journal of Physiology—Cell Physiology*, vol. 286, no. 1, pp. C129–C137, 2004.

[27] C. E. Bond and S. A. Greenfield, "Multiple cascade effects of oxidative stress on astroglia," *Glia*, vol. 55, no. 13, pp. 1348–1361, 2007.

[28] T. Miyake, H. Shirakawa, A. Kusano et al., "TRPM2 contributes to LPS/IFNγ-induced production of nitric oxide via the p38/JNK pathway in microglia," *Biochemical and Biophysical Research Communications*, vol. 444, no. 2, pp. 212–217, 2014.

[29] C. Y. Chiang, S. Zhang, Y. F. Xie et al., "Endogenous ATP involvement in mustard-oil-induced central sensitization in trigeminal subnucleus caudalis (medullary dorsal horn)," *Journal of Neurophysiology*, vol. 94, no. 3, pp. 1751–1760, 2005.

[30] X. Chen, R. Lin, L. Chang et al., "Enhancement of long-term depression by soluble amyloid beta protein in rat hippocampus is mediated by metabotropic glutamate receptor and involves activation of p38MAPK, STEP and caspase-3," *Neuroscience*, vol. 253, pp. 435–443, 2013.

[31] K. Yashiro and B. D. Philpot, "Regulation of NMDA receptor subunit expression and its implications for LTD, LTP, and metaplasticity," *Neuropharmacology*, vol. 55, no. 7, pp. 1081–1094, 2008.

[32] Y. Yamazaki and S. Fujii, "Extracellular ATP modulates synaptic plasticity induced by activation of metabotropic glutamate receptors in the hippocampus," *Biomedical Research*, vol. 36, no. 1, pp. 1–9, 2015.

[33] T. Liu, T. Berta, Z.-Z. Xu et al., "TLR3 deficiency impairs spinal cord synaptic transmission, central sensitization, and pruritus in mice," *Journal of Clinical Investigation*, vol. 122, no. 6, pp. 2195–2207, 2012.

[34] U. Lalo, S. Rasooli-Nejad, and Y. Pankratov, "Exocytosis of gliotransmitters from cortical astrocytes: implications for synaptic plasticity and aging," *Biochemical Society Transactions*, vol. 42, pp. 1275–1281, 2014.

[35] S. Rasooli-Nejad, O. Palygin, U. Lalo, and Y. Pankratov, "Cannabinoid receptors contribute to astroglial Ca^{2+}-signalling and control of synaptic plasticity in the neocortex," *Philosophical Transactions of the Royal Society B: Biological Sciences*, vol. 369, no. 1654, 2014.

[36] Y. Hayashi and H. Nakanishi, "Synaptic plasticity and synaptic reorganization regulated by microglia," *Nihon Shinkei Seishin Yakurigaku Zasshi*, vol. 33, no. 5-6, pp. 211–216, 2013.

[37] C. N. Parkhurst, G. Yang, I. Ninan et al., "Microglia promote learning-dependent synapse formation through brain-derived neurotrophic factor," *Cell*, vol. 155, no. 7, pp. 1596–1609, 2013.

[38] K. Koga, G. Descalzi, T. Chen et al., "Coexistence of two forms of LTP in ACC provides a synaptic mechanism for the interactions between anxiety and chronic pain," *Neuron*, vol. 85, no. 2, pp. 377–389, 2015.

[39] Y.-F. Xie, J. C. Belrose, G. Lei et al., "Dependence of NMDA/GSK-3β mediated metaplasticity on TRPM2 channels at hippocampal CA3-CA1 synapses," *Molecular Brain*, vol. 4, article 44, 2011.

[40] E. P. Azevedo, J. H. Ledo, G. Barbosa et al., "Activated microglia mediate synapse loss and short-term memory deficits in a mouse model of transthyretin-related oculoleptomeningeal amyloidosis," *Cell Death and Disease*, vol. 4, no. 9, article e789, 2013.

[41] R. L. Frozza, A. Bernardi, J. B. Hoppe et al., "Neuroprotective effects of resveratrol against Aβ administration in rats are improved by lipid-core nanocapsules," *Molecular Neurobiology*, vol. 47, no. 3, pp. 1066–1080, 2013.

[42] S. Jo, O. Yarishkin, Y. J. Hwang et al., "GABA from reactive astrocytes impairs memory in mouse models of Alzheimer's disease," *Nature Medicine*, vol. 20, no. 8, pp. 886–896, 2014.

[43] C.-Y. Ko, W.-L. Wang, S.-M. Wang, Y.-Y. Chu, W.-C. Chang, and J.-M. Wang, "Glycogen synthase kinase-3β-mediated CCAAT/enhancer-binding protein delta phosphorylation in astrocytes promot es migration and activation of microglia/macrophages," *Neurobiology of Aging*, vol. 35, no. 1, pp. 24–34, 2014.

[44] M. Jeffrey, G. McGovern, R. Barron, and F. Baumann, "Membrane pathology and microglial activation of mice expressing membrane anchored or membrane released forms of Aβ and mutated human Alzheimer's precursor protein (APP)," *Neuropathology and Applied Neurobiology*, vol. 41, no. 4, pp. 458–470, 2015.

[45] V. G. Ostapchenko, F. H. Beraldo, A. H. Mohammad et al., "The prion protein ligand, stress-inducible phosphoprotein 1, regulates amyloid-beta oligomer toxicity," *Journal of Neuroscience*, vol. 33, no. 42, pp. 16552–16564, 2013.

[46] V. Yürüker, M. Nazıroğlu, and N. Şenol, "Reduction in traumatic brain injury-induced oxidative stress, apoptosis, and calcium entry in rat hippocampus by melatonin: possible involvement of TRPM2 channels," *Metabolic Brain Disease*, vol. 30, no. 1, pp. 223–231, 2014.

[47] S. Saharan and P. K. Mandal, "The emerging role of glutathione in Alzheimer's disease," *Journal of Alzheimer's Disease*, vol. 40, no. 3, pp. 519–529, 2014.

[48] J. C. Belrose, Y.-F. Xie, L. J. Gierszewski, J. F. MacDonald, and M. F. Jackson, "Loss of glutathione homeostasis associated with neuronal senescence facilitates TRPM2 channel activation in cultured hippocampal pyramidal neurons," *Molecular Brain*, vol. 5, article 11, 2012.

[49] I. S. Övey and M. Naziroğlu, "Homocysteine and cytosolic GSH depletion induce apoptosis and oxidative toxicity through cytosolic calcium overload in the hippocampus of aged mice: involvement of TRPM2 and TRPV1 channels," *Neuroscience*, vol. 284, pp. 225–233, 2015.

[50] E. Sözbir and M. Nazıroğlu, "Diabetes enhances oxidative stress-induced TRPM2 channel activity and its control by N-acetylcysteine in rat dorsal root ganglion and brain," *Metabolic Brain Disease*, 2015.

[51] J. Zou, J. F. Ainscough, W. Yang et al., "A differential role of macrophage TRPM2 channels in Ca^{2+} signaling and cell death in early responses to H_2O_2," *American Journal of Physiology—Cell Physiology*, vol. 305, no. 1, pp. C61–C69, 2013.

[52] E. Fonfria, I. C. B. Marshall, I. Boyfield et al., "Amyloid β-peptide(1-42) and hydrogen peroxide-induced toxicity are mediated by TRPM2 in rat primary striatal cultures," *Journal of Neurochemistry*, vol. 95, no. 3, pp. 715–723, 2005.

[53] N. L. Cook, R. Vink, S. C. Helps, J. Manavis, and C. van den Heuvel, "Transient receptor potential melastatin 2 expression is increased following experimental traumatic brain injury in rats," *Journal of Molecular Neuroscience*, vol. 42, no. 2, pp. 192–199, 2010.

[54] I. Alim, L. Teves, R. Li, Y. Mori, and M. Tymianski, "Modulation of NMDAR subunit expression by TRPM2 channels regulates neuronal vulnerability to ischemic cell death," *The Journal of Neuroscience*, vol. 33, no. 44, pp. 17264–17277, 2013.

[55] M. Ishii, A. Oyama, T. Hagiwara et al., "Facilitation of H_2O_2-induced A172 human glioblastoma cell death by insertion of oxidative stress-sensitive TRPM2 channels," *Anticancer Research*, vol. 27, no. 6, pp. 3987–3992, 2007.

[56] C. M. Hecquet and A. B. Malik, "Role of H_2O_2-activated TRPM2 calcium channel in oxidant-induced endothelial injury," *Thrombosis and Haemostasis*, vol. 101, no. 4, pp. 619–625, 2009.

Hindawi Publishing Corporation
Neural Plasticity
Volume 2016, Article ID 2412958, 12 pages
http://dx.doi.org/10.1155/2016/2412958

Research Article

Value of Functionalized Superparamagnetic Iron Oxide Nanoparticles in the Diagnosis and Treatment of Acute Temporal Lobe Epilepsy on MRI

Tingting Fu,[1] Qingxia Kong,[1] Huaqiang Sheng,[2] and Lingyun Gao[2]

[1]*Department of Neurology, Affiliated Hospital of Jining Medical University, Guhuai Road, No. 79, Jining, Shandong 272000, China*
[2]*Department of Magnetic Resonance Imaging, Affiliated Hospital of Jining Medical University, Guhuai Road, No. 79, Jining, Shandong 272000, China*

Correspondence should be addressed to Qingxia Kong; 438274162@qq.com

Received 23 October 2015; Revised 27 December 2015; Accepted 3 January 2016

Academic Editor: Alfredo Pereira Jr.

Purpose. Although active targeting of drugs using a magnetic-targeted drug delivery system (MTDS) with superparamagnetic iron oxide nanoparticles (SPIONs) is a very effective treatment approach for tumors and other illnesses, successful results of drug-resistant temporal lobe epilepsy (TLE) are unprecedented. A hallmark in the neuropathology of TLE is brain inflammation, in particular the activation of interleukin-1β (IL-1β) induced by activated glial cells, which has been considered a new mechanistic target for treatment. The purpose of this study was to determine the feasibility of the functionalized SPIONs with anti-IL-1β monoclonal antibody (mAb) attached to render MRI diagnoses and simultaneously provide targeted therapy with the neutralization of IL-1β overexpressed in epileptogenic zone of an acute rat model of TLE. *Experimental Design.* The anti-IL-1β mAb-SPIONs were studied in vivo versus plain SPIONs and saline. Lithium-chloride pilocarpine-induced TLE models ($n = 60$) were followed by Western blot, Perl's iron staining, Nissl staining, and immunofluorescent double-label staining after MRI examination. *Results.* The magnetic anti-IL-1β mAb-SPION administered intravenously, which crossed the BBB and was concentrated in the astrocytes and neurons in epileptogenic tissues, rendered these tissues visible on MRI and simultaneously delivered anti-IL-1β mAb to the epileptogenic focus. *Conclusions.* Our study provides the first evidence that the novel approach enhanced accumulation and the therapeutic effect of anti-IL-1β mAb by MTDS using SPIONs.

1. Introduction

Temporal lobe epilepsy (TLE) is the most prevalent form of adult focal onset epilepsy (a condition characterized by recurrent, unpredictable, and spontaneous seizures) and is often associated with pharmacological resistance [1], thus medically refractory epilepsy. According to statistics, as many as 75% of patients with TLE are considered to have drug-resistant epilepsy [2], which is a condition defined by the International League Against Epilepsy as persistent seizures, in spite of having used at least two appropriate and adequate antiepileptic drug (AED) treatments [3]. Despite many other approaches, such as surgery (resection or removal of small areas of the brain where the seizures originate) [4], vagus nerve stimulation (VNS) [5, 6], electrical stimulation [7], or dietary treatment (the classic ketogenic diet and its variants) [8] to treat refractory patients, these alternative treatments all remain arguably mostly underutilized because of various reasons such as lacking early identification and referral of appropriate surgical candidates, and patients with medically refractory epilepsy are too often not referred to epilepsy centers or referred too late to prevent irreversible disability [9]. Thus, a novel effective noninvasive strategy is clearly needed. Of note, the therapeutic deficiency with respect to AEDs in patients with medically refractory epilepsy includes resistance to drugs, nonspecificity towards a pathologic site, low local concentration, nonspecific toxicity, other adverse side effects [10], and the high suicide risk [11, 12]. In the

present study, we attempted to solve these shortcomings by combining anti-interleukin- (IL-) 1β monoclonal antibody (mAb) with the a magnetic-targeted drug delivery system (MTDS) [13–16]. In this study, anti-IL-1β mAb, as an anti-epileptogenic therapeutic targeting proteins, was chelated to superparamagnetic iron oxide nanoparticles (SPIONs), composed of iron oxide and polyethylene glycol (PEG), and intravenous tail injections were performed and the possibility of epileptogenic focus imaging and simultaneous targeted therapy of new drug-delivery particles using MRI providing an external magnetic field was explored in a rat model of TLE.

Previous experimental evidence supports the notion that anti-IL-1β mAb may be a promising antiepileptogenic therapeutic agent for TLE by acting on IL-1β, a novel molecular target [17, 18]. More recently, the rapidly growing body of clinical and experimental evidence has provided strong support to the hypothesis that immunity and inflammation are considered to be key elements in the pathobiology of a number of human TLE and convulsive disorders [19, 20]. A growing body of research has shown that the immune exemption of the central nervous system (CNS) is related. The CNS has a kind of special immune defense, including microglia, astrocytes, and endothelial cells, that participates in the immune response within the brain. Microglia are "the sentinel" of the CNS immune system and maintain a steady state in the CNS environment. The biological function of the microglia is similar to the peripheral system of macrophages and is inherent in immune defense within the CNS. Microglia are relatively small in number, representing approximately 5% of all glial cells. When the CNS is infected and impaired, the function of static microglia is active, becomes macrophages, and participates in the adaptive immune response with circulating T cells. Excessive activation of microglia produces neurotoxicity, which is an important source of proinflammatory factors and oxidative stress. Activated microglia cells can release toxic substances, such as cytokines. Astrocytes, one of the largest glial cells and 10-fold the number of neurons, are an important member of the nervous system, which can guide neuromobility, provide the energy for neurons, and regulate the excitability of neurons. Astrocytes are an important "energy library" in the CNS and the astrocyte network, which are connected by gap junction channels and can provide energy for neurons to maintain glutamate synaptic transmission and discharge.

Astrocytes also express some cytokine receptors, especially IL-1 receptors [21], the proinflammatory cytokine, IL-1β, activated intracellular signaling pathways by acting on the IL-1R, and may increase reactive glial cell proliferation and signal amplification inflammation in TLE [22, 23]. IL-1β can trigger the neuronal endogenous inflammatory response by activating the PI3K/Akt/mTOR signaling pathway, and activation of this pathway participates in seizure generation and pathogenesis [23]. In addition, IL-1β can aggravate the occurrence and development of epilepsy and can rapidly lower the focal ictal event threshold [24]. The reverse results could be obtained when blocking IL-1β signaling [25, 26]. These findings strengthen the possibility targeting these inflammatory pathways and IL-1β may represent an effective therapeutic strategy to prevent seizures.

Thus, IL-1β should be considered as a new molecular target in the design of AEDs, which might not only inhibit the symptoms of this disorder, but also prevent or abrogate disease pathogenesis [27]; however, the use of anti-IL-1β mAb as a neuroprotective therapeutic can be limited by the hindered mobility through the BBB. An increasing body of experimental evidence suggests that MTDS can overcome the BBB issue [28–30]. Guiding magnetic nanoparticles (MNPs), with the help of an external magnetic field to its target, is the principle for the development of MTDS [31, 32]. SPIONs are small synthetic γ-Fe_2O_3 (maghemite), Fe_3O_4 (magnetite), or α-Fe_2O_3 (hematite) particles with a core ranging from 10 to 100 nm in diameter [33]. In addition, due to the essential characteristics, SPIONs exhibit unique electronic, optical, and magnetic properties that have been widely used in *in vivo* biomedical applications [33, 34], especially MRI contrast enhancement [35, 36] and drug delivery [37], where SPIONs facilitate laboratory diagnostics and therapeutics. Further studies have demonstrated that SPIONs with proper surface architecture and conjugated targeting ligands/proteins have shown great potential in nanomedicine. For example, functionalized SPIONs conjugated to targeting ligands, such as alpha methyl tryptophan (AMT) and 2-deoxy glucose (2DG), are capable of crossing the BBB and concentrating in the epileptogenic tissues and are approved for MRI contrast agents in an epilepsy model [38, 39]. Similarly, SPIONs with drugs loaded can be guided to the desired target area (epileptogenic tissues) using an external magnetic field, while simultaneously tracking the biodistribution of the particles on MRI [40]. More specifically, the current research involving SPIONs is opening up wide horizons for their use as diagnostic agents in MRI and simultaneously as drug delivery vehicles [41].

In this study, we demonstrated the remarkable capability of anti-IL-1β mAb-SPION to specifically deliver neutralizing-IL-1β antibody into the epileptogenic zone, thus significantly increasing the efficacy of therapy and simultaneously rendering these tissues visible on MRI as a contrast-enhancing agent. The new approach, anti-IL-1β mAb-SPION-MRI, provides a safe theranostic platform, which integrates targeted delivery of antibody drugs and enhances MR imaging of TLE. Thus, this new approach using a functionalized SPION-MRI drugs delivery system truly makes them theranostic (therapeutic and diagnostic) [40].

2. Materials and Methods

2.1. Particles. Two types of functionalized nanoparticles (plain [P] SPIONs and anti-IL-1β mAb-SPIONs) were used in this study. P-SPIONs (unconjugated) were prepared by a procedure similar to that described by Akhtari et al. [38]. The particle consists of monocrystalline iron oxide cores of maghemite (γ-Fe_2O_3) coated with a PEG layer using a precipitation reaction, with an average diameter of 10–20 nm (an average iron-oxide core diameter of 2-3 nm). Anti-IL-1β mAb was then covalently conjugated to the plain particles with the same characteristics (solid content, 5 mg/mL; iron concentration, 2.4 mg/mL; antibody concentration, 10 μg/mg Fe). All of the particles used for this study were provided by MicroMod Company (Rostock, Germany).

2.2. Experimental Animals. All procedures described in this study were approved by the Medical University of Jining Institutional Animal Care and Use Committee. Sprague-Dawley rats (8–10 weeks old; LuKang Pharmaceutical Co., Shandong, China), weighing 250–300 g, were used in all experiments. All rats were housed individually or in pairs at an ambient temperature of 20–25°C and relative humidity of 50%–60% and 12 h light/dark cycle with access to food and water *ad libitum*. All studies were performed in the Key Laboratory of Molecular Pathology of Jining Medical University (Shandong, China).

2.3. Pilocarpine-Status Epilepticus (SE) Model. 127 mg/kg of lithium chloride (Sigma-Aldrich, St. Louis, MO, USA) was administered to all of the rats via a peritoneal injection. After 18–20 h, the rats were injected with a low dose of methylscopolamine (1 mg/kg intraperitoneally in 0.9% NaCl; Sigma-Aldrich) 15–30 min before pilocarpine (Sigma-Aldrich) injections to minimize peripheral effects of cholinergic stimulation. A single dose of pilocarpine was administered (330–345 mg/kg intraperitoneally in 0.9% saline) following 30 min later to induce SE. The period of SE was alleviated after 90 min with 1 diazepam injection (10 mg/kg in saline, intraperitoneal; Xupu Pharma, China). The rats were observed for 1 h and scored according to a modified Racine seizure scale [42] as follows: 1 = facial movements; 2 = head nodding and chewing; 3 = unilateral forelimb clonus; 4 = bilateral forelimb clonus; and 5 = bilateral forelimb clonus, rearing, and loss of balance. The models of TLE that scored ≥ 4 were employed in the following study. All animals were injected with 5% dextrose in lactate Ringer's solution (5 mL intraperitoneal bid) and hand-fed moistened cookies for approximately 3 days and thereafter when needed. Then, randomly select 45 of the successful and survival rat epileptic models, then divided into 3 groups (saline control group (n = 15), P-SPIONs control group (n = 15), and the anti-IL-1β mAb-SPION group (n = 15)).

2.4. MRI Study. MRI was performed using a clinical 3.0 T MRI scanner (Siemens Magnetom, version 3.0 T; Berlin, Germany) along with general 3-inch circular coil at room temperature. T2-weighted images were acquired using the following parameters: repetition time (TR)/echo time (TE), 2500/70; 6 echoes, 192 * 192; slices, 12; thickness slice, 2.0 mm; field of view (FOV), 80 mm; and acquisition time, 6.5 min. MRI scans were acquired on all models 72 h after SE (acute state). MR images were acquired before the injection of anti-IL-1β mAb-SPION (15 mg/kg), plain SPIONs (15 mg/kg), and saline (equivalent dose) in the tail vein 72 h after SE as well as ~4 h after tail vein injection to compare the differences between images. All animals were denied food for at least 12 h before injection. T2 relaxation data were acquired using T2 mapping.

2.5. Tissue Processing. After the MRI study, mice (n = 10 per group) were anesthetized and perfused transcardially using 0.9% saline followed by 0.1% sodium sulfide and 4% paraformaldehyde (0.1 M (pH 7.4)). Brains were immediately removed after perfusion and immersed in 4% paraformaldehyde overnight for additional fixation followed by being arranged to sink in 20% and/or 30% sucrose solution in PBS for 24 h at 4°C. Brains were extracted and were cut on a freezing sliding microtome at a thickness of 5 μm with consecutive coronal slices from all brains throughout the septotemporal extension of the hippocampus for neuropathology. One slice was taken for every interval of 6 and a total of 10 slices were taken from each specimen. Two slices were randomly selected, respectively, for Perl's iron staining, Nissl staining, FJB staining, and immunofluorescence, and subjected to statistical analysis. In addition, remnant animals (n = 5 per group) were decapitated under anesthesia. The brains were removed rapidly and hippocampal tissues were isolated and stored in liquid nitrogen until use for Western blot analysis.

2.6. Western Blot. The tissue samples were dissected out at 4°C and homogenized in lysis buffer and PMSF (nos. p0013 ST506; Beyotime Institute of Biotechnology, Jiangsu, China) for 30 min and centrifuged at 12,000 g for 15 min at 4°C to separate and extract proteins. Total proteins (30 μg per lane; Bio-tanon, Shanghai, China) were separated using 8%–12% sodium dodecyl sulfate (SDS) polyacrylamide gels, and 10% acrylamide and transferred to polyvinylidene fluoride (PVDF) membranes, and each sample was run in duplicate. Proteins were transferred to Millipore polyvinylidene fluoride membranes by electroblotting. The membrane was blocked with 5% nonfat milk in Tween-TBS (TBST) for 2 h at room temperature and incubated at 4°C overnight with primary antibodies against IL-1β (1 : 500 dilution; Santa Cruz Biotechnology Inc., Santa Cruz, CA, USA) or against IL-1R1 (1 : 500 dilution; Santa Cruz Biotechnology Inc.). After rinsing, the membranes were appropriately incubated with horseradish peroxidase- (HRP-) conjugated goat anti-rabbit IgG (1 : 5000 dilution; Santa Cruz Biotechnology Inc.) for 2 h at room temperature. Protein bands were visualized by ECL Western blot detection reagents (ECL, no. P0018; Beyotime Institute of Biotechnology) and were exposed to X-ray film. All experiments were repeated at least three times. Optical density values in each sample were normalized using the corresponding amount of β-actin.

2.7. Histology. In order to observe the distribution of iron particles in the brain tissue of each sample, Perl's iron staining of the sections was performed following the procedure of Perl's iron stain kit (Solarbio, Beijing, China). The sections were incubated in a stock potassium ferrocyanide solution (10%) for 5 min. Immediately prior to use, a working potassium ferrocyanide solution was prepared (70 mL stock potassium ferrocyanide + 30 mL 10% HCl) and applied for 20 min. Sections were counterstained with Nuclear Fast Red for 5 min.

To investigate the antiepileptic effect of anti-IL-1β mAb-SPIONs on the neuronal damage in the hippocampus induced by SE, Nissl staining, Fluoro-Jade (F-J) B staining, and immunofluorescent double-label staining were performed.

To evaluate the degree of hippocampal sclerosis and the overall cellular death, brain sections of each specimen underwent Nissl staining with toluidine blue according to

the well-known Nissl staining protocol, and samples were dried at room temperature. After 3 washes with distilled water, the slides were dipped in 0.1% cresyl violet (Sigma-Aldrich) for 30 seconds, washed again, and then dehydrated. The sections were permeabilized with xylene and mounted with neutral resin. Four randomly chosen nonoverlapping fields were selected to calculate the number of hippocampal CA3 pyramidal cells under a light microscope (Olympus, Hamburg, Germany) at 400x magnification. The mean was taken as the average number of each type of neuron in the hippocampus. F-J B is a high affinity fluorescent marker for the localization of neuronal degeneration. The staining was performed with the following procedure: the slides were first immersed in a solution containing 1% sodium hydroxide in 80% alcohol (20 mL of 5% NaOH added to 80 mL of absolute alcohol) for 5 min. This was followed by a 2-minute immersion in 70% alcohol and 2 min in distilled water. The sections were then transferred to 0.06% potassium permanganate and then a 0.0004% F-J B solution (Millipore, Massachusetts, USA). After washing in distilled water, the sections were placed on a slide warmer at 50°C until they fully dried. The tissue was then examined using an epifluorescent microscope (ZEISS, Oberkochen, Germany) with blue (450–490 nm) excitation light and a barrier filter.

To highlight the differences in the levels of activated nuclear factor-kappa B (NF-κB) p65 and astrocyte hyperplasia within the CA3 region of the hippocampus, double labeling of GFAP and NF-κB p65 was carried out. The brain sections were thawed and fixed in ice-cold acetone for 1 min. Nonspecific binding was blocked using 10% normal goat serum in PBS with 0.1% Triton X-100 for 2 h. The brain sections then were incubated with primary anti-NF-κB p65 antibody (1 : 500 dilution; Abcam, Shanghai, China) and astrocyte-specific primary antibody (rabbit anti-GFAP antibody-Cy3, 1 : 400 dilution; Abcam) in PBS overnight at 4°C following preincubation in 10% normal goat serum to block nonspecific binding, washed with PBS and then with a secondary antibody (Alexa Fluor 488 donkey anti-rabbit IgG antibody, 1 : 500 dilution; Abcam) for 1 h at room temperature. Finally, cells were washed three times and coverslips were mounted using Immu-Mount (Thermo Scientific, Germany). All brain sections were observed under a fluorescence microscope (ZEISS).

2.8. Statistical Analyses. All results are expressed as the mean ± standard deviation (SD). Analysis of variance for repeated measures was performed with SPSS 19.0 statistical software. One-way analysis of variance (ANOVA) was used for comparisons between groups, followed by the LSD test for between-group comparisons. The results of MRI T2 values before and after injection in each group were compared with t-tests. $P < 0.05$ was considered statistically significant and $P < 0.01$ was considered highly significant.

3. Results

3.1. MRI Studies. Prior to particle injection, the baseline T2-weighted MR images of the brains in the three groups all showed areas of positive contrast enhancement (increased signal intensity) of acute lesions of the TLE model (Figures 1(a), 1(c), and 1(e)). We chose the side of the macroscopic lesion to carry out the statistical analysis. The MR signal intensity at the lesion site before particle injection between the three groups was not significantly different ($P > 0.05$; Figure 1(g)). The postinjection images of rats to whom anti-IL-1β mAb-SPION was administered (Figure 1(f)) showed areas of negative enhancement (red arrow) in the regional zone of the brain lesion, in agreement with a significant decrease in T2 values by 21.5% in comparison to the preinjection image of epilepsy ($P < 0.01$; Figure 1(g)). The hypointense region within the epileptogenic lesion is indicative of nanoparticle accumulation, which causes a reduction in signal intensity on T2-weighted image. After injection of P-SPIONs, the MR images of P-SPIONs groups showed areas of negligible negative enhancement (arrows; Figure 1(d)) of partial lesions with no significant difference in T2 values ($P > 0.05$; Figure 1(g)). The MR signal intensity of the saline group showed no significant difference in comparison to preinjection ($P > 0.05$), corresponding to almost no signal reduction within the epileptogenic tissues (Figure 1(b)).

3.2. Distribution of Magnetic Nanoparticles in Rat Brains of the Acute TLE Model. To confirm that the signal intensity change of epileptogenic lesions following administration of anti-IL-1β mAb-SPIONs was due to the accumulation of SPIONs in the epileptogenic tissues, we performed Perl's iron staining of the brain tissue after MR imaging (Figure 2). Perl's iron staining of coronal sections from brain tissues showed uptake of anti-IL-1β mAb-SPIONs (arrows; Figure 2(f)), crossing of the BBB, and intracellular localization in the hippocampus CA3; this accumulation manifested as areas of negative enhancement of the MRI seen in Figure 1, with statistical significance compared with the saline control group ($P < 0.01$; Figure 2(g)). Additionally, little brown iron particles were observed in the P-SPIONs control group (arrows; Figure 2(d)), and there was significant difference ($P < 0.05$) compared with the saline group.

3.3. Anti-IL-1β mAb-SPIONs: Neutralization of IL-1β Ameliorates Pilocarpine-Induced Epilepsy. Western blot for investigating the neutralization of IL-1β protein and expression of IL-1R1 protein was performed (Figure 3). After injection of particles, the P-SPIONs group showed few changes ($P > 0.05$; Figure 3(b)) in the level of IL-1β protein and IL-1R1 protein in comparison to the saline group (Figure 3(a)); however, compared with the two control groups, the anti-IL-1β mAb-SPIONs-treated group had a significant decrease ($P < 0.01$) in the level of IL-1β protein, with no significant decrease ($P > 0.05$) in the level of IL-1R1 protein.

To explore the effect of anti-IL-1β mAb-SPIONs on neuronal damage of brain regions induced by pilocarpine-induced SE, Nissl staining of the brain sections was performed. Representative photomicrographs of Nissl staining results are shown in Figure 3. Nissl staining of samples revealed typical neuropathologic changes, including neuronal loss, organizational structure disorders (nucleus

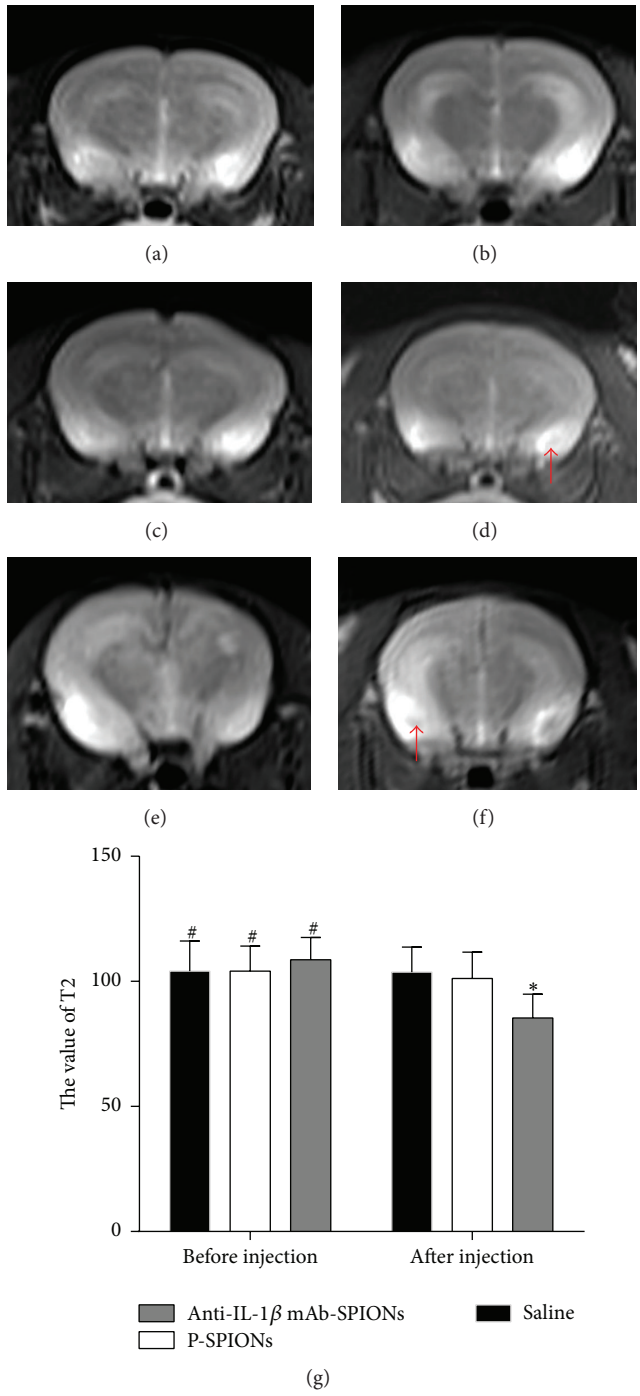

Figure 1: MR images of rat brains in the three groups are shown before and after tail vein injection of particles (15 mg/kg). ((a), (c), and (e)) Baseline MRI prior to injection with saline, P-SPIONs, anti-IL-1β, and mAb-SPIONs; (b) MR images acquired 4 h after saline injection. (d) MR image acquired 4 h after P-SPIONs injection; area of negligible negative enhancement is not visible (red arrow). (f) MR images acquired 4 h after anti-IL-1β mAb-SPIONs injection; area of negative enhancement is visible (red arrow) in CA3 showing unilateral uptake of particles; (g) the changes in the value of T2 before and after injection in the three groups. Data represent mean ± SD of 10 pilocarpine-SE rats per group. $^{*}P < 0.05$ versus preinjection. $^{\#}P > 0.05$ between three groups when preinjected.

shrinkage or disappearance of Nissl bodies) of the hippocampal CA3 area in the control groups (saline and P-SPIONs group; Figures 4(a) and 4(b)); however, after injection of the novel drug, anti-IL-1β mAb-SPIONs, improvement of organizational structure in the hippocampal CA3 area was observed in the experimental group (Figure 4(c)). F-J B staining selectively marked the damaged neurons in agreement with the results of Nissl staining of the hippocampal CA3

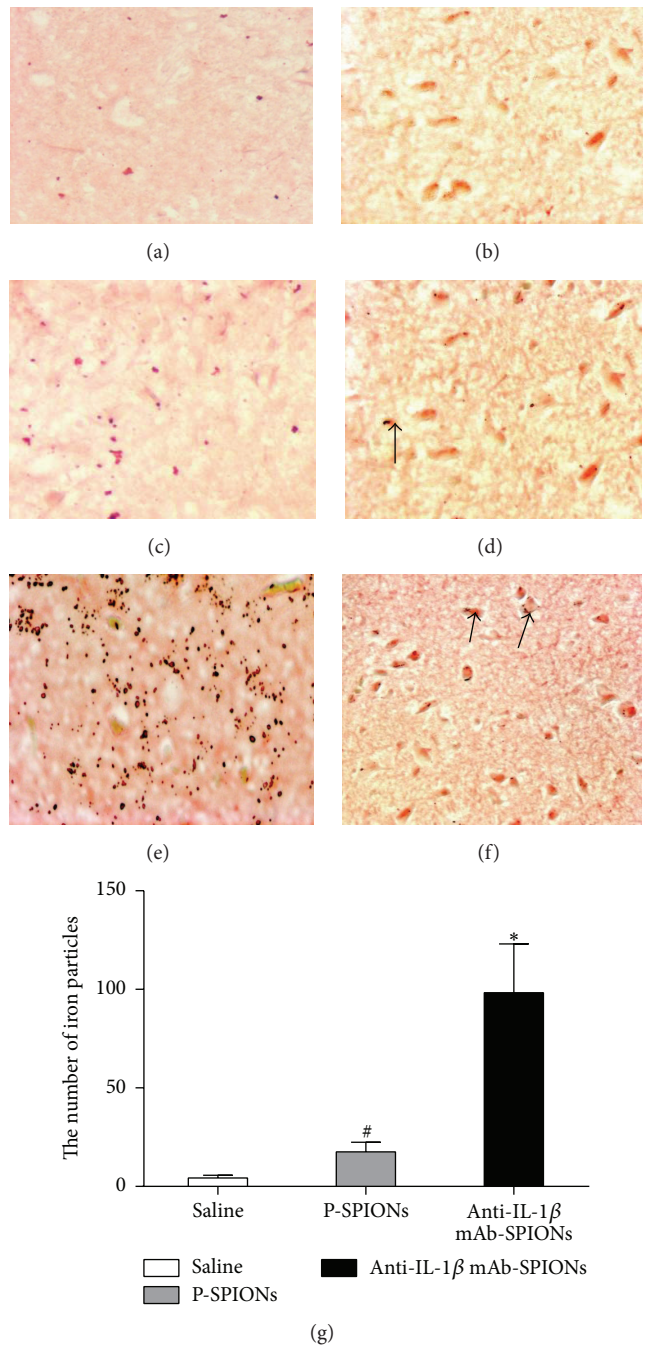

Figure 2: The distribution of iron particles in the hippocampus CA3 of models of TLE at 72 h post-SE after tail vein injection of particles. ((a)-(b)) Perl's iron staining of saline group; ((c)-(d)) Perl's iron staining of P-SPIONs group; ((e)-(f)) Perl's iron staining of anti-IL-1β mAb-SPIONs group. ((a), (c), and (e)) Magnification 40; ((b), (d), and (f)) magnification 400; (g) shows bar graphs (mean ± SD, $n = 10$) for the number of iron particles. $^{*}P < 0.01$ versus saline group. $^{\#}P > 0.05$ versus saline group and anti-IL-1β mAb-SPIONs group.

area showing a trend towards neuronal loss. Compared to the control groups, a decrease in the number of F-J B-positive neurons was observed in the anti-IL-1β mAb-SPIONs group after the injection of the novel drug ($P < 0.05$; Figures 4(d)–4(g)). This extensive cell loss was accompanied by microglial proliferation and the activation of NF-κB p65 in the brain hippocampus. We studied NF-κB p65 expression and astrocytes hyperplasia in the hippocampus CA3 of epileptic rats treated with anti-IL-1β mAb-SPIONs versus saline and P-SPIONs (Figure 5). The activation of GFAP-positive astrocytes and the nuclear transfer of NF-κB p65 in astrocytes were observed in saline group (Figures 5(a1)–5(a4)) and P-SPIONs group (Figures 5(b1)–5(b4)); there was no statistical significance ($P > 0.05$; Figure 5(d)) between groups. Compared with

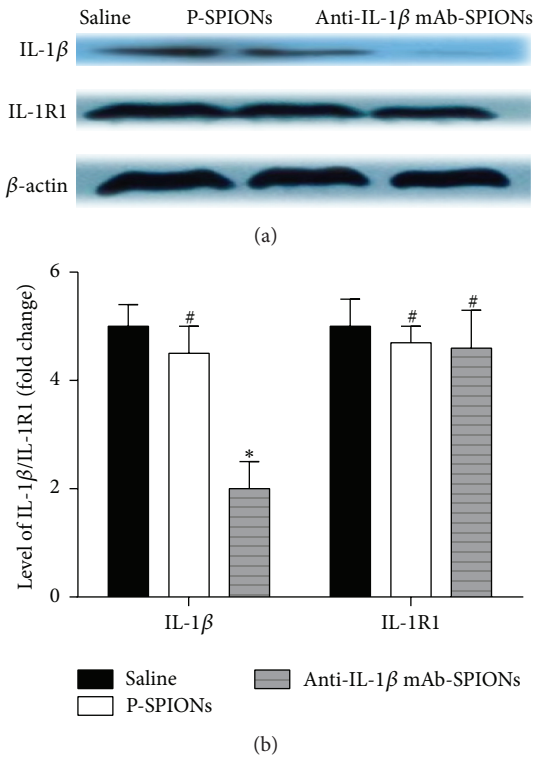

FIGURE 3: The protein expression of IL-1β/IL-1R1 (mean ± SD, $n = 5$) measured in the rat hippocampus after particle injection, as assessed by Western blot. (a) Western immunoblots for IL-1β and IL-1R1 protein expression in the saline, P-SPIONs, and anti-IL-1β mAb-SPIONs groups. (b) shows bar graphs for IL-1β and IL-1R1 protein expression plotted on the vertical-axis as a fold change relative to the saline group. $^{*}P < 0.05$ versus saline group and P-SPIONs group; $^{\#}P > 0.05$ versus saline group.

the control groups, the model rats of TLE treated with anti-IL-1β mAb-SPIONs showed the inhibition of NF-κB p65 expressed in the nuclei of astrocytes of hippocampus CA3 (Figure 5(c4)). Although the cell nucleus of astrocytes did not express NF-κB p65 during antibody treatment, the astrocytes still showed an activated phenotype (Figures 5(c1) and 5(d)).

4. Discussion

The results of this study provide important proof of principle for several aspects of the hypothesis that anti-IL-1β mAb-SPIONs, which cross the BBB, can be used to localize and delineate specific cerebral functions, such as the epileptogenic focus, and simultaneously have a powerful targeted anti-epileptic effect after tail vein administration in a rat model of acute seizures with neuropathologic features mimicking TLE. Most importantly, the improvement of neuropathology and neurotomy (decreased neuronal cell loss and astrocyte proliferation and inhibition of the NF-κB p65 activation) of epileptogenic tissues in rat brain provides evidence that the novel treatment showed high penetration of the antibody into the epileptogenic zone of the brain hippocampus of epileptic rats.

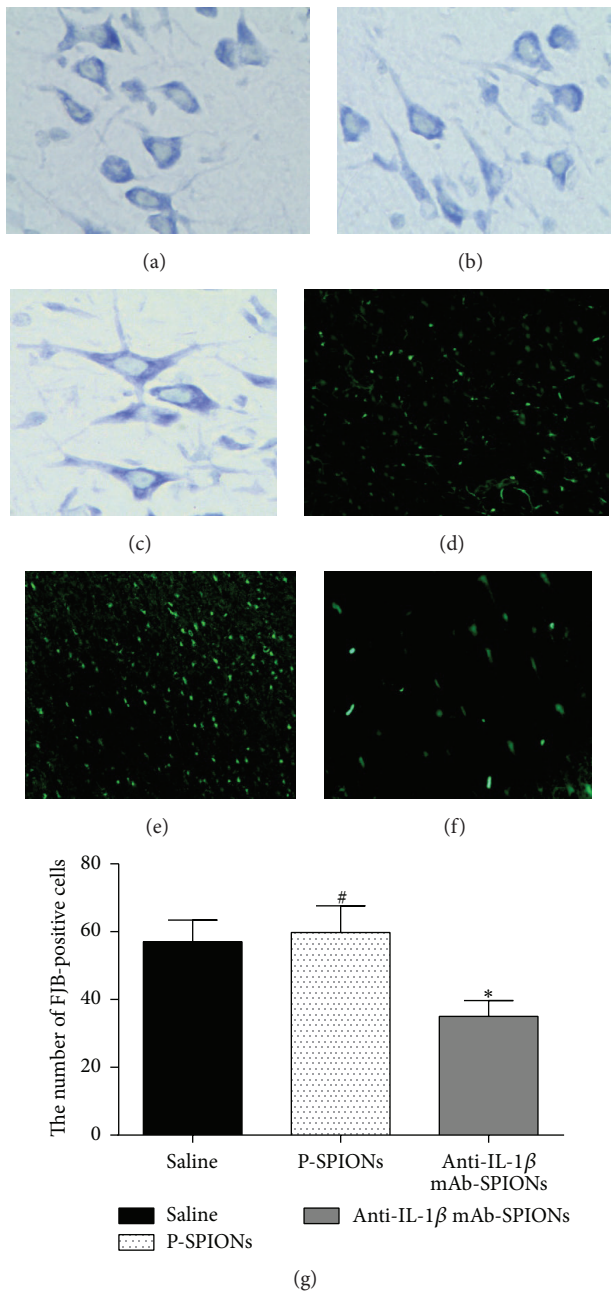

FIGURE 4: Effect of anti-IL-1β mAb-SPIONs dependency on SE-induced neuronal cell loss of hippocampus CA3 at 72 h post-SE after injection. ((a)–(c)) The Nissl staining (400x); ((d)-(e)) the FJB staining (40x) showed FJB-positive cells; ((a), (d)) saline group; ((b), (e)) P-SPIONs group; ((c), (f)) anti-IL-1β mAb-SPIONs group. (g) Data (mean ± SD, $n = 10$) present the number of the FJB-positive cells. $^{*}P < 0.05$ versus saline group and P-SPIONs group; $^{\#}P > 0.05$ versus saline group.

In the present study, we first focused on the uptake of the SPIONs particles and then the ability of crossing the BBB in the brain by the method of tracking even small amounts of magnetite-labeled nanoparticles in the rat brain using MRI [43] and Perl's iron staining. The T2-negative enhancement in epileptogenic tissues of the MRI patterns

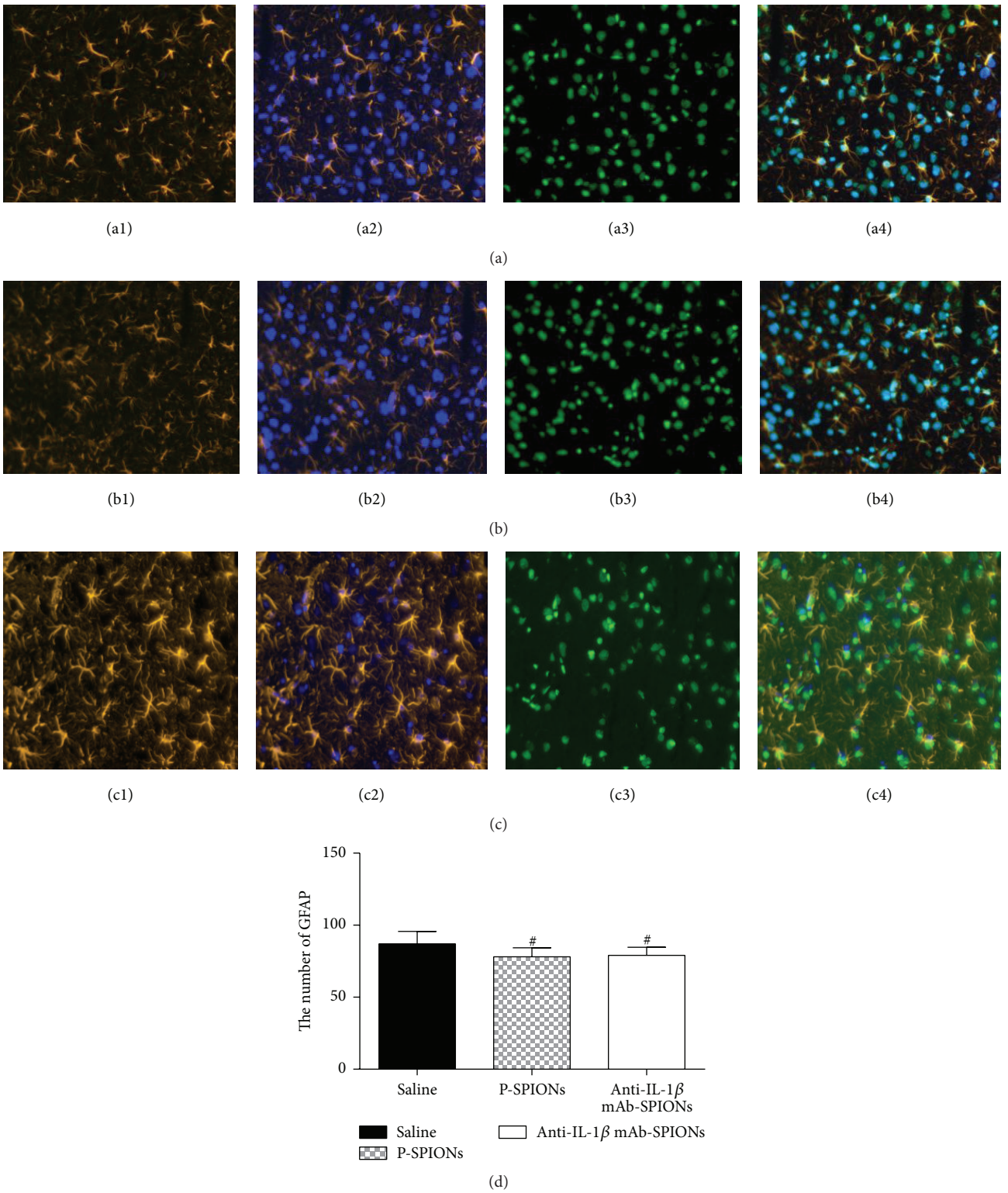

Figure 5: NF-kappa B p65 expression and astrocyte hyperplasia in the hippocampus CA3 of epileptic rats treated with anti-IL-1β mAb-SPIONs versus saline and P-SPIONs (20x); ((a1)–(b4)) show the activation of GFAP-positive astrocytes and the expression of NF-kappa B p65 in astrocyte nucleus was observed in the saline ((a1)–(a4)) and P-SPIONs groups ((b1)–(b4)). Colocalization panels ((a4)–(c4)) show NF-κB p65 expression in activated astrocytes in the hippocampus CA3 of epileptic rats; (c4) notes the inhibition of NF-κB p65 nucleus transfer in anti-IL-1β mAb-SPIONS-treated rats; (c1) shows that the astrocytes still have an activated phenotype. (d) shows the number of positive-GFAP astrocytes (mean ± SD, $n = 10$). $^{\#}P > 0.05$ versus saline group.

performed before and after anti-IL-1β mAb-SPIONs injection confirms previous results showing that these functionalized magnetized particles were taken up by brain parenchyma and then crossed the BBB in this epilepsy model [38, 44]. The results of the distribution of particles in the brain by Perl's iron staining showed that the number of iron particles of epileptogenic tissues in the experimental group exceeds the control groups, corresponding to the negative enhancement changes of MRI images. As a macromolecule, anti-IL-1β mAb cannot aggregate sufficiently to the brain because of an inability to cross the BBB. The results of the present *in vivo* study indicated that MTDS significantly improved the accumulation of the anti-IL-1β mAb in pathologic sites and decreased the undesirable side effects. The mechanisms underlying anti-IL-1β mAb-SPIONs crossing the BBB accounted for a number of observations. First, the inflammation induced by epileptic seizures and epileptic activity itself can result in BBB dysfunction (the disturbances of its integrity and functionality), including an increase in cerebral capillary permeability [45] and an increase in pinocytosis at the level of the cerebral endothelium [46]. Second, the inherent property of nanoparticles, such as the small size, can stick to the cell surface and participate in the material transfer between cells [30]. Previous evidence has shown that antibody-mediated targeting of iron oxide nanoparticles can cross the BBB by the method of receptor-mediated transcytosis [47]. Therefore, monoclonal antibodies, when chelated to the SPIONs, not only influence the specificity of drug delivery, but also penetrate and distribute anti-IL-1β mAb-SPIONs by rendering them capable of selectively binding certain antigens (IL-1β) overexpressed on epileptogenic tissues. The external magnetic field of MTDS, with the major advantage of combining simplicity, a modest cost, enhanced localization of deficient delivery, and reductions in both incubation time and vector doses [31], has directed the delivery of drug coupled to magnetic particles to further enhance selective brain deposition [32]. Recent information suggests that using a combined strategy of ultrasound, magnetic targeting, and drug-loaded nanoparticles can also improve the outcome of targeted delivery of chemotherapy drugs to the brain [48, 49]. The fact that SPIONs should be considered as a strong T2 contrast-enhancing agent, certified by the phantom study, is suggested by changes in negative enhancement between the MRI pattern seen with anti-IL-1β mAb-SPIONs and plain SPIONs or saline during the acute phase.

Although a number of previous studies have shown that IL-1β contributes to epileptic seizures and can be considered as a therapeutic target for TLE, few of the studies have attempted to use specific neutralizing antibody in the treatment of TLE. Here, we found the potential neuroprotective and anti-epileptic effect of anti-IL-1β mAb. In this study, the downregulation of IL-1β protein in Western blot after novel drug injection indicated that anti-IL-1β mAb, which binds tightly to IL-1β with a neutralization potency > 10 times higher than the marketed antibody, canakinumab [50], was highly sensitive and specific for IL-1β protein overexpressed in epileptogenic tissues. Previous evidence showed that neuroinflammation, triggered by the activation of the IL-1β/IL-1 receptor type 1 (IL-1R1) axis, played a key role in epileptogenic brain areas. IL-1R1-mediated posttranscriptional signaling in neurons, which was induced by IL-1β, promoted hyperexcitability, seizures, and excitotoxicity by enhancing neuronal Ca^{2+} influx. However, this study showed no statistical significance in expression of IL-1R1 protein after antibody treatment. Even so, this study demonstrated that neutralization of IL-1β simultaneously led to neuroprotective effects, remarkable reduction of hippocampal neuronal loss, and the improvement of neuronal organizational structure, on SE-associated neuronal damage in the CA3 area of the hippocampus as well as performing targeted location on MRI. The combined sensitivity and specificity of anti-IL-1β mAb-SPIONs provided a robust and safe theranostic platform for TLE.

Among the classical AEDs and the nonclassical anti-seizure drugs, vinpocetine and carbamazepine, with a mechanism of action that involves a decrease in Na^+ channel permeability, were investigated and shown to be highly effective in reducing the cerebral inflammatory IL-1β expression to render reducing the increased brain excitability accompanying seizures [51]. The neutralizing anti-interleukin-1β antibodies, as an anti-inflammatory drug, also have significant positive effects on other pathologic conditions. Recently, some researchers have found that in the fetus, the anti-IL-1β mAb which be taken up by brain in ischemia-reperfusion injury, can then attenuates ischemia-reperfusion related fetal BBB dysfunction [52]. In traumatic brain injury (TBI), similar to our studies, the neutralization of IL-1β was associated with improved histologic and cognitive outcome [53], modification of the inflammatory response, reduced loss of hemispheric tissue, and attenuation of the microglial activation caused by TBI [54]. However, in the present study, the behavioral analysis of epileptic rats after antibody treatment was not performed.

To evaluate potential mechanisms of action for the anti-inflammatory antibody, we then used immunofluorescent double-labeling staining of the CA3 region of the hippocampus to evaluate changes in activated NF-κB p65 and astrocyte hyperplasia induced by SE. The experimental results showed that the role of anti-IL-1β mAb-SPIONs on treatment for epilepsy is not affected by decreased proliferation of astrocytes, implying that astrocytes which affect the development of epilepsy are related to many mechanisms, such as ion channels and water channels, amino acid metabolism of the excitatory, and inhibitory amino acids in the inside and outside of cells, cell factors, and gap junctions. In terms of ion channels and water channels, previous study showed that astrocytes lost the ability of removal of K in patients with temporal lobe epilepsy and the marked increase in the neurons in a highly excited state [55]. In addition, the experiments have proved the existence of glutamate receptors on AST cell membranes, which is a type of excitatory neurotransmitter associated with seizures, and extracellular glutamate levels in the brain are increased. Glutamic acid can stimulate a paroxysmal depolarization offset [56], leading to an epileptic discharge. A study confirmed that IL-1 may reduce the production of glutamine by reducing Glu transporter activity, indirectly reducing Glu synthesis. IL-1β and high mobility group protein 1 (high mobility group box 1

protein (HMGB1)) may play a role in promoting the epileptic attack by making N-methyl-D-aspartate 2 B (N-methyl-D-aspartate (NMDA2B)) phosphorylation [57].

It is generally known that anti-inflammatory response and antiepileptic effect are complementary to each other. These experimental results suggest that the antiepileptic effect of anti-IL-1β mAb-SPIONs, which have decreased the number of IL-1β molecules, was realized by reducing the reaction of IL-1β with receptors on the surface of the astrocytes and then reduced the activation of inflammation in the cell signaling pathways in order for the inhibition of the occurrence of epilepsy by reducing the signal of the inflammation. Previous study showed that the downstream mediators of IL-1β signaling, for example, the activation of NF-κB, are attenuated and inhibition of nucleus transfer after neutralizing IL-1β after injection of antibody is associated with IL-1β upregulation following SE. These data are similar to previous evidence [58] and suggested that the proinflammatory cytokine, IL-1β, contributes to the process leading to increased cell death following TLE and is a key regulator of acute inflammatory processes in the CNS. Despite inflammatory processes, IL-1β was involved in the entire process of epilepsy; however, the postictal suppression (PS) phase, a common and important period following SE, is an important period of IL-1β action. Thus, only the acute stage (24 h after SE) was discussed. Nevertheless, the optimum concentration of anti-IL-1β mAb-SPIONs warrants further study.

5. Conclusion

In summary, this study provides the first direct evidence of the feasibility of a novel approach, integration of the anti-inflammatory drug, and functionalized SPIONs (MTDS), which crosses the BBB, in the simultaneous diagnosis and therapy of epileptic rats in acute stage of TLE *in vivo*. Magnetic field-guided delivery of the anti-IL-1β mAb-SPIONs enabled much more efficient uptake of SPIONs by brain tissues, significantly enhancing the neuroprotective effect of the delivered anti-inflammatory drug neutralizing-IL-1β antibody. Moreover, the anti-IL-1β mAb-SPIONS displayed much higher MRI T2 sensitivity than plain SPIONs, which makes them a very advantaged and safe therapeutic-diagnostic platform for simultaneous magnetic-targeted drugs and MRI diagnosis of other CNS diseases. Further *in vivo* studies to explore this potential are currently under way in our laboratory.

Conflict of Interests

The authors declare that they have no conflict of interests.

Acknowledgments

National Natural Science Foundation of China (Grant no. 81371423) has supported this work. The authors are greatly indebted to Department of Pathological Teaching and Research of Affiliated Hospital Jining Medical University and Key Laboratory of Molecular Pathology of Jining Medical University for invaluable technical assistance.

References

[1] P. Kwan, A. Arzimanoglou, A. T. Berg et al., "Definition of drug resistant epilepsy: consensus proposal by the ad hoc Task Force of the ILAE Commission on Therapeutic Strategies," *Epilepsia*, vol. 51, no. 6, pp. 1069–1077, 2010.

[2] C. A. Espinosa-Jovel and F. E. Sobrino-Mejía, "Drug resistant epilepsy. Clinical and neurobiological concepts," *Revista de Neurologia*, vol. 61, no. 4, pp. 159–166, 2015.

[3] C. A. Espinosa-Jovel and F. E. Sobrino-Mejia, "Drug resistant epilepsy. Clinical and neurobiological concepts," *Revue Neurologique*, vol. 61, no. 4, pp. 159–166, 2015.

[4] J. Gomez-Alonso and P. Bellas-Lamas, "Surgical treatment for drug-resistant epilepsy," *The Journal of the American Medical Association*, vol. 313, no. 15, article 1572, 2015.

[5] C. B. Nemeroff, H. S. Mayberg, S. E. Krahl et al., "VNS therapy in treatment-resistant depression: clinical evidence and putative neurobiological mechanisms," *Neuropsychopharmacology*, vol. 31, no. 7, pp. 1345–1355, 2006.

[6] M. Herring, "Commentary on 'vagus nerve stimulation therapy for treatment of drug-resistant epilepsy and depression'," *Perspectives in Vascular Surgery and Endovascular Therapy*, vol. 18, no. 4, p. 328, 2006.

[7] A. Chambers and J. M. Bowen, "Electrical stimulation for drug-resistant epilepsy—an evidence-based analysis," *Ontario Health Technology Assessment Series*, vol. 13, no. 18, pp. 1–37, 2013.

[8] A. W. C. Yuen and J. W. Sander, "Rationale for using intermittent calorie restriction as a dietary treatment for drug resistant epilepsy," *Epilepsy and Behavior*, vol. 33, pp. 110–114, 2014.

[9] J. J. Engel, "Approaches to refractory epilepsy," *Annals of Indian Academy of Neurology*, vol. 17, supplement 1, pp. S12–S17, 2014.

[10] R. S. Greenwood, "Adverse effects of antiepileptic drugs," *Epilepsia*, vol. 41, supplement 2, pp. S42–S52, 2000.

[11] K. Bates, "Epilepsy: current evidence-based paradigms for diagnosis and treatment," *Primary Care: Clinics in Office Practice*, vol. 42, no. 2, pp. 217–232, 2015.

[12] M. Bagary, "Epilepsy, antiepileptic drugs and suicidality," *Current Opinion in Neurology*, vol. 24, no. 2, pp. 177–182, 2011.

[13] T. Kubo, T. Sugita, S. Shimose, Y. Nitta, Y. Ikuta, and T. Murakami, "Targeted delivery of anticancer drugs with intravenously administered magnetic liposomes in osteosarcoma-bearing hamsters," *International Journal of Oncology*, vol. 17, no. 2, pp. 309–315, 2000.

[14] T. Kato, R. Nemoto, H. Mori et al., "Magnetic microcapsules for targeted delivery of anticancer drugs," *Applied Biochemistry and Biotechnology*, vol. 10, no. 1–3, pp. 199–211, 1984.

[15] A. Mardinoglu and P. J. Cregg, "Modelling the effect of SPION size in a stent assisted magnetic drug targeting system with interparticle interactions," *The Scientific World Journal*, vol. 2015, Article ID 618658, 7 pages, 2015.

[16] J. Zhang and R. D. K. Misra, "Magnetic drug-targeting carrier encapsulated with thermosensitive smart polymer: core-shell nanoparticle carrier and drug release response," *Acta Biomaterialia*, vol. 3, no. 6, pp. 838–850, 2007.

[17] R. M. Kaminski, M. A. Rogawski, and H. Klitgaard, "The potential of antiseizure drugs and agents that act on novel molecular targets as antiepileptogenic treatments," *Neurotherapeutics*, vol. 11, no. 2, pp. 385–400, 2014.

[18] M. Falip, X. Salas-Puig, and C. Cara, "Causes of CNS inflammation and potential targets for anticonvulsants," *CNS Drugs*, vol. 27, no. 8, pp. 611–623, 2013.

[19] M. A. Galic, K. Riazi, and Q. J. Pittman, "Cytokines and brain excitability," *Frontiers in Neuroendocrinology*, vol. 33, no. 1, pp. 116–125, 2012.

[20] A. Vezzani, "Innate immunity and inflammation in temporal lobe epilepsy: new emphasis on the role of complement activation," *Epilepsy Currents*, vol. 8, no. 3, pp. 75–77, 2008.

[21] M. Rizzi, C. Perego, M. Aliprandi et al., "Glia activation and cytokine increase in rat hippocampus by kainic acid-induced status epilepticus during postnatal development," *Neurobiology of Disease*, vol. 14, no. 3, pp. 494–503, 2003.

[22] C. Dube, A. Vezzani, M. Behrens, T. Bartfai, and T. Baram, "Interleukin-1beta contributes to the generation of experimental febrile seizures," *Annals of Neurology*, vol. 57, no. 1, pp. 152–155, 2005.

[23] Z. Xiao, J. Peng, L. Yang, H. Kong, and F. Yin, "Interleukin-1β plays a role in the pathogenesis of mesial temporal lobe epilepsy through the PI3K/Akt/mTOR signaling pathway in hippocampal neurons," *Journal of Neuroimmunology*, vol. 282, pp. 110–117, 2015.

[24] A. Chiavegato, E. Zurolo, G. Losi, E. Aronica, and G. Carmignoto, "The inflammatory molecules IL-1β and HMGB1 can rapidly enhance focal seizure generation in a brain slice model of temporal lobe epilepsy," *Frontiers in Cellular Neuroscience*, vol. 8, article 155, 2014.

[25] T. Ravizza, F. Noé, D. Zardoni, V. Vaghi, M. Sifringer, and A. Vezzani, "Interleukin converting enzyme inhibition impairs kindling epileptogenesis in rats by blocking astrocytic IL-1β production," *Neurobiology of Disease*, vol. 31, no. 3, pp. 327–333, 2008.

[26] A. Vezzani and B. Viviani, "Neuromodulatory properties of inflammatory cytokines and their impact on neuronal excitability," *Neuropharmacology*, vol. 96, pp. 70–82, 2015.

[27] A. Vezzani, J. French, T. Bartfai, and T. Z. Baram, "The role of inflammation in epilepsy," *Nature Reviews Neurology*, vol. 7, no. 1, pp. 31–40, 2011.

[28] Y. S. Yim, J. Choi, G. T. Kim et al., "A facile approach for the delivery of inorganic nanoparticles into the brain by passing through the Blood–Brain Barrier (BBB)," *Chemical Communications*, vol. 48, no. 1, pp. 61–63, 2012.

[29] M. Tajes, E. Ramos-Fernández, X. Weng-Jiang et al., "The blood-brain barrier: structure, function and therapeutic approaches to cross it," *Molecular Membrane Biology*, vol. 31, no. 5, pp. 152–167, 2014.

[30] R. Vidu, M. Rahman, M. Mahmoudi, M. Enachescu, T. D. Poteca, and I. Opris, "Nanostructures: a platform for brain repair and augmentation," *Frontiers in Systems Neuroscience*, vol. 8, article 91, 2014.

[31] J. Estelrich, E. Escribano, J. Queralt, and M. Busquets, "Iron oxide nanoparticles for magnetically-guided and magnetically-responsive drug delivery," *International Journal of Molecular Sciences*, vol. 16, no. 4, pp. 8070–8101, 2015.

[32] T. Wiedmann, X. Yuanyuan, and Z. Pengyun, "Magnetic targeted drug delivery," *Songklanakarin Journal of Science and Technology*, vol. 31, no. 3, pp. 409–417, 2009.

[33] M. Mahmoudi, S. Sant, B. Wang, S. Laurent, and T. Sen, "Superparamagnetic iron oxide nanoparticles (SPIONs): development, surface modification and applications in chemotherapy," *Advanced Drug Delivery Reviews*, vol. 63, no. 1-2, pp. 24–46, 2011.

[34] S. Yoffe, T. Leshuk, P. Everett, and F. Gu, "Superparamagnetic iron oxide nanoparticles (SPIONs): synthesis and surface modification techniques for use with MRI and other biomedical applications," *Current Pharmaceutical Design*, vol. 19, no. 3, pp. 493–509, 2013.

[35] B. R. Smith, J. Heverhagen, M. Knopp et al., "Localization to atherosclerotic plaque and biodistribution of biochemically derivatized superparamagnetic iron oxide nanoparticles (SPIONs) contrast particles for magnetic resonance imaging (MRI)," *Biomedical Microdevices*, vol. 9, no. 5, pp. 719–727, 2007.

[36] S. Mahajan, V. Koul, V. Choudhary, G. Shishodia, and A. C. Bharti, "Preparation and in vitro evaluation of folate-receptor-targeted SPION-polymer micelle hybrids for MRI contrast enhancement in cancer imaging," *Nanotechnology*, vol. 24, no. 1, Article ID 015603, 2013.

[37] Wahajuddin and S. Arora, "Superparamagnetic iron oxide nanoparticles: magnetic nanoplatforms as drug carriers," *International Journal of Nanomedicine*, vol. 7, pp. 3445–3471, 2012.

[38] M. Akhtari, A. Bragin, M. Cohen et al., "Functionalized magnetonanoparticles for MRI diagnosis and localization in epilepsy," *Epilepsia*, vol. 49, no. 8, pp. 1419–1430, 2008.

[39] M. Akhtari, A. Bragin, R. Moats, A. Frew, and M. Mandelkern, "Imaging brain neuronal activity using functionalized magnetonanoparticles and MRI," *Brain Topography*, vol. 25, no. 4, pp. 374–388, 2012.

[40] V. I. Shubayev, T. R. Pisanic II, and S. Jin, "Magnetic nanoparticles for theragnostics," *Advanced Drug Delivery Reviews*, vol. 61, no. 6, pp. 467–477, 2009.

[41] C. Wang, S. Ravi, U. S. Garapati et al., "Multifunctional Chitosan Magnetic-Graphene (CMG) nanoparticles: a theranostic platform for tumor-targeted co-delivery of drugs, genes and MRI contrast agents," *Journal of Materials Chemistry B*, vol. 1, no. 35, pp. 4396–4405, 2013.

[42] R. J. Racine, "Modification of seizure activity by electrical stimulation: I. After-discharge threshold," *Electroencephalography and Clinical Neurophysiology*, vol. 32, no. 3, pp. 269–279, 1972.

[43] N. P. Martínez Vera, R. Schmidt, K. Langer et al., "Tracking of magnetite labeled nanoparticles in the rat brain using MRI," *PLoS ONE*, vol. 9, no. 3, Article ID e92068, 2014.

[44] J. A. Loureiro, B. Gomes, M. A. N. Coelho, M. Do Carmo Pereira, and S. Rocha, "Targeting nanoparticles across the blood-brain barrier with monoclonal antibodies," *Nanomedicine*, vol. 9, no. 5, pp. 709–722, 2014.

[45] S. H. Sheen, J.-E. Kim, H. J. Ryu, Y. Yang, K.-C. Choi, and T.-C. Kang, "Decrease in dystrophin expression prior to disruption of brain-blood barrier within the rat piriform cortex following status epilepticus," *Brain Research*, vol. 1369, pp. 173–183, 2011.

[46] E. Oby and D. Janigro, "The blood-brain barrier and epilepsy," *Epilepsia*, vol. 47, no. 11, pp. 1761–1774, 2006.

[47] K. Griswold, C. Ndong, S. Toraya-Brown et al., "Antibody-mediated targeting of iron oxide nanoparticles to the folate receptor alpha increases tumor cell association in vitro and in vivo," *International Journal of Nanomedicine*, vol. 2015, no. 10, pp. 2595–2617, 2015.

[48] C. X. Deng and X. Huang, "Improved outcome of targeted delivery of chemotherapy drugs to the brain using a combined strategy of ultrasound, magnetic targeting and drug-loaded nanoparticles," *Therapeutic Delivery*, vol. 2, no. 2, pp. 137–141, 2011.

[49] C. C. Chen, P. S. Sheeran, S.-Y. Wu, O. O. Olumolade, P. A. Dayton, and E. E. Konofagou, "Targeted drug delivery

with focused ultrasound-induced blood-brain barrier opening using acoustically-activated nanodroplets," *Journal of Controlled Release*, vol. 172, no. 3, pp. 795–804, 2013.

[50] A. X. H. Goh, S. Bertin-Maghit, S. P. Yeo et al., "A novel human anti-interleukin-1β neutralizing monoclonal antibody showing in vivo efficacy," *mAbs*, vol. 6, no. 3, pp. 765–773, 2014.

[51] C. D. Gómez, R. M. Buijs, and M. Sitges, "The anti-seizure drugs vinpocetine and carbamazepine, but not valproic acid, reduce inflammatory IL-1β and TNF-α expression in rat hippocampus," *Journal of Neurochemistry*, vol. 130, no. 6, pp. 770–779, 2014.

[52] X. Chen, G. B. Sadowska, J. Zhang et al., "Neutralizing anti-interleukin-1β antibodies modulate fetal blood-brain barrier function after ischemia," *Neurobiology of Disease*, vol. 73, pp. 118–129, 2015.

[53] F. Clausen, A. Hånell, M. Björk et al., "Neutralization of interleukin-1β modifies the inflammatory response and improves histological and cognitive outcome following traumatic brain injury in mice," *European Journal of Neuroscience*, vol. 30, no. 3, pp. 385–396, 2009.

[54] F. Clausen, A. Hånell, C. Israelsson et al., "Neutralization of interleukin-1β reduces cerebral edema and tissue loss and improves late cognitive outcome following traumatic brain injury in mice," *European Journal of Neuroscience*, vol. 34, no. 1, pp. 110–123, 2011.

[55] A. Das, G. C. Wallace IV, C. Holmes et al., "Hippocampal tissue of patients with refractory temporal lobe epilepsy is associated with astrocyte activation, inflammation, and altered expression of channels and receptors," *Neuroscience*, vol. 220, pp. 237–246, 2012.

[56] N. Siva, "Astrocytes have a key role in epilepsy," *The Lancet Neurology*, vol. 4, no. 10, p. 601, 2005.

[57] P. Karki, K. Smith, J. Johnson Jr., M. Aschner, and E. Y. Lee, "Genetic dys-regulation of astrocytic glutamate transporter EAAT2 and its implications in neurological disorders and manganese toxicity," *Neurochemical Research*, vol. 40, no. 2, pp. 380–388, 2015.

[58] M. L. Diamond, A. C. Ritter, M. D. Failla et al., "IL-1β associations with posttraumatic epilepsy development: a genetics and biomarker cohort study," *Epilepsia*, vol. 55, no. 7, pp. 1109–1119, 2014.

Hindawi Publishing Corporation
Neural Plasticity
Volume 2016, Article ID 5249893, 8 pages
http://dx.doi.org/10.1155/2016/5249893

Research Article

Dynamic Alterations of miR-34c Expression in the Hypothalamus of Male Rats after Early Adolescent Traumatic Stress

Chuting Li, Yuan Liu, Dexiang Liu, Hong Jiang, and Fang Pan

Department of Medical Psychology, Shandong University School of Medicine, No. 44 Wenhua Xi Road, Jinan, Shandong 250012, China

Correspondence should be addressed to Fang Pan; panfangsdu@126.com

Received 14 November 2015; Revised 4 January 2016; Accepted 6 January 2016

Academic Editor: Alfredo Pereira Jr.

Several types of microRNA (miRNA) overexpression in the brain are associated with stress. One of the targets of miR-34c is the stress-related corticotrophin releasing factor receptor 1 mRNA (CRFR1 mRNA). Here we will probe into the short-term effect and long-term effect of early adolescent traumatic stress on the expression of miR-34c and CRFR1 mRNA. Traumatic stress was established by electric foot shock for six consecutive days using 28-day rats. The anxiety-like behaviors, memory damage, CRFR1 protein, CRFR1 mRNA, and miR-34c expression were detected in our study. The results of our study proved that exposure to acute traumatic stress in early adolescent can cause permanent changes in neural network, resulting in dysregulation of CRFR1 expression and CRFR1 mRNA and miR-34c expression in hypothalamus, anxiety-like behavior, and memory impairment, suggesting that the miR-34c expression in hypothalamus may be an important factor involved in susceptibility to PTSD.

1. Introduction

Posttraumatic stress disorder (PTSD) is a prevalent anxiety disorder triggered by the traumatic experiences which produce strong negative feelings, such as horror, intense fear, and helplessness [1]. The hypothalamic-pituitary-adrenal (HPA) axis plays a pivotal role in stress induced neural plasticity, so that dysregulation of HPA axis is responsible for susceptibility to certain anxiety disorders [2]. Further, as the key upstream factors in HPA axis, CRHR1 was considered as a critical factor in etiology and vulnerability of PTSD [3]. One study has showed that CRHR1 could strengthen the traumatic memories in limbic system of mice after exposure to foot shock stress [3]. Our previous study also showed that traumatic stress in early adolescence triggered long-term effect on central CRFR1 expression and induced dysfunction of HPA axis in adulthood [4].

MicroRNAs (miRNAs), a subset of endogenous small RNA molecules, are widely expressed in astrocytes and neurons in the brain and perform crucial regulatory functions in gene expression in the central nerve system [5, 6]. Previous studies have found that dicer1 and miR-17 expression were increased in reactive astrocyte, and it is also reported that dicer1 plays an important role in astrocyte development [7]. miRNAs exert their function via base-pairing with complementary sequences within mRNA molecules. Upon sequence-specific binding of miRNAs, mRNA molecules are destabilized through shortening of their poly(A) tails or degraded by cleavage of the mRNA strand or less efficiently translated into proteins by ribosomes [8, 9]. One study has observed that miRNAs are expressed differentially in patients with different psychiatric diseases. Meanwhile, stress, glucocorticoids, and mood stabilizers altered the miRNAs level of the patients, suggesting that miRNAs may be the potential vital factors of the pathophysiology and therapeutics of mental diseases [10]. More studies also pointed out that certain miRNAs may act as epigenetic modulators of gene expression in psychiatric disorders like autism, schizophrenia, major depression, and anxiety [10–12]; specific miRNAs were related to neuronal differentiation and synaptic plasticity and the treatment target of anxiety disorders [13]. Those studies indicated that the alterations of certain miRNAs expression had implication in pathogenesis of PTSD [10, 14].

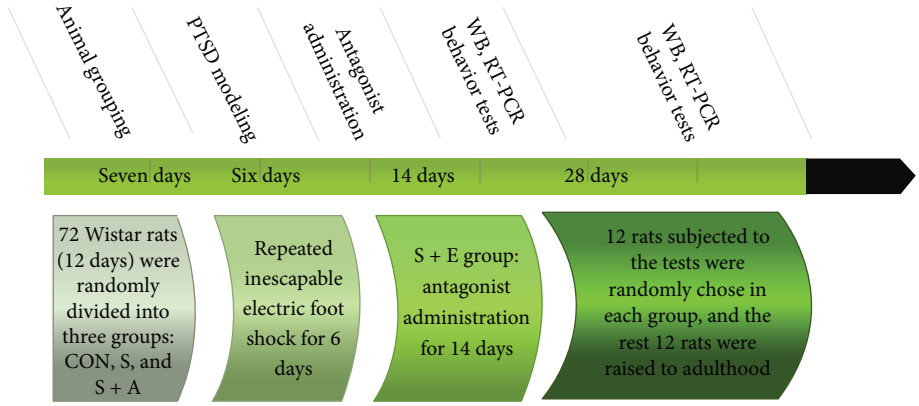

Figure 1

miR-34c is a stress-related miRNA which was prominently increased after traumatic stress and associated with decreased anxiety-like behaviors. What caught our attention was that CRFR1 mRNA is the target of miR-34c. Previous work has confirmed that miR-34c combined with an evolutionarily conserved region in the 3′UTR of CRFR1 mRNA perform its effect. miR-34c reduces the expression of stress-related proteins (such as CRFR1) and plays a role in the recovery process of stress reaction, suggesting that it might have vital implication in vulnerability to PTSD and might become a new target for the prevention and treatment of stress-related disorders [15].

Adolescence is a very rapid development period, which had increased susceptibility to stress. Recent studies have showed that early life stress may have more influence on epigenetic states and brain function than similar stress exposure later in life [16]. Our previous study showed that early life stress increased susceptibility to stress through CRFR1 expression in brain [4]; another study has observed that early life stress activated REST4-mediated gene transcription in the medial prefrontal cortex [17]. Those studies provided new insights that miRNAs could regulate gene expression which alters susceptibility to developing stress-related diseases in adulthood after early life stress. However, miR-34c expression and the association between miR-34c and CRF1 expression in hypothalamus in adult rats after adolescent stress had not clarified.

In the present study, we used our previously established rat model for PTSD, which replicates the specific neuroendocrinological abnormalities observed in PTSD patients [4, 18]. We would observe miR-34c expression in the hypothalamus after adolescent stress because this brain region is a complex region considered to be part of the limbic system and integrate the nervous system and the endocrine system and act as a "switching station" in the brain [19]. The purpose of the study was first to detect dynamic changes, including short-term state and long-term state of miR-34c expression after early adolescent exposure to the stress. Second, we probe into the question whether miR-34c expression could timely regulate CRFR1 expression by using CRFR1 antagonist to block the CRFR1 activity.

2. Methods and Materials

2.1. Animals. A total of 72 male Wistar rats (21 days old, obtained from the experimental animal center of Shandong University, China) were group-caged (two or three per cage) under controlled lighting conditions (07:00–19:00 h) and temperatures (25 ± 2°C) with food and water made available ad libitum and allowed to acclimate for seven days prior to experimental testing. The study was approved by the Institutional Animal Care Committee of Shandong University. Rats were randomly divided into three groups (n = 24 in each group): the control group (CON), the stress group (S), and the stress and antagonist group (S + A). After animal modeling and drug administration (two weeks after foot shock), 12 rats randomly chosen from each group were sacrificed after behavioral tests. The rest of the animals were raised to adulthood (six weeks after foot shock) and were sacrificed after behavioral tests (see Figure 1).

2.2. Animal Model of PTSD. With the exception of the control group, the rats received the repeated inescapable electric foot shock for six consecutive days, according to the previously published method [4, 18]. In each day, there were two trials which lasted for 30 minutes; the interval between the two trials was not less than 4 hours. In each trial, electric foot shock continued for 6 seconds and repeated 20 times with a random interval. The current intensity of electric foot shock was 0.5 mA.

2.3. Antagonist Administration. CRFR1 antagonist CP-154, 526 (Sigma-Aldrich, USA) was administered intraperitoneally. The rats in S + A group were treated with CP-154, 526 (3.2 mg/kg/day, in vehicle) for 14 days after the foot shock stress. Rats in other groups were treated with vehicle (80% polyethylene glycol 400) to balance the systematic error. The dose of CP-154, 526 was determined according to a previous study [20].

2.4. Elevated Plus Maze (EPM). The elevated plus maze consisted of three parts and two opposite closed arms (50 × 10 cm^2) with 40 cm tall nontransparent walls, two opposite

open arms ($50 \times 10\,cm^2$), and a central part ($10 \times 10\,cm^2$), which was elevated 50 cm above the floor. The laboratory room was maintained with controlled levels of light and temperatures. The rats were individually placed in the center part of the maze facing an open arm and allowed free exploration for 5 minutes. The apparatus was completely cleaned with 75% ethanol between two sessions. The number of entries into each arm and the total time spent in each arm were recorded by the SMART video tracking system (SMART v3.0, Panlab, Spain). Ratio entry was defined as the total entries into the open arms divided by the total entries into any arm of the maze. Ratio time was defined as the total time spent in the open arms divided by the total time spent in any arm of the maze. Anxiety score was calculated as anxiety score = 1 − (ratio time + ratio entry/2). Anxious rats were more likely to stay in the closed arms so that a reduced ratio entry or ratio time indicates a more anxious status. When the ratio entry and ratio time are zero, the anxiety score is 1, which means extreme anxiety [21].

2.5. Morris Water Maze. The test was carried out within 24 h after EPM test. The water maze was a cylindrical black galvanized metal container that was 120 cm in diameter and equipped with a platform 1-2 cm below the water surface. The visual objects were placed at fixed positions to serve as visual cues for the location of the platform. The swimming track of the animals in the water maze was recorded and measured by the SMART video tracking system (SMART v3.0, Panlab, Spain). At the start of learning trail, animals were placed on the platform for 10 s to familiarize themselves with the environment. Then the animals were individually placed in the water facing the wall of the water maze and trained to find the platform from different locations (E, S, W, and N) around the edge of the container for 5 consecutive days. Once the animals reach the platform, the trial was terminated. If the animals failed to find the platform within 60 s, the animal was placed on the platform for 10 s and the latency was recorded as 60 s. The time(s) of escape latency to find the platform was recorded and measured by the SMART video tracking system (SMART v3.0, Panlab, Spain). On day 6, the original platform was removed and this quadrant was defined as target quadrant. The animals were placed in the quadrant opposite the platform and allowed free exploration for 1 min. The entries to the target quadrant and cumulative time spending in the target quadrant were recorded and measured by the SMART video tracking system (SMART v3.0, Panlab, Spain).

2.6. Western Blotting

2.6.1. Tissue Preparation. Six rats in each group were decapitated immediately after behavioral tests. The rat's skull was cut and both sides of the frontal and the parietal bone were pulled off to collect the whole brain from the cranial cavity. After that, the hypothalamus was collected and immersed immediately in liquid nitrogen and stored at −80°C for further protein isolation.

2.6.2. Protein Isolation. To isolate protein sample, the brain tissue was homogenized in the lysis buffer (50 mM Tris (pH 7.4), 150 mM NaCl, 1% Triton X-100, 1% sodium deoxycholate, 0.1% SDS, sodium orthovanadate, sodium fluoride, EDTA, and leupeptin) supplemented with 1% protease inhibitor phenylmethanesulfonyl fluoride (PMSF) in a ratio of 1 : 5 (1 g tissue/5 mL reagent). The lysed tissue sample was centrifuged at 14000 g at 4°C for 30 min, and then the protein-containing supernatant obtained was either immediately used or stored at −80°C. The protein concentration was detected by BCA Protein Assay Kit (Beyotime Institute of Biotechnology) using the iMark Microplate Absorbance Reader (Bio-Rad, CA, USA).

2.6.3. CRFR1 Western Blotting. Brain protein samples containing the same amount of total proteins were mixed with a 6x Laemmli loading buffer (Tris-HCl, 50 mM, pH 6.8; dithiothreitol, 0.1 M, pH 6.8; glycerol, 10%; sodium dodecyl sulfate (SDS), 2%; and bromophenol blue, 0.02 mg/mL). The mixed protein sample was heated at 99°C for 5 min to cause protein denaturation, and then 20 μg of protein sample was separated on 12% sodium dodecyl sulfate-polyacrylamide (SDS-PAGE) gel and electrotransferred to polyvinylidene difluoride (PVDF) membranes (Bio-Rad, CA, USA). The membrane was blocked with 5% BSA in TBS containing 0.1% tween-20 (TBST) for 1 h and incubated with primary antibodies against CRFR1 (1 : 4000, Sigma-Aldrich, USA, SAB4500465) or GAPDH (1 : 4000, Biogot Technology, Co., Ltd.) at 4°C overnight in a refrigerator. On the following day, after washing with TBST for 5 min three times, the PVDF membrane was incubated for 1 h at room temperature with the horseradish peroxidase- (HRP-) conjugated secondary antibody (1 : 10000). Then, the PVDF membrane was washed again with TBST for 15 min three times, the Western blots were visualized after being incubated with ECL solution (Millipore Corp., Billerica, Massachusetts, USA) for 1 min and exposed onto photographic films (Eastman Kodak Company, Rochester, New York, USA) for 10–90 sec. Signal intensities were quantified by the Image J 14.0 software and the density value of the objective protein band was normalized according to that of the GAPDH band of the same sample.

2.7. Real-Time PCR Assay. Six rats in each group were used to detected CRFR1 mRNA and miR-34c expression. Each hypothalamus was mixed with 1 mL Trizol (Invitrogen) to extract total RNA from frozen samples. 1 mL of RNA was used to measure the expression of CRFR1 mRNA or miR-34c by RT-PCR. The expression of GAPDH or U6 was used as internal control. The expression of CRFR1 mRNA or miR-34c was calculated according to the threshold cycle (Ct); the CT of the target gene for each sample was corrected by subtracting the CT of the internal control (ΔCT). The controls were chosen as reference samples with mean ΔCT for the control samples being subtracted from the ΔCT for all the experimental samples (ΔΔCT). Finally, relative expression levels were calculated as $2^{-[(\text{Ct of CRFR1 mRNA})-(\text{Ct of GAPDH})]}$ or $2^{-[(\text{Ct of miR-34c})-(\text{Ct of U6})]}$. Real-time PCR experiments were performed by Kangchen Bio-Tech, Shanghai, China.

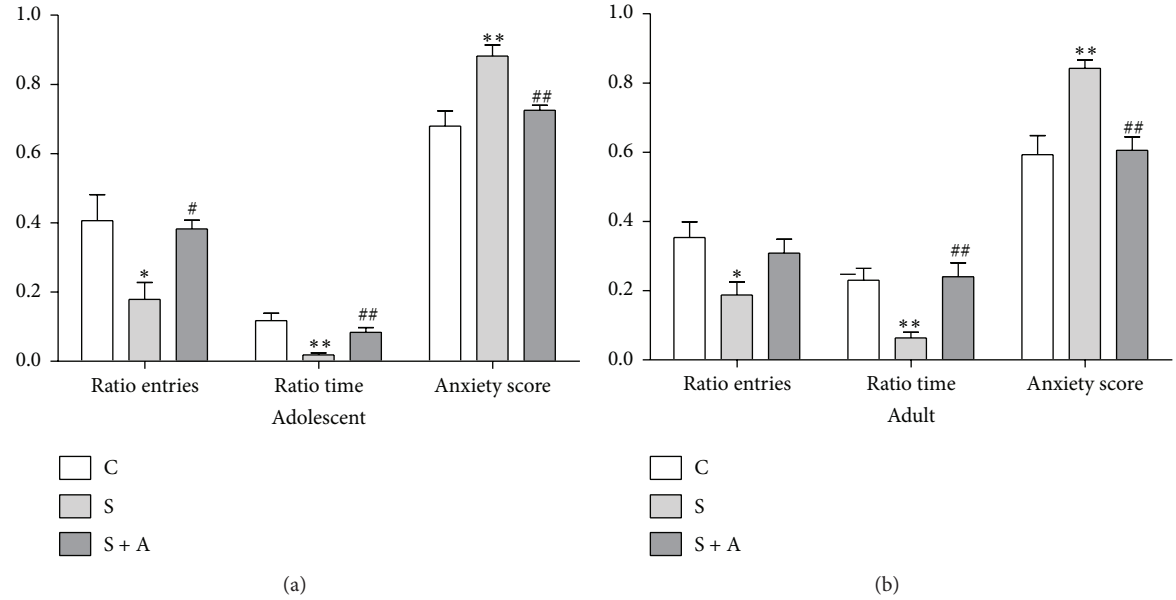

Figure 2: Anxiety-like behavior in the EPM test ($n = 8$ in each group). (a) Anxiety-like behavior of rats in the EPM test in adolescence. (b) Anxiety-like behavior of rats in the EPM test in adulthood. Ratio entry was defined as the total entries into the open arms divided by the total entries into any arm of the maze. Ratio time was defined as the total time spent in the open arms divided by the total time spent in any arm of the maze. Anxiety score was calculated as anxiety score = 1 − (ratio time + ratio entry/2). Values were expressed as mean ± SEM. ∗ and ∗∗ indicate $p < 0.05$ and $p < 0.01$ versus CON, respectively; # and ## indicate $p < 0.05$ and $p < 0.01$ versus S, respectively.

2.8. Statistical Analysis. All analyses were carried out using the statistical software SPSS18.0. The repeated-measures analysis of variance (ANOVA) was used for the analysis of the escape latency among different groups in the Morris water maze. One-way ANOVA was used for the analysis of the other dates. Post hoc analyses consisted of F tests for simple effects and Turkey's and Games-Howell tests where appropriate. Results were expressed as the mean ± standard error of the mean (SEM). Significances were accepted to be present at $p < 0.05$.

3. Results

3.1. Behavioral Test

3.1.1. EPM Test. Figure 2(a) shows the ratio entry to the open arm [$F(2, 22) = 5.444$, $p = 0.012$], ratio time in the open arm [$F(2, 22) = 10.914$, $p = 0.001$], and anxiety score [$F(2, 22) = 10.575$, $p = 0.001$] displayed by the rats two weeks after foot shook. S group had lower ratio entry than the CON ($p = 0.018$) and S + A ($p = 0.035$) groups. Ratio time in the open arm was lower in the S group than the CON ($p = 0.005$) and S + A ($p = 0.005$) groups. Anxiety scores were higher in the S group than the CON ($p = 0.007$) and S + A ($p = 0.003$) groups. Figure 2(b) shows the long-lasting effects of adolescent foot shock on anxiety-like behaviors of rats later in adulthood. Similar group differences were observed in ratio entry to the open arm [$F(2, 22) = 4.32$, $p = 0.027$], ration time in the open arm [$F(2, 22) = 9.495$, $p = 0.001$], and anxiety score [$F(2, 22) = 11.473$, $p = 0.000$]. S group had lower ratio entry than the CON group ($p = 0.025$), lower ratio time than the CON ($p = 0.004$) and S + A ($p = 0.002$) groups, and higher anxiety score than the CON ($p = 0.001$) and S + A ($p = 0.002$) groups.

3.1.2. Memory Function Test. The Morris water maze was performed two weeks and six weeks after foot shock. The mean time to find the platform in the training days is shown in Figures 3(a) and 3(b), and repeated-measures ANOVA confirmed that there was no obvious difference among these groups. One-way ANOVA showed similar differences in the number of entries (Figure 3(c)) and the time spent in the target quadrants (Figure 3(d)) of the adolescent rats and adult rats. Two weeks after foot shock, S group performed less entries to the target quadrants than CON ($p = 0.004$) and S + A ($p = 0.026$) groups [$F(2, 22) = 7.252$, $p = 0.003$] and lower time spent in the target quadrants than CON ($p = 0.004$) and S + A ($p = 0.026$) groups [$F(2, 22) = 13.482$, $p = 0.000$]. Six weeks after foot shock, S group performed less entries to the target quadrants than CON ($p = 0.001$) and S + A ($p = 0.031$) groups [$F(2, 22) = 9.88$, $p = 0.001$] and lower time spent in the target quadrants than CON ($p = 0.000$) group [$F(2, 22) = 11.883$, $p = 0.000$].

3.2. CRFR1 Expression in Hypothalamus. In the adolescent hypothalamus [$F(2, 16) = 9.275$, $p = 0.002$; see Figure 4], the S group ($p = 0.021$) and S + A group ($p = 0.002$) had lower CRFR1 expression than the CON group. However, in the adult hypothalamus [$F(2, 16) = 9.706$, $p = 0.002$; see Figure 4], S group exhibited higher CRFR1 expressions than the CON group ($p = 0.002$) and S + A group ($p = 0.032$).

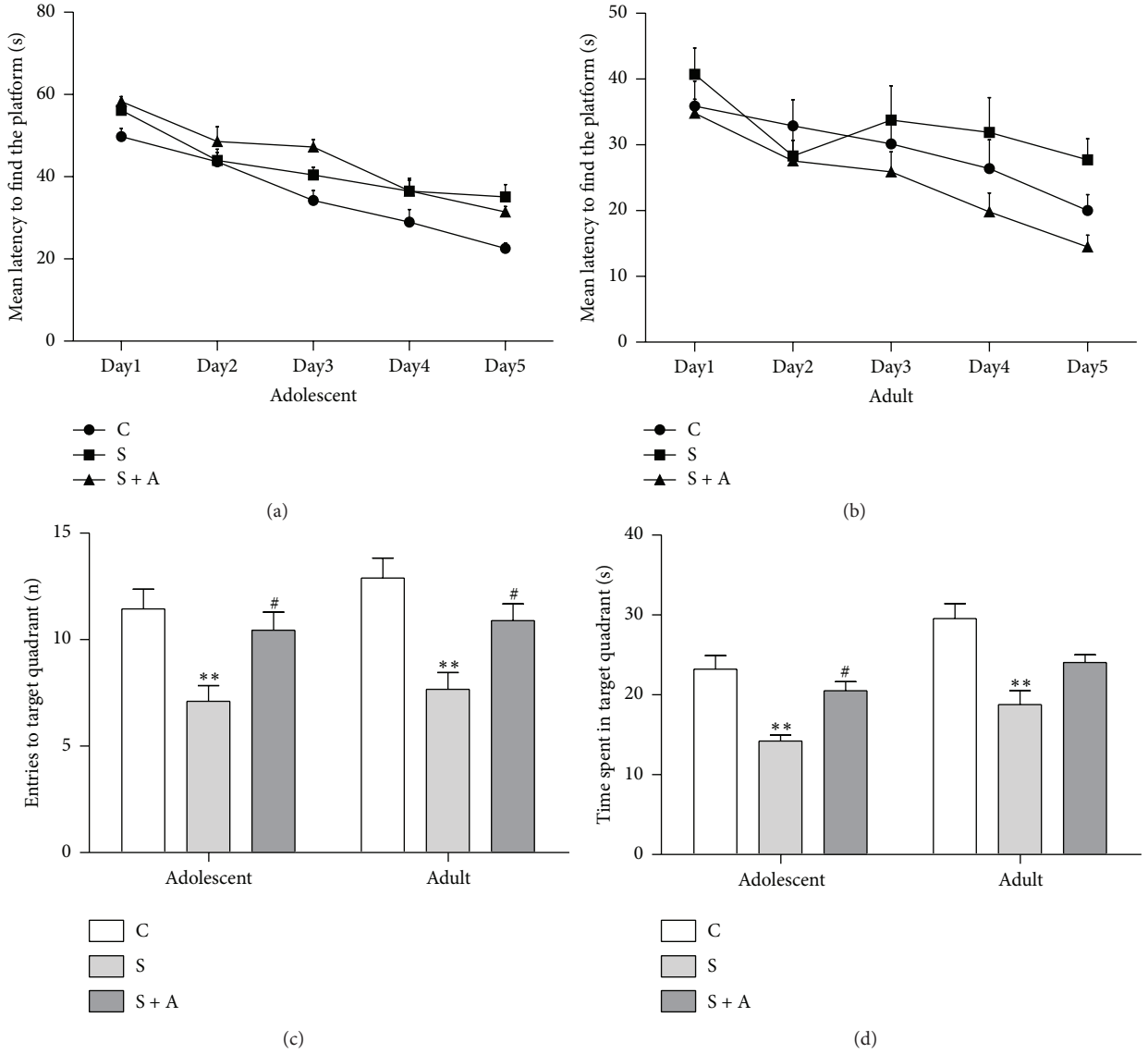

Figure 3: Spatial memory performance in the Morris water maze ($n = 8$ in each group). (a) Mean escape latency to the platform in the Morris water maze in adolescence. (b) Mean escape latency to the platform in the Morris water maze in adulthood. (c) Entries to the target quadrant in adolescence and adulthood. (d) Time spent in the target quadrant in adolescence and adulthood. Values were expressed as mean ± SEM. ∗∗ indicates $p < 0.01$ versus CON; # indicates $p < 0.05$ versus S.

3.3. CRFR1 mRNA Expression and miR-34c Expression in Hypothalamus. The level of CRFR1 mRNA was lower in the adolescent hypothalamus in the S + A group than CON ($p = 0.009$) and S groups ($p = 0.002$) [$F(2, 16) = 10.493$, $p = 0.001$; see Figure 5]. In the adult hypothalamus [$F(2, 16) = 24.650$, $p = 0.000$; see Figure 5], the S ($p = 0.004$) and S + A ($p = 0.01$) groups had lower level of CRFR1 mRNA than the CON group.

In the adolescent hypothalamus [$F(2, 16) = 9.272$, $p = 0.002$; see Figure 6], the S group ($p = 0.011$) and the S + A group ($p = 0.003$) had higher miR-34c expression than the CON group. However, in the adult hypothalamus [$F(2, 16) = 8.547$, $p = 0.003$; see Figure 6], the S + A group exhibited higher miR-34c expressions than the CON group ($p = 0.005$) and S group ($p = 0.012$).

4. Discussion

Early life adverse conditions may lead to abnormal behavioral, neuroendocrine, and genetic responses which might be involved in the pathogenesis of psychiatric disorders [22–27]. Stressful experiences and individual psychology hereditary quality are recognized as risk factors for PTSD [28, 29]. In this study, we focused on the short-term and long-term effects of adolescent foot shock on anxiety-like behavior, memory damage, protein CRFR1 expression, CRFR1 mRNA, and miR-34c levels in the hypothalamus of male Wistar rats.

Behavioral tests were carried out two weeks and six weeks after the stressful foot shock, which acts as models of short-term and long-term effects of adolescent stress, like what to be observed in the PTSD patients. We found that foot

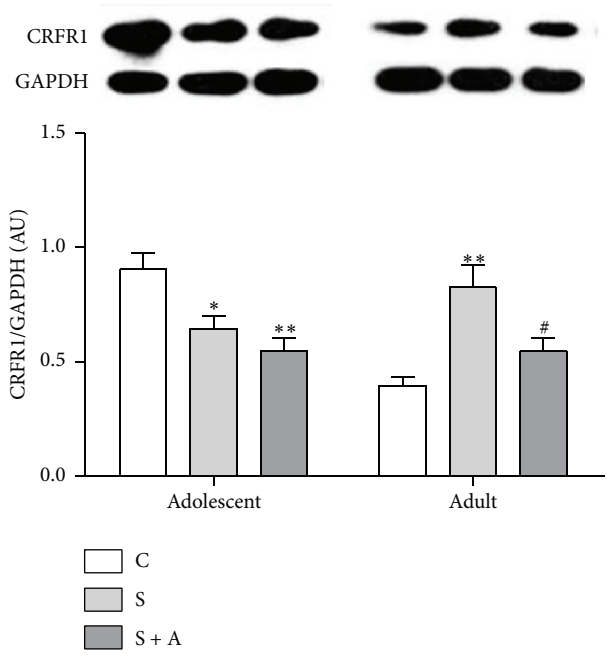

Figure 4: Representative images of Western blotting for CRFR1 expression in adolescent and adult hypothalamus. Values were expressed as mean ± SEM. ∗ and ∗∗ indicate $p < 0.05$ and $p < 0.01$ versus CON, respectively; # indicates $p < 0.05$ versus S.

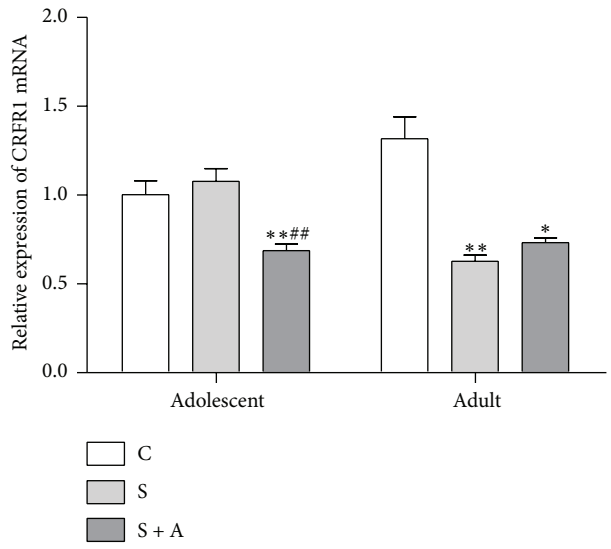

Figure 5: Relative expression of CRFR1 mRNA in adolescent and adult hypothalamus. Values were expressed as mean ± SEM. ∗ and ∗∗ indicate $p < 0.05$ and $p < 0.01$ versus CON, respectively; ## indicates $p < 0.01$ versus S.

shock had both short-term and prolonged negative effects on anxiety-like behavior and memory. Gratifyingly, CRFR1 antagonist performed positive effects. Adolescent foot shock triggered more anxiety-like behaviors and reduced open arm exploration in the EPM test, and passing time did not erase the anxiety of the stressed rats. Since the stressed rats performed fewer entries to the target quadrant and spent less time there than the controls, we speculated that

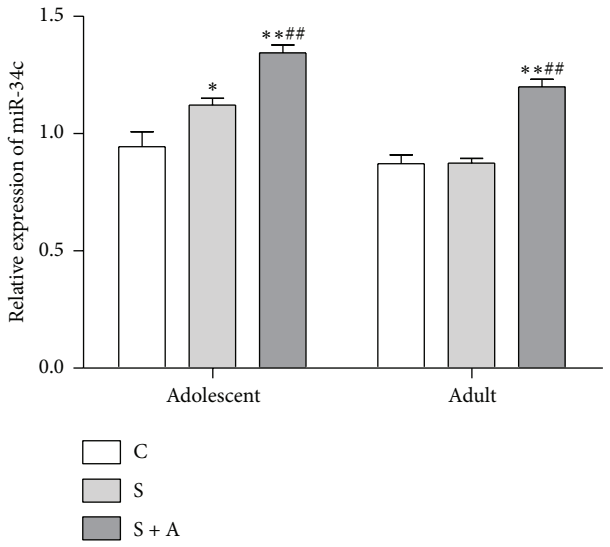

Figure 6: Relative expression of miR-34c in adolescent and adult hypothalamus. Values were expressed as mean ± SEM. ∗ and ∗∗ indicate $p < 0.05$ and $p < 0.01$ versus CON, respectively; # indicates $p < 0.05$ versus S.

rats exposed to foot shock suffered memory damage which lasted to adulthood. Administration of CRFR1 antagonist CP-154,526 after foot shock was proved useful for alleviation of anxiety and memory damage immediately and persistently. Our results supported the conclusions that early life stress resulted in a persisted anxiety behavior and PTSD patients or animal models may develop memory impairments [30–32], which are also affected by individual characters and the type and intensity of stress [26, 30].

Our previous study found that early adolescent stress led to lasting and profound changes in central CRFR1 expression [4]. Therefore, we want to reveal whether the changes of CRFR1 expression occur with the accompanying changes in CRFR1 mRNA expression and miR-34c expression in the hypothalamus, as one of the miR-34c targets is the CRFR1 mRNA, which was regulated via the complementary site on its 3′UTR [15]. In adolescent study, stressed rats showed similar level of CRFR1 mRNA, increased miR-34c expression, and decreased CRFR1 expression compared with the controls in hypothalamus. These results supported the idea that traumatic stress could induce increased miR-34c and decreased CRFR1 expression, which is consistent with the mechanism about miRNA influencing the protein translation [8]. As a marker in stress recovery process, higher level of miR-34c was observed in S + A group. Combined with the result of improved behaviors in CRFR1 antagonist group, our study suggested that CRFR1 antagonist could target a positive process including increased level of miR-34c during acute stress reaction and give a new certification that miR-34c might be closely related with vulnerability to PTSD.

The study focused on the relationship among levels of CRFR1, CRFR1 mRNA, and miR-34c expression in adult stressed rats. In consistent with our hypothesis, stressed rats showed lower level of CRFR1 mRNA, similar level of miR-34c, and increased CRFR1 expression compared with

the unstressed rats. This means although the behavioral performance is the same between adolescence and adulthood of rats after adolescent stress, the CRFR1 mRNA, miR-34c, and protein CRFR1 displayed different dynamic changes after certain period of passing time. The reasons may be explained partially with the homeostasis theory of stress: when individual confronts stress stimulus, organisms would start self-defense mechanism to cope with the stress and induced physiological change to maintain homeostasis. For instance, miR-34c was upregulated after exposure to acute stress, performing anxiolytic properties [15]. In our study, after adolescent foot shock, stressed rats showed increased level of miR-34c in the short term which trigged lower expression of CRFR1 in the hypothalamus to fight against the anxiety. After a protracted struggle which did not work, the level of miR-34c expression returned to normal gradually, while the level of CRFR1 expression was upregulated, as we observed in the hypothalamus six weeks after foot shock. In addition, the sustained upregulated CRFR1 expression might trigger a negative feedback action on the CRFR1 mRNA to maintain the homeostasis. Both positive and negative stress adaptations induce the experience epigenetic changes that affect its future responses [33]. The other reasons including the epigenetic factors such as DNA methylation, histone acetylation, and other types of noncoding RNAs [16, 34, 35] might also influence the CRFR1 expression. For instance, Elliott et al. revealed CRH promoter was demethylated in stress-vulnerability mice while imipramine treatment could reverse the alterations of CRH promoter methylation, mRNA expression, and behavior [36]. It is noticed that there were prominent higher levels of miR-34c in both adolescent and adult CRFR1 antagonist group in the study. The results indicated CRF1 antagonist might improve anxiety-like behavior and memory by alteration of miR-34c expression in hypothalamus.

5. Conclusions

Our results demonstrated that severe traumatic stress in early adolescent induced lasting effects on anxiety-like behavior and spatial memory damage, different alterations of CRFR1 expression, and CRFR1 mRNA and miR-34c expression in hypothalamus between adolescent and adult period, which suggested that the miR-34c expression in hypothalamus may be unique regulator of stress reaction and may play a role in vulnerability to PTSD following exposure to traumatic experience.

Abbreviations

ANOVA: Analysis of variance
CRF: Corticotrophin releasing factor
CRFR1: Corticotrophin releasing factor receptor 1
EPM: Elevated plus maze
HPA: Hypothalamic-pituitary-adrenal
PFC: Prefrontal cortex
PTSD: Posttraumatic stress disorder
PVDF: Polyvinylidene difluoride
SEM: Standard error of the mean
SDS-PAGE: Sodium dodecyl sulfate-polyacrylamide.

Conflict of Interests

The authors declare that there are no competing financial interests. The authors have no conflict of interests to declare.

Authors' Contribution

Fang Pan was involved in study design and date interpretation; Chuting Li performed the majority of the laboratory work and contributed to the analysis of date and writing of the paper; Yuan Liu, Dexiang Liu and Hong Jiang were responsible for the animal model.

Acknowledgments

This work was supported by funding from National Natural Science Foundation of China (no. 31371036). Real-time PCR experiments were performed by Kangchen Bio-Tech, Shanghai, China.

References

[1] S. Goswami, O. Rodríguez-Sierra, M. Cascardi, and D. Paré, "Animal models of post-traumatic stress disorder: face validity," *Frontiers in Neuroscience*, vol. 7, article 89, 2013.

[2] B. S. McEwen, "Sex, stress and the hippocampus: allostasis, allostatic load and the aging process," *Neurobiology of Aging*, vol. 23, no. 5, pp. 921–939, 2002.

[3] A. B. Amstadter, N. R. Nugent, B.-Z. Yang et al., "Corticotrophin-releasing hormone type 1 receptor gene (CRHR1) variants predict posttraumatic stress disorder onset and course in pediatric injury patients," *Disease Markers*, vol. 30, no. 2-3, pp. 89–99, 2011.

[4] C. Li, Y. Liu, S. Yin et al., "Long-term effects of early adolescent stress: dysregulation of hypothalamic-pituitary-adrenal axis and central corticotropin releasing factor receptor 1 expression in adult male rats," *Behavioural Brain Research*, vol. 288, pp. 39–49, 2015.

[5] A. W. Kuss and W. Chen, "MicroRNAs in brain function and disease," *Current Neurology and Neuroscience Reports*, vol. 8, no. 3, pp. 190–197, 2008.

[6] B. K. Sun and H. Tsao, "Small RNAs in development and disease," *Journal of the American Academy of Dermatology*, vol. 59, no. 5, pp. 725–737, 2008.

[7] S.-Y. B. Howng, Y. Huang, L. Ptáček, and Y.-H. Fu, "Understanding the role of dicer in astrocyte development," *PLoS ONE*, vol. 10, no. 5, Article ID e0126667, 2015.

[8] D. P. Bartel, "MicroRNAs: target recognition and regulatory functions," *Cell*, vol. 136, no. 2, pp. 215–233, 2009.

[9] T. R. Cech and J. A. Steitz, "The noncoding RNA revolution—trashing old rules to forge new ones," *Cell*, vol. 157, no. 1, pp. 77–94, 2014.

[10] J. G. Hunsberger, D. R. Austin, G. Chen, and H. K. Manji, "MicroRNAs in mental health: from biological underpinnings to potential therapies," *Neuromolecular Medicine*, vol. 11, no. 3, pp. 173–182, 2009.

[11] S. Mouillet-Richard, A. Baudry, J.-M. Launay, and O. Kellermann, "MicroRNAs and depression," *Neurobiology of Disease*, vol. 46, no. 2, pp. 272–278, 2012.

[12] B. Xu, P.-K. Hsu, M. Karayiorgou, and J. A. Gogos, "MicroRNA dysregulation in neuropsychiatric disorders and cognitive dysfunction," *Neurobiology of Disease*, vol. 46, no. 2, pp. 291–301, 2012.

[13] S. Malan-Müller, S. M. Joanna Hemmings, and S. Seedat, "Big effects of small RNAs: a review of MicroRNAs in anxiety," *Molecular Neurobiology*, vol. 47, no. 2, pp. 726–739, 2013.

[14] U. Schmidt, M. E. Keck, and D. R. Buell, "miRNAs and other non-coding RNAs in posttraumatic stress disorder: a systematic review of clinical and animal studies," *Journal of Psychiatric Research*, vol. 65, pp. 1–8, 2015.

[15] S. Haramati, I. Navon, O. Issler et al., "microRNA as repressors of stress-induced anxiety: the case of amygdalar miR-34," *Journal of Neuroscience*, vol. 31, no. 40, pp. 14191–14203, 2011.

[16] C. J. Peña, R. C. Bagot, B. Labonté, and E. J. Nestler, "Epigenetic signaling in psychiatric disorders," *Journal of Molecular Biology*, vol. 426, no. 20, pp. 3389–3412, 2014.

[17] S. Uchida, K. Hara, A. Kobayashi et al., "Early life stress enhances behavioral vulnerability to stress through the activation of REST4-mediated gene transcription in the medial prefrontal cortex of rodents," *The Journal of Neuroscience*, vol. 30, no. 45, pp. 15007–15018, 2010.

[18] H. Hendriksen, J. Prins, B. Olivier, and R. S. Oosting, "Environmental enrichment induces behavioral recovery and enhanced hippocampal cell proliferation in an antidepressant-resistant animal model for PTSD," *PLoS ONE*, vol. 5, no. 8, Article ID e11943, 2010.

[19] A. Bowirrat, T. J. H. Chen, K. Blum et al., "Neuropsychopharmacogenetics and neurological antecedents of posttraumatic stress disorder: unlocking the mysteries of resilience and vulnerability," *Current Neuropharmacology*, vol. 8, no. 4, pp. 335–358, 2010.

[20] L. Arborelius, K. H. Skelton, K. V. Thrivikraman, P. M. Plotsky, D. W. Schulz, and M. J. Owens, "Chronic administration of the selective corticotropin-releasing factor 1 receptor antagonist CP-154,526: behavioral, endocrine and neurochemical effects in the rat," *The Journal of Pharmacology and Experimental Therapeutics*, vol. 294, no. 2, pp. 588–597, 2000.

[21] R. Adamec, M. Hebert, J. Blundell, and R. F. Mervis, "Dendritic morphology of amygdala and hippocampal neurons in more and less predator stress responsive rats and more and less spontaneously anxious handled controls," *Behavioural Brain Research*, vol. 226, no. 1, pp. 133–146, 2012.

[22] M. F. Juruena, "Early-life stress and HPA axis trigger recurrent adulthood depression," *Epilepsy & Behavior*, vol. 38, pp. 148–159, 2014.

[23] Y. Litvin, P. Tovote, N. S. Pentkowski et al., "Maternal separation modulates short-term behavioral and physiological indices of the stress response," *Hormones and Behavior*, vol. 58, no. 2, pp. 241–249, 2010.

[24] M. Nishi, N. Horii-Hayashi, and T. Sasagawa, "Effects of early life adverse experiences on the brain: implications from maternal separation models in rodents," *Frontiers in Neuroscience*, vol. 8, article 166, 2014.

[25] M. M. Sánchez, C. O. Ladd, and P. M. Plotsky, "Early adverse experience as a developmental risk factor for later psychopathology: evidence from rodent and primate models," *Development and Psychopathology*, vol. 13, no. 3, pp. 419–449, 2001.

[26] T. A. Kosten, J. J. Kim, and H. J. Lee, "Early life manipulations alter learning and memory in rats," *Neuroscience & Biobehavioral Reviews*, vol. 36, no. 9, pp. 1985–2006, 2012.

[27] R. Yehuda, J. D. Flory, L. C. Pratchett, J. Buxbaum, M. Ising, and F. Holsboer, "Putative biological mechanisms for the association between early life adversity and the subsequent development of PTSD," *Psychopharmacology*, vol. 212, no. 3, pp. 405–417, 2010.

[28] J. D. Flory, R. Yehuda, V. Passarelli, and L. J. Siever, "Joint effect of childhood abuse and family history of major depressive disorder on rates of PTSD in people with personality disorders," *Depression Research and Treatment*, vol. 2012, Article ID 350461, 7 pages, 2012.

[29] R. A. Lanius, P. A. Frewen, E. Vermetten, and R. Yehuda, "Fear conditioning and early life vulnerabilities: two distinct pathways of emotional dysregulation and brain dysfunction in PTSD," *European Journal of Psychotraumatology*, vol. 1, article 5467, pp. 1–10, 2010.

[30] L. A. Diehl, L. O. Alvares, C. Noschang et al., "Long-lasting effects of maternal separation on an animal model of post-traumatic stress disorder: effects on memory and hippocampal oxidative stress," *Neurochemical Research*, vol. 37, no. 4, pp. 700–707, 2012.

[31] B. H. Johnsen, J. Eid, T. Løvstad, and L. T. Michelsen, "Posttraumatic stress symptoms in nonexposed, victims, and spontaneous rescuers after an avalanche," *Journal of Traumatic Stress*, vol. 10, no. 1, pp. 133–140, 1997.

[32] C.-Y. Su, K.-Y. Tsai, F. H.-C. Chou, W.-W. Ho, R. Liu, and W.-K. Lin, "A three-year follow-up study of the psychosocial predictors of delayed and unresolved post-traumatic stress disorder in Taiwan Chi-Chi earthquake survivors," *Psychiatry and Clinical Neurosciences*, vol. 64, no. 3, pp. 239–248, 2010.

[33] B. B. Griffiths and R. G. Hunter, "Neuroepigenetics of stress," *Neuroscience*, vol. 275, pp. 420–435, 2014.

[34] A. Holmes, A. M. Le Guisquet, E. Vogel, R. A. Millstein, S. Leman, and C. Belzung, "Early life genetic, epigenetic and environmental factors shaping emotionality in rodents," *Neuroscience and Biobehavioral Reviews*, vol. 29, no. 8, pp. 1335–1346, 2005.

[35] R. Yehuda and L. M. Bierer, "The relevance of epigenetics to PTSD: implications for the *DSM-V*," *Journal of Traumatic Stress*, vol. 22, no. 5, pp. 427–434, 2009.

[36] E. Elliott, G. Ezra-Nevo, L. Regev, A. Neufeld-Cohen, and A. Chen, "Resilience to social stress coincides with functional DNA methylation of the Crf gene in adult mice," *Nature Neuroscience*, vol. 13, no. 11, pp. 1351–1353, 2010.